Hydrogel Systems for Triggered Release of Bacteriophage K and Directed Cell Growth

Bean, Jessica

Award date:
2015

Awarding institution:
University of Bath

HYDROGEL SYSTEMS FOR TRIGGERED RELEASE OF BACTERIOPHAGE K AND DIRECTED CELL GROWTH

Jessica Eleanor Bean

A thesis submitted for the degree of Doctor of Philosophy

University of Bath

Department of Chemistry

August 2015

COPYRIGHT

Acknowledgements

Firstly I would like to thank my supervisor, Dr Toby Jenkins, whose supervision, ideas and guidance made this research possible. I thank him also for giving me the freedom to research independently (with varying degrees of success) and opportunity to travel to so many countries and meet so many brilliant researchers. Thank you to Prof Mark Enright, my second supervisor, for his experienced advice on bacterial infections and bacteriophage. Without his guidance, the world of microbiology would have been so much harder to understand for a lowly chemist. Additionally, I thank the University of Bath Chemistry department, which has been my academic home since 2007; the exciting and diverse research carried out by the department can only flourish in the future. Special thanks go to the BBSRC for funding through the Smartwound project, and to the DAAD for funding my research stay in Germany.

I would like to thank the dynamic past and present members of the Jenkins research group, who have continually been a joy to work with, both socially and academically: Dr Maisem Laabei, Dr Dave Jamieson, Dr Serena Marshall, Dr Sunny Hong, Dr Naing Tun Thet, Dr Diana Alves, Hollie Hathaway, Scarlet Milo and Dr June Mercer-Chalmers. Their help during my PhD has been invaluable, and although beginning as colleagues I will leave them as good friends.

I would also like to thank all those who made my research placement at the Universität Siegen such a wonderful experience. Firstly, my supervisor Prof Holger Schönherr, who allowed me to work as part of the Physical Chemistry I research group and who gave such good guidance during my stay. Secondly, all of the members of the Physical Chemistry I and Macromolecular research groups who were so welcoming and made my stay so rewarding. Special thanks are given to Ping Li, for her excellent supervision, Katrin-Stephanie Tücking, for looking after me in a new country, and Cleiton Kunzler, for the salsa lessons.

Finally I would like to thank my friends and family for their unconditional support over the past 4 years. To you all, you have been wonderful and I could not have done any of this without you. Additional thanks to my sister, Sarah, Diana and Katy for proof-reading.

“For a moment, nothing happened. Then, after a second or so, nothing continued to happen” - *Douglas Adams, The Hitchhiker’s Guide to the Galaxy*

Dissemination of Research Work

List of Patents and Publications

Enhancement of the Antimicrobial Properties of Bacteriophage-K via Stabilization using Oil-in-Water Nano-Emulsions, Esteban, P. P.; Alves, D. R.; Enright, M. C.; Bean, J. E.; Gaudion, A.; Jenkins, A.T.A.; Young, A. E. R.; Arnot, T. C. *Biotechnology Progress*, **2014**, 30, 932-944.

Combined Use of Bacteriophage K and a Novel Bacteriophage to Reduce *Staphylococcus aureus* Biofilm Formation, Alves, D. R.; Gaudion, A.; Bean, J. E.; Esteban, P. P.; Arnot, T. C.; Harper, D. R.; Kot, W.; Hansen, L. H.; Enright, M. C.; Jenkins, A.T.A. *Applied and Environmental Microbiology*, **2014**, 80, 6694 - 6703.

Triggered Release of Bacteriophage K from Agarose/Hyaluronan Hydrogel Matrixes by *Staphylococcus aureus* Virulence Factors, Bean, J. E.; Alves, D. R.; Laabei, M.; Esteban, P. P.; Thet, N. T.; Enright, M. C.; Jenkins, A.T.A, *Chemistry of Materials*, **2014**, 26, 7201 – 7208.

Poly(N-isopropylacrylamide-co-allylamine) (PNIPAM-co-ALA) Nanospheres for the Thermally Triggered Release of Bacteriophage K, Hathaway, H; Alves, D. R.; Bean, J. E.; Esteban, P. P.; Ouadi, K.; Sutton, J. M.; Jenkins, A.T.A., *European Journal of Pharmaceutics and Biopharmaceutics*, **2015**, 96, 437 – 441.

A novel bacteriophage cocktail reduces and disperses *Pseudomonas aeruginosa* biofilms under static and flow conditions, Alves, D. R.; Esteban, P. P.; Kot, W.; Bean, J. E.; Arnot, T. C.; Hansen, L. H.; Enright, M. C.; Jenkins, A.T.A., *Microbial Biotechnology*, **2015**, accepted for publication

Prototype Development of the Intelligent Hydrogel Wound Dressing and Its Efficacy in the Detection of Model Pathogenic Wound Biofilms, Thet, N. T.; Alves, D. R.; Bean, J. E.; Booth, S.; Nzakizwanayo, J.; Young, A. E. R.; Jones, B. V.; Jenkins, A. T. A., *ACS Applied Materials & Interfaces*, **2015**, accepted for publication

Patents

- **"Hydrogel",** Bean, J. E.; Jenkins, A. T. A.; 2015; UK Patent (Application no: GB1500204.1)

Awards

May 2012 - 1st Year physical and computational poster prize (sponsored by BP)

June 2014 – Wrote and was awarded DAAD Research Grant €3000 for 6 month placement in Germany

March 2015 - £400 University of Bath Conference Travel grant

List of Presentations

Jul 2012 – Colloids and Nanomedicine 2012, Amsterdam, the Netherlands

Poster - "Encapsulation of bacteriophage and bacteriophage lysins into responsive nanoparticles

Jan 2013 – KOALA Nanyang Technological University Meeting, Singapore

Poster - "Engineering of hydrogel scaffolds for delivery of lysostaphin and bacteriophage lysins"

Jan 2014 – Exploiting bacteriophages for bioscience, biotechnology and medicine, O2 Arena, London, UK

Sep 2013 – Phages 2013: Bacteriophage in medicine, food and biotechnology, Oxford, UK

2011 - 2015 yearly – BioNano Summer School, Hirschegg, Austria

2015 talk - "Hydrogel matrices for triggered release of new antimicrobial therapeutics"

May 2015 – EMRS Spring Meeting, Lille, France

Table of Contents

ACKNOWLEDGEMENTS i
DISSEMINATION OF RESEARCH WORK iii
TABLE OF CONTENTS v
LIST OF FIGURES xiii
LIST OF TABLES xviii
ACRONYMS AND ABBREVIATIONS xix
ABSTRACT xxiii

CHAPTER 1: INTRODUCTION AND LITERATURE REVIEW 1

1.1. Bacterial Infections 2
1.1.1. Clinical problem 4
1.1.2. Wounds and wound infections 6
1.1.3. Biofilms 7
1.1.4. *Staphylococcus aureus* 8
1.1.4.1. Virulence Factors 9
1.1.4.2. Regulation of *S. aureus* virulence factors 9
1.1.5. Antibiotic resistance 11
1.1.5.1. Methicillin resistant *S. aureus*, MRSA 11
1.1.5.2. Alternatives to antibiotics 12
1.2. Bacteriophage 13
1.2.1. Discovery and historical use 13
1.2.2. Classification and morphology 14
1.2.3. Bacteriophage life cycle 15
1.2.3.1 The Lytic Cycle 16
1.2.3.2 The Lysogenic Cycle 17
1.2.4. Advantages of bacteriophage therapy 17
1.2.5. Disadvantages of bacteriophage therapy 18
1.2.6. Bacteriophage as a therapeutic 19
1.2.7. Bacteriophage and biofilms 20
1.2.8. Bacteriophage lysins 21
1.3. Vesicles 23
1.4. Hydrogels 24
1.4.1. Hydrogel wound dressings 24

1.4.2. Natural polymers 26
1.4.3. Synthetic polymers 27
1.4.4. Hyaluronic acid 28
1.4.4.1. Role of hyaluronic acid in wound healing 29
1.4.4.2. Hyaluronic acid crosslinking 30
1.4.4.2.1. Modification of hyaluronic acid carboxylic acid 30
1.4.4.2.2. Crosslinking of hyaluronic acid alcohols 31
1.4.4.2.3. Crosslinking of hyaluronic acid derivatives 32
1.4.4.3. Hyaluronic acid hydrogel dressings 33
1.4.4.4. Hyaluronidase in prokaryotes 34
1.4.4.5. Hyaluronidase in eukaryotic cells 35
1.4.5. 'Smart' hydrogel systems 35
1.4.5.1. pH sensitive hydrogels 35
1.4.5.2. Temperature sensitive hydrogels 36
1.4.5.3. Enzyme sensitive hydrogels 36
1.5. Aims and Objectives 37
1.6. References 38

CHAPTER 2: MATERIALS, GENERAL METHODS AND EXPERIMENTAL THEORY 45
2.1. Materials 45
2.2. General Methods 45
2.2.1. Preparation of bacteria 45
2.2.1.1. Bacterial live culture preparation 46
2.2.1.2. Bacterial supernatant preparation 46
2.2.1.3. Bacterial concentration calculation 46
2.2.1.4. Bacterial strains used 47
2.2.1.5. PCR of bacterial DNA 49
2.2.2. Preparation of bacteriophage 49
2.2.2.1. Bacteriophage extraction 49
2.2.2.2. Bacteriophage isolation 50
2.2.2.3. Bacteriophage propagation (double overlay method) 50
2.2.2.4. Bacteriophage titration 50
2.2.2.5. Bacteriophage sensitivity assay 51

2.2.2.6. PEG purification of bacteriophage 51
2.2.2.7. Fluorescent tagging of bacteriophage 52
2.2.2.8. Incubation of bacteriophage with live bacterial culture 52
2.2.3. NIH-3T3 fibroblast cell culture 52
2.2.4. Preparation of vesicles 53
2.2.4.1. Vesicle buffer solutions 53
2.2.4.2. Giant Unilamellar Vesicle (GUV) preparation 53
2.2.4.3. Large Unilamellar Vesicle (LUV) preparation 54
2.2.4.4. Incubation of vesicles with bacterial supernatant 54
2.2.5. Hydrogel swelling ratio 55
2.3. Instrumentation 55
2.4. General Experimental Theory 56
2.4.1. Fluorescence Spectroscopy 56
2.4.2. UV-visible Spectroscopy 57
2.4.3. Microscopy 58
2.4.3.1. Light microscopy 58
2.4.3.2. Fluorescence microscopy 58
2.4.3.3. Confocal Laser Scanning Microscopy (CLSM) 59
2.4.3.4. Scanning Electron Microscopy (SEM) 60
2.4.3.5. Transmission Electron Microscopy (TEM) 60
2.4.4. Dynamic Light Scattering (DLS) 61
2.5. Polymerisation 61
2.6. Principles of Radical Polymerisation 64
2.6.1. Initiation 64
2.6.2. Propagation 65
2.6.3. Termination 65
2.6.4. Kinetics of radical polymerisation 66
2.6.5. Thermodynamics of radical polymerisation 67
2.7. Principles of Hydrogel Chemistry 68
2.7.1. Rheology 69
2.7.2. Swelling 70
2.8. Enzyme kinetics 71
2.9. References 73

CHAPTER 3: PRELIMINARY WORK 75

3.1. Introduction 75

3.2. Preliminary Results and Discussion 76

3.3. Conclusions 83

3.4. References 84

CHAPTER 4: DIFFUSION AND INFECTION OF BACTERIOPHAGE K IN HYDROGEL MATRICES 85

4.1. Introduction 85

4.2. Materials and Methods 86

4.2.1. Formation of PVA 86

4.2.2. Formation of agarose 87

4.2.3. Bacteriophage methods 87

4.2.4.1. Disc diffusion assay 87

4.2.3.2. Temperature stability of Bacteriophage K 87

4.2.4.3. UV stability of Bacteriophage K 87

4.3. Results and Discussion 88

4.3.1. Bacteriophage 88

4.3.1.1. Bacteriophage isolation and plaque morphology 88

4.3.1.2. TEM imaging of bacteriophage 88

4.3.1.3. Bacterial sensitivity to bacteriophage 89

4.3.1.4. Bacteriophage growth curves in liquid culture 92

4.3.1.5. Temperature stability of Bacteriophage K 93

4.3.1.6. UV stability of Bacteriophage K 95

4.3.1.7. Use of Bacteriophage K for further development 96

4.3.2. Bacteriophage K in poly(vinyl alcohol) (PVA) hydrogels 97

4.3.2.1. PVA hydrogels 97

4.3.2.2. SEM imaging of PVA hydrogels 99

4.3.2.3. Release of bacteriophage from PVA hydrogels 101

4.3.2.4. Kinetics of bacteriophage release 102

4.3.2.5. Zones of inhibition 104

4.3.2.6. Bacteriophage hydrogels in overnight culture 105

4.3.2.7. UV irradiation 106

4.3.2.8. Overview 107

4.3.3. Bacteriophage K in agarose hydrogels....108
4.3.3.1. Agarose hydrogels....108
4.3.3.2. SEM imaging of agarose hydrogels....110
4.3.3.3. Release of bacteriophage from agarose hydrogels....112
4.3.3.4. Kinetics of bacteriophage release from hydrogels....113
4.3.3.5. Zones of inhibition....114
4.3.3.6. Bacteriophage hydrogels in overnight culture....115
4.3.3.7. UV irradiation....116
4.3.3.8. Overview....118
4.4. Conclusions....118
4.5. References....118

CHAPTER 5: DEVELOPMENT OF CROSSLINKABLE HYALURONIC ACID AND SUBSEQUENT SENISITIVITY TO *STAPHYLOCOCCAL* HYALURONIDASE....121
5.1. Introduction....121
5.2. Materials and Methods....122
5.2.1. Carbodiimide crosslinking....123
5.2.2. Aldehyde/adipic dihydrazide crosslinking....123
5.2.2.1. Synthesis of oxidised hyaluronic acid (oxi-HA)....123
5.2.2.2. TNBS assay....123
5.2.2.3. Crosslinking of oxi-HA with adipic dihydrazide....124
5.2.3. Photopolymerisation crosslinking....124
5.2.3.1. Synthesis of hyaluronic acid methacrylate (HAMA)....124
5.2.3.2. Photopolymerisation of HAMA....124
5.2.4. Carbazole assay....124
5.2.5. Hyaluronidase production in biofilms....125
5.2.5.1. *S. aureus* biofilm formation....125
5.2.5.2. Crystal violet assay....125
5.3. Results and Discussion....126
5.3.1. Crosslinking of HA....126
5.3.1.1. Carbodiimide crosslinking....126
5.3.1.2. Aldehyde/adipic dihydrazide crosslinking....130
5.3.1.3. Photopolymerisation crosslinking....133

5.3.2. Hyaluronidase production by *S. aureus* 139
5.3.2.1. Screen of bacterial hyaluronidase activity 139
5.3.2.2. Hyaluronidase expression during *S. aureus* growth 141
5.3.2.3. Expression of hyaluronidase by *S. aureus* biofilms 142
5.3.3. Sensitivity of HAMA-co-PEG films to hyaluronidase 144
5.3.4. Sensitivity of HAMA-co-PEG films to *S. aureus* supernatant 146
5.4. Conclusions 148
5.5. References 149

CHAPTER 6: A BILAYERED HYDROGEL SYSTEM FOR TRIGGERED RELEASE OF BACTERIOPHAGE K BY *STAPHYLOCOCCAL* HYALURONIDASE 151
6.1. Introduction 151
6.2. Materials and Methods 152
6.2.1. Formation of bilayer hydrogel 152
6.2.2. Measurement of bacteriophage release by hyaluronidase 153
6.2.3. Measurement of bacteriophage release by bacterial supernatant 153
6.2.4. Live culture with bilayer hydrogels 154
6.3. Results and Discussion 155
6.3.1. Bilayer hydrogels 155
6.3.2. Optimisation of HAMA crosslinking 155
6.3.3. Optimisation of agarose hydrogels 157
6.3.4. 0.4% agarose bilayer hydrogel 158
6.3.4.1. Triggered release of Bacteriophage K by hyaluronidase 158
6.3.4.2. Triggered release of Bacteriophage K by bacterial supernatant 160
6.3.5. 0.7% agarose bilayer hydrogel 161
6.3.5.1. Triggered release of Bacteriophage K by hyaluronidase 161
6.3.5.2. Triggered release of Bacteriophage K by bacterial supernatant 162
6.3.5.3. Triggered release of Bacteriophage K by multiple bacterial supernatants 163
6.3.6. 2% agarose bilayer hydrogel 164
6.3.6.1. Triggered release of Bacteriophage K by hyaluronidase 164
6.3.6.2. Triggered release of Bacteriophage K by bacterial supernatant 165
6.3.6.3. Triggered release of Bacteriophage K by multiple bacterial supernatants 166

6.3.6.4. Incubation with live *S. aureus* culture 167
6.4. Conclusions 168
6.5. References 169

CHAPTER 7: NANO-IMPRINT LITHOGRAPY OF PHOTOCROSSLINKABLE HYALURONIC ACID/GELATIN HYDROGELS FOR DIRECTED CELL GROWTH AND PROLIFERATION 171
7.1. Introduction 171
7.2. Materials and Methods 172
7.2.1. Cast moulding of lithographic prints through Hot Embossing 172
7.2.2. Crosslinking of hydrogels 172
7.2.3. Characterisation of polystyrene prints and printed hydrogels.....173
7.2.4. Cell culture on HAMA hydrogels.....173
7.2.5. Preparation of GelMA 173
7.2.6. Cytotoxicity of Irgacure 2959.....173
7.2.7. MTT assay.....174
7.2.8. Hyaluronidase degradation of HA and Gelatin based co-gels 174
7.3. Results and Discussion..... 175
7.3.1. Printing of hydrogels.....175
7.3.1.1. Cast moulding of lithographic prints through Hot Embossing .. 175
7.3.1.2. Printing of HAMA hydrogels 176
7.3.2. NIH-3T3 culture on HAMA hydrogels 178
7.3.2.1. Culture of NIH-3T3 fibroblasts.....178
7.3.2.2. Cell culture on flat HAMA hydrogels 179
7.3.2.3. Cell culture on printed HAMA hydrogels.....180
7.3.2.4. Printing of HA hydrogels with varying concentration of HA 181
7.3.2.5. Cytotoxicity of Irgacure 2959 183
7.3.3. NIH-3T3 culture on HAMA/gelatin hydrogels.....185
7.3.3.1. Cell culture on HAMA-gelatin co-gels with 0.1% Irgacure 2959.187
7.3.3.2. Cell culture on HAMA-gelatin co-gels with prewashing 188
7.3.4. NIH-3T3 culture on gelatin methacrylate (GelMA) hydrogels.....189
7.3.4.1. Preparation of GelMA 189
7.3.4.2. Swelling of GelMA hydrogels 191
7.3.4.3. Cell culture on GelMA.....192

7.3.4.4. Cell culture on HAMA-GelMA co-gels.....192
7.3.4.5. Cell culture on 5% GelMA hydrogels with and without HA and PEGDA 194
7.3.4.6. Hyaluronidase degradation of GelMA gels containing HA 196
7.3.4.7. Hyaluronidase degradation of GelMA gels containing HAMA ...197
7.4. Conclusions 197
7.5. References.....198

CHAPTER 8: CONCLUSIONS AND FUTURE WORK 199
8.1. General Conclusions.....199
8.1.1. Limitations of the presented work 200
8.2. Future Project Development 201
8.2.1. Bacteriophage cocktails 201
8.2.2. Theranostic wound dressings 202
8.2.3. Triggered release hydrogels.....202
8.2.4. Testing with established biofilms 203
8.2.5. In vivo testing.....203
8.2.6. Hydrogels for eukaryotic cell culture.....203
8.2.7. Lithographic printing of hydrogels 204

List of Figures

Figure 1.1: Schematic diagram of prokaryotic (left) and eukaryotic (right) cells.....2
Figure 1.2: Diagram of the cell wall composition of Gram-positive (left) and Gram-negative (right) bacteria.....3
Figure 1.3: Diagram of bacterial growth phases: the lag phase, exponential phase, stationary phase and death phase 3
Figure 1.4: Number of approved antibiotics between 1980 and 2011. Reproduced with permission from Bassetti et al.....5
Figure 1.5: Stages of biofilm development. Reproduced with permission from Sauer et al, ...7
Figure 1.6: False-coloured SEM image of *S. aureus* ©J. H. Carr, Public Health Image Library 8
Figure 1.7: Diagram explaining the self-regulating function of the *agr* system. Reproduced with permission from Novick et al.....10
Figure 1.8: TEM images of (left) Initial bacteriophage adsorption onto the host bacterium, ©Graham Colm, (right) bacterial lysis due to bacteriophage infection, ©Biozentrum, University of Basel/Science Photo Library.....13
Figure 1.9: Lytic and lysogenic life cycles of bacteriophage. Reproduced with permission from Campbell et al.....16
Figure 1.10: Pyobacteriophage preparations for use in broad-range infections ©Eliava Institute20
Figure 1.11: Murein hydrolase enzyme sites of attack: 1. N-acetylmuramoyl-L-alanine amidase, 2. L-alanoyl-D-glutamate endopeptidase, 3. Interpeptide bridge endopeptidase, 4. N-acetyl-β-D-muramidase, 5. Transglycosylase, 6. N-acetyl-β-D-glucosaminidase.....22
Figure 1.12: Structure of the phospholipid DPPC 23
Figure 1.13: Vesicle, micelle and bilayer structures formed from phospholipid bilayers 24
Figure 1.14: a) Hartmann Hydrosorb™ hydrogel wound dressing sheet, b) Medicare Burnshield hydrogel spray for burns and scalds, c) Sorbact® antimicrobial hydrogel 25
Figure 1.15: Characteristics for optimal wound dressings and devices. Reproduced with permission from Mayet et al 26
Figure 1.16: Chemical structures of a) poly(vinyl alcohol), PVA b) poly(ethylene glycol), PEG c) poly(caprolactone) d) poly(lactic acid) e) polyvinylpyrrolidone, PVA and f) poly(hydroxyethyl methacrylate) 28
Figure 1.17: Repeating unit structure of hyaluronic acid.....28
Figure 1.18: HA crosslinking through a) amine bond formation, b) ester bond formation and c) hydrazide bond formation.....31
Figure 1.19: HA crosslinking through free radical polymerisation of methacrylated HA 32
Figure 1.20: Positions of cleavage of HAase molecules - 1. hyaluronate-3-glycanohydrolases, 2. hyaluronate-4-glycanohydrolases and 3. hyaluronate lyases. 34
Figure 2.1: Bacteriophage dilution plating on bacterial lawn for concentration determination...51
Figure 2.2: Jablonski diagram showing fluorescence and phosphorescence from various excited electronic states 56
Figure 2.3: a) Chemical structure of 5(6)-carboxyfluorescein, b) Left vial containing unquenched fluorescing 5 mM dye, right vial containing quenched non-fluorescent 50 mM dye under UV light57
Figure 2.4: Schematic diagram of visible light excitation and emission in a fluorescent microscope 59
Figure 2.5: a) Random copolymer, b) alternating copolymer, c) block copolymer, d) graft copolymer.....62
Figure 2.6: a) Addition polymerisation of ethene to form poly (ethene), b) condensation polymerisation of 1, 4-phenylene diamine and 1, 4-benzenedicarbonyl chloride to form Kevlar™ and HCl by-product.....63
Figure 2.7: Free radical initiation of monomer unit.....64
Figure 2.8: Propagation of polymer chains in free radical polymerisation.....65

Figure 2.9: Combination and Disproportionation termination mechanisms in free radical polymerisations..... 66
Figure 2.10: Structure of ideal crosslinked polymer network for use in hydrogels 68
Figure 2.11: a) Diagram of hydrogel sample between one rotating and one stationary plate in DMA, b) shearing of a hydrogel block by a force, F 69
Figure 2.12: ΔE change difference in catalysed and uncatalysed reactions..... 71
Figure 2.13: a) initial reversible binding of enzyme to substrate, b) conversion of substrate to products in the enzyme active site, c) release of products from the enzyme..... 72
Figure 3.1: Schematic of antimicrobial or dye filled vesicles which become degraded by bacterial virulence factors, leading to the killing of bacteria or the release of dye molecules..... 75
Figure 3.2: (left) Fluorescence intensity of 5(6) carboxyfluorescein vesicles incubated with bacterial supernatant over 2 hours, (right) Endpoint fluorescence intensity after 2 hours..... 77
Figure 3.3: Confocal microscopy images of DPPC GUVs containing 5 mM 5(6)-carboxyfluorescein (left) from the z direction and (right) from the x direction 78
Figure 3.4: a) red, b) green and c) combined laser images of 5(6)-carboxyfluorescein GUVs doped with Texas Red labelled DHPE. Scale bar = 2 µm..... 78
Figure 3.5: (left) Fluorescence intensity of 5(6) carboxyfluorescein GUVs incubated with bacterial supernatant over 2 hours, (right) Endpoint fluorescence intensity after 2 hours..... 79
Figure 3.6: (left) *S. aureus* MSSA 476 and (right) *S. aureus* RN9611 incubated with GUVs containing Bacteriophage K 80
Figure 3.7: Reaction scheme for the fluorescent tagging of bacteriophage capsid primary amines with (5)-carboxyfluorescein N-succinimidyl ester 81
Figure 3.8: Emission spectra of pure 5-carboxyfluorescein N-succinimidyl ester and 5-carboxyfluorescein N-succinimidyl ester tagged Bacteriophage K..... 82
Figure 3.9: a) red, b) green and c) combined laser images of Texas Red labelled DHPE GUVs containing CF-NSE labelled bacteriophage 82
Figure 4.1: Bacteriophage diffusion out of hydrogel matrices and subsequent killing of bacteria85
Figure 4.2: a) Bacteriophage K dilutions used for concentration calculation with 10^{-3}, 10^{-4}, 10^{-5} and 10^{-6} phage lysate dilutions. b) Individual Bacteriophage K plaques 88
Figure 4.3: TEM images of Bacteriophage K stained with 1% uranyl acetate. Bacteriophage K with extended tail (left), Bacteriophage K with contracted tail and injection mechanism (right). Imaging carried out by Diana Alves 89
Figure 4.4: Streak test examples of *S. aureus* strains deemed susceptible (left), intermediate (centre) and resistant (right) to Bacteriophage K infection..... 90
Figure 4.5: Overnight bacterial growth curves of a) Bacteriophage K sensitive *S. aureus* H560, b) Bacteriophage K intermediate sensitivity *S. aureus* RN6390B and c) Bacteriophage resistant S. aureus ST239 µ2..... 92
Figure 4.6: Titer of Bacteriophage K solutions incubated at -20, 4, 25, 37, 45, 60 and 70 °C for one hour..... 94
Figure 4.7: Titer of Bacteriophage K exposed to UV flood irradiation for 30 seconds, 1, 2 and 5 minutes 95
Figure 4.8: Structure of PVA repeating unit 97
Figure 4.9: 10 mm discs of freeze/thawed hydrogels containing (left to right) 2%, 5% and 10% PVA..... 98
Figure 4.10: Swelling ratio measurements of 2%, 5% and 10% PVA hydrogels 98
Figure 4.11: Water loss measurements of 5% PVA hydrogels at 4, 25, 37, 45 and 60 °C 99
Figure 4.12: SEM images of a) 2%, b) 5% and c) 10% PVA hydrogels formed by freeze thawing at -20 °C. Scale bar = 5 µm. 100
Figure 4.13: Bacteriophage release from 2%, 5% and 10% PVA hydrogels..... 101
Figure 4.14: Graph of C_t/C_0 of 2%, 5% and 10% PVA hydrogels 102
Figure 4.15: Diffusion coefficient values (10^{-11} m^2sec^{-1}) for 2%, 5% and 10% PVA..... 103

Figure 4.16: (left) Zone of inhibition measurements of 8 mm diameter PVA hydrogels containing 10^8 pfu/mL Bacteriophage K on S. aureus H560. (right) Image of zone of inhibition surrounding 7% PVA.....104
Figure 4.17: Growth curves of *S. aureus* H560 liquid cultures incubated with 2%, 5% and 10% PVA containing 10^8 pfu/mL Bacteriophage K. 105
Figure 4.18: Incubation of *S. aureus* H560 with 5% PVA containing 10^8 pfu/mL Bacteriophage K which has been irradiated with flood UV for 10, 30 and 60 seconds 106
Figure 4.19: Structure of agarose repeating unit.....108
Figure 4.20: 10 mm discs of hydrogels containing (from left to right) 0.2%, 0.4%, 0.7%, 1.4% and 2% agarose 109
Figure 4.21: Swelling ratio measurements of 0.2%, 0.4%, 0.7%, 1.4% and 2% agarose hydrogels 109
Figure 4.22: Water loss measurements of 0.7% agarose hydrogels at 4, 25, 37, 45 and 60 °C...110
Figure 4.23: SEM images of a) 0.2%, b) 0.4%, c) 0.7%, d) 1.4 and e) 2% w/v agarose hydrogels. Scale bar = 10 µm 111
Figure 4.24: Bacteriophage release from 0.2%, 0.7% and 2% agarose hydrogels 112
Figure 4.25: Graph of C_t/C_0 0.2%, 0.7% and 2% agarose hydrogels.....113
Figure 4.26: Diffusion coefficient values (10^{-11} m^2sec^{-1}) for 0.2%, 0.7% and 2% agarose.....114
Figure 4.27: (left) Zone of inhibition measurements of 8 mm diameter agarose hydrogels containing 10^8 pfu/mL Bacteriophage K on *S. aureus* H560. (right) Image of zone of inhibition surrounding 0.4% agarose.....115
Figure 4.28: Growth curves of *S. aureus* H560 liquid cultures incubated with 0.4%, 0.7%, 1.4% and 2% agarose containing 10^8 pfu/mL Bacteriophage K. 116
Figure 4.29: Incubation of *S. aureus* H560 with a) 0.4%, b) 0.7%, c)1.4% and d)2% agarose containing 10^8 pfu/mL Bacteriophage K which has been irradiated with flood UV for 10, 30 and 60 seconds.....117
Figure 5.1: Schematic diagram of bilayered hydrogel system: upper hydrogel layer containing degradable crosslinked HA. 121
Figure 5.2: Reaction scheme for the crosslinking of HA with EDC and PEG diglycidyl ether.....126
Figure 5.3: Reaction mechanism for the EDC mediated crosslinking of HA 127
Figure 5.4: a) dry HA film before crosslinking, b) crosslinked HA film (10 mM EDC, 10 mM HCl, 250 mM PEG diglycidyl ether) after swelling in PBS buffer overnight 127
Figure 5.5: FTIR spectrum of HA and HA sheets crosslinked with 10 mM EDC, 10 mM HCl and 250 mM PEG diglycidyl ether. 128
Figure 5.6: Reaction scheme for the oxidation of HA by sodium periodate.....130
Figure 5.7: Reaction mechanism for the nucleophilic addition of adipic dihydrazide to oxi-HA.131
Figure 5.8: FTIR spectrum of HA, oxidised HA and oxidised HA crosslinked with adipic dihydrazide. 131
Figure 5.9: Standard curve of OD_{340} measurements of 0 – 30 mM tert-butyl carbazate used to calculate aldehyde concentration in oxidised HA 132
Figure 5.10: a) 6% oxi-HA solution, b) 8% ADH solution and c) oxi-HA/ADH crosslinked.....133
Figure 5.11: Reaction scheme for the methacrylation of HA using glycidyl methacrylate.....134
Figure 5.12: Reaction mechanism of radical formation of Irgacure 2959 by UV light and subsequent polymerisation initiation of HAMA. 134
Figure 5.13: Crosslinked HAMA hydrogels containing 1% w/v Irgacure 2959 and 1%, 2% and 5% a) PEG diacrylate, b) ethylene glycol dimethacrylate and c) ethylene diacrylate after 1 minute UV irradiation.....135
Figure 5.14: FTIR spectra of hyaluronic acid and hyaluronic acid methacrylate (HAMA).....136
Figure 5.15: ^1H NMR spectrum of HAMA in D_2O. Resonances at 5.6 and 6.2 ppm verified the presence of methylene protons. 136

Figure 5.16: Swelling ratio measurements of 2% HAMA hydrogels containing varying % PEG diacrylate with 1% initiator and 1 minute UV exposure 137
Figure 5.17: Side-on SEM images of 2% HAMA hydrogels containing 0, 1, 5 and 10% v/v PEG diacrylate with 1% initiator and 1 minute UV exposure. 138
Figure 5.18: 2% agarose gels of hysA gene in JE2, NE334 (hys-), TW20, ST239 μ2 and ST239 μ20. Ladder =1 kB 139
Figure 5.19: HAase activity screen of 116 bacterial strains 140
Figure 5.20: HAase production during the growth of *S. aureus* H560 141
Figure 5.21: HAase production during the growth of *S. aureus* ST239 μ2 142
Figure 5.22: (left) HAase activity and (right) biofilm biomass in *S. aureus* C3, H560 and hys- 143
Figure 5.23: Example biofilm plate stained with 0.1% crystal violet solution after 24 hours growth 143
Figure 5.24: Concentration of NAG from 2% HAMA /1% PEGDA gels, after incubation with PBS, 0.01, 0.1 and 1 mg/mL HAase 144
Figure 5.25: Top view SEM images after 2 hour incubation of 1% PEG diacrylate + 2% HAMA hydrogels with a) PBS, b) 0.01 mg/mL HAase and c) 1 mg/mL HAase 145
Figure 5.26: Degradation of HAMA hydrogels containing 0%, 1%, 5% and 10% PEGDA by HAase... 146
Figure 5.27: SEM images of HAMA hydrogels after 2h incubation with *S. aureus* supernatant. HAase positive strains: a) RN6390B, b) H560, c) lac. HAase negative strains: d) hys-, e) ST239 μ2, and f) TSB. 147
Figure 5.28: Degradation of HAMA hydrogels by HAase positive (green) and HAase negative (red) *S. aureus* supernatant. 148
Figure 6.1: Schematic diagram of bilayered hydrogel system: degradation of the upper HAMA layer causes release of immobilised bacteriophage, causing bacterial death 151
Figure 6.2: Schematic diagram of bilayer hydrogel formation 153
Figure 6.3: 12-well plate layout for 1 mg/mL hyaluronidase breakdown measurements of bilayer hydrogel experiments 153
Figure 6.4: 12-well plate layout for bacterial supernatant breakdown measurements of bilayer hydrogel experiments 154
Figure 6.5: (left) Bilayered 2% agarose hydrogel with HAMA layer, (right) bilayered 5% PVA hydrogel with HAMA layer 155
Figure 6.6: Swelling ratio measurements of HAMA hydrogels after 10, 20, 30 and 60 sec UV irradiation 156
Figure 6.7: Degradation of HAMA hydrogels crosslinked for 10, 20, 30 and 60 seconds with 1 mg/mL HAase 156
Figure 6.8: Bacteriophage K concentration released from agarose hydrogels exposed to no and 10 sec UV after 4 hours 158
Figure 6.9: Bacteriophage titer after hyaluronidase degradation of bilayer 0.4% agarose / HAMA hydrogel 159
Figure 6.10: Bacteriophage titer after *S. aureus* C3 and hys- supernatant degradation of bilayer 0.4% agarose / HAMA hydrogel 160
Figure 6.11: Bacteriophage titer after hyaluronidase degradation of bilayer 0.7% agarose / HAMA hydrogel 161
Figure 6.12: Bacteriophage titer after *S. aureus* C3 and hys- supernatant degradation of bilayer 0.7% agarose / HAMA hydrogel 162
Figure 6.13: Bacteriophage titer after 4 hour incubation of bilayered 0.7% agarose / HAMA hydrogels with 8 HAase positive and 8 HAase negative strains 163
Figure 6.14: Bacteriophage titer after hyaluronidase degradation of bilayer 2% agarose / HAMA hydrogel 164

Figure 6.15: Bacteriophage titer after *S. aureus* C3 and hys- supernatant degradation of bilayer 2% agarose / HAMA hydrogel 165
Figure 6.16: Bacteriophage titer after 4 hour incubation of bilayered 2% agarose / HAMA hydrogels with 8 HAase positive and 8 HAase negative strains 166
Figure 6.17: 2% agarose/ HAMA bilayer hydrogels containing Bacteriophage K incubated with (left) S. aureus H560 and (right) *S. aureus* hys- live culture 167
Figure 7.1: Diagram of nano-imprint lithography using PDMS moulds to print photo-crosslinkable polymers. Diagram by Ping Li 172
Figure 7.2: Structure of the tetrazolium dye MTT and its subsequent reduction by mitochondrial reductase to the insoluble purple product Formazan.....174
Figure 7.3: a) Silicon wafer line patterned with photoresist b) Large silicon wafer with multiple photoresist patterns c) PDMS mould of patterned silicon wafer leads to a negative patterning d) Polystyrene print formed through hot embossing with PDMS mould.....175
Figure 7.4: Scanning Electron Microscopy (SEM) images of 10, 15 and 80 µm polystyrene prints formed by Hot Embossing. Scale bar = 50 µm. Images courtesy of Ping Li.....176
Figure 7.5: Light microscopy images of a) 10 µm, b) 15 µm, c) 50 µm and d) 80 µm line width prints formed on 2% HAMA/1%PEGDA/1%I2959 hydrogels. Scale bar = 100 µm 177
Figure 7.6: Light microscopy images of a) 50 µm and b) 80 µm line width prints formed on 2% HAMA/ 1%PEGDA/ 1%I2959 hydrogels after 24 hours swelling in PBS buffer. Scale bar = 100 µm 178
Figure 7.7: Light microscopy images of NIH-3T3 fibroblasts cultured on polystyrene cell culture flasks in DMEM medium after a) 2 hours, b) 24 hours and c) 48 hours growth. Scale bar = 100 µm 179
Figure 7.8: Light microscopy images of NIH-3T3 fibroblasts grown on unprinted 2% HAMA /1%I2959 hydrogels. Hydrogels contained a) 0% PEGDA, b) 1% PEGDA, c) 5% PEGDA and d) 10% PEGDA. Scale bar = 100 µm 180
Figure 7.9: Light microscopy images of NIH-3T3 fibroblasts grown on printed 2% HAMA/1% I2959/1% PEGDA hydrogels for 48h. Hydrogels were printed with a) 10 µm, b) 15 µm, c) 50 µm and d) 80 µm. Scale bar = 100 µm.....181
Figure 7.10: Swelling ratio values for varying 1% PEGDA/1% I2959 HAMA hydrogels containing 1 – 6% HAMA.....182
Figure 7.11: NIH-3T3 fibroblast growth on 80 µm hydrogel prints formed from varying HAMA concentrations – a) 2%, b) 3%, c) 4% d) 6% w/v HAMA/1% PEGDA/1% I2959. Scale bar = 100 µm 183
Figure 7.12: % live NIH-3T3 fibroblast cells after 24 hours incubation with 0, 0.03, 0.05 and 0.1% Irgacure 2959.....184
Figure 7.13: NIH-3T3 cell growth in (left) 0% gelatin and (right) 5% gelatin hydrogels after 48 hours. Scale bar = 100 µm 185
Figure 7.14: NIH-3T3 cell growth in 5% gelatin + 1% Irgacure 2959 after 48 hours. Scale bar = 100 µm.....186
Figure 7.15: NIH-3T3 cell growth in 80 µm printed 3% HAMA/ 10% gelatin hydrogels after 48 hours. Scale bar = 100 µm 186
Figure 7.16: NIH-3T3 cell growth in 80 µm printed 3% HAMA hydrogels containing a) 0%, b) 3%, c) 5% and d)10% gelatin and 0.1% Irgacure 2959 after 48 hours. Scale bar = 100 µm.....188
Figure 7.17: NIH-3T3 cell growth in non-printed (left) and 80 µm printed (right) 3% HAMA/ 10% gelatin hydrogels after 48 hours with prewashing. Scale bar = 100 µm 189
Figure 7.18: Reaction scheme for gelatin methacrylation with methacrylic anhydride.....190
Figure 7.19: ^{1}H NMR spectrum of gelatin methacrylate in D_2O.....190
Figure 7.20: Swelling ratio values for hydrogels containing 1 – 3% HA (a) or HAMA (b) and 0 – 10% GelMA. 191

Figure 7.21: NIH-3T3 fibroblast growth on 5% GelMA hydrogels containing 0.1% (left) and 1% (right) I2959. Scale bar = 100 µm. Images courtesy of Ping Li 192
Figure 7.22: NIH-3T3 cell growth on 3% HAMA 80 µm printed hydrogels after 48 hours with (left) 0% GelMA and (right) 10% GelMA. Scale bar = 100 µm 193
Figure 7.23: NIH-3T3 cell growth on 3% HAMA 80 µm printed hydrogels after 48 hours with (left) 0% GelMA and (right) 10% GelMA with prewashing. Scale bar = 100 µm 193
Figure 7.24: NIH-3T3 cell growth on crosslinked GelMA hydrogels containing no HA. No print with a) no PEGDA and b) 1% PEGDA. 80 µm line print with c) no PEGDA and d) 1% PEGDA. Scale bar = 100 µm 194
Figure 7.25: NIH-3T3 cell growth on crosslinked GelMA hydrogels containing 1% HA. No print with a) no PEGDA and b) 1% PEGDA. 80 µm line print with c) no PEGDA and d) 1% PEGDA. Scale bar = 100 µm 195
Figure 7.26: Weight loss of GelMA/HA hydrogels through degradation with 1 mg/mL hyaluronidase. (left) 5% GelMA and (right) 10% GelMA 196
Figure 7.27: Weight loss of GelMA/HAMA hydrogels through degradation with 1 mg/mL hyaluronidase. a) 1% HAMA, b) 2% HAMA and c) 3% HAMA 197

List of Tables

Table 1.1: Morphology and genetic properties of bacteriophage families 15
Table 1.2: Commercial products used for a range of therapies which contain HA as a major component 33
Table 2.1: *S. aureus* strains, origin and SCCmec type used in this investigation 48
Table 2.2: Non *S. aureus* strains used in this investigation 48
Table 2.3: Specifications of forward and reverse primers used from hysA amplification 49
Table 2.4: Constituents of HEPES buffer 53
Table 2.5: Constituents of CF50 HEPES buffer 53
Table 4.1: Sensitivity of *S. aureus* species to Bacteriophage K. Tests were carried out jointly by Jessica Bean and Diana Alves 91
Table 4.2: Sensitivity of other bacterial species to Bacteriophage K. Tests were carried out by Diana Alves 91
Table 4.3: D_{app} calculations for Bacteriophage K diffusion from 2%, 5% and 10% PVA hydrogels 103
Table 4.4: D_{app} calculations for Bacteriophage K diffusion from 0.2%, 0.7% and 2% agarose hydrogels 113
Table 5.1: Swelling ratio calculations for HA sheets crosslinked with EDC (1 – 100 mM), HCl (10 – 50 mM) and PEG diglycidyl ether (0 – 500 mM) 129

Acronyms and Abbreviations

ADH	Adipic dihydrazide
agr	Accessory Gene Regulator
AIBN	Azobisisobutyronitrile
AIP	Auto Inducing Peptide
ATRP	Atom-transfer radical-polymerization
au	Arbitrary units
BDDE	1,4 butanediol diglycidyl ether
CA-MRSA	Community acquired Methicillin Resistant S. aureus
CDC	Centres for Disease and Control
CF	5(6)-carboxyfluorescein
CF-NSE	(5)-carboxyfluorescein N-succinimidyl ester
cfu	Colony forming units
CHO	Cholesterol
CLSM	Confocal Laser Scanning Microscopy
CMC	Critical Micelle Concentration
CRISPR	Clustered regularly interspaced short palindromic repeats
D_{app}	Diffusion coefficient
DCC	N,N'-dicyclohexylcarbodiimide
DHPE	1,2-dihexadecanoyl-sn-glycero-3-phosphoethanolamine
DLS	Dynamic Light Scattering
DMA	Dynamic mechanical analysis
DMAB	p-dimethylaminobenzaldehyde
DMEM	Dulbecco's Modified Eagle Medium
DMP	Dess – Martin periodinane
DMSO	Dimethyl sulphoxide
DNA	Deoxyribonucleic Acid
dNTP	Deoxynucleotide
DPPC	1,2-dipalmitoyl-sn-glycero-3-phosphocholine
DPPE	1,2-dipalmitoyl-sn-glycero-3-phosphoethanolamine
ds	Double stranded
DVS	Divinyl sulphone
E. coli	*Escherichia coli*
EDC	1-Ethyl-3-(3-dimethylaminopropyl)carbodiimide
EDTA	Ethylene Diamine Tetraacetic Acid
EPS	Extracellular polymeric substance
FCS	Fetal Calf Serum
FDA	Food and Drug Administration
FITC	Fluorescein isothiocyanate
FTIR	Fourier Transform Infrared
GelMA	Gelatin methacrylate
GI	Gastrointestinal
GMA	Glycidyl methacrylate
GUV	Giant Unilamellar Vesicles

HA	Hyaluronic Acid
HAase	Hyaluronidase
HAMA	Hyaluronic Acid Methacrylate
HA-MRSA	Hospital acquired Methicillin Resistant S. aureus
HEPES	4-(2-hydroxyethyl)-1-piperazineethanesulfonic acid
I2959	Irgacure 2959
IPN	Interpenetrating Polymer Network
LB	Luria Bertani
LCST	Lower critical solution temperature
LUV	Large Unilamellar Vesicle
MDR	Multi-drug resistant
MDR-TB	Multi-drug resistant Tuberculosis
MMP	Matrix metalloproteinase
MRSA	Methicillin resistant Staphylococcus aureus
MTT	3-[4,5-dimethylthiazol-2-yl]-2,5 diphenyl tetrazolium bromide
M_w	Molecular weight
NAG	N-acetyl Glucosamine
NHS	N-hydroxysuccinimide
NMR	Nuclear Magnetic Resonance
OD_{600}	Optical density at 600 nm
oxi-HA	Oxidised hyaluronic acid
P. aeruginosa	*Pseudomonas aeruginosa*
PBS	Phosphate buffered saline
PCR	Polymerase chain reaction
PDMS	Polydimethylsiloxane
PEG	Poly (ethylene glycol)
PEGDA	Poly (ethylene glycol) diacrylate
PEGDE	Poly (ethylene glycol) diglycidyl ether
pfu	Plaque forming unit
pHEMA	Poly(2-hydroxyethyl methacrylate)
PhK	Bacteriophage K
PNIPAAm	Poly(N-isopropylacrylamide)
PVA	Poly (vinyl alcohol)
PVL	Panton – Valentine Leukocidin
PVP	Poly (vinyl pyrrolidone)
RAFT	Reversible addition−fragmentation chain-transfer polymerisation
RHAMM	Receptor for hyaluronan-mediated motility
RGD	Amino acid sequence = Arginine-Glycine-Aspartic acid
RNA	Ribonucleic acid
ROMP	Ring-opening metathesis polymerisation
S. aureus	*Staphylococcus aureus*
S. epidermidis	*Staphylococcus epidermidis*
SDS	Sodium dodecyl sulphate
SLS	Static Light Scattering
S. pneumoniae	*Streptococcus pneumoniae*
S. pyogenes	*Streptococcus pyogenes*

sar	*Staphylococcal* accessory regulator
SCCmec	*Staphylococcal* cassette chromosome *mec*
SEM	Scanning Electron Microscopy
ss	Single stranded
SSSS	*Staphylococcal* scalded skin syndrome
SSTI	Skin and Soft Tissue Infection
SUV	Small Unilamellar Vesicle
TBAB	Tetra butyl ammonium bromide
t-BC	*Tert*-butyl carbazate
TCDA	10,12-tricosodiynoic acid
TEA	Triethylamine
TEM	Transmission Electron Microscopy
T_m	Melting point
TNBS	2,4,6-trinitrobenzene sulfonic acid
TS	Tryptic Soy
TSS	Toxic Shock Syndrome
VRE	Vancomycin-resistant *Enterococcus*
WHO	World Health Organisation

Abstract

Hydrogels have been increasingly used in the treatment of skin and soft tissue wounds in recent years due to their superb water holding and cell-growth promoting properties. When impregnated with antibiotics, they can also treat or prevent bacterial infections. Due to the global increase in antibiotic resistance, antibiotics are now becoming less effective and bacteriophage (viruses able to kill bacteria) offer a new alternative. Triggered release mechanisms also slow resistance development, as bacteria are not continually exposed to sub-lethal levels of therapeutic. Here, *Staphylococcus aureus* (*S. aureus*) was focussed on as it is the most common pathogen present in skin and soft tissue infections. The main aim of this work was to form biocompatible hydrogel systems which were able to give passive or triggered release of bacteriophage particles by *S. aureus* virulence factors. Micropatterned hydrogels were also investigated to assess the response in eukaryotic systems.

This study found that Bacteriophage K was highly infective against *S. aureus*, with 94% strains (out of 86 strains) showing complete or intermediate sensitivity. Bacteriophage were immobilised into PVA and agarose hydrogel systems without a significant loss in concentration or efficacy. A photocrosslinkable polymer, HAMA (hyaluronic acid methacrylate) was also investigated which could be crosslinked in situ into a robust hydrogel; this hydrogel was sensitive to hyaluronidase (HAase), an enzyme secreted by the majority of *S. aureus* strains. On incubation with purified HAase and *S. aureus* supernatant, hydrogel degradation was recorded (Carbazole assay and SEM imaging) compared to buffer and HAase – negative *S. aureus* strains.

When combined into a bilayered hydrogel system, 2% agarose/HAMA hydrogels gave triggered release of bacteriophage by pure HAase and HAase positive bacterial supernatant. However, in live culture triggered killing was not possible. HAMA could also be successfully printed, and NIH-3T3 fibroblasts showed directed aggregation but no adhesion to HAMA hydrogels.

In general, hydrogel systems which gave triggered release of Bacteriophage K only in the presence of *S. aureus* HAase were successfully formed. However, the passive leakage of bacteriophage into the wider environment was seen in live culture. This could be remedied by direct coupling of the bacteriophage to the polymer network, and is a possible avenue for future work. This system was significant as it proved that *S. aureus* HAase can be used as a trigger for bacteriophage release from hydrogel systems. In eukaryotic cells, HAMA hydrogels did not promote cell growth, although some promise was seen in gelatin-based gels.

Chapter 1 : Introduction and Literature Review

Hydrogel dressings are now widely used in skin and soft tissue wound treatment due to their optimal properties. They provide a highly hydrated environment which promotes wound repair, allowing cell migration and proliferation, as well as drainage of the wound site. Hydrogels can also be incorporated with a variety of additional therapeutics (e.g. antibiotics, antimicrobial peptides or antimicrobial polymers) which can prevent infection. Topical wounds, such as burns, surgical sites or diabetic ulcers are frequently susceptible to infection due to the natural presence of bacteria on the skin and the surrounding environment; by far in the majority of cases, infections are due to *Staphylococcus aureus* or later *Pseudomonas aeruginosa*[1]. The use of antibiotics to treat these infections is being hindered by the recent upsurge in antibiotic resistance, where bacteria previously susceptible to an antibiotic become resistant.

Over the past few decades, research into tackling antibiotic resistance has focussed on the development of novel active synthetic antibiotics with different chemical structures. Until recently this has generally been sufficient, however increased globalisation has put pressure on this approach. Bacteriophage (naturally occurring viruses able to infect and kill bacteria) are a little used antimicrobial therapeutic which offer a promising alternative to antibiotics. Another way that the development of antibiotic resistance can be slowed is by preventing the prophylactic or passive application of antibiotics, and only using them when an infection is present. In a hospital setting, this can only be done if the infecting bacterial strain is known; determining what is present is notoriously slow and can result in patient mortality. A system which can detect and treat an infection in situ would aid infection treatment and patient care.

With this in mind, this research aimed to create hydrogel systems which were able to selectively release bacteriophage *only* when a bacterial infection was present. The approach offers a number of advantages. Firstly any infection would be quickly treated in situ, without the need of dressing removal or medical intervention. Also, the unnecessary or passive release of bacteriophage would be prevented, which in turn would slow any development of resistance. The burst release of a high concentration of bacteriophage, versus a sustained low concentration release is more likely to completely treat an infection. Here, *S. aureus* sensitive systems were investigated as the virulence of the organism is well understood and it is the most common Gram-positive bacterium present in wound infections.

1.1. Bacterial Infections

Bacteria are a large group of single celled, prokaryotic organisms which are found in all corners of the planet including soil and radioactive waste. There are thought to be approximately 5 x 10^{30} bacteria on earth[2]. Due to their innate simplicity, bacteria are extremely proficient at adapting to extreme conditions, and are able to undergo aerobic and anaerobic respiration (as well as switching between the two), and fermentation.

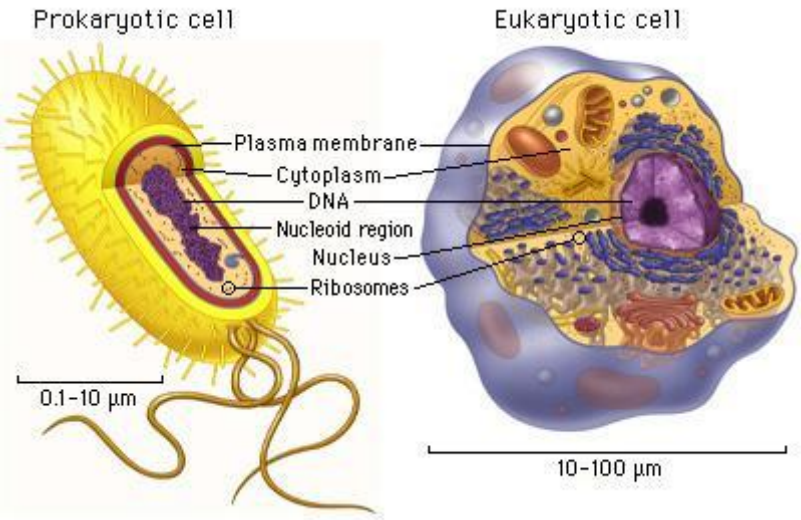

Bacteria range in size from 10^{-7} to 10^{-4} m and are found in a variety of shapes including spheres (cocci), rods (bacilli) and coiled (spirochetes). They are far simpler than eukaryotic cells (Figure 1.1) as they lack complex membrane-bound organelles such as the nucleus, mitochondria, endoplasmic reticulum and Golgi apparatus. Bacteria however can also have flagella, which aid cell movement, and pili, which are involved in bacterial conjugation and gene exchange, which are not present in eukaryotic cells. In eukaryotes mimic these through use of cilia.

The bacterial cell wall structure can be different depending on bacterial species, and is seen in Figure 1.2. Bacteria are either Gram-positive or negative, depending on the presence of an outer membrane layer, which gives additional protection and stability to the cell. Certain molecules on the bacterial surface such as lipopolysaccharides act as antigens to the body, which stimulate an immune response[3].

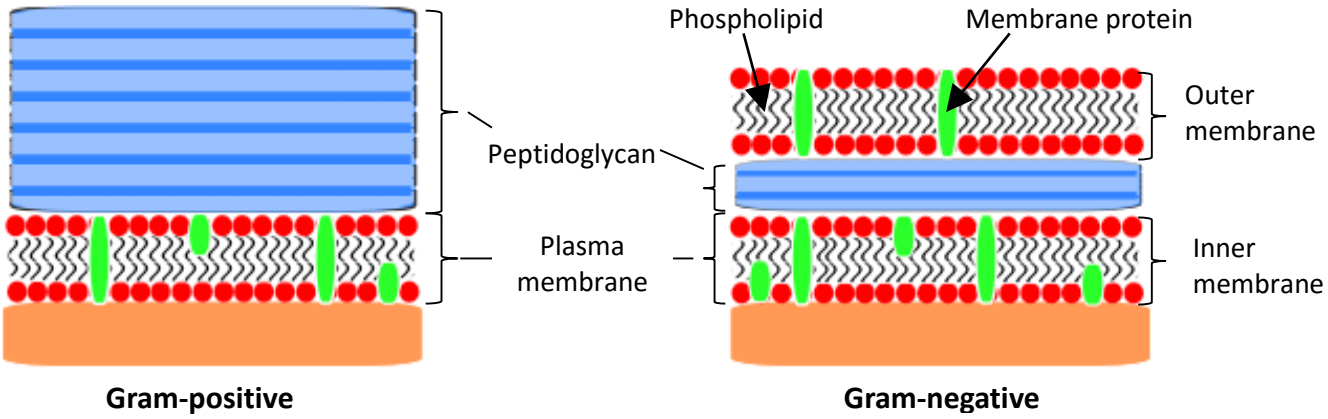

Bacteria replicate through a process known as binary fission – where each bacterium divides into two separate daughter cells. Bacterial growth can be modelled in four phases, shown in Figure 1.3: the lag phase, log phase, stationary phase and death phase. The lag phase (A) involves the initial adaption of bacteria to the new growth conditions; bacteria do not divide, but synthesise the new RNA, enzymes, etc. required for growth in the new environment. Once bacteria are able to efficiently replicate, growth moves into the exponential phase (B). With an excess of nutrients, bacteria divide every few minutes at a constant exponential rate (e.g. the doubling time of *E. coli* in optimum conditions is every 20 minutes).

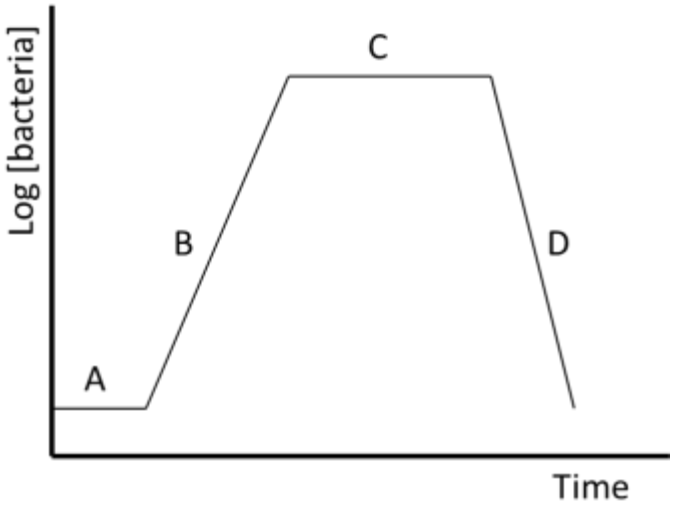

During the stationary stage (C) the rate of growth slows due to nutrient loss and the accumulation of toxic by-products. Eventually the rate of death is higher than the rate of growth and growth enters the death phase (D); all nutrients have been used up and the bacteria die.

Bacteria are notorious opportunistic pathogens. They take advantage of a compromised host and go on to infect causing tissue damage, disease and significant morbidity and mortality. Infection frequently occurs more in immunocompromised or immunosuppressed patients where the body's natural defences have been lowered. These include those with skin wounds (e.g. burns, diabetic ulcers and surgical site wounds), cancer or HIV/AIDS, as well as the very young, elderly, or pregnant women.

1.1.1. Clinical problem

One of the most significant scientific breakthroughs of the 20th century has been the discovery and development of antibiotics against bacterial infections. Before antibiotics, bacterial infections were the leading cause of human morbidity and mortality for the majority of human existence. Perhaps the most devastating example of these occurred in the 14th century, where the Black Death (a bubonic plague caused by the bacterium *Yersinia pestis*) killed between 30 – 60% of the entire population of Europe[4]. Later, diseases such as tuberculosis, Scarlet Fever, meningitis and pneumonia, as well as sexually transmitted diseases, were frequently common and fatal[5]. Surgery and childbirth were all both highly dangerous due to subsequent bacterial infection.

The discovery of the penicillins and sulphonamides in the 1940s revolutionised medicine. The work of Fleming, Florey and Chain on penicillin, and Ernst on the sulphonamides began a period of unprecedented research into new effective antibiotics which treated large swathes of previously deadly diseases. As a result, mortality rate significantly decreased. The organ transplants and chemotherapy that is so essential for medicine today would not be possible without antibiotics.

In recent years however, the chronic use of antibiotics has led to the emergence of bacteria resistant to a range of antibiotic drugs, as well as providing optimal environments for the selection and spread of resistance[6]. For example, the treatment of acute respiratory infections with antibiotics is a common procedure, even though the cause is in most cases viral[7, 8]. In healthcare, the over or unnecessary prescription of antibiotics by physicians, as well as incorrect self-dosing by patients (either through lack of information or negligence) drives this

development. In developing countries, antibiotic resistance is exacerbated by the unregulated sale of antibiotics over the counter.

Antibiotics are additionally used in huge quantities in agriculture as a prophylactic and as a growth promoter, creating a 'reservoir' where resistance can evolve. Although in 2006, the EU banned the use of all antibiotics as growth promoters, the practise is still widespread in the US and other countries[9]. Antibiotics in agriculture are also able to seep into the surrounding soil and watercourses, facilitating the transfer of resistance to the wider microbial population.

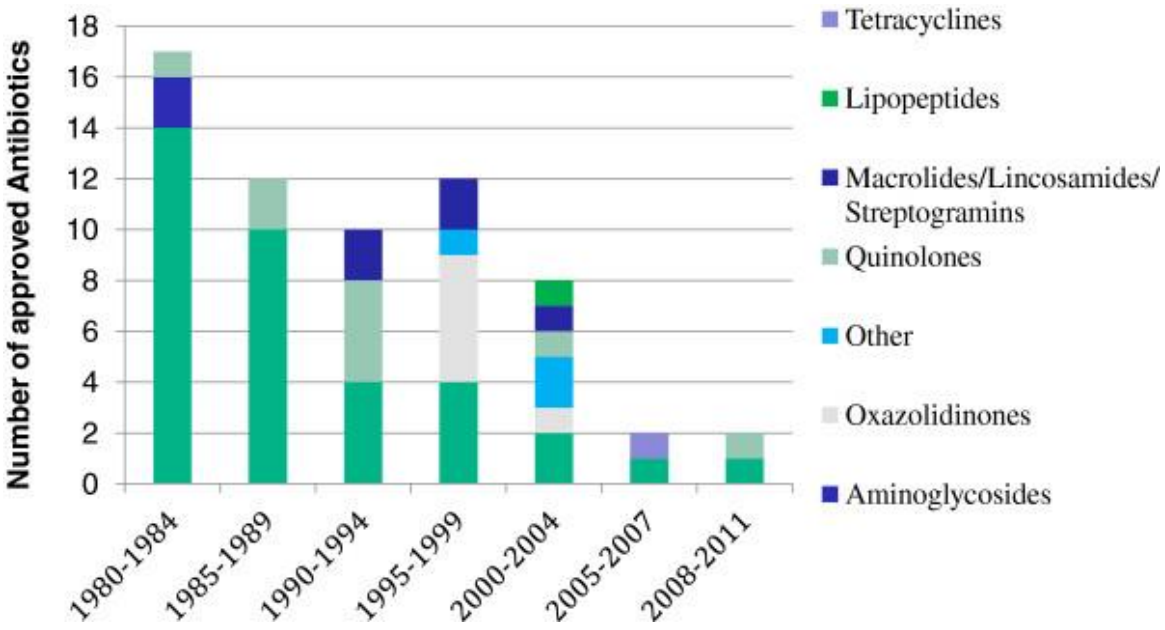

The situation is worsened by the lack of new antibiotics coming onto the market. The comparative 'boom' of the second half of the 20th century has been surpassed with fewer and fewer antibiotics now being approved; only two between 2008 and 2011 (Figure 1.4)[10]. This drastically limits the choice of drugs clinicians have available for infection treatment. In 2015, Teicoplanin was documented as possibly the first new class of antibiotics in a decade; the drug has efficacy against *S. aureus* and *Mycobacterium tuberculosis* in mice, but is yet to go into human trials[11]. In that case, the way in which the drug was discovered is more significant than the drug itself.

Antibiotics are not commercially viable for large pharmaceutical companies to research compared to chronic and lifestyle-associated diseases where drugs are taken long-term. It is estimated that to bring a novel antibiotic to market takes 10 years and between $800 million

and $1.7 billion, all without the guarantee of approval at the end[12]. There have been efforts to tackle this "market failure"; agencies such as the EU are funding incentives such as the 'Innovative Medicines Initiative' which works to promote and speed up the development of new medicines.

The critical rise in antibiotic resistance and fall in antibiotic discovery is a severe public health concern. In 2009, the World Health Organisation (WHO) announced that antibiotic resistance was one of the three greatest threats to health[13]. In 2011 the UK Government's chief scientific officer, Professor Dame Sally Davies, described that antibiotic resistance posed a "catastrophic threat". The post-antibiotic era described by the WHO in 2014 is a stark reminder of the very real possibility of a world where antibiotics are ineffectual[14]. Without antibiotics common infections and minor injuries could kill; routine operations, cancer therapy or transplants would not occur.

1.1.2. Wounds and wound infections

In recent years, the bacteria named by the Infectious Diseases Society of America as 'ESKAPE' pathogens have been targeted as the main cause of hospital-acquired infections. Linked by their ability to 'escape' treatment by antibiotics, ESKAPE pathogens comprise *Enterococcus faecium*, *Staphylococcus aureus*, *Klebsiella pneumoniae*, *Acinetobacter baumannii*, *Pseudomonas aeruginosa* and *Enterobacter* species; there is also a case for including the gut bacterium *Clostridium difficile* in the group[15-17]. All of these pathogens, as well as causing the majority of infections in healthcare settings, represent paradigms of pathogenesis, transmission, and resistance that if understood can be applied to all other infections.

Skin and soft tissue wounds are particularly vulnerable to opportunistic infections, which cause considerable damage as they metabolise and proliferate. The most common bacteria associated with skin and soft tissue infections are the normal host flora: *S. aureus* and *Streptococcus pyogenes*[1]. In 2009, skin and soft tissue infections (SSTIs) were responsible for 51% of all hospitalisations attributed to *S. aureus* in the US, with each case costing $11,622 to treat[18]. Gram-negative organisms such as *P. aeruginosa, Escherichia coli* and *Acinetobacter* are not normally found on the skin, but can be acquired from the environment and go on to cause infection at later stages[19].

Bacterial infections of skin and soft tissue (cellulitis), wounds, surgical sites and burns cause damage to the surrounding tissue including redness, pain, pus and tissue destruction and necrosis as bacteria grow and proliferate[20]. The severity of further infection is determined by the

extent and depth of the wound, as well as the number of colonising bacteria. The release of a range of virulence factors by bacteria facilitates adhesion, immune system evasion, leukocyte killing and tissue destruction[21].

1.1.3. Biofilms

The majority of microorganisms in the environment do not exist as planktonic, floating, single cells; most form complex communities which irreversibly adhere to surfaces called biofilms. Biofilms can contain either single or multiple strains or species of bacteria. Bacteria in biofilms are surrounded by a self-produced extracellular polymeric substance (EPS) which comprises genetic material, proteins and polysaccharides.

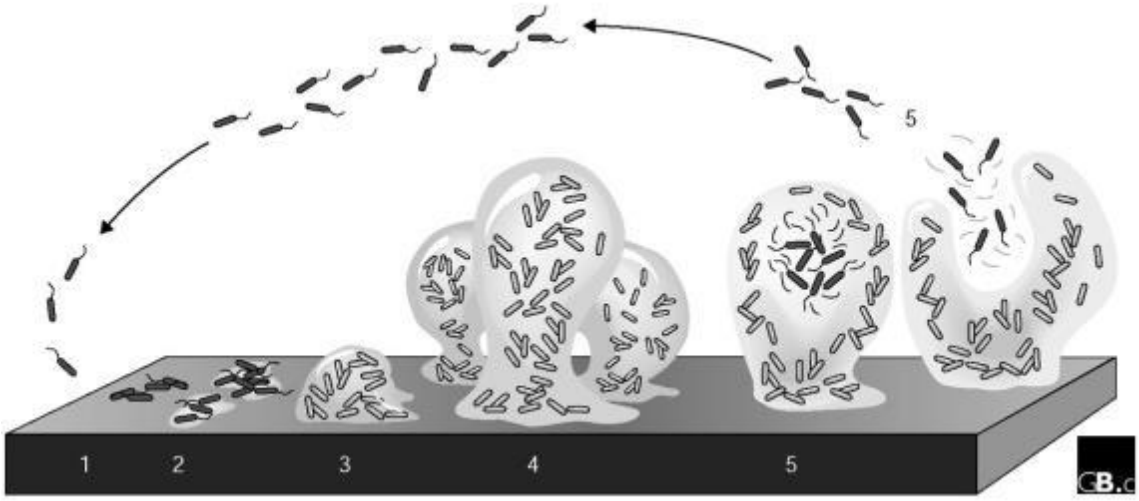

Figure 1.5: Stages of biofilm development. Reproduced with permission from Sauer et al

The structure and development of biofilms on surfaces has been well characterised, and can be described in five distinct stages as described in Figure 1.5[22-24]: (1) Reversible attachment - bacterial cells reversibly attach to a surface using a variety of sensing mechanisms, e.g. flagella, pili and outer membrane proteins. (2) Irreversible attachment - bacteria irreversibly bind to the surface and secrete EPS to adhere. (3) Growth and replication – adsorbed cells grow and multiply forming microcolonies which become encapsulated by EPS. (4) Maturation – a three-dimensional structure develops with an established microbial community 'glued' in EPS. (5) Detachment – some cells detach and disperse into the bulk fluid, going on to form new biofilms.

Biofilms frequently form on surfaces within the body where they cause persistent and chronic infections on catheters, shunts, implants and prostheses, as well as burn wounds[25, 26]. For example, indwelling catheters are the most common cause of healthcare associated bloodstream infections, with 200,000 infection cases a year associated with their use[27-29]. A

number of Gram-positive and Gram-negative organisms have been isolated from these environments including ESKAPE pathogens and *Proteus mirabilis*.

Biofilms are inherently more tolerant to the immune response, antibiotics, biocides and hydrodynamic shear forces compared to planktonic bacteria due to the impermeable EPS[30]. This makes these established infections particularly hard to treat. Bacteria growing in a biofilm also exhibit a phenotypic 'switch' when in a biofilm where the growth rate and regulation of many genes is altered, including phenotypes for antimicrobial resistance, which similarly hinders treatment[31, 32].

1.1.4. *Staphylococcus aureus*

Staphylococcus aureus (*S. aureus*) is a Gram-positive, coagulase positive, facultative anaerobic coccus which appears as yellow, grape-like clusters; the name is derived from the Greek '*staphylē kókkos'* meaning 'bunch of grapes', and the Latin '*aureus*' meaning 'gold' (Figure 1.6). *S. aureus* is found naturally on the mucous membranes of the upper respiratory tract and skin microbiota. It is thought that approximately 20% of the population are persistent and 60% are intermittent carriers[33]. *S. aureus* can cause both community and hospital acquired infections, resulting in $14.5 billion in healthcare costs in the US annually[34].

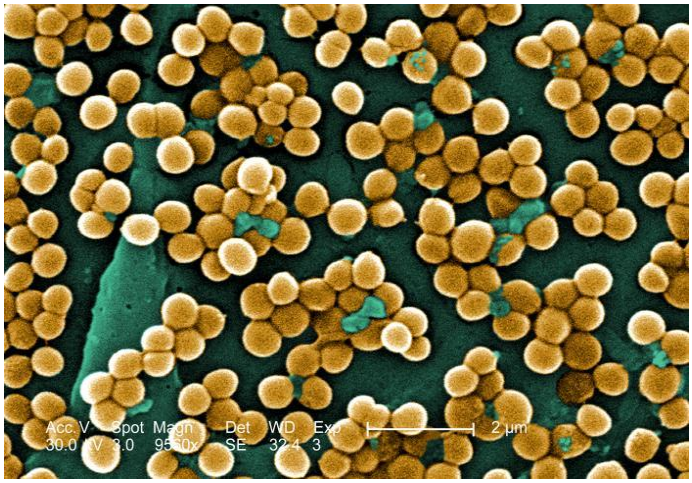

S. aureus is a leading cause of morbidity and mortality worldwide, and is responsible for a range of varying severity diseases[35]. It usually causes minor infections of the skin and soft tissues, resulting in pimples, furuncles, boils and impetigo[36]. However, if able to systemically invade, it can cause serious deep-seated infections such as pneumonia, osteomyelitis, meningitis, endocarditis and bacteremia which can be fatal. Gram-positive species are frequently associated

with burn and soft tissue infections. *S. aureus* is also notorious for its toxicity; secreted exotoxins are capable of initiating systemic shock and organ failure such as that seen in Toxic Shock Syndrome (TSS) and *Staphylococcal* Scalded-skin Syndrome (SSSS) [37, 38].

1.1.4.1. Virulence Factors

S. aureus secretes a wide range of toxins (exotoxins) into its surrounding environment which are thought to be used by the bacterium to invade and break down tissue into usable nutrients. These include cytotoxins, superantigens (Enterotoxins A, B, C and D, exfoliatin and TSS toxin) and enzymes (coagulase, proteases, lipases, nucleases, hyaluronidase and collagenase) [39, 40]. These molecules are highly potent and stimulate a strong immune response when detected.

Cytotoxins are small protein molecules - α, β, γ, and δ-haemolysin, Panton-Valentine leukocidin (PVL), and Phenol-soluble modulins - which cause the lysis of eukaryotic cells to aid bacterial invasion. Protein units exist as soluble monomers which assemble to form β-folded 'barrels'. The protein barrels associate with the cell membrane and form a pore – this facilitates the free movement of water and ions through the cell membrane, eventually causing cell lysis. PVL is a cytotoxin known to lyse human leukocytes (white blood cells); it is associated with increased virulence in *S. aureus* and is common in the majority of community-acquired MRSA isolates[41, 42].

Collagenase and hyaluronidase, HAase, are both secreted to break down the main polymers (collagen and hyaluronic acid) which make up connective tissues and skin. For the purposes of this report, the function and mechanism of hyaluronidase excretion in *S. aureus* will be discussed in detail in Section 1.4.4.4. Coagulase is an interesting enzyme in that it converts the glycoprotein fibrinogen to fibrin – with *S. aureus* the fibrin covers the bacterium, and on contact with blood forms a clot which is thought to protect the microbe from phagocytosis.

1.1.4.2. Regulation of *S. aureus* virulence factors

The accessory gene regulator (*agr*) and the *staphylococcal* accessory regulator (*sar*) are the main regulatory mechanisms that control the production of *S. aureus* virulence factors (Figure 1.7)[43]. *S. aureus* relies on a mechanism called quorum sensing to detect changes in the outside environment, which is dependent on population density.

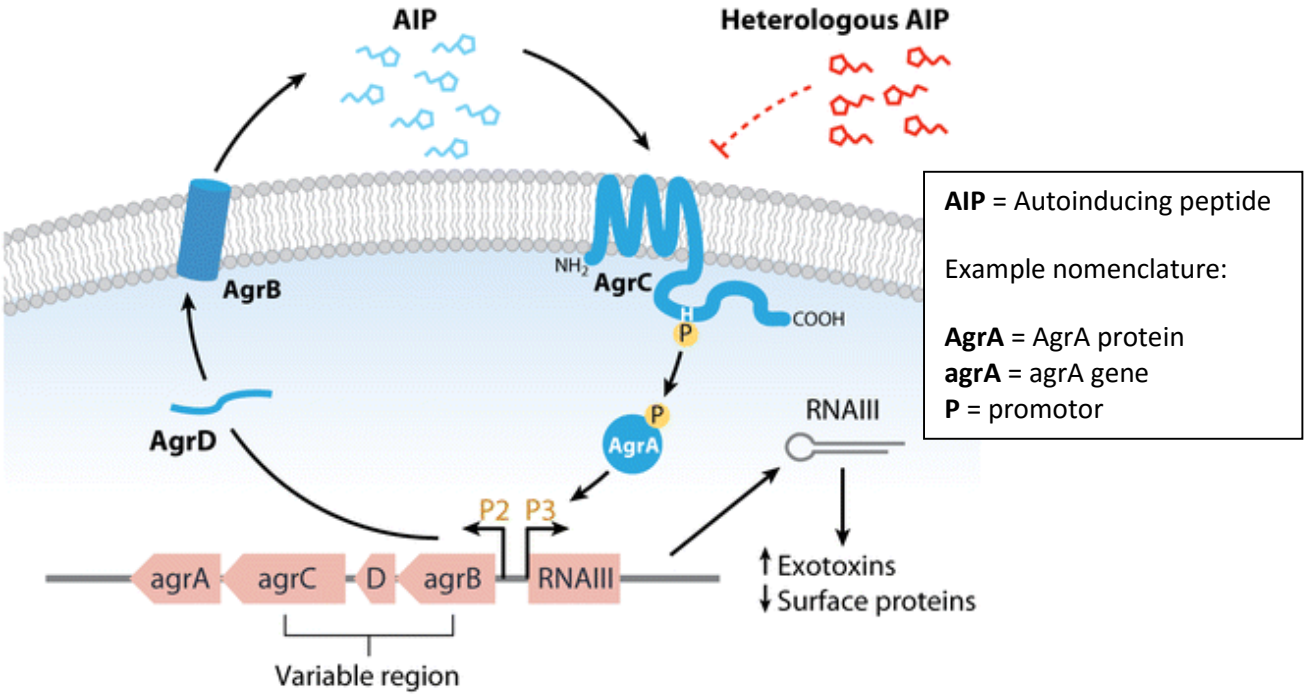

As bacteria grow, they secrete small molecules called auto-inducing peptides (AIPs); as the population gets larger, so then does the concentration of AIPs. Over a threshold concentration, AIPs bind to a membrane associated histidine kinase, AgrC, on the bacterial surface. This then initiates the phosphorylation of an internal protein, AgrA inside the bacterium. Phosphorylated AgrA then activates is own promoter P2 on the gene, but also the promoter P3, which drives the transcription of RNAIII. RNAIII modulates the expression of virulence factors; an upregulation of RNAIII results in increased exotoxin production and virulence, and a decrease in surface proteins[43].

In *S. aureus*, *sar* has also been found to play an important part in virulence factor regulation. The *sar* locus encodes for the SarA protein, which binds to bacterial DNA and modulates gene expression[44].

In *S. aureus*, hyaluronidase is expressed by the gene *hysA*. Until very recently, little has been known about the regulation of this enzyme; the full sequencing of *hysA* in 1995 has now led to a more comprehensive outlook. Hyaluronidase expression is thought to be activated by the regulator *agr* and repressed by *sar* in a similar way to other *S. aureus* virulence factors[45, 46]. When the *agr* system is activated, HAase levels increase until *agr* is deactivated. This is the same system as described earlier, making HAase expression to a certain extent RNAIII dependent.

Recent work by Ibbensen et al has found that by creating mutations in the global regulator CodY, they were able to show that not only does CodY directly influence both the *agr* system and the *hysA* gene, but also could play a part in the link between virulence and nutrient availability[47].

1.1.5. Antibiotic resistance

Antibiotic resistance occurs when bacterial DNA either mutates or acquires other genetic material through horizontal gene transfer, which enables bacteria to become resistant to one or a class of antibiotics. Bacteria acquire these genes from integrons (transferable genetic elements), plasmids or bacteriophage. The emergence of a number of clinically acute antibiotic resistant strains, including methicillin-resistant *S. aureus* (MRSA), vancomycin-resistant *Enterococcus* (VRE) and multidrug-resistant tuberculosis (MDR-TB), is now widespread. The WHO estimates that antibiotic resistant infections cost the EU approximately €1.5 billion and the US $30 billion a year[48].

The acquisition and interchanging of genetic material is a natural phenomenon commonly seen in bacteria. This is due to the speed at which bacteria replicate and the ease at which they can exchange genetic material. The overuse of antibiotics gives an added selection pressure which drives for resistant strains[49]. The most common mechanisms that bacteria become resistant to antibiotics include: alteration of the target site, alteration to target site access (e.g. efflux pumps or decreasing cell wall permeability) and production of enzymes which modify or destroy the antibiotic[50].

One way of slowing the emergence of antibiotic resistant strains is to only use antibiotics when an infection is present. When antibiotics are present in low concentrations in the environment, a reservoir is formed where there is a selection pressure on any bacteria present to become resistant. In this way, a triggered high dose of antibiotics will be more successful in killing all bacteria and preventing resistance from evolving than a low constant dose[51].

1.1.5.1. Methicillin resistant *S. aureus*, MRSA

The emergence of MRSA was reported in 1961, a year after the introduction of the β-lactam antibiotic methicillin. MRSA now encompasses any strain of *S. aureus* which is resistant to β-lactam antibiotics such as penicillins, cephalosporins and carbapenems. Over recent years the prevalence of MRSA in *S. aureus* infections has escalated dramatically – MRSA is currently the most common antibiotic resistant pathogen in US hospitals[52]. In 2008 MRSA was responsible for more deaths in the US than HIV/AIDS and tuberculosis combined[53].

Although the number of cases has been decreasing since its peak in 2008, the US Centres for Disease and Control (CDC) reported over 80,000 cases of MRSA infection in 2011[54]. Originally, MRSA was confined to the hospital environment, termed hospital-associated MRSA (HA-MRSA), where the high usage of antibiotics in the environment drove resistance. Now however, certain MRSA strains have appeared in the wider community only, going on to infect young healthy patients (community-associated MRSA, CA-MRSA). The higher morbidity and mortality associated with CA-MRSA, as well as its increased genetic diversity, virulence and ability to resist broader classes of antibiotics make CA-MRSA a serious concern[55].

S. aureus resistance to methicillin occurs due to the production of an altered penicillin binding protein known as PBP2a, which has a decreased affinity to β-lactam antibiotics. PBP2a is encoded by the *mecA* gene, which is found on a mobile genetic island known as the *Staphylococcal* cassette chromosome *mec*, SCC*mec*. The SCC*mec* element also contains additional regulatory genes, and sequences to aid integration and excision into host DNA. At least five different SCCmec types have been described. Types I - III are associated with HA-MRSA; type IV and V are most common in CA-MRSA with the SCCmec generally smaller in size to aid horizontal gene transfer[56-58].

1.1.5.2. Alternatives to antibiotics

A number of alternatives to antibiotics are being investigated, and are becoming more promising in the light of the emergence of antibiotic resistance. Firstly, various methods can be implemented to prevent antibiotic infection in the first place, with vaccination being the primary choice. Vaccines of attenuated bacteria have been used for decades to impart immunity against disease causing bacteria. The Bacillus Calmette–Guérin (BCG) vaccine for example, uses attenuated *Mycobacterium bovis* to protect against tuberculosis. Investigations into vaccines against more clinically relevant species such as *C. difficile*, *S. pneumoniae*, *E. coli*, *Salmonella* and *Listeria monocytogenes* have all been reported[59].

In the event of an infection becoming established, there are also many alternatives that have been overshadowed by antibiotics since their discovery. Bacteriophage and bacteriophage lysins are in many ways the most promising alternative. These are natural predators of bacteria, and are discussed in detail in Section 1.2. Although it is unlikely that antibiotics will ever be completely replaced, these alternatives offer a new method of treating resistant infections either in conjunction or singly.

1.2. Bacteriophage

Bacteriophage, or phage, viruses are the most common biological entity on the planet with an estimated population of 10^{31}, outnumbering bacteria by a factor of ten[60]. They are the natural viral predators of bacteria, and are responsible for the removal of half the world's bacterial population every 48 hours[61]. Bacteriophage are ubiquitous, with phage most commonly found in areas containing high bacterial populations such as soil, river water and sewage. In humans, they are found naturally in the mucosal membranes and GI tract living symbiotically with commensal bacteria[62]. They are able to infect bacteria (but crucially no other cells) through their cell wall and cause the bacterium to lyse and die (Figure 1.8). Phages can have a very narrow host range due to their very specific bacterial binding sites. They are also a common element in horizontal gene transfer between bacteria, facilitating bacterial genetic diversity[63].

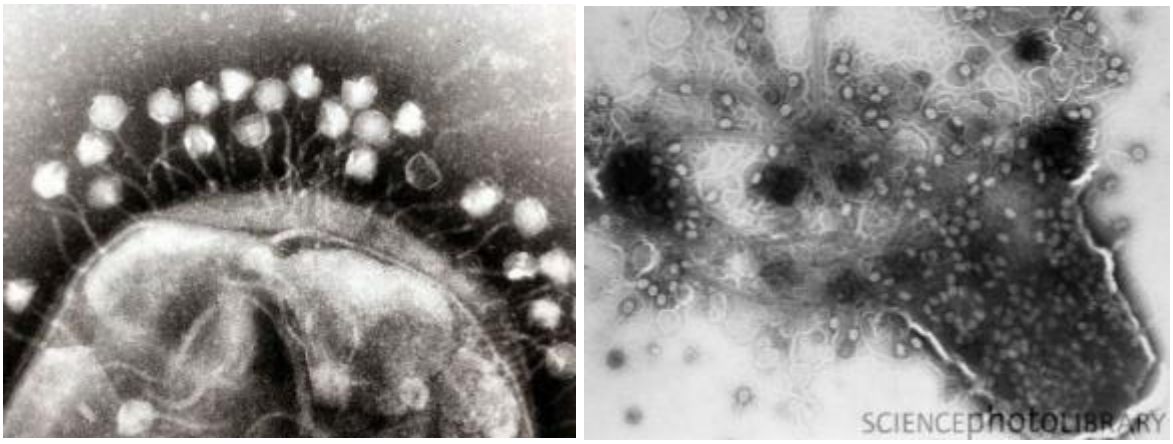

1.2.1. Discovery and historical use

Bacteriophage were discovered independently a century ago by Twort and d'Hérelle in 1915 and 1917 respectively[64]. D'Hérelle was the first to propose the name 'bacteriophage' for the viruses after *bacteria* and *phagein* (from the Greek: φαγεῖν, to devour). Although not investigated further by Twort due to the outbreak of WW1, research into bacteriophage and their possibilities was continued by d'Hérelle[64]. In 1923, d'Hérelle, along with microbiologist George Eliava, founded the Eliava institute in Tbilisi, Georgia, which to this day is a centre for bacteriophage therapy and research.

At the time companies initially seized on bacteriophage as a new therapy against infectious diseases. The 'Société Française de Teintures Inoffensives pour Cheveux', a forerunner to

L'Oréal, released a range of phage preparations for infectious diseases (e.g. Bacté-coli-phage, Bacté-pyo-phage and Bacté-staphy-phage)[65]. In the US, large pharmaceutical companies such as Eli Lily also developed phage products[66].

The age of antibiotics, beginning with the development of sulfa drugs in the 1930s and penicillin in the 1940s bought about a sharp decline in the research and use of bacteriophage for infection treatment. In the West, bacteriophage were superseded by the apparent glut of easily manufactured, broad spectrum antibiotics which were reliable and could be mass produced. However, phage therapy remained prevalent in Eastern European counties, notably the ex-Soviet countries of Russia, Poland and Georgia. Now, in an era where bacterial resistance to antibiotics is sadly all too common, bacteriophage therapy has undergone a renaissance as a possible alternative.

1.2.2. Classification and morphology

Due to the sheer number and diversity of bacteriophage in our ecosystem, phage can be classified in a number of different ways through their morphology, type of genetic material (DNA or RNA), their host organism or their life cycle. The current standard method of phage classification was set out in 1971 by the International Committee on the Taxonomy of Viruses after a seminal report by Bradley[67, 68]. A brief description of the 10 main bacteriophage classes can be seen in Table 1.1, adapted from Ackerman et al[68].

The vast majority of bacteriophage (approximately 96%) fall into the order Caudovirales, which comprise the familes *Myoviridae*, *Sipoviridae* and *Podoviridae*. These bacteriophage all contain double stranded DNA encapsulated in an icosahedral capsid head, and either a contractile, long non-contractile or short tail respectively. Bacteriophage tails frequently contain tail fibres which are essential for adsorption onto host bacteria; it is these fibres that impart the narrow host-range of infection seen in phage.

	Family	Nucleic acid, properties and size	Example
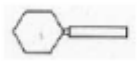	*Myoviridae*	dsDNA, contractile tail	T2, P2, T4
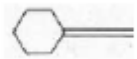	*Siphoviridae*	dsDNA, long non-contractile tail	λ
	*Podoviridae*	dsDNA, short tail	T7, P22
	*Microviridae*	ssDNA 27 nm, 12 knoblike capsomers	ΦX174
	*Corticoviridae*	dsDNA 63 nm complex lipidic capsid	PM2
	*Tectiviridae*	dsDNA inner lipid vesicle	PRD1
	*Leviviridae*	ssRNA 23 nm polio virus-like	MS2
	*Cystoviridae*	dsRNA, segmented, lipidic envelope 70-80 nm	Φ6
	*Inoviridae*	ssDNA, filaments or rods	M13, fd
	*Plasmaviridae*	dsDNA, lipidic envelope, no capsid	MVL2

Table 1.1: Morphology and genetic properties of bacteriophage families, adapted from Ackerman et al

1.2.3. Bacteriophage life cycle

The life cycle of bacteriophage and how they infect host bacteria has been well characterised. As mentioned above, bacteriophage tail fibres are involved in the initial viral adsorption onto the bacterial surface. In general, in Gram-positive bacteria phage tail fibres are able to bind to specific receptors made from the peptidoglycan and teichoic acids in the cell wall. In Gram-negative bacteria, other receptors are involved which are part of the outer membrane; protein (such as OmpA, C and F, and Lam) and lipopolysaccharide receptors are the most common in these bacteria.

After initial adsorption to surface receptors, the bacteriophage tail binds irreversibly to the bacterial cell wall. Generally, the tail then contracts; this drives its central tail tube through the bacterial outer membrane in a similar fashion to a hypodermic needle. Phage DNA is then injected into the cytoplasm of the host bacterium and further replication can commence[69].

Once inside the bacterial cytoplasm, phage can undergo two different replication cycles depending on the phage type and external factors. These are known as the lytic cycle (seen in

virulent bacteriophage) and the lysogenic cycle (seen in temperate bacteriophage). These are described in further detail below (Figure 1.9[70, 71]).

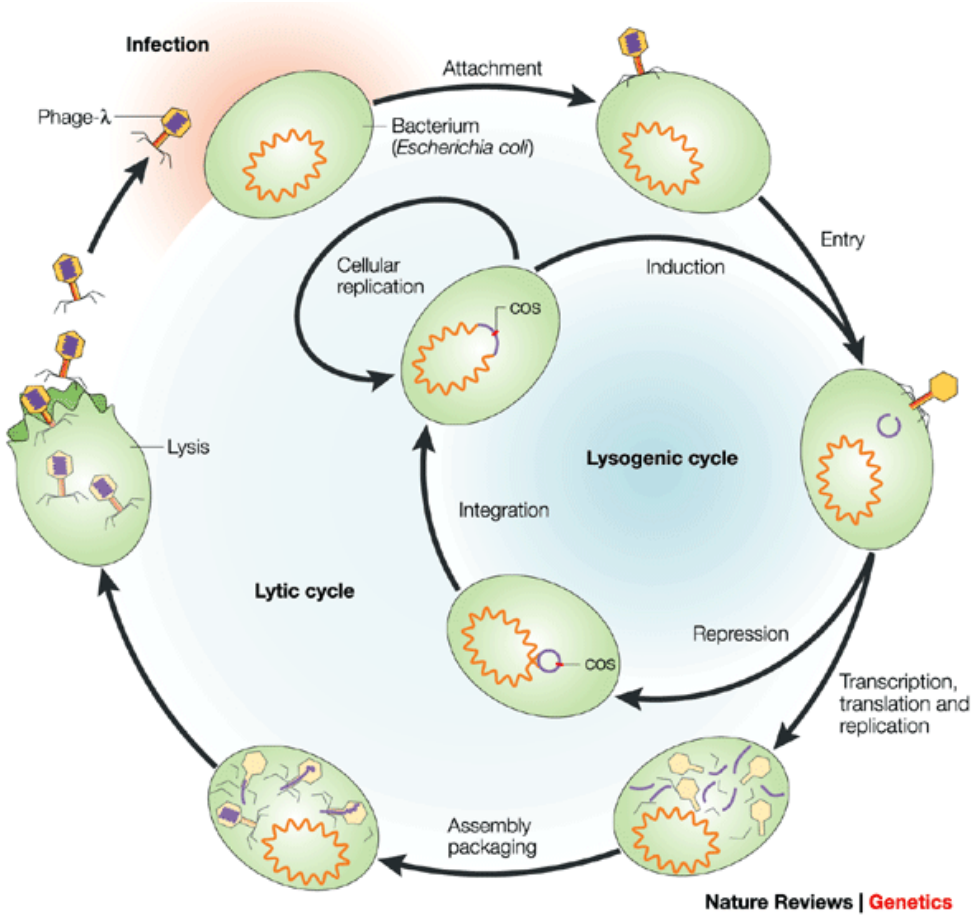

1.2.3.1 The Lytic Cycle

The lytic cycle is undergone by the majority of bacteriophage as their standard replicative mechanism. Once the bacteriophage DNA has reached the cytoplasm, it integrates into host DNA and immediately expresses proteins which inhibit bacterial defence mechanisms (e.g. DNA restriction enzymes and proteases). The genes then take over bacterial metabolism and initiate the production of new phage virions. The head, tail and tail fibres are constructed separately and then assembled at the last moments. Proteins are then expressed which break down the bacterial cell wall to enable phage release. These are known as holins and lysins, and are discussed in further detail in Section 1.2.8. The released bacteriophage then go on to infect new host bacteria, leaving the destroyed original cell; the cycle is repeated until no host bacteria are left.

1.2.3.2 The Lysogenic Cycle

The lysogenic cycle is the second, less common replicative pathway undergone by bacteriophage. Lysogeny is characterised by two main factors which differ from the lytic cycle[72]. Firstly, after the incorporation of phage DNA (now called the "prophage") into the host genome, this DNA is replicated as normal through bacterial binary fission and passed down to every daughter cell. Secondly, lysogenic phage infection is not infective; it does not produce phage virions.

In bacteria infected with lysogenic phage, the prophage can exist either in the host genome or as a plasmid. The prophage remains integrated and passed down in the bacterial chromosome until a process known as induction. During induction, an environmental or genetic trigger initiates the excision of prophage from the bacterial DNA; this then induces the phage to go into the lytic cycle and new whole bacteriophage are made. All bacteriophage undergo the lytic cycle at some stage, however some go through lysogeny beforehand.

1.2.4. Advantages of bacteriophage therapy

The specific advantages of bacteriophage as antimicrobials have been collated in a recent review by Loc-Carillo et al[73]. Firstly, compared to antibiotics the side effects sustained through phage therapy are minimal. Whereas multiple side effects have been reported with antibiotics (intestinal disorders, allergies and secondary infections), because bacteriophage are comprised of only nucleic acids and proteins, they are inherently non-toxic. Although phage could interact with the body and cause an immune response, with the use of highly pure phage preparations in medical studies this is not a significant concern.

Secondly, on infection with lytic bacteriophage, bacteria are lysed completely, eliminating the chance of bacterial regrowth. In the case of bacteriostatic antibiotics such as macrolides and tetracyclines, this is not the case. Also, bacteriophage are able to infect regardless of antibiotic susceptibility as they use completely different mechanisms action; this gives them a high activity against MDR strains such as MRSA [74, 75].

On application, bacteriophage congregate at the site of infection. The phage will continue to replicate and infect the host organism until that organism is removed. This is known as "auto-dosing"; a small amount of phage solution increases in concentration in response to the host concentration. This not only means that a low initial dose is needed, but the phage are concentrated at the site of infection. With antibiotics, concentration does not change in

response to the number of bacteria; antibiotic is distributed throughout the body and eventually metabolised and excreted regardless of the state of infection.

The narrow host range of bacteriophage reduces the chances of resistance occurring across a whole bacterial species. Any mutations that a bacterium develops to resist a specific phage are only suitable for that phage/bacterium interaction. This also allows the preservation of normal gut flora, giving none of the gastrointestinal problems associated with antibiotics. Some broad spectrum antibiotics are able to cause secondary infections such as *Clostridium difficile* colitis due to this disruption[76].

In the event of resistance developing against bacteriophage, finding new infective phages is quick, straight-forward and relatively cheap, taking days to weeks. Bacteriophage also exhibit versatility in terms of application, being active in liquids, emulsions, creams and on solids[77-80]. In general, although never a complete replacement to antibiotics, bacteriophage offer an additional treatment with certain favourable characteristics.

1.2.5. Disadvantages of bacteriophage therapy

There remain certain limitations in the use of whole bacteriophage as a therapeutic. Firstly, any bacteriophage which will eventually be used as a therapeutic must be lytic. As temperate phage are able to insert their DNA into the host genome, this alters host DNA and carries the risk of horizontal transfer of virulent or cell cytochemistry changing genetic elements. For example, the gene responsible for methicillin resistance in strains of MRSA, *mecA*, is thought to have originally come from a lysogenic phage[81, 82]. This problem can be remedied by gene sequencing of the whole phage genome to rule out lysogenic components.

It is also possible for bacteria to develop resistance to bacteriophage themselves through alteration or removal of the surface receptors necessary for phage binding[83], abortive infection or production of intracellular enzymes (whereby on phage infection the enzymes cleave the structures needed for phage assembly, e.g. DNA or capsid proteins) [84, 85]. In 2007, Barrangou et al also reported that CRISPR (Clustered Regularly Interspaced Short Palindromic Repeats) in the bacterial genome were able to transfer resistance against bacteriophage to other organisms[86]. Despite this, it is important to note that bacteriophage can then evolve in retaliation against these changes to continue infecting.

The specificity of a bacteriophage can be a disadvantage in a clinical setting. The narrow host range of phage means that the exact strain of bacterium must be known in order to choose the

appropriate phage. Phage cannot be used in the same manner as broad-spectrum antibiotics, where treatment can be given before the exact infective organism is known. To counteract this, bacteriophage are most effectively administered in phage 'cocktails'[87, 88]. These are mixtures of different phages which combined give treatment over a broad spectrum compared to single bacteriophage.

As bacteriophage can be recognised as foreign bodies, a certain response is expected by the immune system when exogenous phage are administered to the body. At low concentrations, phage are usually completely cleared from the blood and internal organs through elimination by the liver and spleen[89]. Immune response of phage is largely based on the type and concentration of phage, and route of administration; topically administered phage rarely elicit a response, however high concentrations of systemic phage can initiate antibody release[90, 91]. Another concern is that the lysis of high concentrations of bacteria by phage can release exotoxins and superantigens into the system, stimulating an inflammatory response. This can be controlled to a certain extent through the use of lysis-deficient phage[92].

Large pharmaceutical companies remain hesitant to invest in bacteriophage therapy. Bacteriophage are considered by the FDA as a biological product, meaning clinical trials must be stopped in the event of phage mutation, regardless of if this mutation is dangerous. Standard protocols for the isolation and production of phage cocktails suitable for clinical trials were published by Merabishvili in 2009[93]. Also, it is very hard to secure patent protection for phage products. Even if phage were regulated, compared to antibiotics, bacteriophage are generally harder to manufacture, store and purify on a large scale.

1.2.6. Bacteriophage as a therapeutic

The majority of phage products seen today are licenced for agricultural or food use; for example preparations against *E. coli*, *Campylobacter*, *Salmonella* and *Listeria* have all been licenced to prevent food poisoning[94]. Some preparations are also available for medical use in Eastern Europe, e.g. from the former Soviet Union (Georgia and Russia) (Figure 1.10). Despite the general promise of bacteriophage as a medical therapeutic, there are currently no phage preparations that have been approved or are in Phase III clinical trials in the EU or USA[95]. Although used for decades, there are few clinical trials to support bacteriophage as a safe, reliable and potent therapeutic; in the West phage were forgotten, and when therapy was continued in Eastern Europe trials were frequently not carried out to international standards.

The major hurdle that prevents more bacteriophage products going into clinical trials is the regulatory 'grey-area' in which phage are placed[96, 97]. At the moment they are regulated in a similar way to antibiotics, however as viruses that are able to evolve, it is hoped that phage will be treated in a similar way to the seasonal influenza vaccine.

Although no phage preparations have been licenced as a medical treatment, many hundreds of studies have been carried out in small-scale research settings which seem promising. These have been extensively reported and have been collated in a number of comprehensive reviews [65, 98, 99]. For example in 2009 a small scale, randomised, double-blind, placebo controlled trial of phage was successful in treating the majority of patients with chronic otitis caused by antibiotic-resistant *P. aeruginosa* infection[100]. There has also been research reported on different forms of bacteriophage delivery; a recent study by Lehman et al has described the beneficial use of bacteriophage-hydrogel coated catheters in *P. aeruginosa* and *P. mirabilis* infections[103].

Perhaps an indication of the drive of the international community to make phage therapy a viable alternative in infection control can be seen with the PhagoBurn project[97]. PhagoBurn is a new phage research program funded by a €3.8 million FP-7 grant from the European Commission that involves researchers from France, Belgium and Switzerland. Their aim is to coordinate a two year Phase I/II clinical trial to assess the use of phage therapy against *E. coli* and *P. aeruginosa* burn wound infections. The results from these trials and lessons learnt from large scale manufacturing are hoped to form the basis of future regulatory guidelines for phage therapy.

1.2.7. Bacteriophage and biofilms

As described earlier, biofilms are sessile communities of bacteria which offer a safe haven against pH, osmotic shock and even UV light. Biofilms also are notoriously resistant to antibiotics

due to poor diffusion inside the matrix; the systemic administration of antibiotics against biofilms on indwelling catheters for example, is usually ineffective with a failure rate of at least 30%[101]. With this in mind, bacteriophage are a new therapy thought to be particularly beneficial in the removal of bacterial biofilms [102, 103].

Firstly, bacteriophage secrete enzymes known as polysaccharide depolymerases (originally to degrade the bacterial cell wall after phage assembly) which degrade the biofilm EPS matrix. As the EPS breaks down, the biofilm becomes more fragile and bacteria are now more susceptible to the environment, antibiotics and indeed bacteriophage themselves. In 2007, Lu et al were able to engineer a T7 phage with a biofilm-degrading enzyme which reduced *E. coli* biofilm cell counts by 4.5 orders of magnitude[104].

Secondly, once bacteriophage have degraded the EPS matrix they can go on to infect and lyse bacteria present. The phage infect and multiply as they go through the matrix, eroding at the biofilm. Doolittle et al were able to follow this diffusion with fluorescently labelled phage[105] A drawback of using phage in this way is that some biofilms can contain many different bacterial strains and species; phage infection is so strain specific that full killing could possibly not occur. A compromise can be used by firstly administering phage, and then treating with antibiotics; this is known as dual therapy. The phage breaks down the EPS matrix (the main barrier to antibiotic diffusion) and then allows better diffusion and subsequent efficacy of antibiotics. This was seen by Kirby et al in 2012 for example, with gentamicin and *S. aureus* phage SA5 showing higher bacterial killing when used in combination than as separate treatments[106].

1.2.8. Bacteriophage Lysins

Bacteriophage lysins are phage-encoded murein hydrolase enzymes. They are secreted by bacteriophage during the final stage of the lytic cycle and facilitate the release of whole phage from the bacterium into the surrounding environment after assembly. Firstly, bacteriophage-encoded proteins, holins, are excreted into the cytoplasm and form pores in the bacterial cell membrane. Bacteriophage lysins are then able to move through these pores, which then gives access to the peptidoglycan. These degrade specific bonds of the peptidoglycan depending on which bond is the specific target; they are classified into six groups (Figure 1.11)[107]. After enzymatic degradation, the bacterial cell loses structural integrity; water is able to move through the now porous peptidoglycan into the cytoplasm, causing the cell to eventually burst[108].

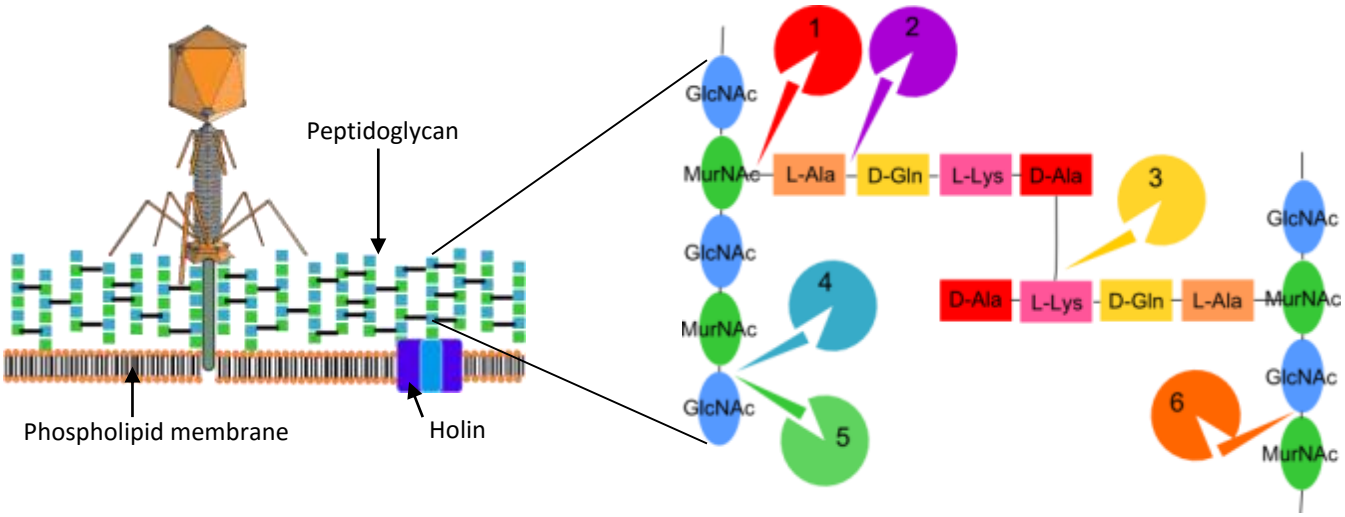

When applied exogenously, recombinantly expressed purified bacteriophage lysins can elicit the same response without the addition of holins (as there is now no barrier to bacterial peptidoglycan) or bacteriophage. Because of this action, lysins are thought to be a promising alternative to current antibiotics and phage therapy[109-111]. Currently many extensive reviews and investigations have been carried out into lysins as antimicrobials, especially in Gram-positive species with active lysins found against all clinically relevant Gram-positive bacteria[112, 113].

Lysins have a number of advantageous properties over antibiotics and whole bacteriophage[114, 115]. They have a broader host range than some bacteriophage with lysins able to lyse many strains of a species, regardless of antibiotic resistance. For example, the anti-*Staphylococcal* lysin LysK exhibits killing over a number of clinically relevant *S. aureus* species including MRSA[116].Optimal properties of bacteriophage lysins can be fine-tuned with the chemical tailoring of enzymes. The truncated lysin CHAPk is derived from LysK – the catalytic amidase-2 domain and cell-binding SH3b domain were both removed and lytic activity was retained. Compared to whole bacteriophage, lysins are far quicker in initiating bacterial cell lysis. The enzymes are active immediately, as opposed to whole phage which rely on bacteria being in the exponential growth phase. Also, because lysins do not carry genetic material, they eliminate the risk of transduction of virulence factors into bacterial DNA. The acquisition of resistance to lysins is additionally very low (if seen at all) as it is thought the target structure for lysin attack (peptidoglycan) is not easily changed by the bacterium[117].

Although a promising lead against Gram-positive infections, lysins retain a lack of efficacy against Gram-negative bacteria. This is due to the presence of the thick outer membrane, which

surrounds and protects the Gram-negatives. Bacteriophage lysins are unable to permeate this membrane and so cannot go on to degrade cell peptidoglycan. Despite this, some active lysins have been characterised. For example, in 2012 Lukacik et al succeeded in lysing strains of Gram-negative *Y. pestis* and *E. coli* by fusing a T4 phage lysin to a membrane transporter binding domain[118].

1.3. Vesicles

Phospholipid molecules are the major constituent of cell membranes, consisting of a hydrophilic phosphate 'head' and a hydrophobic lipid 'tail' (Figure 1.12). Because of these dual properties in the same molecule, phospholipids are described as being amphiphilic. The hydrophilic headgroup is most commonly a choline, ethanolamine, serine or glycerol linked to a negatively charged phosphate group. Phospholipid tails consist of two hydrocarbon chains, either saturated or unsaturated.

In aqueous solution the amphiphilic nature of phospholipids causes molecules to self-assemble over a certain concentration into supramolecular aggregates. This concentration is known as the Critical Micelle Concentration (CMC). Phospholipids initially align at the interface, with headgroups in the aqueous and tails in the air layers. Above the CMC the whole interface is covered and the only way for more phospholipids to go into solution is to form aggregates. Which aggregate is formed is dependent on the concentration and shape of the phospholipid used.

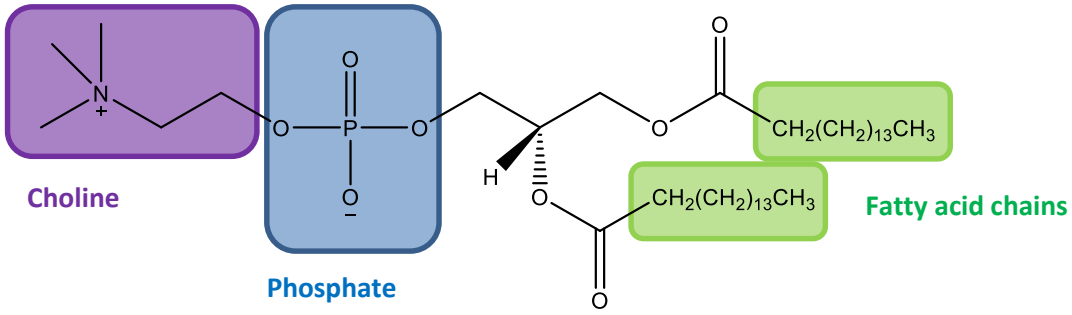

Figure 1.12: Structure of the phospholipid DPPC

What kind of aggregate forms is determined by the phospholipid head size and tail length (Figure 1.13). If the projection area of the tail is smaller than the headgroup, micelles are formed as this is most favourable. Phospholipids in micelles are aligned so the headgroup is in contact with the aqueous media and tails are inside, forming a lipophilic core. Micelles are useful for the in encapsulation of lipophilic molecules in aqueous media because of this. If tails are very similar

in size to the headgroup, thin membranes known as phospholipid bilayers are formed. Vesicles are formed by lipids with a large tail in comparison to the headgroup (>16 carbons). They are ideally formed to encapsulate aqueous materials such as dye molecules, drugs and other chemicals. Recently there has been renewed interest in vesicles due to their similarity in size and shape to cell membranes.

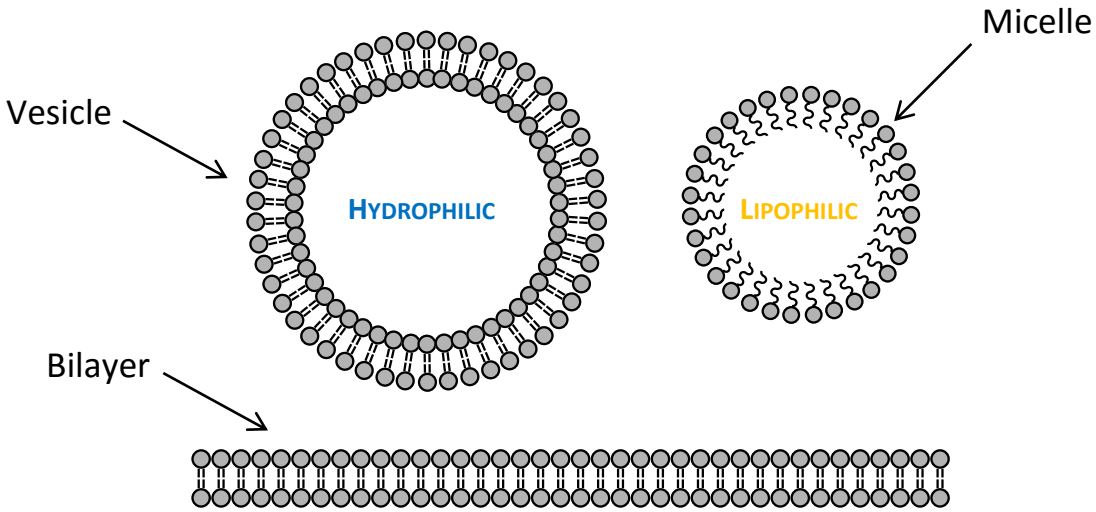

Figure 1.13: Vesicle, micelle and bilayer structures formed from phospholipid bilayers

Vesicles can form in varying sizes, ranging from small unilamellar vesicles (20 – 50 nm) to giant unilamellar vesicles (> 1 µm). They have many uses in biomedicine as delivery systems, as they are able to increase the stability of previously unstable drugs. Inside the body they are advantageous as they do not initiate an immune response and are able to pass through the Blood Brain Barrier (BBB). Liposomal formulations of many drugs such as Doxorubicin and Paclitaxel are being researched or are already on the market. For example, Doxil, a liposomal formulation of doxorubicin is a drug recently approved by the FDA for Kaposi's sarcoma and ovarian cancer. Vaccines for influenza and hepatitis A have been developed in vesicular forms which were found to increase in vivo stability[119-121].

1.4. Hydrogels

1.4.1. Hydrogel wound dressings

Following a wound occurring, the healing process as well as the healing time will depend on the depth and severity of the wound. It is imperative for this process to be as quick as possible to minimise the risk of scarring, and more importantly, the risk of infection by commensal skin flora

or opportunistic pathogens. The standard treatment method for burns and other skin and soft tissue wounds is initial debridement of the wound, and then application of bandages or gauze to protect the wound as it heals. This however has a number of drawbacks: wound fluid cannot drain, bandages can adhere to the wound, the progress of healing cannot be seen without bandage removal and a perfect environment for bacterial infection is established. Increasingly, research is turning to polymeric hydrogels as better dressing alternatives.

Hydrogels exhibit the optimal characteristics of solids and liquids, as they can be both strong and flexible, as well as having high water content with good diffusive properties. They are crosslinked polymer networks that can hold vast quantities of water for their weight (> 90%). Hydrogels are also able to reversibly absorb and release water in response to external stimuli, e.g. temperature, pH and ionic strength, allowing the development of 'smart' and 'triggered release' hydrogels. Currently there are many hydrogel formulations on the market for wound treatment, especially for burns (Figure 1.13), as well as in cell culture and tissue engineering[122].

Hydrogel dressings are ideal for the promotion and facilitation of wound healing. Firstly hydrogels are able to absorb wound exudate, which promotes the free movement of the keratinocytes and fibroblasts needed for re-epithelialisation. Hydrogels are also more flexible, comfortable and soothing than conventional dressings. The highly hydrophilic environment can prevent cell attachment and so hydrogels can generally be non-adhesive; this reduces the pain and discomfort associated with dressing changes.

Currently a vast range of formulations have been investigated which aim to improve and advance current wound dressings. As well as hydrogel dressings, other novel approaches include hydrocolloid, alginate, adhesive film, foam and biological dressings. Dressings can additionally be incorporated with other factors which promote healing or prevent infection such as growth factors, supplements and antimicrobials; these are easily able to diffuse through the porous structure to the wound site. The optimal characteristics for a wound dressing are summarised in Figure 1.15[123]. Although many dressings will comprise the majority of these characteristics, no dressing as yet has been all-encompassing.

Currently there has been a general trend to form hydrogels which are formed from multiple polymeric materials (natural and synthetic). This not only aids in creating hydrogels with the best physical properties, but also can help with different aspects of wound healing and management (e.g. re-epithelialisation, collagen synthesis or infection control)[124, 125]. Hydrogels derived from polysaccharides have additional benefits of excellent biocompatibility, biodegradability and natural abundance[126].

1.4.2. Natural polymers

Natural polymers are defined as polymers which are obtained from natural sources, such as animals, microbes or vegetables. Natural polymers are inherently biocompatible, biodegradable and similar to the extracellular matrix (ECM), and so are ideal for use in wound dressings.

The most common natural polymers used are polysaccharides (chitin, chitosan, hyaluronic acid, alginate, cellulose) and proteins (collagen, gelatin, fibrin and keratin). Chitosan is one of the most abundant natural polymers used in wound dressings, and as well as having all the beneficial properties of a natural polymer, also exhibits anti-bacterial and wound healing affects[127]. Hyaluronic acid has received increased attention in recent years due to its role in wound healing, and will be discussed in detail in Section 1.4.4. Collagen is the major and most abundant structural component in connective tissues, and so is commonly used in wound dressings; it is known to stimulate wound healing, tissue development and wound debridement. Although collagen has favourable qualities in vivo, in vitro the protein loses structure and elasticity. This can be overcome to a certain extent with crosslinking of fibres to retain structure; in 2013, Tronci et al functionalised collagen lysine residues with photo-active methacrylate groups, enabling subsequent photo-crosslinking[128]. Collagen can also be used in coatings for implants and medical devices, as well as in artificial skin.

Although natural polymers possess a number of advantageous properties, frequently their high biodegradability combined with low tensile strength and high cost means that they become unsuitable for biomedical applications. To overcome this, natural polymers can be mixed with either multiple natural polymers or, more commonly, mixed with synthetic polymers.

1.4.3. Synthetic polymers

The control of synthesis and chemical modification of polymers is a major advantage of synthetic polymers over natural polymers. Synthetic polymers can be made to specific requirements of functionality, m, purity, homogeneity and reactivity, making them far easier to understand and use[123, 129]. These polymers can be biologically inert (e.g. PEG); they do not aid wound healing however they equally to not illicit an immune response.

Poly(vinyl alcohol), PVA, is one of the most commonly used synthetic polymers. It can be moulded into multiple forms (e.g. sheets, fibres and foams) and shows good biocompatibility, water absorption and oxygen permiability[130, 131]. A number of natural polymers have been combined with PVA to form wound dressings with improved properties, most commonly chitosan[132, 133]. Drug and biologically important molecules have been coupled to the inert

poly(ethylene glycol), PEG, to improve solubility, reduce immunogenicity and provide 'stealth' delivery; for example the Crohn's disease drug Cimzia is delivered as the PEGylated form[134, 135]. Again, in a wound dressing PEG is frequently used as a scaffold for more biologically active molecules. Other non-toxic and non-immunogenic polymers such as poly(hydroxyethyl methacrylate), pHEMA, and poly(vinylpyrrolidone), PVP, as well as the biodegradable polymers poly(lactic acid) and poly(caprolactone), have all been widely used as hydrogel scaffolds to promote wound healing (Figure 1.16).

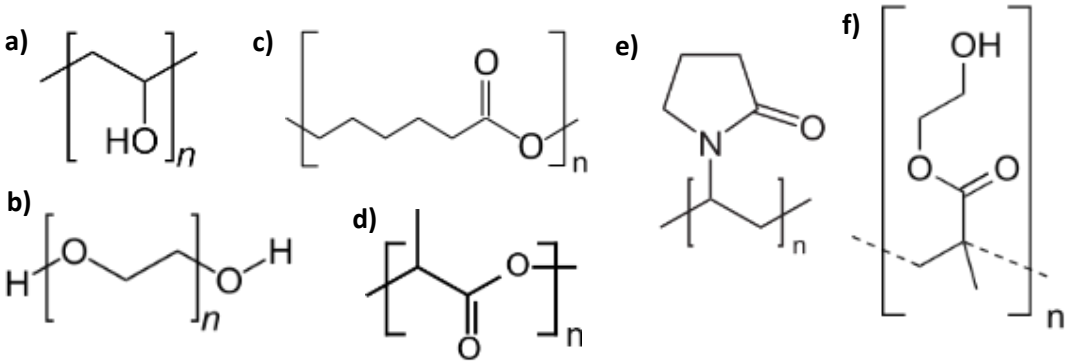

Figure 1.16: Chemical structures of a) poly(vinyl alcohol), PVA b) poly(ethylene glycol), PEG c) poly(caprolactone) d) poly(lactic acid) e) polyvinylpyrrolidone, PVA and f) poly(hydroxyethyl methacrylate)

1.4.4. Hyaluronic acid

Hyaluronic acid, sometimes known as hyaluronan (HA), is a high molecular weight, linear polysaccharide biopolymer made up of glucuronic acid and N-acetyl glucosamine sugars linked by alternating β-1,3 and β-1,4 glycosidic bonds (Figure 1.17). Although classed as a glycosaminoglycan (along with heparin and chondroitin sulphate), the polymer differs in that it is non-sulphated, non-protein bound and can have a molecular weight of up to 10^6 g/mol. HA is found in almost all tissues of all vertebrates, but in humans is a major constituent of the connective tissues, umbilical cord, synovial fluid, eye vitreous humour and especially the skin. It plays an active role in the body; with approximately 5 g HA (1/3 of the whole body amount) metabolised every day[136, 137].

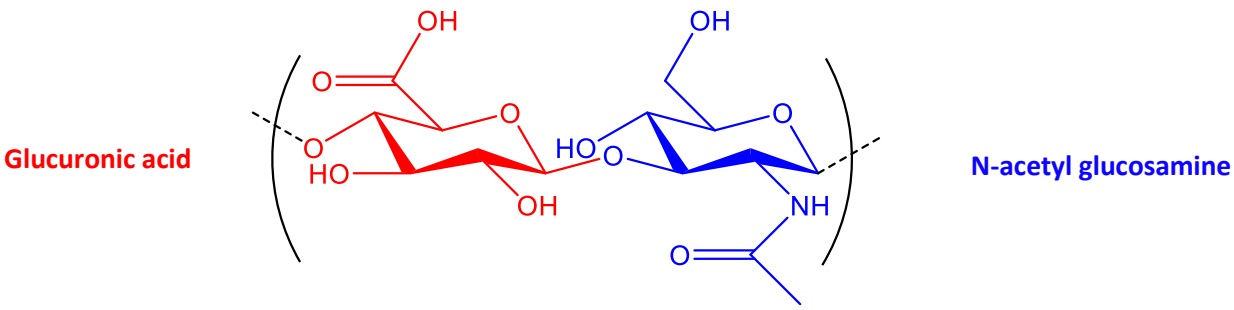

Figure 1.17: Repeating unit structure of hyaluronic acid

In the body, HA is synthesised by three different hyaluronan synthase enzymes (HAS1, HAS2 and HAS3) which are situated in the cell membrane; the polymer is directly extruded onto the cell surface or into the extracellular matrix. HA is able to interact with eukaryotic cells through cell membrane receptors; these include CD44 (Cluster of Differentiation 44) and RHAMM (Receptor for HA-mediated motility) [138]. The structure of HA is highly conserved throughout vertebrates, implying it has an important biological role.

HA has both a structural and active function in the body. Firstly, it has incredible water holding properties compared to other biopolymers. It is able to occupy a large volume in tissues with a high concentration of associated water molecules, making it able to easily maintain tissue structure and hydration. The molecule also acts as a lubricant for joints due to its viscoelastic nature. The major role of HA in the body is in wound healing, and is discussed in Section 1.4.4.1., however in other areas of the body, HA has an active role in embryo development, carcinogenesis, inflammation, cell signalling and ageing[139].

The unique viscoelastic and water holding properties of HA, as well as its biocompatibility and non-immunogenicity make the molecule highly suitable for medical applications in wound healing, drug delivery and tissue engineering[140, 141]. Chemically, the molecule contains a number of easily modifiable functional groups which allow crosslinking and conjugation with biologically active molecules and proteins[142].

1.4.4.1. Role of hyaluronic acid in wound healing

Hyaluronic acid is known to play an active and beneficial role in all stages of wound healing. On initial wounding, HA synthesis is upregulated and long chain HA (> 1000 – 5000 saccharides) is secreted from cells, binding to fibrinogen in the blood to start clot formation[143, 144]. The long chain HA is then degraded into smaller and smaller lengths over the course of wound healing. The influx of HA to the wound also causes swelling and opens up the tissue facilitating movement of neutrophils into the wound site; here long chain HA is acting as an immunosuppressant.

In the inflammatory stage, the stimulation of inflammatory cytokines such as TNF-α and interleukin occurs due to smaller HA fragments (< 1000 saccharides)[145]. In the next proliferative phase, even smaller HA fragments (6 – 20 saccharides) stimulate fibroblast and keratinocyte migration to the wound site and subsequent proliferation, as well as synthesis of collagen[144, 146]. By the maturation phase excess short chain HA is broken down further which then goes on to stimulate angiogenesis (sprouting of blood vessels in the ECM)[147, 148].

A number of studies have found that the application of exogenous HA to a wound site has a positive effect on wound healing, especially in burns, surgical wounds and chronic wounds (e.g. diabetic ulcers). In 2012 Voigt et al carried out a systemic review and meta-analysis of the use of HA in wound healing compared to conventional therapies or placebos[149]. In eight out of nine randomised controlled trials investigated, HA significantly improved wound healing. HA based therapeutics are currently in use in both medical and cosmetic areas; these are discussed in more detail in Section 1.4.4.3.

1.4.4.2. Hyaluronic acid crosslinking

In aqueous solution HA forms highly swollen gels which lack mechanical strength and shape, and so are unsuitable for use in wound dressings. Also, as mentioned earlier, in the body native HA is degraded extremely quickly. In order to form a usable hydrogel for medical applications HA can be crosslinked. This is predominantly through 3 routes: reaction of HA with itself (through coupling of the carboxylic acid, alcohol and acetamide groups), addition of a crosslinking molecule which reacts with HA, or by a two-step process where HA is first modified and then crosslinked. Crosslinking of HA has been summarised in a number of reviews by Schanté (2011) and Burdick (2011)[150, 151].

1.4.4.2.1. Modification of hyaluronic acid carboxylic acid

One of the most common and facile approaches to crosslink polysaccharides including HA is the reaction with carbodiimides, which are molecules with the formula RN=C=NR. Carbodiimides form ‘zero-length’ crosslinks and do not directly combine into the structure; they are preferable as they are biocompatible and only produce urea based by-products[152]. One of the first carbodiimides investigated for HA crosslinking was DCC (N, N’-dicyclohexylcarbodiimide), although this reaction was toxic and required unfavourable non-aqueous conditions. Because of this, the water-soluble analogue EDC (1-Ethyl-3-(3-dimethylaminopropyl) carbodiimide) is more commonly used[153, 154].

HA carboxylic acid groups become activated to the reactive O-acyl-isourea intermediate on addition of carbodiimides such as EDC (Figure 1.18). The activated HA is then able to either react with other HA hydroxyl groups forming a ‘zero-length’ ester bond, or amine groups that can be added as crosslinking molecules (typically in the form of diamines and dihydrazides).

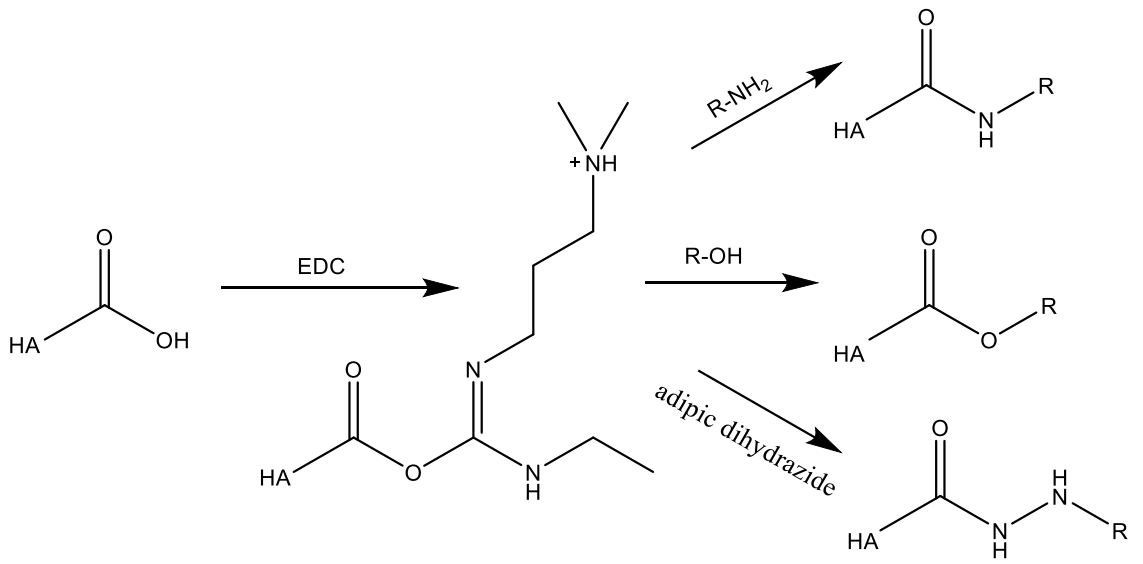

Figure 1.18: HA crosslinking through a) amide bond formation, b) ester bond formation and c) hydrazide bond formation

Another approach which utilises HA carboxylic acids is the Ugi condensation, which involves the reaction of HA in acidic conditions with a diamine crosslinker (e.g. 1,5 pentanediamine), formaldehyde and cyclohexyl isocyanide[155]. This results in the formation of a diamine crosslinked HA (through the HA carboxylic acid groups) that has additional secondary amide and pendant cyclohexyl functionality.

1.4.4.2.2. Crosslinking of hyaluronic acid alcohols

Primary and secondary hydroxyl groups can also be involved in crosslinking reactions. Firstly, hydroxyl groups can react with bi-functional ethers to form ether crosslinked HA; the most common crosslinker used in HA hydrogels on the market is 1,4 butanediol diglycidyl ether (BDDE). It is cheap and easy to synthesise, and so far degradation products have not shown significant toxicity[156]. It is also possible for BDDE to form crosslinks with HA carboxylic acid groups in acidic conditions, however in alkaline solution (pH 10) the alcohol esterification predominates with more stable products[148].

In alkaline media (pH > 13), divinylsulphone (DVS) forms a sulphonyl ether crosslink between the hydroxyl groups of HA. DVS itself is highly reactive and toxic; in 2010, Ibrahim et al showed the high concentrations of DVS needed to form solid gels compromised biocompatibility and gels formed were of poor quality[157].

The aldehyde functionality has been used for HA crosslinking in two main ways. Firstly, alcohol groups found on the HA sugars can be selectively oxidised to form aldehyde groups, which can

then react with diamines or dihydrazides to form crosslinks through imine bonds[158, 159]. Which hydroxyl groups will be oxidised is determined by the choice of oxidising agent[160]. The use of sodium periodate ($NAIO_4$) results in the ring opening of the glucuronic acid sugar, and the formation of two aldehyde groups from the C2 and C3 carbons. Dess-Martin periodinane selectively oxidises the N-acetyl glucosamine primary alcohol to the corresponding aldehyde with no destruction of the HA structure[161]. Secondly, HA hydroxyl groups can be crosslinked by the dialdehyde glutaraldehyde, forming a hemiacetal; however this reaction is known to be toxic and crosslinks are easily hydrolysed[150].

1.4.4.2.3. Crosslinking of hyaluronic acid derivatives

The Huisgen cycloaddition, or 'Click' crosslinking, is a relatively new method of crosslinking which has been successfully applied to HA. The process involves the initial functionalisation of separate HA carboxylates with azide or alkyne groups[162]; in the presence of Cu^+ catalyst a 1, 3 cycloaddition then occurs forming a 5-membered ring and a crosslink. In 2007, Crescenzi et al successfully crosslinked HA that had been functionalised with propargylamine and 11-Azido-3,6,9-trioxaundecan-1-amine in an aqueous, room temperature reaction with 1% CuCl[163].

Another method described by several authors is the crosslinking of HA by photo-polymerisation. Initially, HA is functionalised with acrylate or methacrylate groups (frequently through coupling to glycidyl methacrylate or methacrylic anhydride), as these groups react rapidly with free radicals. When mixed with a photo-active initiator and exposed to UV light, HA methacrylate (HAMA) is able to form crosslinks between methacrylate groups via a free-radical polymerisation mechanism (Figure 1.19).

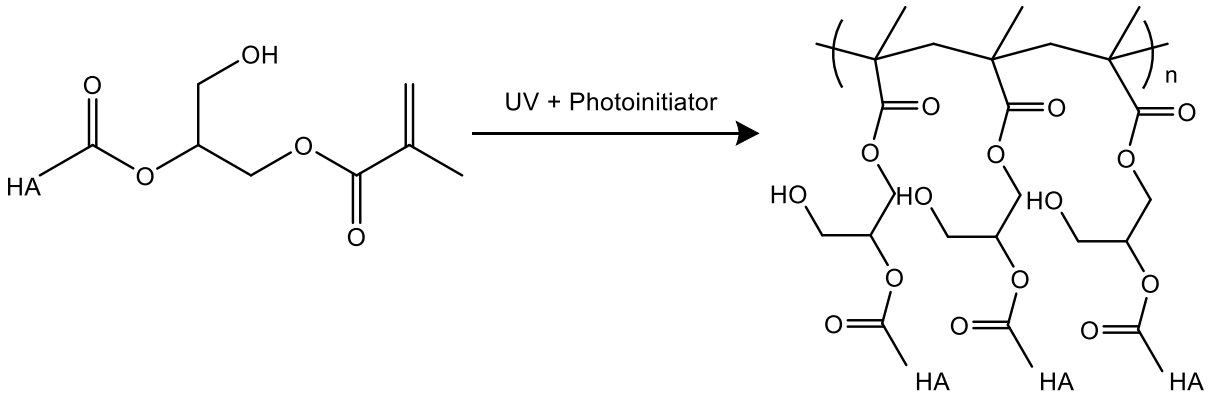

Figure 1.19: HA crosslinking through free radical polymerisation of methacrylated HA

Common radical initiators used include benzophenone and benzoin derivatives such as 2-hydroxy-4'-(2-hydroxyethoxy)-2-methylpropiophenone (Irgacure 2959). Other acrylated molecules can also be incorporated into the mixture prior to polymerisation to enhance the hydrogel structure and properties; these include acrylated PEG derivatives, proteins or collagen.

Photopolymerisation offers a better control of hydrogel properties through alteration of the concentration of macromer, methacrylate groups or initiator[164, 165]. Interpenetrating networks (IPNs) of crosslinked HAMA can also be easily formed around existing polymer scaffolds which greatly increase the hydrogel strength and properties[166].

1.4.4.3. Hyaluronic acid hydrogel dressings

HA can be found in many products available to the public, both medical and cosmetic (Table 1.2). These products mainly use HA in two ways. Firstly, they can contain free unmodified HA of varying molecular weights which has been mixed in with other ingredients to form a liquid or cream, for example in cosmetics or products such as Hyalgan®. Secondly, they can be crosslinked HA hydrogels. Juvederm® is a temporary dermal filler used for the treatment of wrinkles, which is lightly crosslinked with the diether BDDE[167]. Many HA hydrogels available for use in wounds (especially for skin and soft tissue injuries) are wound dressing-like sheets of crosslinked polymers.

Therapeutic area	Applications	Commercial Products	References
Osteoarthritis	Lubrication and mechanical support for joints	Hyalgan®, Artz®, ORTHOVISC®, Healon®, Syinocrom®	168, 169
Surgery and wound healing	Aids cell proliferation, migration and wound healing	Hyalomatrix®, Bionect®, HYAFF®, Connettivina®, Jossalind®, Hyalofill®	146, 170, 171
Embryo Implantation	Promotes implantation after embryo transfer in *in vitro* fertilisation	EmbryoGlue®	172, 173
Antiaging	Rehydration and replacement of HA in skin	Juvederm®, Restylane®, Perlane®, Surgiderm®	167, 174
Cosmetics	Moisturisation	RevitaLift® (L'Oréal), Eucerin® Hyaluronan Filler, Rimmel® Moisture Renew Lipstick	
Burns	Aids cell proliferation, migration and wound healing	Hyalosafe®, Hyalomatrix®	149, 175

Table 1.2: Commercial products used for a range of therapies which contain HA as a major component

1.4.4.4. Hyaluronidase in prokaryotes

Hyaluronidase (HAase) is an extracellular enzyme which facilitates the cleavage of HA. Enzymatic degradation of this molecule results in a drop in tissue viscosity, a breakdown of tissue structure and a higher chance of bacterial invasion.

HAase enzymes can be sub-divided into three different classes[176, 177]: hyaluronate-4-glycanohydrolases (testicular HAase), hyaluronate-3-glycanohydrolases (leech HAase) and hyaluronate lyase (bacterial HAase). The first two types are both found in eukaryotes and cleave the HA molecule by hydrolysis of the glycosidic bonds. The hyaluronate lyases are only found in bacteria and cleave the HA molecule through β-elimination of the β-1, 4 glycosidic bond (Figure 1.20).

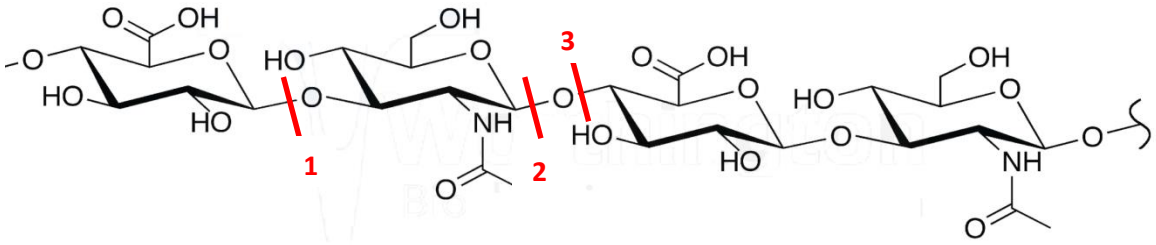

Figure 1.20: Positions of cleavage of HAase molecules - 1. hyaluronate-3-glycanohydrolases, 2. hyaluronate-4-glycanohydrolases and 3. hyaluronate lyases.

The structure of bacterial HAase has been studied in *S. pneumoniae*[178, 179] and *Streptococcus agalactiae*[180], with *S. aureus* HAase thought to have a similar structure. The size of HAase enzymes differs between species, with a weight of 84 kDa in *S. aureus* and 40 kDa for *S. pyogenes* for example[136].

In bacteria, HAase is used as a "spreading factor" to aid the invasion of host tissues, and to break down HA into a usable carbon source. Although seen in both Gram-positive and Gram-negative bacteria, the enzyme is predominantly secreted as an exotoxin in Gram-positives (in Gram-negative organisms the enzyme remains periplasmic). The most common bacteria known to secrete HAase are *S. aureus*, *S. pyogenes* and *Clostridium* [176] - species which are all common in soft tissue infections[181]. In 1980, Essers and Radebold reported that in a screen of 210 *S. aureus* strains, only one isolate was found to be HAase negative. In the same study, all but one of 150 coagulase-negative *Staphylococci* (i.e. not *S. aureus*) showed no HAase activity at all[182]. Unfortunately more recent studies into the extent of HAase production in clinically relevant *S. aureus* have not been prevalent.

1.4.4.5. Hyaluronidase in eukaryotic cells

Eukaryotic cells are also able to produce HAase, which plays a key role in the natural metabolism of HA in the body. The concentration of hyaluronidase in human serum is approximately 2.6 U/mL[183]. There are six known genes that code for hyaluronidase in humans: Hyal-1, Hyal-2, Hyal-3, Hyal-4, PH-20/Spam1 and Phyal-1 (a pseudogene transcribed in humans but not translated)[184]. Of these, Hyal-1 and Hyal-2 are the major HAases found in tissue.

As mentioned in Section 1.4.4.2., native unmodified HA has an extremely short residence time in the body of approximately 24 hours in skin and a few weeks in tissues. It is rapidly degraded by human HAase and used, and subsequently replaced, by the body. The crosslinking of HA to a certain extent prevents HA breakdown by human HAases, increasing hydrogel residence time as well as mechanical properties[185].

1.4.5. 'Smart' hydrogel systems

Synthetic hydrogels can be tailored to exhibit triggered swelling that is dependent on an external stimulus; these are sometimes known as 'smart' hydrogels as they automatically respond to their external environment. Hydrogels have been developed which are responsive to stimuli including pH, temperature, ionic strength, an enzymatic or chemical reaction, as well as magnetism or an electric current[186]. Stimuli are able to chemically modify the structure of the hydrogel and cause changes in the polymer network, most commonly by causing a change in swelling.

1.4.5.1. pH sensitive hydrogels

pH sensitive hydrogels are ionic polymer networks all containing either acidic (carboxylic acid or sulphonic acids) or basic (ammonium salts) pendant groups[187]. These groups are able to accept or donate protons depending on the external pH, and swelling is initiated due to electrostatic repulsions between charges on the polymer chain (releasing encapsulated agents). The most frequently used cationic polymers include poly (acrylic acid), poly(methacrylic acid), PMAA, whilst anionic polymers include poly(N,N' -diethylamino ethyl methacrylate) (PDEAMA).

A number of drug molecules have been successfully administered through triggered pH release from hydrogels by taking advantage of pH changes in the body[188, 189]. In 2014, Car et al reported on the use of poly(dimethylsiloxane)-b-poly(2-dimethylamino ethyl methacrylate) (PDMS-b-PDEAMA) for triggered release of the anti-cancer drug doxorubicin; cancer cells are known to be more acidic compared to healthy cells and so drug will only be released to cancer cells[190]. pH

sensitive hydrogels can also be formed with polysaccharides such as hyaluronic acid, chitosan and dextran as the carboxylic acid and amine groups present can become ionised[191]. For example in 2014 Kwon et al investigated cellulose/HA complexes for pH-triggered release of Isoliquiritigenin[192].

1.4.5.2. Temperature sensitive hydrogels

Temperature sensitive hydrogels are one of the most well-studied 'smart' hydrogel systems, with the majority of hydrogels based on poly(N-isopropylacrylamide), PNIPAAm. These hydrogels undergo a reversible phase transition at a critical temperature (the lower critical solution temperature, LCST) over which results in hydrogel collapse and a decrease in polymer solubility[187, 193]. PNIPAAm is particularly advantageous in a biomedical setting as its LCST is approximately 32 °C, being in the region of normal body temperature; this LCST can be altered by addition of hydrophilic or hydrophobic copolymers.

Temperature responsive polymers can be used to entrap a wide range of drug molecules[194], enzymes and cells, which go on to give a triggered release over the LCST[195]. They are also best used for topical delivery to skin and soft tissue wounds such as burns, as these injuries frequently show an increased temperature compared to the external environment. PNIPAAm has also been used for non-enzymatic removal of cultured cell sheets from culture vessels[196]. Increasingly, the thermoresponsive properties of PNIPAAm are being combined with pH responsive polymers for added sensitivity[197, 198].

1.4.5.3. Enzyme sensitive hydrogels

A far smaller research area compared to pH and temperature responsive hydrogels are enzyme sensitive hydrogels; these are hydrogels which use enzymatic processes as a trigger mechanism for therapeutic release. Targeting enzymes has a number of advantages over more common triggers such as temperature and pH. Enzymes can be very specific to a target substrate and normally are most active at normal body temperature and pH. They are also highly prevalent in both healthy and diseased tissue; for example, certain enzymes are only secreted in the event of a certain disease or trauma[199].

A number of approaches have been taken by researchers targeting specific enzymes to initiate triggered release of therapeutics. Various PEG based polymer hydrogels have been developed which can be degraded by matrix metalloproteases (MMPs); in 2012 Yang et al formed peptide crosslinked PEG hydrogels which released dexamethasone in the presence of MMPs[112, 200]. Other enzymes can also be targeted which are known to be secreted in certain situations. For example,

the upregulation of elastase production by neutrophils in wound sites has been used as a trigger in a number of studies[201-203]. There have also been reports of polymers formed which have sensitivity to bacterial enzymes. In 2004, Lee et al reported on the development of an enzyme-responsive peptide drug conjugate. This conjugate was susceptible to the enzyme Penicillin G amidase (PGA); on the incubation of *E. coli* (which contained the PGA gene) with this conjugate, breakdown and triggered release of drug was seen[204].

In 2014, Komnatnyy et al reported on the selective killing of bacteria by lipase sensitive polymers[205]. On incubation with lipase secreting bacteria (in this case *P. aeruginosa*), the lipase was able to break an enzyme-sensitive linkage between surface attached PEG and the antibiotic ciprofloxacin. Triggered antibiotic killing was observed where wild-type lipase secreting *P. aeruginosa* was selectively killed compared to lipase mutants.

Triggered release of certain molecules by hyaluronidase has been recently reported by some groups. In 2013, sulphorhodamine and polyhexanide were selectively released from HA-starch nanocapsules by HAase, and in 2015 a triggered release of 7-amino-4-methylcoumarin was reported from HA-b-poly(caprolactone) block copolymer vesicles[206, 207]. In a recent 2015 paper by Wu et al, release of amoxicillin was described from HA coated nanoparticles, with the intention of using HAase secreted by *S. aureus* as a trigger. Although these particles did show high bacterial killing, subsequent investigation into HAase triggered release was not investigated[208]. In all of these cases, no trigger mechanism was reported which used enzymes to initiate triggered release of bacteriophage, especially using HAase secreted by live *S. aureus*.

1.5. Aims and Objectives

The aim of this project was to develop bacteria-triggered release systems for the delivery of bacteriophage for use in topical wound dressings. In this way, bacteriophage would be released *only* when pathogenic bacterial infection is present. This not only prevents the unnecessary use of therapeutic, but also decreases the probability of bacterial resistance emerging. As a viable alternative to antibiotics, bacteriophage offer a range of advantages over antibiotics which lend them to use in wound dressings. The systems investigated used bacterial virulence factors naturally secreted during growth to initiate triggered release, predominantly by the Gram-positive organism *S. aureus*.

This project focussed on two main trigger mechanisms. Firstly, previous work on phospholipid vesicles in the group had used the secretion of the holin molecule δ-haemolysin by *S. aureus* to

selectively release dye and antimicrobial molecules. The use of larger giant unilamellar vesicles was investigated to encapsulate bacteriophage and to give triggered release in a similar manner.

The second trigger mechanism developed was the use of crosslinked HA as an enzyme sensitive barrier for bacteriophage release. Hydrogel wound dressings are already widespread and can actively promote wound healing through combination with natural polymers such as collagen and hyaluronic acid. *S. aureus* secretes hyaluronidase, and so on *S. aureus* infection the hydrogel matrix is degraded and bacteriophage release is seen. In the presence of no *S. aureus*, the matrix acts as a typical hydrogel dressing that benefits from the wound healing properties of HA.

As well as providing an antibacterial therapy in the event of bacterial infection, it was also important to investigate how eukaryotic cells responded to the hydrogel environment. Following on from this, the printing of crosslinked hyaluronic acid was carried out using nano-imprint lithography to investigate its effect on NIH-3T3 fibroblasts. By imparting a surface roughness, it could also be possible to grow cells in a directed fashion (a more ordered cell growth would be more reflective of the highly ordered skin layers).

1.6. References

1. A. Giacometti, O. Cirioni, A. M. Schimizzi, M. S. Del Prete, F. Barchiesi, M. M. D'Errico, E. Petrelli and G. Scalise, *Journal of Clinical Microbiology*, 2000, **38**, 918-922.
2. W. B. Whitman, D. C. Coleman and W. J. Wiebe, *Proc Natl Acad Sci U S A*, 1998, **95**, 6578-6583.
3. A. Weintraub, *Carbohydr Res*, 2003, **338**, 2539-2547.
4. S. A. Alchon, *A Pest in the Land: New World Epidemics in a Global Perspective* University of New Mexico Press, 2003.
5. R. I. Aminov, *Frontiers in Microbiology*, 2010, **1**, 134.
6. J. N. Pendleton, S. P. Gorman and B. F. Gilmore, *Expert Rev Anti Infect Ther*, 2013, **11**, 297-308.
7. R. Gonzales, D. C. Malone, J. H. Maselli and M. A. Sande, *Clinical Infectious Diseases*, 2001, **33**, 757-762.
8. I. Welschen, M. Kuyvenhoven, A. Hoes and T. Verheij, *Fam Practice*, 2004, **21**, 234-237.
9. D. F. Maron, T. J. S. Smith and K. E. Nachman, *Globalization and Health*, 2013, **9**, 48-48.
10. M. Bassetti, M. Merelli, C. Temperoni and A. Astilean, *Ann Clin Microbiol Antimicrob*, 2013, **12**, 22.
11. L. L. Ling, T. Schneider, A. J. Peoples, A. L. Spoering, I. Engels, B. P. Conlon, A. Mueller, T. F. Schaberle, D. E. Hughes, S. Epstein, M. Jones, L. Lazarides, V. A. Steadman, D. R. Cohen, C. R. Felix, K. A. Fetterman, W. P. Millett, A. G. Nitti, A. M. Zullo, C. Chen and K. Lewis, *Nature*, 2015, **517**, 455-459.
12. *Bad bugs, no drugs as antibiotic discovery stagnates -- a public health crisis brews.*, Infectious Diseases Society of America, 2004.
13. L. J. V. Piddock, *The Lancet Infectious Diseases*, 2012, **12**, 249-253.
14. S. Reardon, *Nature News*, 2014.
15. F. G. De Rosa, S. Corcione, N. Pagani and G. Di Perri, *Clinical infectious diseases : an official publication of the Infectious Diseases Society of America*, 2015, **60**, 1289-1290.

16. L. B. Rice, *Journal of Infectious Diseases*, 2008, **197**, 1079-1081.
17. L. B. Rice, *Infection Control & Hospital Epidemiology*, 2010, **31**, S7-S10.
18. J. A. Suaya, R. M. Mera, A. Cassidy, P. O'Hara, H. Amrine-Madsen, S. Burstin and L. G. Miller, *BMC Infect Dis*, 2014, **14**, 296.
19. K. Chiller, B. A. Selkin and G. J. Murakawa, *J Investig Dermatol Symp Proc*, 2001, **6**, 170-174.
20. A. A. Salyers and D. D. Whitt, *Bacterial Pathogenesis: A Molecular Approach*, ASM Press, USA, 2 edn., 2002.
21. D. Church, S. Elsayed, O. Reid, B. Winston and R. Lindsay, *Clin Microbiol Rev*, 2006, **19**, 403-434.
22. L. D. Renner and D. B. Weibel, *MRS bulletin / Materials Research Society*, 2011, **36**, 347-355.
23. L. Hall-Stoodley, J. W. Costerton and P. Stoodley, *Nat Rev Micro*, 2004, **2**, 95-108.
24. K. Sauer, *Genome Biol*, 2003, **4**, 219.
25. R. M. Donlan, *Clinical Infectious Diseases*, 2001, **33**, 1387-1392.
26. R. M. Donlan, *Emerg Infect Dis*, 2001, **7**, 277-281.
27. S. Aslam, *Am J Infect Control*, 2008, **36**, S175 e179-111.
28. I. Francolini and G. Donelli, *FEMS Immunol Med Microbiol*, 2010, **59**, 227-238.
29. L. A. Mermel, B. M. Farr, R. J. Sherertz, Raad, II, N. O'Grady, J. S. Harris and D. E. Craven, *Clin Infect Dis*, 2001, **32**, 1249-1272.
30. N. Høiby, T. Bjarnsholt, M. Givskov, S. Molin and O. Ciofu, *International Journal of Antimicrobial Agents*, 2010, **35**, 322-332.
31. A. Resch, B. Fehrenbacher, K. Eisele, M. Schaller and F. Gotz, *FEMS Microbiol Lett*, 2005, **252**, 89-96.
32. K. Sauer, A. K. Camper, G. D. Ehrlich, J. W. Costerton and D. G. Davies, *Journal of Bacteriology*, 2002, **184**, 1140-1154.
33. T. J. Foster, *Journal of Clinical Investigation*, 2004, **114**, 1693-1696.
34. G. A. Noskin, R. J. Rubin, J. J. Schentag, J. Kluytmans, E. C. Hedblom, C. Jacobson, M. Smulders, E. Gemmen and M. Bharmal, *Clinical Infectious Diseases*, 2007, **45**, 1132-1140.
35. F. D. Lowy, *Journal of Clinical Investigation*, 2003, **111**, 1265-1273.
36. E. Rezaei, H. Safari, M. Naderinasab and H. Aliakbarian, *Burns*, 2011, **37**, 805-807.
37. K. Kulhankova, J. King and W. Salgado-Pabon, *Immunologic Research*, 2014, **59**, 182-187.
38. A. J. Brosnahan and P. M. Schlievert, *Febs Journal*, 2011, **278**, 4649-4667.
39. M. M. Dinges, P. M. Orwin and P. M. Schlievert, *Clin Microbiol Rev*, 2000, **13**, 16-34, table of contents.
40. D. E. Fry and P. S. Barie, *Surg Infect (Larchmt)*, 2011, **12**, 191-203.
41. S. Szmigielski, G. Prévost, H. Monteil, D. A. Colin and J. Jeljaszewicz, *Zentralblatt für Bakteriologie*, 1999, **289**, 185-201.
42. J. Kaneko and Y. Kamio, *Bioscience, Biotechnology, and Biochemistry*, 2004, **68**, 981-1003.
43. R. P. Novick and E. Geisinger, *Annu Rev Genet*, 2008, **42**, 541-564.
44. J. M. Morrison, K. L. Anderson, K. E. Beenken, M. S. Smeltzer and P. M. Dunman, *Front Cell Infect Microbiol*, 2012, **2**, 26.
45. G. Makris, J. D. Wright, E. Ingham and K. T. Holland, *Microbiology*, 2004, **150**, 2005-2013.
46. M. E. Hart, L. H. Tsang, J. Deck, S. T. Daily, R. C. Jones, H. Liu, H. Hu, M. J. Hart and M. S. Smeltzer, *Microbiology*, 2013, **159**, 782-791.
47. C. B. Ibberson, C. L. Jones, S. Singh, M. C. Wise, M. E. Hart, D. V. Zurawski and A. R. Horswill, *Infect Immun*, 2014, **82**, 4253-4264.
48. E. Leung, D. E. Weil, M. Raviglione and H. Nakatani, *Bull World Health Organ*, 2011, **89**, 390-392.

49. B. Spellberg, J. G. Bartlett and D. N. Gilbert, *New England Journal of Medicine*, 2013, **368**, 299-302.
50. R. V. Goering, *Mims' medical microbiology*, St. Louis, Mo. : Mosby, St. Louis, Mo.], 4th ed. edn., 2008.
51. H. C. Neu, *Science*, 1992, **257**, 1064-1073.
52. D. J. Diekema, B. J. BootsMiller, T. E. Vaughn, R. F. Woolson, J. W. Yankey, E. J. Ernst, S. D. Flach, M. M. Ward, C. L. Franciscus, M. A. Pfaller and B. N. Doebbeling, *Clin Infect Dis*, 2004, **38**, 78-85.
53. H. W. Boucher and G. R. Corey, *Clinical Infectious Diseases*, 2008, **46**, S344-S349.
54. R. Dantes, Y. Mu, R. Belflower and et al., *JAMA Internal Medicine*, 2013, **173**, 1970-1978.
55. N. Zetola, J. S. Francis, E. L. Nuermberger and W. R. Bishai, *Lancet Infectious Diseases*, 2005, **5**, 275-286.
56. M. C. Enright, *Current Opinion in Pharmacology*, 2003, **3**, 474-479.
57. S. Deresinski, *Clin Infect Dis*, 2005, **40**, 562-573.
58. R. S. Daum, T. Ito, K. Hiramatsu, F. Hussain, K. Mongkolrattanothai, M. Jamklang and S. Boyle-Vavra, *J Infect Dis*, 2002, **186**, 1344-1347.
59. R. Curtiss, III, *The Journal of Clinical Investigation*, 2002, **110**, 1061-1066.
60. E. Kutter and A. Sulakvelidze, *Bacteriophages - Biology and Applications*, CRC Press, FL USA, 2005.
61. R. W. Hendrix, *Theor Popul Biol*, 2002, **61**, 471-480.
62. A. Letarov and E. Kulikov, *Journal of Applied Microbiology*, 2009, **107**, 1-13.
63. T. Kenzaka, K. Tani, A. Sakotani, N. Yamaguchi and M. Nasu, *Applied and Environmental Microbiology*, 2007, **73**, 3291-3299.
64. X. Wittebole, S. De Roock and S. M. Opal, *Virulence*, 2014, **5**, 226-235.
65. A. Sulakvelidze, Z. Alavidze and J. G. Morris, Jr., *Antimicrob Agents Chemother*, 2001, **45**, 649-659.
66. S. Deresinski, *Clin Infect Dis*, 2009, **48**, 1096-1101.
67. D. E. Bradley, *Bacteriological Reviews*, 1967, **31**, 230-314.
68. H.-W. Ackerman, *Microbiol. Aus.*, 2011, **32**, 90-94.
69. M. G. Rossmann, V. V. Mesyanzhinov, F. Arisaka and P. G. Leiman, *Curr Opin Struct Biol*, 2004, **14**, 171-180.
70. J. B. Reece, M. R. Taylor, E. J. Simon, J. Dickey and N. A. Campbell, *Campbell biology : concepts & connections*, Benjamin Cummings, Boston, [Massachusetts], Seventh edition, International edition / edn., 2012.
71. A. Campbell, *Nat Rev Genet*, 2003, **4**, 471-477.
72. P. Hyman and S. T. Abedon, *Bacteriophages in Health and Disease*, CABI International, UK, 2012.
73. C. Loc-Carrillo and S. T. Abedon, *Bacteriophage*, 2011, **1**, 111-114.
74. S. O'Flaherty, R. P. Ross, W. Meaney, G. F. Fitzgerald, M. F. Elbreki and A. Coffey, *Appl Environ Microbiol*, 2005, **71**, 1836-1842.
75. Z. Kazmierczak, A. Gorski and K. Dabrowska, *Viruses*, 2014, **6**, 2551-2570.
76. C. Slimings and T. V. Riley, *Journal of Antimicrobial Chemotherapy*, 2014, **69**, 881-891.
77. G. Sun, X. Zhang, Y. I. Shen, R. Sebastian, L. E. Dickinson, K. Fox-Talbot, M. Reinblatt, C. Steenbergen, J. W. Harmon and S. Gerecht, *Proc Natl Acad Sci U S A*, 2011, **108**, 20976-20981.
78. P. P. Esteban, D. R. Alves, M. C. Enright, J. E. Bean, A. Gaudion, A. T. Jenkins, A. E. Young and T. C. Arnot, *Biotechnol Prog*, 2014, **30**, 932-944.
79. H. A. Pearson, G. S. Sahukhal, M. O. Elasri and M. W. Urban, *Biomacromolecules*, 2013, **14**, 1257-1261.
80. U. Puapermpoonsiri, J. Spencer and C. F. van der Walle, *Eur J Pharm Biopharm*, 2009, **72**, 26-33.

81. R. P. Novick, G. E. Christie and J. R. Penades, *Nat Rev Microbiol*, 2010, **8**, 541-551.
82. J. L. Balcazar, *PLoS Pathog*, 2014, **10**, e1004219.
83. P. Hyman and S. T. Abedon, in *Adv Appl Microbiol*, 2010 Elsevier Inc, United States, 2010, vol. 70, pp. 217-248.
84. R. Barrangou and J. van der Oost, *EMBO J*, 2015, **34**, 134-135.
85. S. J. Labrie, J. E. Samson and S. Moineau, *Nat Rev Microbiol*, 2010, **8**, 317-327.
86. R. Barrangou, C. Fremaux, H. Deveau, M. Richards, P. Boyaval, S. Moineau, D. A. Romero and P. Horvath, *Science*, 2007, **315**, 1709-1712.
87. B. K. Chan, S. T. Abedon and C. Loc-Carrillo, *Future Microbiol*, 2013, **8**, 769-783.
88. D. Kelly, O. McAuliffe, R. P. Ross, J. O'Mahony and A. Coffey, *Bioeng Bugs*, 2011, **2**, 31-37.
89. K. Dabrowska, K. Switala-Jelen, A. Opolski, B. Weber-Dabrowska and A. Gorski, *J Appl Microbiol*, 2005, **98**, 7-13.
90. T. Kaur, N. Nafissi, O. Wasfi, K. Sheldon, S. Wettig and R. Slavcev, *Journal of Nanotechnology*, 2012, **2012**, 1-13.
91. A. Gorski, R. Miedzybrodzki, J. Borysowski, K. Dabrowska, P. Wierzbicki, M. Ohams, G. Korczak-Kowalska, N. Olszowska-Zaremba, M. Lusiak-Szelachowska, M. Klak, E. Jonczyk, E. Kaniuga, A. Golas, S. Purchla, B. Weber-Dabrowska, S. Letkiewicz, W. Fortuna, K. Szufnarowski, Z. Pawelczyk, P. Rogoz and D. Klosowska, *Adv Virus Res*, 2012, **83**, 41-71.
92. T. Matsuda, T. A. Freeman, D. W. Hilbert, M. Duff, M. Fuortes, P. P. Stapleton and J. M. Daly, *Surgery*, 2005, **137**, 639-646.
93. M. Merabishvili, J.-P. Pirnay, G. Verbeken, N. Chanishvili, M. Tediashvili, N. Lashkhi, T. Glonti, V. Krylov, J. Mast, L. Van Parys, R. Lavigne, G. Volckaert, W. Mattheus, G. Verween, P. De Corte, T. Rose, S. Jennes, M. Zizi, D. De Vos and M. Vaneechoutte, *PLoS ONE*, 2009, **4**, e4944.
94. A. B. Monk, C. D. Rees, P. Barrow, S. Hagens and D. R. Harper, *Lett Appl Microbiol*, 2010, **51**, 363-369.
95. B. F. Gilmore, *Expert Rev Anti Infect Ther*, 2012, **10**, 533-535.
96. H. M. R. T. Parracho, B. H. Burrowes, M. C. Enright, M. L. McConville and D. R. Harper, *Journal of Molecular and Genetic Medicine : An International Journal of Biomedical Research*, 2012, **6**, 279-286.
97. S. Reardon, *Nature*, 2014, **510**, 15-16.
98. Z. Golkar, O. Bagasra and D. G. Pace, *J Infect Dev Ctries*, 2014, **8**, 129-136.
99. R. Miedzybrodzki, J. Borysowski, B. Weber-Dabrowska, W. Fortuna, S. Letkiewicz, K. Szufnarowski, Z. Pawelczyk, P. Rogoz, M. Klak, E. Wojtasik and A. Gorski, *Adv Virus Res*, 2012, **83**, 73-121.
100. A. Wright, C. H. Hawkins, E. E. Anggard and D. R. Harper, *Clin Otolaryngol*, 2009, **34**, 349-357.
101. M. P. Lungren, D. Christensen, R. Kankotia, I. Falk, B. E. Paxton and C. Y. Kim, *Bacteriophage*, 2013, **3**, e26825.
102. B. K. Chan and S. T. Abedon, *Curr Pharm Des*, 2015, **21**, 85-99.
103. a) R. M. Donlan, *Trends Microbiol*, 2009, **17**, 66-72. b) S. M. Lehman and R. M. Donlan, *Antimicrob Agents Chemother*, 2015, **59**, 1127 - 1137.
104. T. K. Lu and J. J. Collins, *Proceedings of the National Academy of Sciences*, 2007, **104**, 11197-11202.
105. M. M. Doolittle, J. J. Cooney and D. E. Caldwell, *J Ind Microbiol*, 1996, **16**, 331-341.
106. A. E. Kirby, *PLoS ONE*, 2012, **7**, e51017.
107. M. J. Loessner, *Curr Opin Microbiol*, 2005, **8**, 480-487.
108. L. Rodríguez-Rubio, D. Gutiérrez, D. M. Donovan, B. Martínez, A. Rodríguez and P. García, *Critical Reviews in Biotechnology*, 2015, 1-11.
109. J. A. Hermoso, J. L. Garcia and P. Garcia, *Curr Opin Microbiol*, 2007, **10**, 461-472.
110. M. Schmelcher, D. M. Donovan and M. J. Loessner, *Future Microbiol*, 2012, **7**, 1147-1171.

111. V. A. Fischetti, *Int J Med Microbiol*, 2010, **300**, 357-362.
112. H. Yang, J. Yu and H. Wei, *Frontiers in Microbiology*, 2014, **5**.
113. M. Fenton, P. Ross, O. McAuliffe, J. O'Mahony and A. Coffey, *Bioengineered Bugs*, 2010, **1**, 9-16.
114. V. A. Fischetti, *Curr Opin Microbiol*, 2008, **11**, 393-400.
115. V. A. Fischetti, *Bacteriophage*, 2011, **1**, 188-194.
116. S. C. Becker, J. Foster-Frey and D. M. Donovan, in *FEMS Microbiol Lett*, England, 2008, vol. 287, pp. 185-191.
117. T. M. Viertel, K. Ritter and H. P. Horz, *J Antimicrob Chemother*, 2014, **69**, 2326-2336.
118. P. Lukacik, T. J. Barnard, P. W. Keller, K. S. Chaturvedi, N. Seddiki, J. W. Fairman, N. Noinaj, T. L. Kirby, J. P. Henderson, A. C. Steven, B. J. Hinnebusch and S. K. Buchanan, *Proc Natl Acad Sci U S A*, 2012, **109**, 9857-9862.
119. K. J. Holm and K. L. Goa, *BioDrugs*, 1999, **11**, 137-144.
120. F. Ambrosch, G. Wiedermann, S. Jonas, B. Althaus, B. Finkel, R. Gluck and C. Herzog, *Vaccine*, 1997, **15**, 1209-1213.
121. R. Acevedo, S. Fernandez, C. Zayas, A. Acosta, M. E. Sarmiento, V. A. Ferro, E. Rosenqvist, C. Campa, D. Cardoso, L. Garcia and J. L. Perez, *Front Immunol*, 2014, **5**, 121.
122. S. Van Vlierberghe, P. Dubruel and E. Schacht, *Biomacromolecules*, 2011, **12**, 1387-1408.
123. N. Mayet, Y. E. Choonara, P. Kumar, L. K. Tomar, C. Tyagi, L. C. Du Toit and V. Pillay, *J Pharm Sci*, 2014, **103**, 2211-2230.
124. M. Madaghiele, C. Demitri, A. Sannino and L. Ambrosio, *Burns & Trauma*, 2014, **2**, 153-161.
125. V. W. L. Ng, J. M. W. Chan, H. Sardon, R. J. Ono, J. M. García, Y. Y. Yang and J. L. Hedrick, *Advanced Drug Delivery Reviews*, 2014, **78**, 46-62.
126. H. Li, J. Yang, X. Hu, J. Liang, Y. Fan and X. Zhang, *Journal of Biomedical Materials Research Part A*, 2011, **98A**, 31-39.
127. T. Dai, M. Tanaka, Y. Y. Huang and M. R. Hamblin, *Expert Rev Anti Infect Ther*, 2011, **9**, 857-879.
128. G. Tronci, S. J. Russell and D. J. Wood, *Journal of Materials Chemistry B*, 2013, **1**, 3705.
129. S. P. Zhong, Y. Z. Zhang and C. T. Lim, *Wiley Interdiscip Rev Nanomed Nanobiotechnol*, 2010, **2**, 510-525.
130. E. A. Kamoun, X. Chen, M. S. Mohy Eldin and E.-R. S. Kenawy, *Arabian Journal of Chemistry*, 2015, **8**, 1-14.
131. M. H. Alves, B. E. Jensen, A. A. Smith and A. N. Zelikin, *Macromol Biosci*, 2011, **11**, 1293-1313.
132. D. Zhang, W. Zhou, B. Wei, X. Wang, R. Tang, J. Nie and J. Wang, *Carbohydrate Polymers*, 2015, **125**, 189-199.
133. C. Chen, L. Liu, T. Huang, Q. Wang and Y. Fang, *Int J Biol Macromol*, 2013, **62**, 188-193.
134. K. Knop, R. Hoogenboom, D. Fischer and U. S. Schubert, *Angewandte Chemie International Edition*, 2010, **49**, 6288-6308.
135. A. Kolate, D. Baradia, S. Patil, I. Vhora, G. Kore and A. Misra, *J Control Release*, 2014, **192**, 67-81.
136. K. S. Girish and K. Kemparaju, *Life Sci*, 2007, **80**, 1921-1943.
137. R. Stern, *European Journal of Cell Biology*, 2004, **83**, 317-325.
138. B. P. Toole, *Nat Rev Cancer*, 2004, **4**, 528-539.
139. R. Stern and H. I. Maibach, *Clin Dermatol*, 2008, **26**, 106-122.
140. P. Matricardi, C. Di Meo, T. Coviello, W. E. Hennink and F. Alhaique, *Adv Drug Deliv Rev*, 2013, **65**, 1172-1187.
141. M. N. Collins and C. Birkinshaw, *Carbohydr Polym*, 2013, **92**, 1262-1279.
142. H. Zhang, S. Huang, X. Yang and G. Zhai, *Eur J Med Chem*, 2014, **86**, 310-317.
143. J. S. Frenkel, *Int Wound J*, 2014, **11**, 159-163.

144. R. Stern, A. A. Asari and K. N. Sugahara, *Eur J Cell Biol*, 2006, **85**, 699-715.
145. W. Y. Chen and G. Abatangelo, *Wound Repair Regen*, 1999, **7**, 79-89.
146. R. D. Price, M. G. Berry and H. A. Navsaria, *J Plast Reconstr Aesthet Surg*, 2007, **60**, 1110-1119.
147. D. C. West, I. N. Hampson, F. Arnold and S. Kumar, *Science*, 1985, **228**, 1324-1326.
148. M. A. Selyanin, P. Y. Boykov and V. N. Khabarov, *Hyaluronic Acid: Preparation, Properties, Application in Biology and Medicine*, Wiley, 2015.
149. J. Voigt and V. R. Driver, *Wound Repair Regen*, 2012, **20**, 317-331.
150. C. E. Schanté, G. Zuber, C. Herlin and T. F. Vandamme, *Carbohydrate Polymers*, 2011, **85**, 469-489.
151. J. A. Burdick and G. D. Prestwich, *Adv Mater*, 2011, **23**, H41-56.
152. A. Sannino, S. Pappadà, M. Madaghiele, A. Maffezzoli, L. Ambrosio and L. Nicolais, *Polymer*, 2005, **46**, 11206-11212.
153. J.-Y. Lai, *Materials*, 2012, **5**, 1986-2002.
154. P. L. Lu, J. Y. Lai, D. H. Ma and G. H. Hsiue, *J Biomater Sci Polym Ed*, 2008, **19**, 1-18.
155. A. Maleki, A. L. Kjoniksen and B. Nystrom, *Carbohydr Res*, 2007, **342**, 2776-2792.
156. K. De Boulle, R. Glogau, T. Kono, M. Nathan, A. Tezel, J. X. Roca-Martinez, S. Paliwal and D. Stroumpoulis, *Dermatol Surg*, 2013, **39**, 1758-1766.
157. S. Ibrahim, Q. K. Kang and A. Ramamurthi, *Journal of Biomedical Materials Research Part A*, 2010, **94A**, 355-370.
158. N. Shoham, A. L. Sasson, F.-H. Lin, D. Benayahu, R. Haj-Ali and A. Gefen, *Journal of the Mechanical Behavior of Biomedical Materials*, 2013, **28**, 320-331.
159. W. Y. Su, Y. C. Chen and F. H. Lin, *Acta Biomater*, 2010, **6**, 3044-3055.
160. P. Sedova, R. Buffa, S. Kettou, G. Huerta-Angeles, M. Hermannova, V. Leierova, D. Smejkalova, M. Moravcova and V. Velebny, *Carbohydr Res*, 2013, **371**, 8-15.
161. 2012.
162. A. Takahashi, Y. Suzuki, T. Suhara, K. Omichi, A. Shimizu, K. Hasegawa, N. Kokudo, S. Ohta and T. Ito, *Biomacromolecules*, 2013, **14**, 3581-3588.
163. V. Crescenzi, L. Cornelio, C. Di Meo, S. Nardecchia and R. Lamanna, *Biomacromolecules*, 2007, **8**, 1844-1850.
164. J. A. Burdick, C. Chung, X. Jia, M. A. Randolph and R. Langer, *Biomacromolecules*, 2005, **6**, 386-391.
165. M. H. M. Oudshoorn, R. Rissmann, J. A. Bouwstra and W. E. Hennink, *Polymer*, 2007, **48**, 1915-1920.
166. S. Suri and C. E. Schmidt, *Acta Biomater*, 2009, **5**, 2385-2397.
167. I. Bogdan Allemann and L. Baumann, *Clin Interv Aging*, 2008, **3**, 629-634.
168. D. W. McCarthy, M. T. Downing, D. R. Brigstock, M. H. Luquette, K. D. Brown, M. S. Abad and G. E. Besner, *Journal of Investigative Dermatology*, 1996, **106**, 49-56.
169. S. Colen, M. P. van den Bekerom, M. Mulier and D. Haverkamp, *BioDrugs*, 2012, **26**, 257-268.
170. A. Faga, G. Nicoletti, F. Brenta, S. Scevola, G. Abatangelo and P. Brun, *Int Wound J*, 2013, **10**, 329-335.
171. M. B. Brown and S. A. Jones, *J Eur Acad Dermatol Venereol*, 2005, **19**, 308-318.
172. M. R. Valojerdi, L. Karimian, P. E. Yazdi, M. A. Gilani, T. Madani and A. R. Baghestani, *J Assist Reprod Genet*, 2006, **23**, 207-212.
173. W. D. Hazlett, L. R. Meyer, T. E. Nasta, P. A. Mangan and V. C. Karande, *Fertil Steril*, 2008, **90**, 214-216.
174. I. Sall and G. Férard, *Polymer Degradation and Stability*, 2007, **92**, 915-919.
175. C. Longinotti, *Burns & Trauma*, 2014, **2**, 162 - 168.
176. W. L. Hynes and S. L. Walton, *FEMS Microbiol Lett*, 2000, **183**, 201-207.
177. R. Stern, G. Kogan, M. J. Jedrzejas and L. Soltes, *Biotechnol Adv*, 2007, **25**, 537-557.

178. M. Zheng, H. Zhang and D. Xu, *The Journal of Physical Chemistry B*, 2012, **116**, 11166-11172.
179. M. J. Jedrzejas, L. V. Mello, B. L. de Groot and S. Li, in *J Biol Chem*, United States, 2002, vol. 277, pp. 28287-28297.
180. L. V. Mello, B. L. de Groot, S. Li and M. J. Jedrzejas, *Journal of Biological Chemistry*, 2002, **277**, 36678-36688.
181. V. Ki and C. Rotstein, *The Canadian Journal of Infectious Diseases & Medical Microbiology*, 2008, **19**, 173-184.
182. L. Essers and K. Radebold, *Journal of Clinical Microbiology*, 1980, **12**, 641-643.
183. B. Delpech, P. Bertrand and C. Chauzy, *J Immunol Methods*, 1987, **104**, 223-229.
184. R. Stern and M. J. Jedrzejas, *Chemical reviews*, 2006, **106**, 818-839.
185. C. Schiraldi, A. La Gatta and M. De Rosa, in *Biopolymers*, ed. *M. Elnashar*, InTech, 2010.
186. N. A. Peppas, J. Z. Hilt, A. Khademhosseini and R. Langer, *Advanced Materials*, 2006, **18**, 1345-1360.
187. Y. Qiu and K. Park, *Advanced Drug Delivery Reviews*, 2012, **64, Supplement**, 49-60.
188. N. Sood, A. Bhardwaj, S. Mehta and A. Mehta, *Drug Deliv*, 2014, 1-23.
189. Y. Liu, W. Wang, J. Yang, C. Zhou and J. Sun, *Asian Journal of Pharmaceutical Sciences*, 2013, **8**, 159-167.
190. A. Car, P. Baumann, J. T. Duskey, M. Chami, N. Bruns and W. Meier, *Biomacromolecules*, 2014, **15**, 3235-3245.
191. C. Alvarez-Lorenzo, B. Blanco-Fernandez, A. M. Puga and A. Concheiro, *Advanced Drug Delivery Reviews*, 2013, **65**, 1148-1171.
192. S. S. Kwon, B. J. Kong and S. N. Park, *Eur J Pharm Biopharm*, 2015, **92**, 146 - 154.
193. B. D. Ratner, *Biomaterials science an introduction to materials in medicine*, Amsterdam ; Boston : Elsevier Academic Press, Amsterdam ; Boston, 2nd ed. edn., 2004.
194. C. Gong, T. Qi, X. Wei, Y. Qu, Q. Wu, F. Luo and Z. Qian, *Curr Med Chem*, 2013, **20**, 79-94.
195. L. Klouda and A. G. Mikos, *European Journal of Pharmaceutics and Biopharmaceutics*, 2008, **68**, 34-45.
196. A. Halperin and M. Kroger, *Langmuir*, 2012, **28**, 16623-16637.
197. M. Constantin, S. Bucatariu, V. Harabagiu, I. Popescu, P. Ascenzi and G. Fundueanu, *Eur J Pharm Sci*, 2014, **62**, 86-95.
198. M. Liang, T.-M. Yang, H.-P. Chang and Y.-M. Wang, *Reactive and Functional Polymers*, 2015, **86**, 27-36.
199. R. V. Ulijn, *Journal of Materials Chemistry*, 2006, **16**, 2217-2225.
200. J. A. Gustafson, R. A. Price, J. Frandsen, C. R. Henak, J. Cappello and H. Ghandehari, *Biomacromolecules*, 2013, **14**, 618-625.
201. P. D. Thornton, S. M. Reduwan Billah and N. R. Cameron, *Macromol Rapid Commun*, 2013, **34**, 257-262.
202. C. E. Brubaker and P. B. Messersmith, *Biomacromolecules*, 2011, **12**, 4326-4334.
203. A. A. Aimetti, M. W. Tibbitt and K. S. Anseth, *Biomacromolecules*, 2009, **10**, 1484-1489.
204. M. R. Lee, K. H. Baek, H. J. Jin, Y. G. Jung and I. Shin, *Angew Chem Int Ed Engl*, 2004, **43**, 1675-1678.
205. V. V. Komnatnyy, W. C. Chiang, T. Tolker-Nielsen, M. Givskov and T. E. Nielsen, *Angew Chem Int Ed Engl*, 2014, **53**, 439-441.
206. G. Baier, A. Cavallaro, K. Vasilev, V. Mailander, A. Musyanovych and K. Landfester, *Biomacromolecules*, 2013, **14**, 1103-1112.
207. S. Haas, N. Hain, M. Raoufi, S. Handschuh-Wang, T. Wang, X. Jiang and H. Schönherr, *Biomacromolecules*, 2015, **16**, 832-841.
208. Y. Wu, Y. Long, Q-L. Li, S. Han, J. Ma, Y-W. Yang, H. Guo, *ACS Appl Mater Interfaces*, 2015, **7**, 17255-17263.

Chapter 2 : Materials, General Methods and Experimental Theory

2.1. Materials

All bacterial strains used were part of a strain collection kindly available to the lab from Dr Ruth Massey, University of Bath, UK and Prof Mark Enright, University of Manchester, UK. Tryptic Soy Broth, Tryptic Soy Agar, Luria-Bertani Broth, Luria Bertani Agar, glycerol and microbiological agar were obtained from Sigma-Aldrich (Poole, Dorset, UK).

Magnesium sulphate, gelatin, Tris-HCl, PEG-8000 and carboxyfluorescein N-succinimidyl ester (CF-NSE) were all obtained from Sigma-Aldrich (Poole, Dorset, UK).

Ethylenediaminetetraacetic acid, (EDTA), TritonX-100, 4-(2-Hydroxyethyl) piperazine-1-ethanesulfonic acid, (HEPES), sodium chloride, cholesterol, 5(6)-carboxyfluorescein and 10,12-Tricosadiynoic acid, (TCDA) were all purchased from Sigma-Aldrich (Poole, Dorset, UK). Sodium hydroxide (NaOH) was obtained from Fisher Scientific (Loughborough, Leics., UK). All lipids (DPPC and DPPE) were obtained from Avanti Polar Lipids (Alabaster, AL, USA).

NIH-3T3 embryonic mouse fibroblasts were gained from the University of Munster. Dulbecco's Modified Eagle Medium (DMEM), fetal calf serum (FCS), L-glutamine, penicillin and streptomycin were purchased from Life Technologies, Germany.

2.2. General Methods

2.2.1. Preparation of bacteria

All bacterial isolates were acquired from the University of Bath Biology and Biochemistry Department as 15% glycerol stock solutions stored at -80 °C. Stabs of frozen stock were streaked onto tryptic soy (TS) or Luria Bertani (LB) agar plates (TS for *Staphylococci* and LB for all other species) and spread to form isolated colonies. Plates were grown overnight at 37 °C and afterwards stored at 4 °C until needed.

In all cases where *S. aureus* NE334 (hys-) was used, bacteria were cultured on plates and in TSB supplemented with 5 μg/mL erythromycin.

All *Staphylococcus* isolates were incubated in autoclaved TS broth (30 g in 1 L deionised water), whilst all other species were incubated in autoclaved LB broth (25 g in 1 L deionised water).

2.2.1.1. Bacterial live culture preparation

Bacterial overnight cultures were grown by inoculating 50 mL centrifuge tubes containing 10 mL sterile TS or LB broth with one isolated colony. Tubes were then incubated overnight at 37 °C with 200 rpm shaking; this resulted in cultures of approximately 10^9 cfu/mL. For live culture experiments, bacteria were subcultured to return growth to the lag phase. 10 µL overnight culture was added to 10 mL TS or LB broth and thoroughly mixed before use.

2.2.1.2. Bacterial supernatant preparation

Bacterial overnight cultures were centrifuged at 4000 rpm for 20 minutes to pellet whole cells. The supernatant was then removed and filter sterilised through 0.22 µm filters. Supernatant was stored at -20°C in aliquots until needed.

2.2.1.3. Bacterial concentration calculation

Concentration of bacteria in cultures was calculated through serial dilution. In brief, 100 µL of test bacterial solution was added to 900 µL sterile phosphate buffered saline (PBS) and then vortexed. This was then serially diluted by a factor of 10 until a final dilution of 10^{-8}. 10 µL of each sample dilution was then streaked onto an agar plate, and the plates incubated at 37 °C overnight. All dilutions were plated in triplicate.

Isolated bacterial colonies were then counted, with a dilution giving between 3 and 30 colonies per 10 µL most valid. Bacterial concentration in colony forming units per mL (cfu/mL) was calculated using the formula:

$$\text{cfu/mL original sample} = (1 / \text{dilution}) \times (\text{number of colonies}) \times 100 \qquad (2.1)$$

2.2.1.4. Bacterial strains used

S. aureus strains used in all studies, their origin and their SCCmec type can be seen in Table 2.1. '-'= not methicillin resistant strains.

Strain	Origin	SCCmec	Strain	Origin	SCCmec
15981	Spain	-	**FFP221**	Portugal	I
57/92	Germany	III	**Fin62305**	Finland	IV
8325-4	USA	-	**Fin76167**	Finland	IV
963Small	USA	II	**Fra97392**	France	IV
99ST10345	Ireland	II	**Germany131/98**	Germany	I
BC00691	unknown	unknown	**H399**	UK	-
BK1563	USA	II	**H40**	UK	-
Btn2164	UK	-	**H402**	UK	-
Btn2299	UK	-	**H417**	UK	-
C125	UK	-	**H42**	UK	-
C13	UK	-	**H560**	UK	-
C154	UK	-	**HT2001-634**	Australia	IV
C160	UK	-	**HT2002-0609**	unknown	unknown
C233	UK	-	**HT2002-0635**	Australia	IV
C253	UK	-	**HT2002-664**	UK	IV
C3	UK	-	**HT2004-0991**	Algeria	IV
C390	UK	-	**HT2005-0306**	France	IV
C427	UK	-	**JE2**	USA	IV
C49	UK	-	**KD12943**	UK	I
C56	UK	-	**LAC (USA 300)**	USA	IV
CAN6428-011	Canada	-	**MRSA 252**	UK	II
CAN6820-0616	Canada	-	**82MRSA**	Belgium	I
CDC12	USA	II	**MRSA378**	UK	unknown
CDC16	USA	II	**MRSA4JJ**	UK	unknown
CDC201078-USA700	USA	unknown	**MRSA707**	UK	unknown
CDC201114-USA300	USA	IV	**MRSA71**	UK	unknown
CDC960758-USA100	USA	II	**MSSA 476**	UK	-
CDC980193-USA300	USA	IV	**MU3**	Japan	II
COL	England	I	**MW2 (USA400)**	USA	IV
Cuba4005	Cuba	-	**N315**	Japan	II
Cuba4030	Cuba	-	**NE334 (hys-)**	USA	IV
D22	UK	-	**Newman**	UK	-

D279	UK	-	**Not116**	UK	-
D302	UK	-	**Not161**	UK	-
D316	UK	-	**Not266**	UK	-
D318	UK	-	**Not271**	UK	-
D470	UK	-	**Not290**	UK	-
D473	UK	-	**Not380**	UK	-
D49	UK	-	**Not98-53**	UK	IV
D508	UK	-	**RN4282 (TSST-1)**	USA	-
D551	UK	-	**RN6390B (agr+)**	UK	-
D97	UK	-	**RN6911 (agr-)**	UK	-
D98	UK	-	**ST239 µ1**	Turkey	III
E2260	Denmark	-	**ST239 µ2**	Turkey	III
EMRSA 13	UK	unknown	**ST239 µ20**	Turkey	III
EMRSA 15	UK	IV	**SwedenAO17934/97**	Sweden	IV
EMRSA 16	UK	II	**SwedenON408/99**	Sweden	III
EMRSA 9	UK	III	**SwedN8890/99**	Sweden	IV
EMRSA 6	UK	IV	**TW20**	England	III
H050960412	UK	-	**WBG8343**	Australia	IV
H118	UK	-	**WW2707/97**	Germany	IV
H129	unknown	unknown			

Table 2.1: *S. aureus* strains, origin and SCCmec type used in this investigation

Other non *S. aureus* species investigated can be seen in Table 2.2**.**

Species	**Strain**
E. coli	DH5α
P. aeruginosa	PAO1
S. epidermidis	12228
S. epidermidis	RP62A
S. kloosi	DSM 20676
S. xylosus	ATCC29971
S. lentus	ATCC 29070
S. vitulinus	ATCC51145
S. gallinarum	CCM3572
S. chromogenes	CCM3387
S. arlettae	N910-254
S. simulans	N920-197
S. sciuri subsp. Sciuri	ATCC29062

Table 2.2: Non *S. aureus* strains used in this investigation

2.2.1.5. PCR of bacterial DNA

Bacterial DNA was extracted by standard methods using a High Pure PCR Template Preparation Kit (Roche, UK). In brief, 200 µL bacterial overnight culture (10^8 cfu/mL) was centrifuged at 3,000 x g for 5 minutes, the supernatant removed and replaced with 200 µL PBS. 10 µL 5mg/mL lysostaphin was then added and the vials incubated at 37 °C for 30 minutes. 200 µL Binding Buffer and 40 µL proteinase K were then added, and the vial incubated at 70 °C for 10 minutes. 100 µL isopropanol was added and the solution filtered at 8,000 x g for 1 minute. To isolate bacterial DNA, the solution was washed sequentially with 500 µL Inhibitor Removal Solution, twice with 500 µL Wash Buffer and then finally with 200 µL Elution Buffer.

PCR of bacterial DNA was carried out by incubating the mix below on a standard PCR replication cycle, with an annealing temperature of 65 °C. Analysis of amplified *hysA* gene was then carried out using agarose gel electrophoresis in 2% agarose.

- 1 µL forward *hysA* primer
- 1 µL reverse *hysA* primer
- 10 µL PCR Master mix (*Taq* DNA polymerase, dNTPs, $MgCl_2$ and reaction buffers)
- 1 µL DNA
- 7 µL water

The specifications of forward and reverse primers are detailed in Table 2.3.

	Sequence (5' -> 3')	**M_w (g/mol)**	**T_m (°C)**
Forward primer (FW)	CCCGATGCTACAGAGAAAGAGGC	7091	64.2
Reverse primer (RV)	cccCTCTCCGTTGATACTTTCATAG	7518	63.0

Table 2.3: Specifications of forward and reverse primers used from *hysA* amplification

2.2.2. Preparation of bacteriophage

2.2.2.1. Bacteriophage extraction

Firstly, crude sewage samples were taken from Thames Water PLC (Luton, United Kingdom). In brief, 250 mL sewage/river water was added to 200 mL water containing 15 g TSB, 1 mM $MgSO_4$ and 1 mM $CaCl_2$. The solution was then inoculated with 5 mL per strain of turbid, actively growing culture of the intended host bacterium. This was then gently mixed and incubated at 37 °C overnight. A 10 mL aliquot of the solution was subsequently removed and NaCl dissolved to a concentration of 1 M to remove attached bacteriophage from bacteria. To kill any bacteria in the sample, 500 µL chloroform was added and the vial vortexed and centrifuged at 4,000 rpm for 30

minutes. The aqueous enrichment was removed, filter sterilised (0.22 µm filter) and stored at 4 °C until required.

2.2.2.2. Bacteriophage isolation

Specific bacteriophage strains were isolated from the purified lysate by plaque picking. 100 µL enrichment was added to 3 mL molten Tryptic Soy top agar (TS broth supplemented with 0.65 % w/v bacteriological agar) containing 100 µL host strain overnight culture. This was poured onto TS agar plates and incubated at 37 °C overnight to get isolated plaques. If isolated plaques were not seen, enrichment samples were diluted in SM buffer (100 mM NaCl, 8.5 mM $MgSO_4$, 50 mM Tris-HCl, 0.01 % gelatin) and the test repeated. Isolated plaques of one morphology were picked using pipette tips and resuspended in 300 µL SM buffer.

2.2.2.3. Bacteriophage propagation (double overlay method)

To make stock solutions of pure bacteriophage, 40 µL picked plaque solution was added to 3 mL TS top agar containing 100 µL host strain overnight culture; this was gently mixed and poured onto a TS agar plate. The plate was incubated overnight at 37 °C to form a confluent / semi-confluent lysis plate. 3 mL SM buffer was added to the plate to resuspend the grown bacteriophage, and the plate was incubated with gentle shaking at room temperature for 4 hours (30 rpm, Stuart gyratory rocker SSM4, Bibby Scientific Limited, UK). The resulting liquid was removed and 50 µL chloroform added per 1 mL to kill any live host bacteria. The vial was gently vortexed, centrifuged at 4,000 x g for 20 minutes and the supernatant filter sterilised to form pure stock solutions of one type of bacteriophage. Aliquots were stored at 4 °C until required.

2.2.2.4. Bacteriophage titration

The bacteriophage concentration of samples was calculated by serial dilution. 100 µL phage solution was added to 900 µL sterile SM buffer and vortexed. 100 µL of this solution was then serially diluted by factors of 10 until a dilution of 10^{-8}. Each sample was carried out in triplicate. 100 µL bacterial overnight culture was added to 3 mL molten TS top agar and the solution poured onto a TS agar plate. This was then allowed to set. 10 µL bacteriophage dilution was pipetted onto the set bacterial agar (Figure 2.1). After overnight incubation at 37 °C, plaques were counted and the original phage concentration per mL calculated. Plates containing 3 – 30 plaques were the most accurate for calculating titer.

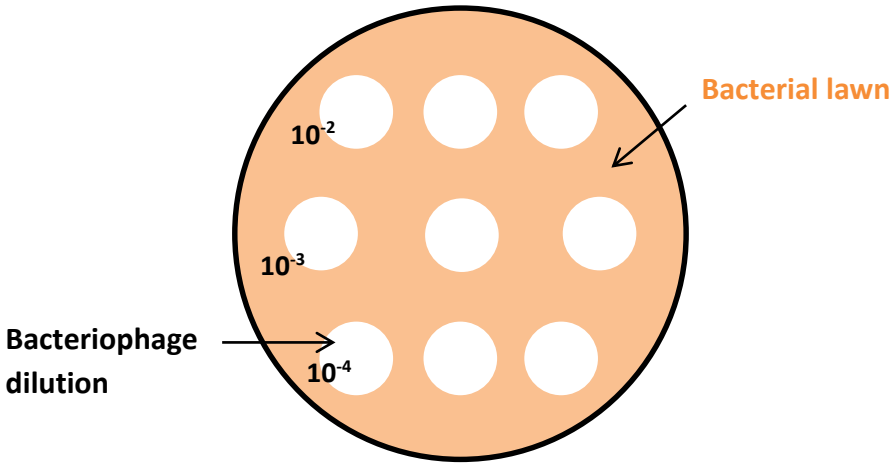

Figure 2.1: Bacteriophage dilution plating on bacterial lawn for concentration determination

The bacteriophage concentration in plaque forming units per mL (pfu/mL) was calculated using the formula:

pfu/mL original sample = (1/dilution) x (number of plaques) x 100 (2.2)

2.2.2.5. Bacteriophage sensitivity assay

The sensitivity of bacterial strains to bacteriophage was assessed using the streak test assay described by Cooper et al[1]. 10 µL bacterial overnight solution was streaked in a line over the surface of a petri dish and air dried at room temperature for 15 minutes. 10 µL bacteriophage solution (10^9 pfu/mL) was then spotted onto the line and allowed to dry at room temperature for 1 hour. Plates were incubated overnight at 37 °C and analysed for bacteriophage activity.

2.2.2.6. PEG purification of bacteriophage

In some cases, very pure bacteriophage samples were required containing no other media by-product contamination, e.g. globules of agar. To gain bacteriophage particles only in buffer, bacteriophage stock was precipitated with 100 mg PEG 8000 + 53.4 mg NaCl per mL. This was incubated at 4 °C for 1 hour and then centrifuged at 11,000 rpm for 10 minutes. The precipitate was resuspended in an equal volume of SM buffer. To remove bound bacteriophage from PEG 8000, an equal volume of chloroform was added to the suspension, gently vortexed and then centrifuged at 4,300 rpm for 15 minutes. The aqueous phase was recovered and stored at 4 °C until needed.

2.2.2.7. Fluorescent tagging of bacteriophage

PEG 8000 precipitated bacteriophage were resuspended in PBS solution and adjusted to pH 8.3 (with tris-acetate buffer). PEG 8000 was then removed with 1:1 addition of chloroform and the aqueous phase recovered. 7 mL phage suspension was incubated with 7 µL (5)-carboxyfluorescein N-succinimidyl ester (10 mg/mL in DMF) at room temperature in the dark for 24 hours. Tagged bacteriophage were then recovered again with PEG precipitation.

2.2.2.8. Incubation of bacteriophage with live bacterial culture

The assessment of bacteriophage infectivity with live bacterial culture was carried out using absorbance at 600 nm (OD_{600}) measurements in a SPECTROstar Omega plate reader. In all experiments, 10 µL bacterial overnight culture was added to 10 mL fresh growth medium (TSB or LB) and 200 µL added per well to a 96-well plate. The plate was then incubated with shaking at 37 °C in the plate reader for 2 hours until bacterial growth entered the exponential phase. After 2 hours, 50 µL per well of bacteriophage solution was added to the bacteria, and the plate was again incubated with shaking at 37 °C overnight. OD_{600} measurements were taken throughout incubation.

2.2.3. NIH-3T3 fibroblast cell culture

NIH-3T3 (mouse embryonic fibroblast cell line) cells were cultured in Dulbecco's modified Eagle's medium (DMEM) containing 10% fetal calf serum (FCS), 2 mM L-glutamine, 100 U/mL penicillin and 100 µg/mL streptomycin at 37 °C at 5% CO_2. Cells were incubated for 2 days and adjusted to 10^4 cells/mL for all experiments. Frozen low-passage number -150 °C stocks were created by standard protocols. 1 mL 2 day cell culture (10^6 cells/mL) in growth medium was mixed 1:1 with 80% FCS + 20% DMSO. 1 mL solution was added per vial; vials were cooled in isopropanol at -80 °C for 2 weeks, and then stored at -150 °C until needed.

To revive cells, 1 mL frozen stock solution was added to a 25 mL cell culture flask containing 15 mL DMEM (10% fetal calf serum (FCS), 2 mM L-glutamine, 100 U/mL penicillin and 100 µg/mL streptomycin). This was then incubated for 24 hours at 37 °C at 5% CO_2. After this time, growth medium was carefully removed, discarded and replaced with another 15 mL to remove dissolved DMSO. The flask was then incubated for a further 24 hours at 37 °C at 5% CO_2.

To passage cells, spent media was removed and cells were washed with 5 mL PBS. This was then removed, and 2.5 mL 0.05% trypsin/EDTA solution was added and the flask incubated at 37 °C at 5% CO_2 for 3 minutes. 10 mL growth medium was added and the flask tapped sharply to dislodge

cells. After all cells were dislodged, the solution was centrifuged at 4,000 rpm for 3 minutes. The supernatant was removed and the cells were then resuspended in 1 mL growth medium.

For all cell tests, 100 µL resuspended cells was added to 15 mL growth medium (10^4 cells/mL) and used directly. Cell counting was carried out using a hemocytometer.

2.2.4. Preparation of vesicles

2.2.4.1. Vesicle buffer solutions

Aqueous HEPES buffers were made up using Table 2.4 and Table 2.5. Compounds were dissolved in deionised water (18.2 MΩcm^{-1}) and left at 4 °C to solvate overnight. HEPES buffer was then autoclaved to sterilise.

Compound	Mass (mg)	Concentration (mM)
HEPES	1191	10
NaCl	3120	100
NaOH	112	5.6
EDTA	146.1	1

Table 2.4: Constituents of HEPES buffer

Compound	Mass (mg)	Concentration (mM)
HEPES	239	10
NaCl	59	10
NaOH	541	135
EDTA	29	97.5
5(6)-Carboxyfluorescein	1879	50

Table 2.5: Constituents of CF50 HEPES buffer

2.2.4.2. Giant Unilamellar Vesicle (GUV) preparation

GUVs were formed following the procedure outlined by Moscho et al [2]. In brief, the desired ratio of lipids was made up using 100 mM chloroform lipid stock solutions. 20 µL or this mixture was then added to a 50 mL round-bottomed flask containing 980 µL chloroform and 150 µL methanol. 6.5 mL of the aqueous phase (containing the desired molecules to encapsulated; namely 5(6)-carboxyfluorescein buffer or bacteriophage suspension) was then carefully added down the side of the round-bottomed flask. Organic solvent was then removed by rotary evaporation above the T_m of the main lipid for two minutes. The formation of an opalescent liquid indicated GUVs had been created in high concentration.

Purification of GUVs was not possible using standard NAP-25 columns as they were too large to pass through. Following Rotary Evaporation, 1 mL aliquots of the opalescent liquid were

centrifuged at 13,200 rpm for 5 minutes and the resulting pellet re-suspended in 1 mL HEPES buffer. This was then repeated a further 2 times and the vesicles stored at 4°C until needed.

2.2.4.3. Large Unilamellar Vesicle (LUV) preparation

100 nm LUVs were formed using the film hydration method. Lipid mixtures with a total volume of 300 µL were measured from 100 mM lipid stocks in chloroform into sintered glass vials. The organic solvent was then evaporated under N_2 for 10 minutes, resulting in a uniform lipid film. Once dry, 5 mL CF50 buffer was added to each vial and vials were incubated above the T_m at 55 °C for 10 minutes. After 10 minutes, vials were vortexed and subsequently put through 3 x freeze-thaw cycles to increase vesicle encapsulation volume. This resulted in the formation of multilamellar vesicles of varied diameter in high yield.

To form unilamellar vesicles of uniform diameter, vesicles were then extruded using a Liposofast™® LF-50 vesicle extruder. In short, the extruder was firstly set up with 2 x 100 nm pore extrusion membranes and pre-washed through with HEPES buffer. The vesicle solution was then passed through the extruder 3 times or until the solution became clear. All extrusion was carried out above the vesicle T_m.

Vesicle purification was carried out using illustra™ NAP-25 columns (#17-0852, GE Healthcare, Little Chalfont, Bucks., UK). Each column was drained and equilibrated with HEPES buffer. 2.5 mL vesicle solution was allowed to completely enter the gel bed and 3.5 mL HEPES buffer was then added. All eluent of a yellow/orange colour (last 3 mL after HEPES addition) was collected and vesicles were then stored at 4 °C until needed.

For those vesicles containing the cross-linking agent TCDA, vesicles were left overnight (before dilution) to equilibrate and then photolysed to crosslink the TCDA. 1 mL of vesicle solution was loaded into quartz cuvettes and placed into the middle of a UV CL1000 Crosslinker (254 nm) (Ultra Violet Products). Photolysis of vesicles was carried out at timer setting 1 (Approx. 6 seconds). Vesicles were then diluted 1:2 with HEPES buffer and stored at 4 °C until needed.

2.2.4.4. Incubation of vesicles with bacterial supernatant

Supernatant aliquots were thawed to room temperature and 50 µL added to 50 µL vesicle solution in a 96-well plate. Plates were then incubated at 37 °C with shaking and the fluorescence intensity measured over 2 hours using a Spectrophotometer.

2.2.5. Hydrogel swelling ratio

Hydrogel swelling studies were carried out by immersing 10 mm gel discs in PBS buffer. Discs were incubated in PBS overnight to achieve total swelling. After 18 hours discs were removed, blotted to remove excess buffer and weighed (W_s). They were then dried at 60 °C overnight until a constant weight was seen (W_d). The swelling ratio was then calculated using the equation below:

$$Swelling\ ratio = \frac{W_S - W_d}{W_d} \tag{2.3}$$

2.3. Instrumentation

Fourier Transform Infrared Spectroscopy (FTIR) was carried out on a Spectrum 100 FTIR fitted with a Universal ATR Accessory (PerkinElmer, USA), using SpectraSuite software to analyse spectra.

Nuclear Magnetic Resonance (NMR) spectra of polymer samples were taken on a 400 MHz Bruker Avance III NMR at approximately 10 mg/mL in D_2O. Spectra were then analysed using SpinWorks 3 software.

Two separate UV crosslinker setups were used depending on what item was to be crosslinked. For TCDA crosslinking in phospholipid vesicles, 1 mL of vesicle solution was loaded into a quartz cuvette and placed into the middle of a UV CL1000 Crosslinker (254 nm) (Ultra Violet Products). Crosslinking was carried out at timer setting 1 (Approx. 6 seconds). For crosslinking of photopolymerisable hyaluronic acid (HAMA), polymer pre-mix was incubated in a Dymax 5000 Flood curing system (400 W) for the desired time.

The size distribution of vesicles was analysed using a Zetasizer Nanoscale Dynamic Light Scatterer (DLS) (Malvern Instruments, Malvern, UK). Vesicle samples were diluted by F200 in HEPES buffer (5 µL vesicle solution in 995 µL buffer) and vortexed; they were then allowed to equilibrate for 10 minutes at the set temperature before measurement.

Absorbance and fluorescence measurements were taken using a SPECTROstar Omega (BMG Labtech, UK) microplate reader fitted with a UV/Vis spectrometer. Data measurement and analysis was carried out with Omega Data Analysis software and Origin Pro 8.

2.4. General Experimental Theory

2.4.1. Fluorescence Spectroscopy

Fluorescent molecules can be used as a useful tool for investigating the dynamics and responses of systems such as hydrogels and phospholipid vesicles. Dye molecules can be encapsulated into vesicles and are released when the phospholipid bilayer breaks, giving a colour or fluorescence change. When added to a hydrogel system, either through direct coupling or entrapment during crosslinking, fluorescent molecules can give a greater insight into hydrogel structure and diffusion properties, as well as potentially being involved in 'smart' triggered release. The phenomenon of fluorescence is described by the Jablonski diagram (Figure 2.2). Common non-toxic, stable dyes used in biological systems include calcein, rhodamine, fluorescein and Alexa Fluor® dyes.

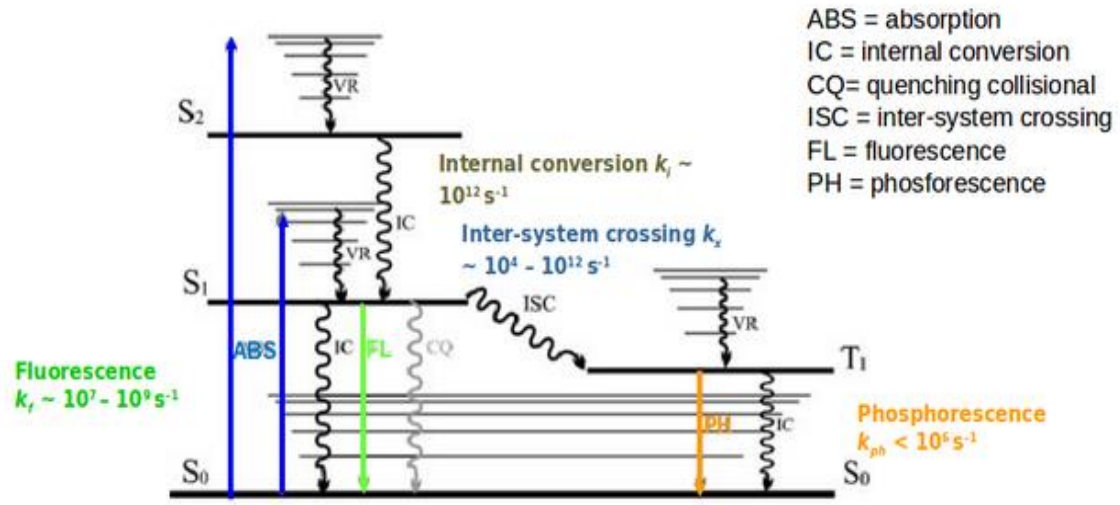

The Jablonski diagram describes the electronic states found in molecules and their subsequent excitations and transitions[3]. On absorption of a photon the molecule is excited from the S_0 vibrational ground state to the S_2 state. This then transfers to a lower S_1 state via intersystem crossing. From this state molecule emissions can go one of two ways. Fluorescence occurs when the molecule relaxes directly from the S_1 state to the S_0 state, emitting a photon. Phosphorescence occurs when the excited molecule has undergone intersystem crossing. This transfers the excited molecule to a state of higher spin multiplicity known as the triplet state. The molecule moves to the lowest triplet state T_1 and then returns to the ground state by

emitting a photon as phosphorescence. Fluorescence occurs on a much faster timescale compared to phosphorescence - ~10^{-8} seconds compared to ~1 second respectively.

The main fluorescent agent used in Chapter 3 was the fluorophore 5(6)-carboxyfluorescein, which has an absorption maximum at 480 nm and an emission maximum at 520 nm. It fluoresces at low concentrations but is known to self-quench above concentrations of 50 mM (Figure 2.3). The mechanism of self-quenching in 5(6)-carboxyfluorescein is not well understood but is thought to involve the formation of a non-fluorescent dimer complex.

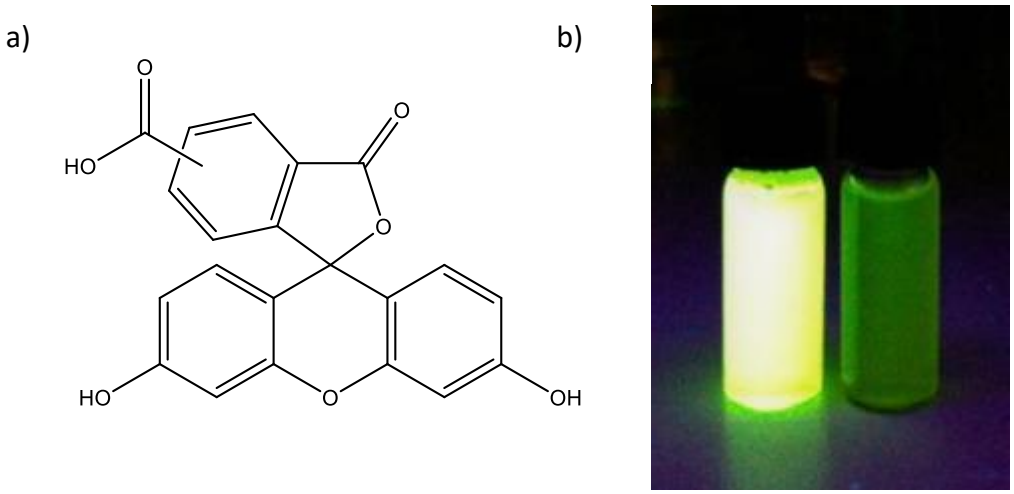

Figure 2.3: a) Chemical structure of 5(6)-carboxyfluorescein, b) Left vial containing unquenched fluorescing 5 mM dye, right vial containing quenched non-fluorescent 50 mM dye under UV light

2.4.2. UV-visible Spectroscopy

UV-visible spectroscopy refers to the investigation of the absorption of UV or visible light by molecules. It is a widely used technique for the analysis of transition elements, organic compounds and biological molecules. Absorbance is easily determined with the use of a spectrophotometer, by shining light through a sample and measuring the intensity change.

Different molecules are able to absorb radiation at different wavelengths, depending on their chemical structure and environment, resulting in different colours. On absorption, outer electrons (σ, π or lone pair electrons) are promoted from the ground state to the excited state. The π to π* transition will be focussed on here as it is the most common transition in organic and biological molecules, and its absorption occurs between 200 – 800 nm (the UV-visible region).

Π to π* transitions occur in molecules which contain unsaturated groups such as double bonds and aromatic rings. In protein molecules, absorption occurs at 280 nm due to tryptophan and phenylalanine amino acids (both aromatic). The more double bonds and conjugation present, the more coloured the compound; for example, the very deeply orange compound β-carotene contains an extensively conjugated π-system. Conjugation (where p-orbital overlap allows movement of delocalised electrons) is electronically favourable as it brings the HOMO and LUMO π orbitals closer together, lowering the amount of energy required to promote to the excited state.

UV-visible absorption can be described by the Beer-Lambert Law, which states that concentration, c, is directly proportional to the absorbance, A, where I_0 is the initial intensity, I is the transmitted intensity, ε is the molar absorptivity and *l* is the path length.

$$A = log_{10}\frac{I_0}{I} = \varepsilon\, l\, c \qquad (2.4)$$

In this work, absorbance measurements were used in two main ways. Firstly, bacteria are known to absorb at 600 nm, and so by measuring the absorbance at 600 nm over the bacterial growth cycle, bacterial concentration can be followed. Secondly, a number of colorimetric assays were used which either used a coloured stain or produced a colour change in the presence of a certain molecule. These included the Carbazole assay (pink/violet = 595 nm), the TNBS assay (orange = 340 nm), the MTT assay (violet = 570 nm) and the staining of bacterial biofilms with Crystal Violet stain (violet = 590 nm).

2.4.3. Microscopy

2.4.3.1. Light microscopy

Light microscopy involves shining white light through a sample at high magnitude in order to gain an image. The light is focussed with single or multiple lenses and has a resolution of between 100 µm and 0.1 µm. Imaging of eukaryotic and bacterial cells is ideal with light microscopy, as these organisms usually have sizes on this scale and it is non-invasive.

During this research, direct imaging of NIH-3T3 fibroblast cells was carried out using a Zeiss AxioCam ERc5s light microscope with no further sample preparation.

2.4.3.2. Fluorescence microscopy

Fluorescent microscopes use fluorescence of samples to create an image. Light of a certain wavelength is focussed onto a sample that has been previously stained with (or contains) a fluorescent compound. The compound is then exited and emits fluorescence of another

wavelength. This is then detected and an image can be formed. Images can either be purely fluorescence or can be combined with visible light images. This has been summarised in Figure 2.4.

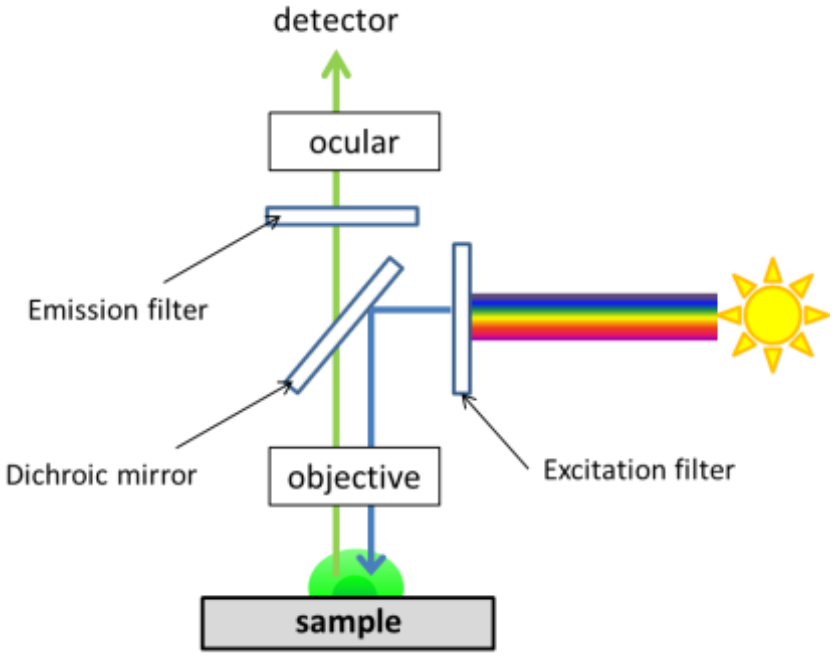

Figure 2.4: Schematic diagram of visible light excitation and emission in a fluorescent microscope

Unlike conventional optical microscopy, fluorescence microscopy gives images with high contrast and visibility. Various fluorescent dyes can be used which selectively bind to certain cell organelles. For example, in cell culture the fluorescent probe 4',6-diamidino-2-phenylindole (DAPI) selectively binds to cell DNA, showing only nuclei as blue in images. One problem sometimes found with fluorescence can be the possibility of photo-bleaching, where the fluorescent molecule is damaged over the course of excitation and fluorescence gradually fades.

2.4.3.3. Confocal Laser Scanning Microscopy (CLSM)

Confocal Laser Scanning Microscopy (CLSM) enables high resolution optical images of fluorescently stained samples to be taken on multiple depths. These can then be collated to form a 3D picture (z-stack). CLSM has a number of advantages over conventional fluorescence microscopy, notably that by using pinhole apertures extraneous light can be filtered out resulting in a sharper image.

CLSM is routinely used for high quality imaging of biological specimens taken from cell biology, microbiology and genetics. A Zeiss LSM510 META Confocal Microscope with LSM Image Browser

software was used in this research to image fluorescently tagged phospholipid vesicles in solution.

2.4.3.4. Scanning Electron Microscopy (SEM)

Scanning Electron Microscopy (SEM) is a high resolution imaging method which uses the interaction of high energy electron beams with conductive surfaces. Firstly, an electron beam is generated (usually from a tungsten filament cathode) and focussed using electromagnetic lenses. To form an image, the focussed electron beam is scanned across the sample under vacuum in a raster pattern. The electron beam excites electrons on the surface and emitted electrons are detected by a detector. By knowing the position of the sample that has been scanned and the intensity of emitted electrons, an image can be formed.

In order to create an image with SEM, the sample surface must be conductive. In biological or non-metallic samples which are not conductive, sputter coating of a thin metal layer (gold, platinum, chromium, etc.) is carried out during sample preparation.

SEM imaging of hydrogels was carried out with help from the University of Bath Microscopy and Analysis Suite. 2 x 2 mm hydrogel samples were firstly immersed in liquid nitrogen for 10 minutes to preserve structure and then freeze dried overnight. Samples were then sputter coated with gold using an Edwards S150B sputter coater. SEM images of hydrogels were taken under vacuum using a JEOL SEM6480LV SEM.

2.4.3.5. Transmission Electron Microscopy (TEM)

Transmission Electron Microscopy (TEM) again uses a high energy electron beam to image at a far higher resolution than traditional light microscopy. TEM can be used to image very small biological materials which range in size from 1 μm to 1 nm, such as viruses. Electrons are emitted at the top of the microscope within a high vacuum and the beam is focussed with electromagnetic lenses. The electron beam then passes through the specimen to a viewing screen below. Unscattered electrons that have passed through the sample appear as light areas, whereas electrons that have been scattered by the sample appear as dark areas.

In TEM, samples are normally negatively stained with heavy metals; frequently used stains include uranyl acetate, osmium tetroxide and phosphotungstic acid. The electron beam then interacts with these ions forming an image.

TEM imaging of bacteriophage was carried out with help from the University of Bath Microscopy and Analysis Suite. For sample preparation, glow discharge grids were firstly exposed to ozone

for 30 minutes to increase surface hydrophilicity. Each grid was then soaked in PEG precipitated bacteriophage stock (10^9 pfu/mL) for 1 minute to allow bacteriophage to adsorb. Excess bacteriophage solution was then removed by blotting the edge with filter paper, and the grids were then lightly washed with distilled water twice. One drop 1% uranyl acetate solution (pH 4) was added to each grid to negatively stain bacteriophage, and the excess was then blotted away. The grids were then left to dry overnight. Images were acquired using a Jeol JEM1200EXII TEM with Gatan Dualvision Digital Camera.

2.4.4. Dynamic Light Scattering (DLS)

Dynamic light scattering (DLS) is a technique used to calculate the size of nano to micro-sized particles such as proteins, polymers, colloids, micelles and vesicles in solution. It can also be used to investigate particle size distribution and zeta-potential.

DLS relies on the underlying Brownian motion of particles in solution to calculate size. A monochromatic laser is shone at the sample and light hits the moving particles, causing the beam to be scattered. This is known as Raleigh Scattering. If particles were stationary, the amount of scattered light would be constant, however as particles are constantly moving interference is seen. The change in wavelength of the scattered light in relation to time can be measured and is used to calculate the diffusion constant, D.

The hydrodynamic radius of spherical particles is calculated using the Stokes-Einstein equation:

$$D = \frac{k_B T}{6\pi\eta r} \tag{2.5}$$

where k_B is the Boltzmann constant, T is the temperature, η is the dynamic viscosity and r is the particle radius. It is important to note that the calculated particle radius is in fact the hydrodynamic radius, which includes a thin dipole layer of solvent molecules which surround the particle.

2.5. Polymerisation

Polymerisation has multiple and far-reaching applications in nearly every aspect of modern life, with polymers prevalent in the natural world, as well as the automotive industry, healthcare, coatings, adhesives, textiles and packaging. It involves the reaction of small molecules (monomers) to form long polymer chains or 3D networks; these can be formed from one or many types of monomer.

Polymer chains which contain only one type of monomer are known as homopolymers. When two or more different monomers are involved, copolymers are formed which exhibit varying configurations. The main configurations can be seen in Figure 2.5.

Random copolymers have a random arrangement of monomer units within the chain. Alternating polymers are more ordered with regularly alternating units. Block copolymers are made up of large blocks of each monomer and are predominantly formed using living polymerisation techniques such as ATRP, ROMP and RAFT. In recent years they have come under increased investigation due to their interesting phase separation and self-assembly properties[4, 5]. Finally, graft polymerisation results in branched copolymers where one polymer block is grafted to another polymer backbone.

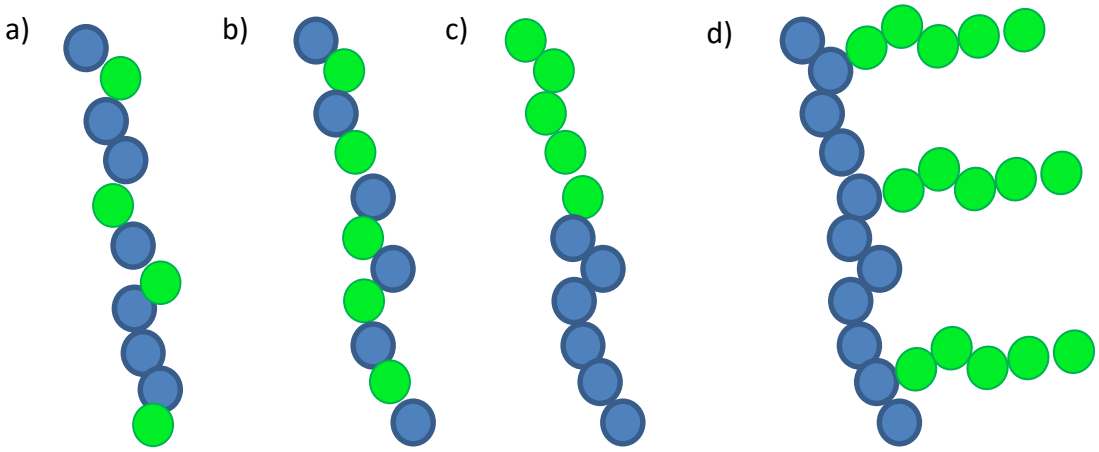

In bulk polymer matrices, two distinct physical phases can be present: the crystalline and amorphous forms. Crystalline structures form when polymers have a regular structure (homopolymers or alternating polymers) which can form highly ordered phases, for example, polyethylene, and isotactic polypropylene. Amorphous polymers have no crystalline structures but form randomly oriented structures with intertwined polymer.

Polymerisation can occur through chain growth or step growth reactions of monomer units. Chain growth polymerisation creates polymers with no by-product molecules formed, whereas in step growth polymerisation small molecules such as water or HCl are created as well as the growing polymer chain (Figure 2.6). In step growth polymerisation, monomer units are most commonly linked through ester, amide and carbonate linkages.

Radical, anionic, cationic and coordination polymerisation processes are all classed as chain growth polymerisations. In these cases, the monomer unit undergoes polymerisation by forming free radicals, carbocations, carbanions or organometallic complexes respectively, which then undergo a chain reaction to form polymers. For the purposes of this work, free radical polymerisation will be discussed in more detail in Section 2.6.

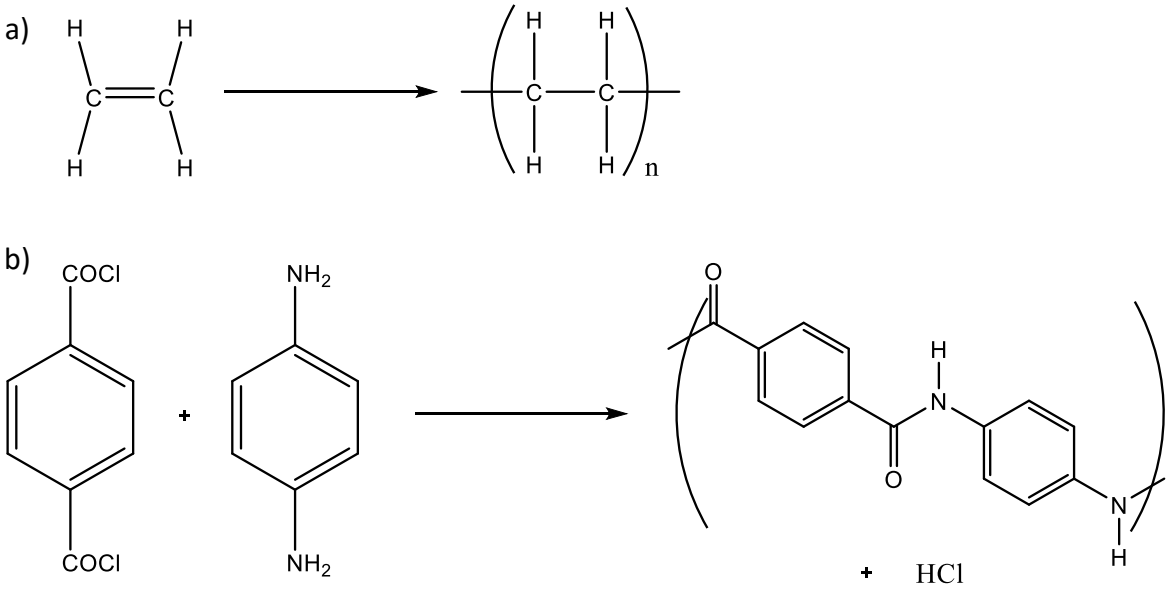

Figure 2.6: a) Chain growth polymerisation of ethene to form poly (ethene), b) Step growth polymerisation of 1, 4-phenylene diamine and 1, 4-benzenedicarbonyl chloride to form Kevlar™ and HCl by-product

Polymer molecular weight (and degree of polymerisation) determines the physical properties of the polymer in question. It can be described by the number average molecular mass, or the weight average molecular mass depending on the number or weight of repeating units. The two equations for number average, $\bar{M}_n$ and weight average, $\bar{M}_w$ molecular weight can be seen in below[6]. Where N_i is the number of molecules and M_i is the molecular weight.

$$\bar{M}_n = \frac{\sum N_i M_i}{\sum N_i} \qquad \bar{M}_w = \frac{\sum N_i {M_i}^2}{\sum N_i M_i} \qquad PDI = Đ = \frac{\bar{M}_w}{\bar{M}_n} \tag{2.6}$$

The ratio between $\bar{M}_w$and $\bar{M}_n$ is known as the (poly)-dispersity index (Đ), which gives an indication of the molecular weight range of polymer chains. The smaller the polydispersity, the narrower the molecular weight range. If all polymer chains have the same molecular weight, the system is described as monodisperse and has a polydispersity of one.

2.6. Principles of Radical Polymerisation

Free radical polymerisation is a chain growth addition polymerisation which creates polymers through the sequential addition of monomer to an active free radical centre at the chain end (suitable monomers consist of vinylic monomers). It is a successful method for large scale production of polymers; more than 70% vinyl polymers (polymers formed from vinylic monomers) have been industrially produced this way[7a]. Although relatively non-specific (e.g. it gives little control over polymer tacticity or polydispersity), it has a number of advantages over other methods as it forms polymers of a high molecular weight very quickly without the formation of by-products. The process occurs in four distinct steps: initiation, propagation, chain transfer and termination[7b].

2.6.1. Initiation

Initiation describes the initial production of radical species which go on to create the radical centres involved in polymerisation. Initiators are frequently small molecules which form radicals after decomposition with either heat or light. These include peroxides, azo compounds (AIBN), redox initiators and photoinitiators (peroxides and azo compounds can dissociate photolytically, as well as benzophenone based molecules).

After dissociation, the primary radical species reacts with a monomer unit, M, to form initiating radicals, which then go on to react with more monomer units in a chain reaction (Figure 2.7). Reaction mainly occurs in a "head-to-tail" orientation, from the least sterically hindered and most electronically favourable side of the monomer.

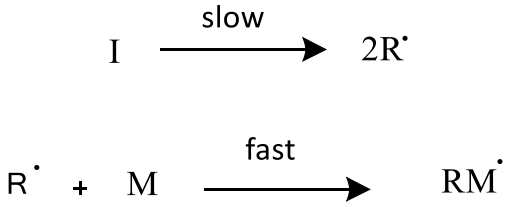

$$rate_{\ init} = \frac{d[R\cdot]}{dt} = 2fk_i[I]$$

Figure 2.7: Free radical initiation of monomer unit

Where k_i is the rate constant for initiator decomposition, f is initiator efficiency and [I] is initiator concentration.

Initiation is frequently not ideal; a number of side reactions, rearrangements and fragmentations can occur in competition with the ideal initiation seen in Figure 2.7. Initiator concentration (with

respect to monomer concentration) also governs polymer chain length; a high initiator concentration (compared to monomer concentration) eventually yields shorter chains, whilst a low initiator concentration gives longer chains.

2.6.2. Propagation

Propagation is the process in which polymers increase chain length by sequential addition of monomers (Figure 2.8). After the radical initiator has reacted with the monomer unit, the monomer radical sequentially attacks each new monomer (usually at bonds which stabilise the radical such as π-bonds), forming a new polymer repeating unit and a radical at a new position. This process will continue until there are no more monomers, or a termination event occurs.

$$RM_n^{\cdot} + M_1 \xrightarrow{k_p} RM_{n+1}^{\cdot} \qquad rate_{prop} = -\frac{d[M]}{dt} = k_p[M][RM_n \cdot]$$

Figure 2.8: Propagation of polymer chains in free radical polymerisation

Where k_p is the rate constant for chain propagation, [M] is monomer concentration and [M·] is monomer radical concentration.

Chain transfer is the side reaction to propagation, and is the transfer of a radical from a growing polymer chain either to a monomer, another radical species, another polymer or the solvent. This results in the formation of both a terminated polymer and a new radical species.

Chain transfer agents are small molecules that can be added to a polymerisation to induce chain transfer through abstraction of a hydrogen or halogen atom. In general, the addition of small amounts of these species forms polymers of reduced molecular weight and polydispersity. The most commonly used chain transfer agents are thiol derivatives and halocarbons because of their weak S-H and C-halogen bonds[8]

2.6.3. Termination

There are two main termination events which stop the polymerisation reaction: combination of two growing polymers (combination), or termination by disproportionation (Figure 2.9). In combination, two radical polymer chains combine together to form one long polymer chain linked with a σ-bond. In radical disproportionation, two radical polymer chains transfer a proton to form two separate non-radical products. The most common disproportionation reaction

occurs when a hydrogen atom is taken from one chain by another, forming one hydrogen-terminated and one double bond-terminated chain.

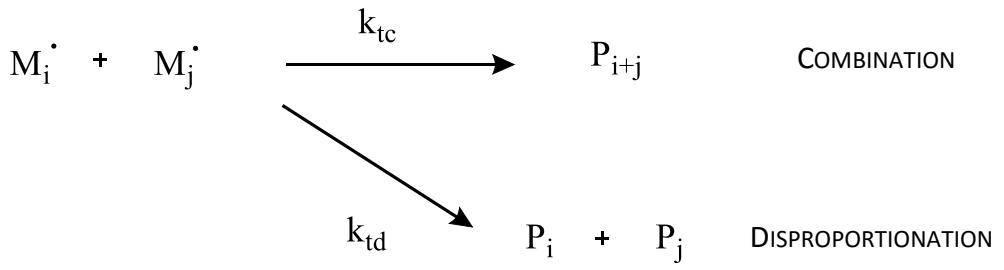

$$rate_{\ term} = -\frac{d[M\cdot]}{dt} = 2k_t[RM_n^{\cdot}]^2 \ where \quad k_t = k_{tc} + k_{td}$$

Figure 2.9: Combination and Disproportionation termination mechanisms in free radical polymerisations

Where k_t is the rate constant for chain termination, k_{tc} is the rate constant for combination termination, k_{td} is the rate constant for disproportionation termination and $[M^{\cdot}]$ is radical chain concentration.

Termination is the major disadvantage of free radical polymerisation compared to other processes. Because the reaction with radical chains is so fast, chains can react quickly and easily with other growing chains. This results in the formation of polymers with a very broad polydispersity and different molecular weights[7]. In order to overcome this, in recent years chemists have turned to controlled radical polymerisation techniques such as atom transfer radical polymerisation (ATRP)[9] and reversible addition-fragmentation chain transfer (RAFT)[10, 11], which give a very narrow relative polydispersity [12-15].

2.6.4. Kinetics of radical polymerisation

The rate equations for initiation, propagation and termination can be combined into a simplified rate equation by using the steady-state approximation. This assumes that during the reaction, the concentration of the intermediate species, $RM_n^{\cdot}$ concentration does not change significantly over time, therefore:

$$\frac{d[RM\cdot]}{dt} = 0 \qquad (2.7)$$

After an induction period, the rate of initiation and termination become equal:

$$2fk_i[I] = 2k_t[M_n^{\cdot}]^2 \quad (2.8)$$

which rearranges to:

$$[RM_n^{\cdot}] = \sqrt{\frac{fk_i[I]}{k_t}} \quad (2.9)$$

By substituting in the rate equation for propagation, we can get an equation for the overall loss of the initial monomer species:

$$rate_{\,prop} = -\frac{d[M]}{dt} = k_p[M]\sqrt{\frac{fk_i[I]}{k_t}} \quad (2.10)$$

which can simplify to Equation 2.11, where k is the overall rate constant for reaction:

$$rate_{\,prop} = k\sqrt{[I]}[M] \quad (2.11)$$

Therefore, by monitoring the monomer concentration over time, the general rate of reaction can be calculated.

2.6.5. Thermodynamics of radical polymerisation

In free radical polymerisation, polymerisation is favoured enthalpically (ΔH = negative), but disfavoured entropically (ΔS = negative). The reaction will take place provided that the change in Gibbs free energy (ΔG) is negative (Equation 2.12); in order for this to occur the enthalpy change must be large and negative, making the process exothermic.

$$\Delta G = \Delta H - T\Delta S < 0 \quad (2.12)$$

In general, the driving force of polymerisation is the enthalpy change, which in turn is dependent on a number of factors. These include the bond energy difference between the monomer and polymer (e.g. if the double bonds on the monomer or polymer are stabilised by resonance), steric effects and electronic effects. As temperature increases, the entropic contribution to the system becomes more important.

2.7. Principles of Hydrogel Chemistry

As mentioned earlier in Chapter 1, hydrogels are crosslinked polymer networks formed from natural or synthetic polymers which contain over 90% water. They can be highly hydrophilic, superabsorbent, biocompatible and non-toxic, as well as displaying similar structural and mechanical properties to human tissues. It is due to these reasons that in recent years, hydrogels have become widely used in biotechnology (e.g. in tissue engineering, wound dressings, medical devices and cell culture).

Hydrogels encompass a vast range of structures and chemistries, and so can be classified depending on varying parameters[16]:

- **Charge:** anionic, cationic, ampholytic or neutral
- **Preparation method:** homo-polymer networks, multi-polymer 'blended' networks, interpenetrating networks or copolymers
- **Chemical composition:** natural or synthetic polymers
- **Structure:** amorphous, semi-crystalline or supramolecular networks
- **Nature of crosslinks:** chemical hydrogels = covalent bonds, physical hydrogels = Van der Waals, molecular entanglements, metal complexes or hydrogen bonds

Either radiation (to induce a chain reaction) or chemical reaction can be used to crosslink polymers into networks. Radiation crosslinking is predominantly through UV irradiation, but can also be through X-rays, γ-rays or electron beams. With 'reactive' chemical crosslinking, small molecular weight molecules can be reacted with polymer chains to form di- or multi- crosslinks. An ideal crosslinked hydrogel structure can be seen in Figure 2.10.

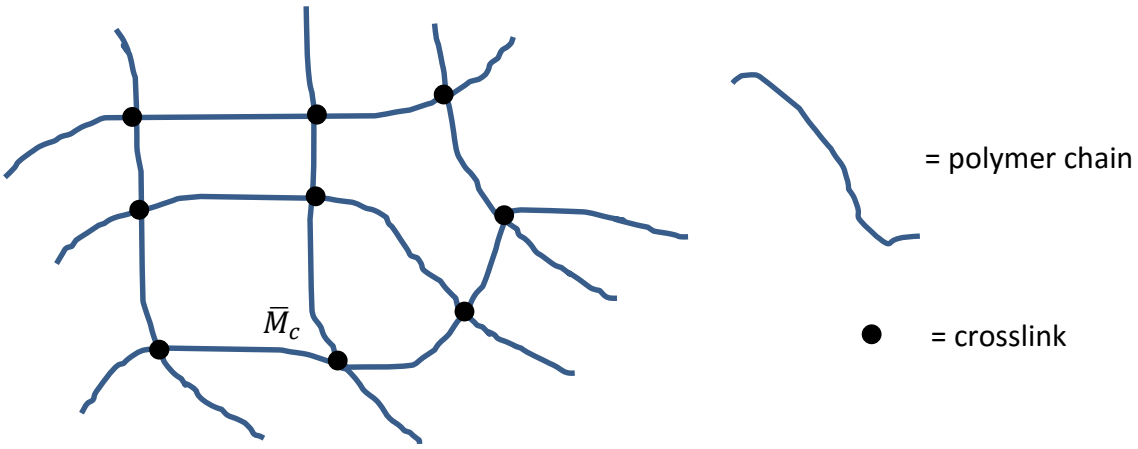

Figure 2.10: Structure of ideal crosslinked polymer network for use in hydrogels

Ideally, a crosslinked polymer network should comprise tetra-functional crosslinks with small size distribution of length between crosslinks, M_c. However, more commonly ideal behaviour is not seen and other crosslinked structures can be present. Polymer chains can be looped together or entangled, or there could be unreacted functionalities or dangling chain ends.

2.7.1. Rheology

The most common method of measuring the viscoelastic mechanical properties of hydrogels is through rheology, using dynamic mechanical analysis, DMA. Rheology is the science of deformation and flow of liquids and semi-solids in response to an applied force. In DMA, the hydrogel is clamped between two plates and a sinusoidal shear strain is applied to one side through rotation of one plate; on the other side, a detector measures stress imparted to the hydrogel (Figure 2.11) [17, 18]. Shear force is a force applied to a sample parallel to the surface.

From this measurement, two important parameters can be calculated: the shear storage (elastic) modulus, G', and the shear loss (viscous) modulus, G'' [16, 19, 20]. In general, G' describes the elasticity and G'' describes the viscosity of the material and energy lost as heat.

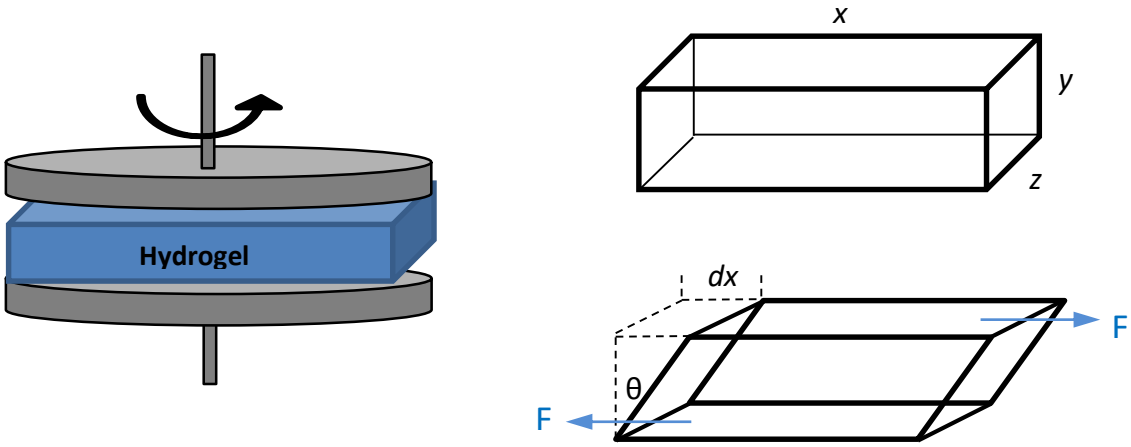

On initial testing of the sample, the material is subjected to sinusoidal strain, described by Equation (2.13), where γ_0 is the shear strain amplitude and ω is the oscillation frequency:

$$\gamma = \gamma_0 \sin(\omega t) \tag{2.13}$$

On interaction with the sample, the wave becomes out of phase with the strain applied by a phase angle, δ, due to additional interactions (viscous and elastic) with the hydrogel. For shear

stress, this can be described by the equation below, where σ is the shear stress and G* is the shear modulus:

$$\sigma = G^*(\omega)\,\gamma_0 \sin(\omega t + \delta) \tag{2.14}$$

If we separate this into an "in-phase" and "out-of-phase" component, and if we define:

$$G'(\omega) = G^* \cos(\delta) \tag{2.15}$$

$$G''(\omega) = G^* \sin(\delta) \tag{2.16}$$

Then, we can obtain an equation to describe G' (the elastic modulus) and G'' (the viscous modulus):

$$\sigma = \gamma_0 \left(G'(\omega) \sin(\omega t) + G''(\omega) \cos(\omega t)\right) \tag{2.17}$$

The ratio of the energy lost to the energy stored by the hydrogel during the plate rotation is described by the loss tangent:

$$\tan\delta = \frac{G''}{G'} \tag{2.18}$$

In general, the technique provides a good indication of the viscoelastic properties of a hydrogel; however for the purposes of this work, rheology of hydrogels was not investigated in detail.

2.7.2. Swelling

The swelling ratio of a hydrogel in a certain solvent can give valuable information on its structure, density and diffusion properties. The most widely used method of investigating the internal structure of a hydrogel is the use of the Flory-Rehner equation[21]. Florey-Rehner analysis assumes the hydrogel structure to be a neutral and tetra-functionally crosslinked network. Although the theory is quite general, it offers a useful indication of hydrogel properties in an ideal system.

A simplified version of the Flory-Rehner equation can be seen in Equation (2.19)[22], where Q_v is the volumetric swelling ratio, $\bar{v}$ is the specific volume of the dry polymer, $\overline{M}_c$is the average molecular weight between crosslinks, V_1 is the molar volume of solvent and χ is the Flory polymer solvent interaction parameter.

$$Q_v^{\frac{5}{3}} \cong \frac{\bar{v}\,\overline{M}_c}{V_1}\left(\frac{1}{2} - \chi\right) \tag{2.19}$$

The volumetric swelling ratio can be determined by standard swelling measurements described in Section 2.2.5. Subsequently, a number of hydrogel characteristics can be calculated. The effective crosslink density of the hydrogel, V_e, can be calculated using Equation (2.20), where ρ_p is the polymer density:

$$V_e = \frac{\rho_p}{\bar{M}_c} \tag{2.20}$$

The mesh size of the hydrogel, ξ, can also be calculated using Equation (2.21), where $\bar{r}^2$ is the distance between crosslinks:

$$\xi = Q_v^{\frac{1}{3}} \sqrt{\bar{r}^{\,2}} \tag{2.21}$$

By knowing these parameters, the diffusional characteristics of the hydrogel can be understood. A highly swelling hydrogel would have a large pore size, giving faster diffusion, whereas in low swelling hydrogels which are denser, slow diffusion is seen.

2.8. Enzyme kinetics

Enzymes are biological protein molecules which act as extremely specific catalysts in chemical reactions by lowering the activation energy of the system. Here, enzymes act as mediators in the transition state between reactants (in the case of enzymes they are referred to as substrates) and products. The enzyme lowers the activation energy, ΔE, required to overcome the energy barrier of the reaction (Figure 2.12).

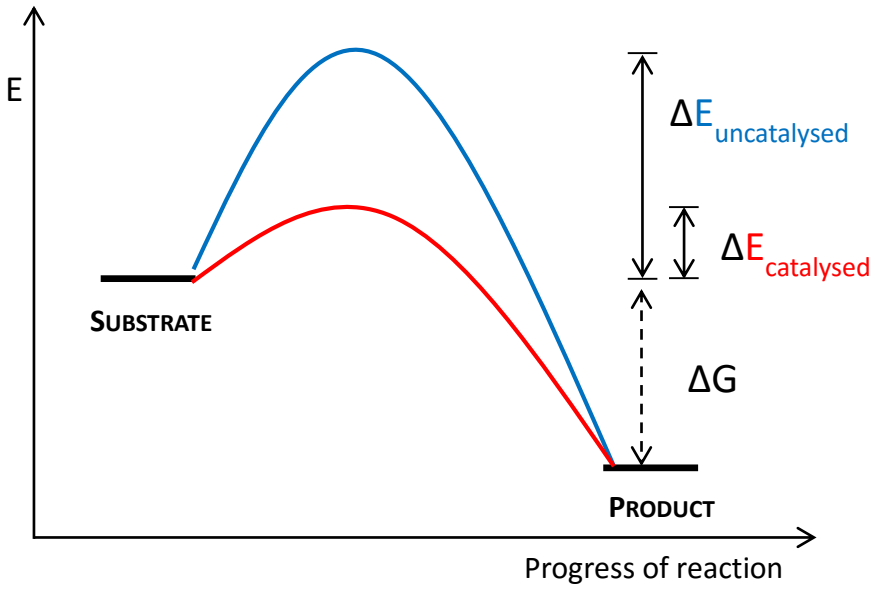

In the

presence of no enzyme, substrate molecules would not have enough thermal energy to overcome this energy barrier to be converted to products. In general, catalysts increase the rate of reaction from substrate to product.

A schematic of substrate interaction with an enzyme, and subsequent reaction can be seen in Figure 2.13. On initial reaction, the enzyme and the substrate bind in equilibrium with the enzyme-substrate complex. The enzyme contains a region, known as the active site, which is completely complementary to the substrate in size, shape and chemical composition. On binding the enzyme-substrate complex lowers the activation energy and promotes the rapid conversion to products.

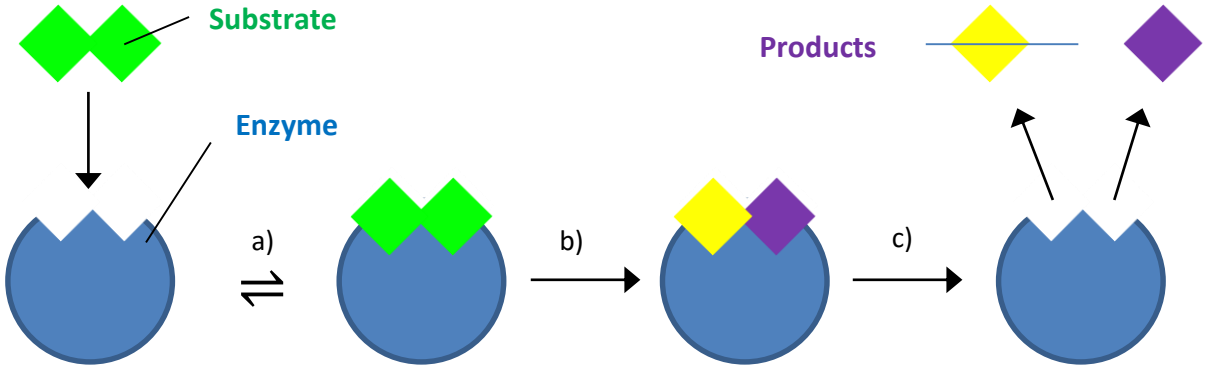

The enzyme-substrate reaction can be described by the Equation (2.22), where E is the enzyme, S is substrate, ES is the enzyme-substrate complex and P is the products:

$$E + S \underset{k_{-1}}{\overset{k_1}{\rightleftharpoons}} \mathrm{ES} \xrightarrow{k_2} E + P \tag{2.22}$$

Taking this equation, the overall rate of reaction can be calculated as described by the Michaelis-Menten equation, where v is the rate, V_{max} is the maximum rate achieved by the system, and K_M is the Michaelis constant:

$$v = \frac{V_{max}\,[S]}{K_M + [S]} \tag{2.23}$$

where:

$$K_M = \frac{k_{-1} + k_2}{k_1}$$

(2.24)

Experimentally, V_{max} is calculated by measuring the rate of product formation versus the substrate concentration. The V_{max} is the maximum rate at which substrate is converted too product. K_M is then subsequently calculated as ½ V_{max}.

In general, the Michaelis-Menten constant can describe two properties of an ES system. Firstly, K_M is the concentration of substrate at which half the active sites are filled. In this way the concentration of substrate needed for significant catalysis to occur can be calculated. Also, K_M gives an indication of how well an enzyme is able to complex with a substrate. If the rate of product formation, $k_{2,}$ is much smaller than the rate of dissociation, k_{-1}, K_M is equal to the dissociation constant for the ES complex. Here, if K_M is high, binding is weak, and if K_M is low, a strong binding is seen.

2.9. References

1. C. J. Cooper, S. P. Denyer and J. Y. Maillard, *J Appl Microbiol*, 2011, **110**, 631-640.
2. A. Moscho, O. Orwar, D. T. Chiu, B. P. Modi and R. N. Zare, *Proc Natl Acad Sci U S A*, 1996, **93**, 11443-11447.
3. in *"Flourescence" Photonics For Life Research Group , Federico II University of Naples*, 2015.
4. H. Hu, M. Gopinadhan and C. O. Osuji, *Soft Matter*, 2014, **10**, 3867-3889.
5. S. B. Darling, *Progress in Polymer Science*, 2007, **32**, 1152-1204.
6. M. P. Stevens, *Polymer chemistry : an introduction*, New York ; Oxford : Oxford University Press, New York ; Oxford, 3rd ed. edn., 1999.
7. a) H. S. Bisht and A. K. Chatterjee, *Journal of Macromolecular Science, Part C*, 2001, **41**, 139-173 b) R. J. Young, P. A. Lovell, *Introduction to Polymers*, 3rd Edition, CRC Press, USA, 2011.
8. C. Henríquez, C. Bueno, E. A. Lissi and M. V. Encinas, *Polymer*, 2003, **44**, 5559-5561.
9. K. Matyjaszewski, *Macromolecules*, 2012, **45**, 4015-4039.
10. D. J. Keddie, G. Moad, E. Rizzardo and S. H. Thang, *Macromolecules*, 2012, **45**, 5321-5342.
11. J. Chiefari, Y. K. Chong, F. Ercole, J. Krstina, J. Jeffery, T. P. T. Le, R. T. A. Mayadunne, G. F. Meijs, C. L. Moad, G. Moad, E. Rizzardo and S. H. Thang, *Macromolecules*, 1998, **31**, 5559-5562.
12. G. Moad, E. Rizzardo and S. H. Thang, *Australian Journal of Chemistry*, 2005, **58**, 379-410.
13. W. A. Braunecker and K. Matyjaszewski, *Progress in Polymer Science*, 2007, **32**, 93-146.
14. O. W. Webster, *Science*, 1991, **251**, 887-893.
15. K. Fukuda, R. Enomoto, K. Ishihara, Y. Morishima and S.-I. Yusa, *Polymers*, 2014, **6**, 846-859.
16. R. Barbucci, *Hydrogels: Physical Properties and Applications*, Springer-Verlag, Milan, Italy, 2009.

17. K. S. Anseth, C. N. Bowman and L. Brannon-Peppas, *Biomaterials*, 1996, **17**, 1647-1657.
18. J. M. G. Cowie and V. Arrighi, *Polymers: Chemistry and Physics of Modern Materials*, CRC Press, 3 edn., 2007.
19. D. S. Jones, *International Journal of Pharmaceutics*, 1999, **179**, 167-178.
20. D. S. Jones, Y. Tian, O. Abu-Diak and G. P. Andrews, *Advanced Drug Delivery Reviews*, 2012, **64**, 440-448.
21. P. J. Flory, *Principles of Polymer Chemistry*, Cornell University Press, USA, 1953.
22. J. Baier Leach, K. A. Bivens, C. W. Patrick, Jr. and C. E. Schmidt, *Biotechnol Bioeng*, 2003, **82**, 578-589.

Chapter 3 : Preliminary work – Bacteriophage encapsulation into GUVs

3.1. Introduction

The initial preliminary work on this project focussed on the use of phospholipid vesicles for triggered release. In recent years, vesicles (formed from either phospholipids or more commonly amphiphilic block copolymers) have been used to encapsulate a range of biologically active molecules including peptides, enzymes, viruses, antimicrobials and drugs[1-4], as well as in imaging.

As previously mentioned in Chapter 1, when growing, bacteria secrete a number of small molecule virulence factors into their surrounding environment. The structure of the phospholipid bilayer of vesicles is very similar to that of the cell membrane, giving them very similar responses to these virulence factors[5].Previous research within the group has investigated how *S. aureus* and *P. aeruginosa* virulence factors cause triggered release of dye and antimicrobial molecules from phospholipid vesicles (Figure 3.1) [6].

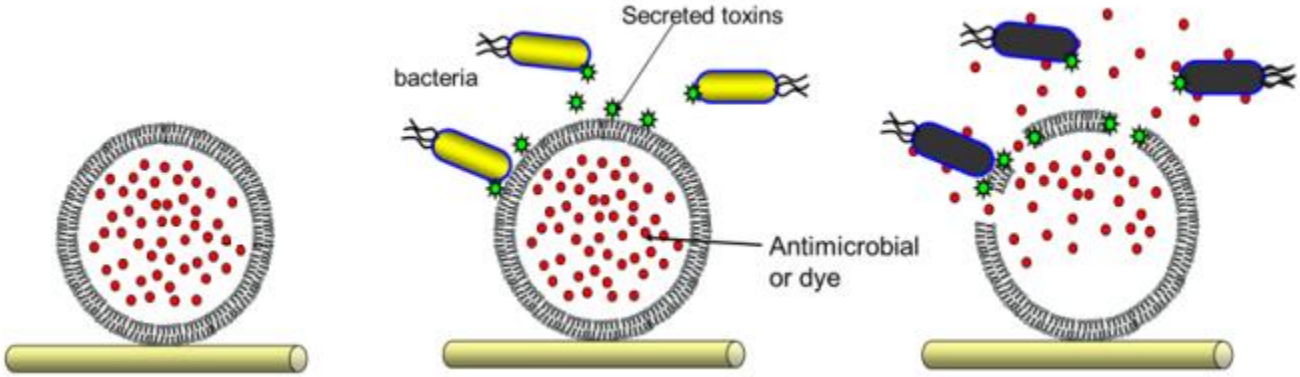

Figure 3.1: Schematic of antimicrobial or dye filled vesicles which become degraded by bacterial virulence factors, leading to the killing of bacteria or the release of dye molecules

As bacteria grow, these small molecules are able to degrade the phospholipid bilayer of the vesicle in the same way as with cell membranes. This causes the vesicle to burst, and depending on what is encapsulated inside the vesicle, a different response is seen. If vesicles contain encapsulated self-quenched fluorescent dye such as 5(6)-carboxyfluorescein, the dye will be released into the surrounding environment and diluted, allowing it to fluoresce. This can be seen as a fluorescent glow under UV light. If antibiotics or other antimicrobials are encapsulated, triggered killing is seen. In the presence of toxic bacteria, the antimicrobials are released and go

on to kill the surrounding bacteria. In non-toxic species, the vesicles remain intact and no killing is seen.

Triggered breakdown of vesicles (and subsequent cargo release) is understood to be due to secreted δ-toxin in *S. aureus* and rhamnolipids in *P. aeruginosa*[7, 8]. δ-toxin is a potent, low molecular weight peptide which causes cell (and vesicle) damage through insertion into the cell membrane phospholipid bilayer. On insertion, the protein forms pore-like barrel structures in the membrane, allowing efflux of water and ions. At higher concentrations the peptide is also thought to cause solubilisation of the membrane in a similar way to surfactant[9, 10]. Rhamnolipids, on the other hand, are rhamnose based glycolipid biosurfactants which solubilise the phospholipid cell membrane[11].

The aim of this chapter was to encapsulate bacteriophage into phospholipid vesicles to create a system which gives triggered release by bacterial virulence factors. In the presence of pathogenic bacteria, the vesicles would become lysed and bacteriophage would be released into the system (killing infecting bacteria). When there is no infection, or the bacteria present are not pathogenic, no vesicle lysis is seen and so bacteriophage are not released. In this way, the constant release of therapeutic is prevented, lowering the selection pressure on bacteria to become resistant. Because of the highly aqueous nature of the vesicles, in order to remain active the vesicles would then be embedded into a hydrogel matrix.

3.2. Preliminary Results and Discussion

Proof of concept was carried out using LUVs previously researched by the group. 100 nm phospholipid LUVs (size verified with DLS) containing DPPC, DPPE, cholesterol and the crosslinker TCDA were formed containing 50 mM 5(6)-carboxyfluorescein. These vesicles were then incubated with bacterial supernatant of pathogenic strains (*S. aureus* RN6390B, lac and MSSA 476 and *P. aeruginosa* PAO1) and non-pathogenic strains (*S. aureus* RN9611 and *E. coli* DH5α), as well as positive and negative controls (the surfactant Triton X100 and buffer).

As seen in Figure 3.2, in the presence of surfactant or pathogenic bacteria, the vesicles become lysed and a fluorescent switch-on was seen. In the presence of non-pathogenic bacteria, no fluorescent response was seen, implying the vesicles were not lysed. From these results we could show that vesicles were able to give triggered release of encapsulated molecules *only* in the presence of pathogenic bacteria and Triton X100 surfactant.

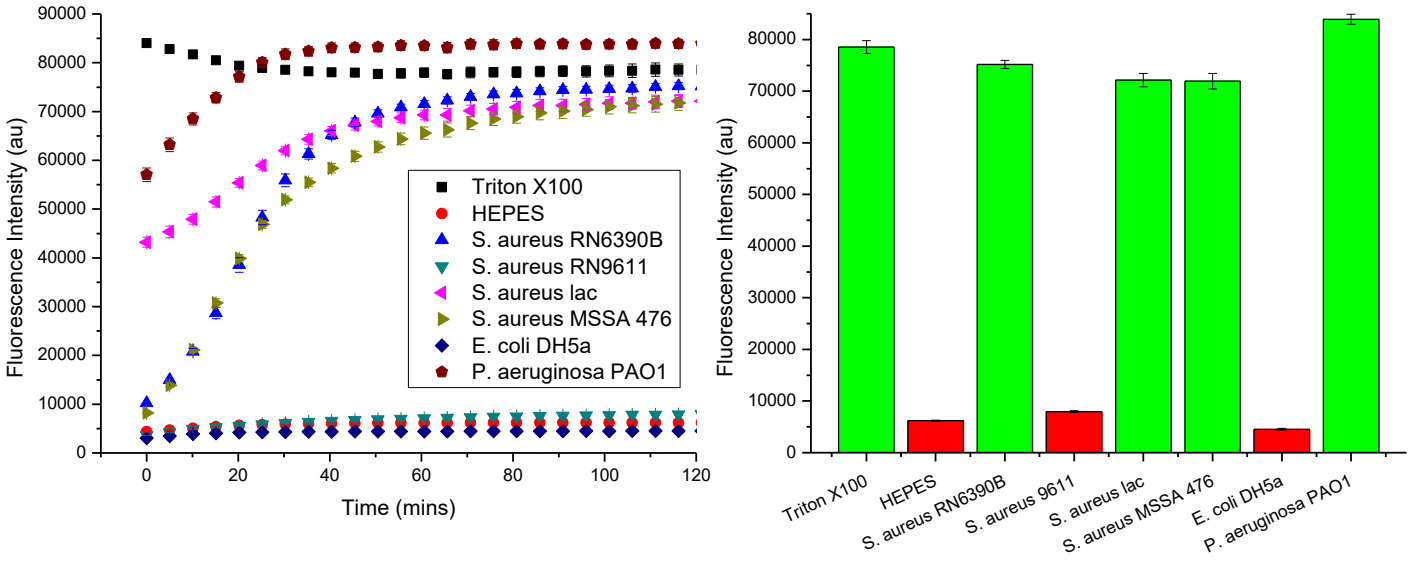

Figure 3.2: (left) Fluorescence intensity of 5(6) carboxyfluorescein vesicles incubated with bacterial supernatant over 2 hours, (right) Endpoint fluorescence intensity after 2 hours

With this in mind, it was initially proposed to use this selective lysis of vesicles by bacterial virulence factors to create a vesicular system for triggered release of the bacteriophage. The vesicles would provide a stable, aqueous environment to protect the bacteriophage, and on lysis by secreted virulence factors, bacteriophage would be released into the system to infect and kill bacteria. Some investigations have been previously carried out into bacteriophage encapsulation by other researchers, however none had used phospholipid vesicles, and none had reported triggered release[12, 13].

Here, the extruded 100 nm LUVs used for the majority of previous research were unsuitable, as they were too small; instead Giant Unilamellar Vesicles (GUVs) formed by rotary evaporation were used which generally have a diameter of over 1 µm[14, 15]. GUVs were initially formed containing 80% DPPC 20% cholesterol encapsulating 5(6)-carboxyfluorescein and then imaged using confocal microscopy (Figure 3.3).

Because GUVs are relatively heavy, they were able to sink down onto the bottom of the glass coverslip; 3D confocal images of these were then formed using z-stacks. The majority of GUVs formed were approximately 1 µm in diameter; however some of up to 10 µm were apparent. Although fluorescence microscopy did give an idea of the size distribution, it did not allow further investigation of vesicle structure, e.g. lamellarity. Also many vesicles appeared aggregated and non-spherical in shape.

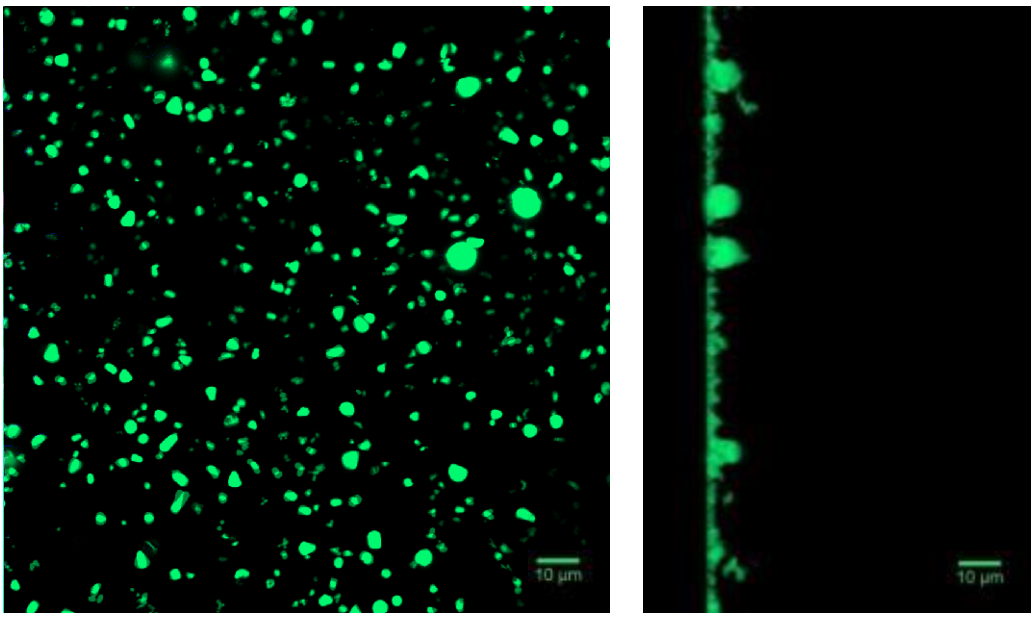

Figure 3.3: Confocal microscopy images of DPPC GUVs containing 5 mM 5(6)-carboxyfluorescein (left) from the z direction and (right) from the x direction

The phospholipid bilayer was then doped with Texas Red labelled phospholipid DHPE in order to visualise the lipid bilayer in more detail. Vesicles with this were formed with encapsulated of 5 mM 5(6)-carboxyfluorescein and then imaged using confocal microscopy (Figure 3.4).

As expected, the Texas Red labelled DHPE (excitation = 595 nm, emission = 613 nm) aggregated into the phospholipid bilayer, allowing the GUV bilayer to be seen. Under excitation, the Texas Red emits a red colour only from the phospholipid membrane. Under excitation at 488 nm however, the encapsulated 5(6)-carboxyfluorescein is seen emitting a green colour from the vesicle inside.

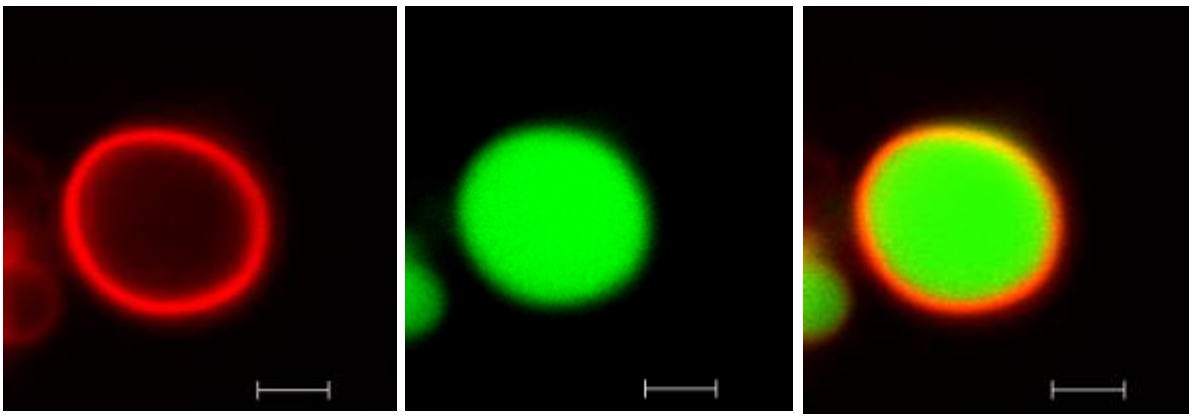

In general, the imaging showed that GUVs could successfully be formed using rotary evaporation; however this technique formed vesicles with a broad size distribution with little control over vesicle lamellarity or shape. Also, the concentration of GUVs formed was very low and the majority of GUVs imaged were small and aggregated. Despite this, the majority of vesicles formed had a diameter of approximately 1 µm, which was sufficient for bacteriophage encapsulation.

GUVs containing self-quenched 50 mM 5(6)-carboxyfluorescein were then incubated with bacterial supernatant in a similar way to LUVs (Figure 3.5).

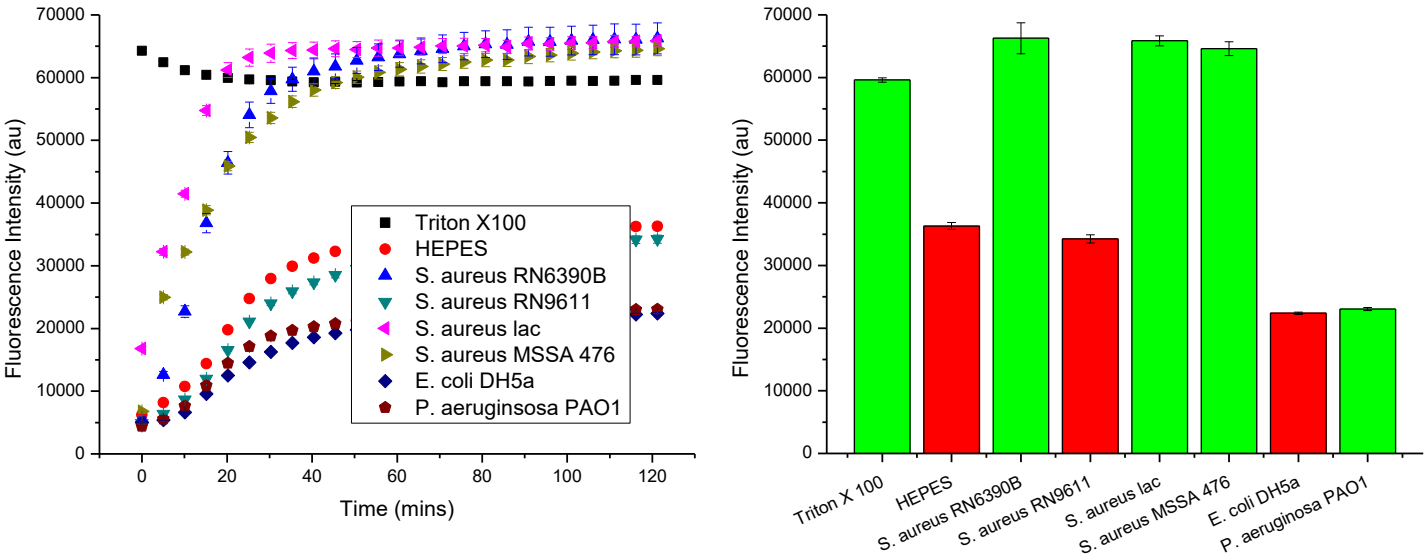

Figure 3.5: (left) Fluorescence intensity of 5(6) carboxyfluorescein GUVs incubated with bacterial supernatant over 2 hours, (right) Endpoint fluorescence intensity after 2 hours

After two hours incubation, GUVs generally exhibited the same response to LUVs, with pathogenic strains showing a higher fluorescent response than non-pathogenic strains or buffer solution. However, far higher background fluorescence was seen, with negative controls exhibiting approximately 10 times more fluorescence intensity than with LUVs; this implied either poor vesicle purification or inherent vesicle instability in solution. Also, the GUVs were not responsive to *P. aeruginosa* PAO1, a strain that secretes rhamnolipid virulence factors which were earlier shown to break down LUVs (Figure 3.2).

As the bacteriophage used was not active against *P. aeruginosa*, this was not necessarily an issue, so GUVs containing encapsulated Bacteriophage K were still investigated. GUVs were found to be successfully purified by centrifugation, as the viral particles did not sediment

compared to GUVs. The bacteriophage were also stable in the elevated temperatures seen during rotary evaporation, as well as being stable in the presence of the organic solvents (chloroform and methanol) used to dissolve the phospholipids. As now a fluorescent marker was not incorporated into the GUVs, lysis was followed using absorbance of bacteria at 600 nm. When incubated with bacteriophage GUVs, bacterial virulence factors would again lyse the vesicle, but this time bacteriophage would be released and a drop in absorbance would be seen as bacteria are lysed.

Here, bacteriophage GUVs were incubated with two *S. aureus* strains which were both sensitive to Bacteriophage K (data shown in Chapter 4), however they had differing abilities to lyse GUVs. *S. aureus* MSSA 476 was used as a strain sensitive to Bacteriophage K, and able to lyse vesicles, whereas *S. aureus* RN9611 was sensitive to Bacteriophage K but unable to lyse vesicles compared to positive and negative controls in 5(6)-carboxyfluorescein GUVs.

With bacterial strains which were sensitive to Bacteriophage K, killing should only be seen in strains which are also able to lyse vesicles (if bacteriophage have been efficiently encapsulated into GUVs). With strains which do not lyse GUVs (e.g. RN9611) but are still sensitive to bacteriophage, normal growth should be seen. If normal growth is seen, in all cases the bacteriophage concentration was too low to cause significant bacterial killing; this would either be due to the reaction conditions killing bacteriophage, or GUVs not being encapsulated inside GUVs in a high enough concentration. Overnight incubation results can be seen in Figure 3.6.

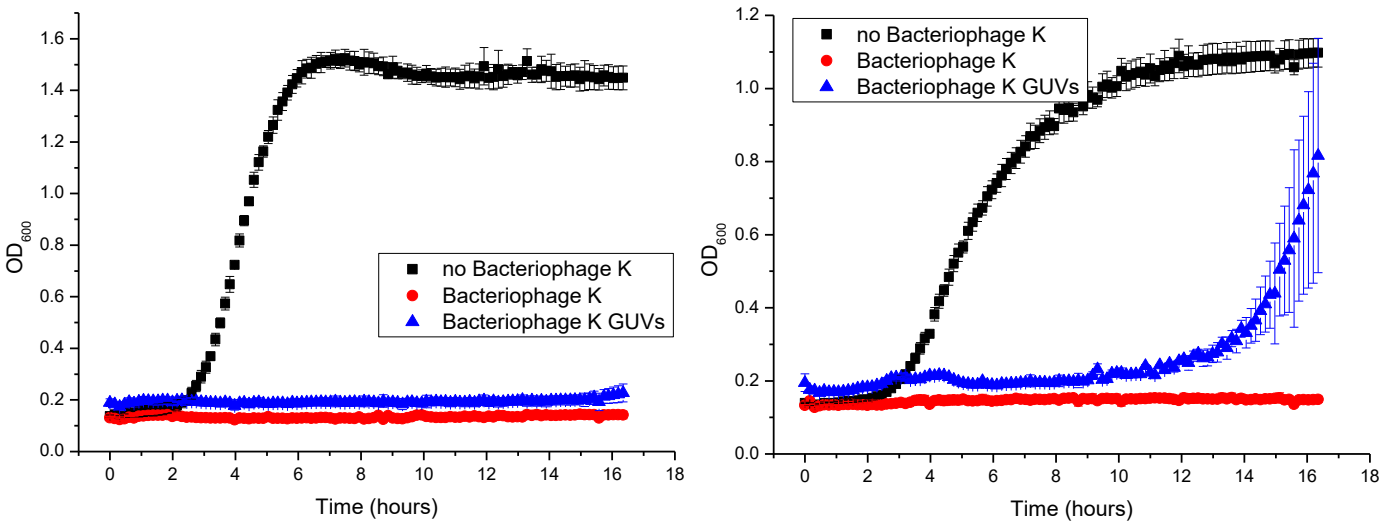

Figure 3.6: (left) *S. aureus* MSSA 476 and (right) *S. aureus* RN9611 incubated with GUVs containing Bacteriophage K

In *S. aureus* MSSA 476 normal responses to Bacteriophage K and Bacteriophage K GUVs were seen, with bacterial lysis in all cases. With *S. aureus* RN9611 however, again bacterial lysis was seen in all cases; a small re-emergence in growth apparent after approximately 12 hours growth can be attributed to bacterial mutation and subsequent resistance to bacteriophage occurring.

From the results of live culture experiments, no triggered release was seen; instead killing was seen in both *S. aureus* species. To assess why this occurred, bacteriophage were tagged with a fluorescent label. By imaging the bacteriophage GUVs using fluorescence confocal microscopy, we could ascertain if bacteriophage were assembling inside the vesicles or in the phospholipid bilayer.

Fluorescent tagging of bacteriophage was carried out by reacting amine groups on the bacteriophage capsid head (predominantly arginine and lysine) with fluorescent labels. 5-carboxyfluorescein N-succinimidyl ester (CF-NSE) and fluorescein isothiocyanate (FITC) were investigated, with CF-NSE the most successful (Figure 3.7).[16, 17]

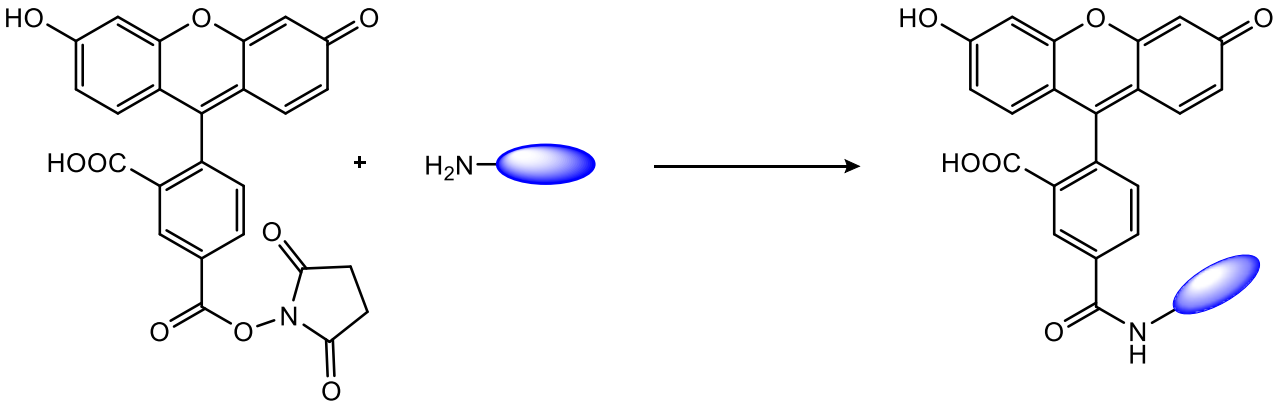

Figure 3.7: Reaction scheme for the fluorescent tagging of bacteriophage capsid primary amines with (5)-carboxyfluorescein N-succinimidyl ester

After purification, the successful tagging of bacteriophage was confirmed using spectroscopy, with the maximum intensity in the emission spectrum of the dye shifting by approximately 10 nm to a lower wavelength (Figure 3.8). This is known as hypsochromic (blue) shift and occurs when the fluorophore is in a different chemical environment, implying attachment to the capsid head.

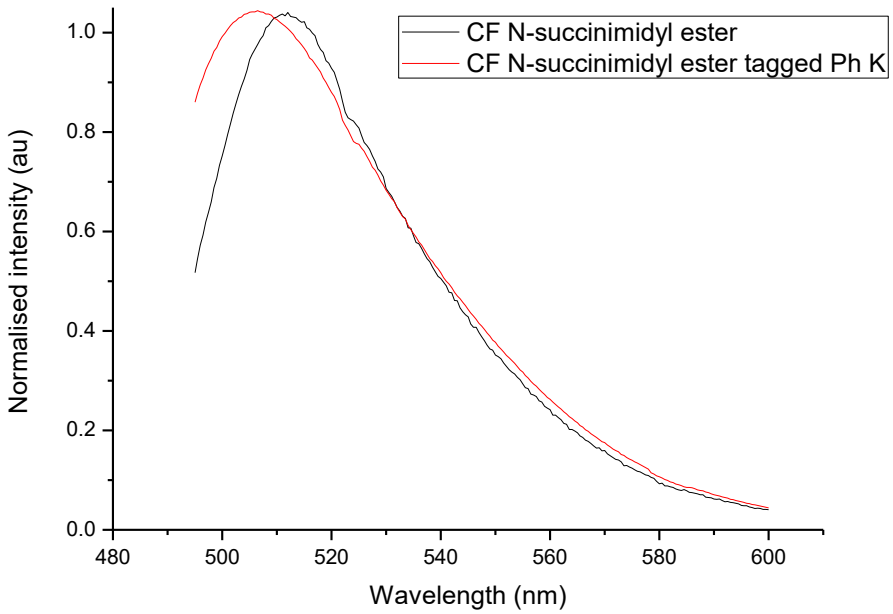

Figure 3.8: Emission spectra of pure 5-carboxyfluorescein N-succinimidyl ester and 5-carboxyfluorescein N-succinimidyl ester tagged Bacteriophage K

The tagged bacteriophage were encapsulated into GUVs through rotary evaporation. Texas Red labelled DHPE was also added in order to label the phospholipid bilayer. Confocal images of the vesicles can be seen in Figure 3.9, where separate images of the labelled phospholipid (a) and bacteriophage (b), as well as combined together in one vesicle (c) are shown.

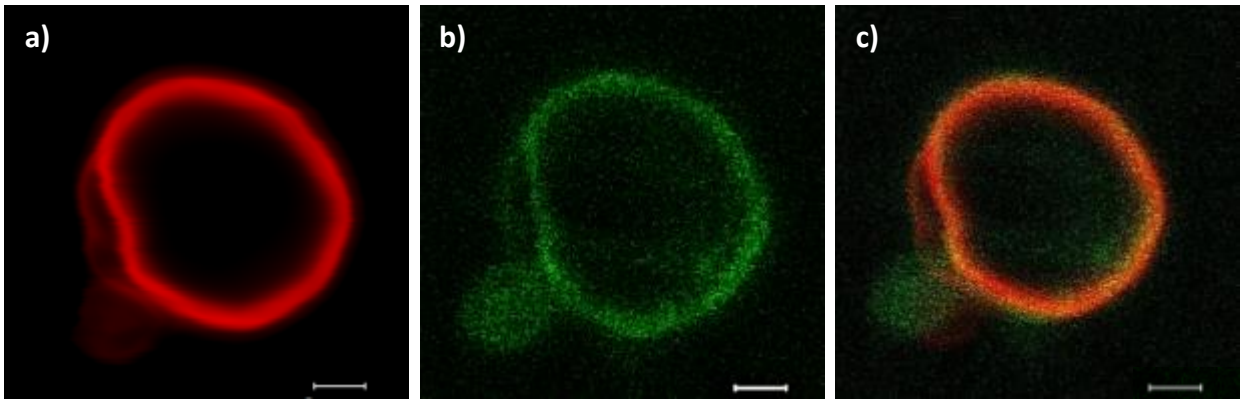

Spherical GUVs could be visualised under confocal microscopy by exciting the Texas Red dye at 543 nm, as seen in image a) in Figure 3.9. When a 488 nm excitation was then used, the carboxyfluorescein labelled bacteriophage could also now be seen (image b), showing where the

bacteriophage in the GUVs could be found. This showed that when formed into GUVs, the bacteriophage aggregated into the phospholipid layer instead of selectively being encapsulated. This could be confirmed by overlaying both images (image c)), where both the phospholipid bilayer and the bacteriophage were in exactly the same position. This meant that on incubation with bacteria, bacteriophage were still free to infect and lyse bacteria as they were not separated by the GUV membrane. Therefore triggered release was not possible by using GUVs.

A recent paper by Nieth et al has similarly described their investigations into the encapsulation of bacteriophage into phospholipid vesicles, however in their case vesicles were used to facilitate cellular uptake[21]. They encountered similar issues with a lack of control of vesicle size and lamellarity, and only gained significant bacteriophage loading by using alternative techniques (gel-assisted GUV formation or inverse emulsion). These techniques could be utilised in order to form more homogenous, stable and highly loaded bacteriophage GUVs for future work.

3.3. Conclusions

Although previous work by the group has used LUVs successfully for triggered release of antimicrobial and dye molecules, this was not as effective when used with GUVs. The sensitivity to bacterial virulence factors and long term stability (data not shown) were significantly poorer than in LUV systems. Also, the control of size distribution and lamellarity was not as precise. On the formation of bacteriophage GUVs, bacteriophage were found to associate with the phospholipid bilayer instead of being isolated in the inside of the vesicle.

Because of this, it was decided not to continue with the use of vesicular systems for the triggered release mechanism of bacteriophage. Instead, an alternative approach was chosen using hydrogels. Hydrogels offer a number of advantages over vesicle systems. Firstly, as described in Chapter 1, they are already commonly and effectively used in medical devices to aid and promote would healing; they can additionally be incorporated with a variety of additives to extend this further. The highly aqueous environment is generally robust to drying effects compared to vesicles, which lyse and collapse on even small amounts of drying. Lastly, hydrogels give excellent control of structure and reactivity through tailoring polymer chemistry. The stabilisation of bacteriophage by hydrogel matrices and their subsequent therapeutic use has been reported; however these systems did not incorporate a triggered release mechanism but instead gave sustained release [18-20].

In recent years, the use of hydrogels for triggered release by using external stimuli-responsive chemistry has been widely reported (e.g. pH, temperature, enzymes or light), as discussed in Chapter 1. In a bacterial system, the use of enzyme-sensitive hydrogels is apt and has been shown to give triggered release, and so the triggered release of bacteriophage from a hydrogel system by bacterial virulence factors was subsequently investigated.

3.4. References

1. X. Xu, A. Costa and D. J. Burgess, *Pharm Res*, 2012, **29**, 1919-1931.
2. K. Kita and C. Dittrich, *Expert Opin Drug Deliv*, 2011, **8**, 329-342.
3. J. Gubernator, *Expert Opin Drug Deliv*, 2011, **8**, 565-580.
4. R. P. Brinkhuis, F. P. J. T. Rutjes and J. C. M. van Hest, *Polymer Chemistry*, 2011, **2**, 1449-1462.
5. T. G. Pomorski, T. Nylander and M. Cárdenas, *Advances in Colloid and Interface Science*, 2014, **205**, 207-220.
6. J. Zhou, A. L. Loftus, G. Mulley and A. T. A. Jenkins, *Journal of the American Chemical Society*, 2010, **132**, 6566-6570.
7. M. Laabei, W. D. Jamieson, S. E. Lewis, S. P. Diggle and A. T. Jenkins, *Appl Microbiol Biotechnol*, 2014, **98**, 7199-7209.
8. M. Laabei, W. D. Jamieson, R. C. Massey and A. T. Jenkins, *PLoS One*, 2014, **9**, e87270.
9. J. Verdon, N. Girardin, C. Lacombe, J. M. Berjeaud and Y. Hechard, *Peptides*, 2009, **30**, 817-823.
10. A. Pokorny, E. M. Kilelee, D. Wu and P. F. Almeida, *Biophys J*, 2008, **95**, 4748-4755.
11. R. M. Maier and G. Soberon-Chavez, *Appl Microbiol Biotechnol*, 2000, **54**, 625-633.
12. U. Puapermpoonsiri, J. Spencer and C. F. van der Walle, *Eur J Pharm Biopharm*, 2009, **72**, 26-33.
13. Y. Ma, J. C. Pacan, Q. Wang, Y. Xu, X. Huang, A. Korenevsky and P. M. Sabour, *Appl Environ Microbiol*, 2008, **74**, 4799-4805.
14. P. Walde, K. Cosentino, H. Engel and P. Stano, *Chembiochem*, 2010, **11**, 848-865.
15. A. Moscho, O. Orwar, D. T. Chiu, B. P. Modi and R. N. Zare, *Proc Natl Acad Sci U S A*, 1996, **93**, 11443-11447.
16. D. L. Jaye, C. M. Geigerman, R. E. Fuller, A. Akyildiz and C. A. Parkos, *J Immunol Methods*, 2004, **295**, 119-127.
17. V. Gitis, A. Adin, A. Nasser, J. Gun and O. Lev, *Water Research*, 2002, **36**, 4227-4234.
18. V. M. Balcao, A. R. Moreira, C. G. Moutinho, M. V. Chaud, M. Tubino and M. M. Vila, *Enzyme Microb Technol*, 2013, **53**, 55-69.
19. E. M. Ryan, S. P. Gorman, R. F. Donnelly and B. F. Gilmore, *Journal of Pharmacy and Pharmacology*, 2011, **63**, 1253-1264.
20. K. Markoishvili, G. Tsitlanadze, R. Katsarava, J. G. Morris, Jr. and A. Sulakvelidze, *Int J Dermatol*, 2002, **41**, 453-458.
21. A. Nieth, C. Versaux, S. Barnert, R. Süss, W. Römer, *Expert Opin. Drug Deliv*. 2015, **12**, 1411 – 1424.

Chapter 4 : Diffusion and Infection of Bacteriophage K in Hydrogel Matrices

4.1. Introduction

This chapter will focus on the immobilisation and diffusion of bacteriophage in hydrogel matrices. Hydrogels offer a protective environment for bacteriophage which prevents virion desiccation during storage, as well as creating an optimal environment for wound healing. The aim of this chapter was to investigate a range of hydrogel formulations which could be used in wound dressings, and to determine if incorporation of bacteriophage affected activity. Bacteriophage will passively diffuse out of the hydrogel and, on bacterial infection, will be able to cause bacterial lysis (Figure 4.1).

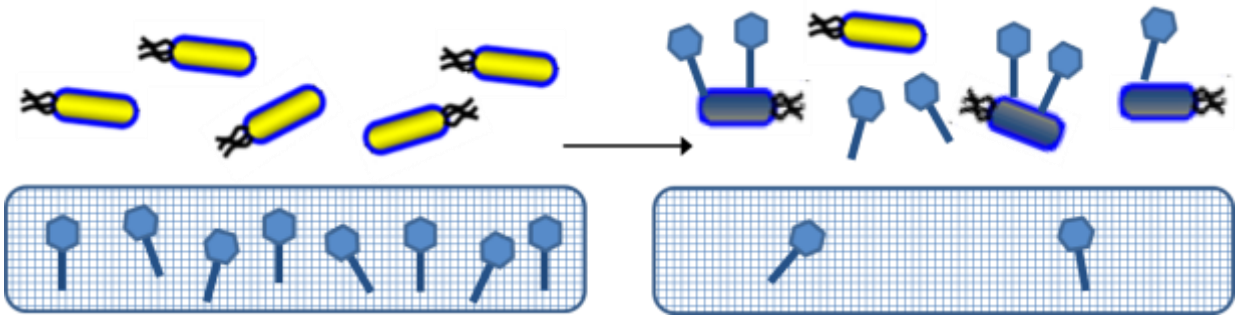

Figure 4.1: Bacteriophage diffusion out of hydrogel matrices and subsequent killing of bacteria

Bacteriophage are the natural viral predators of bacteria, and so due to the increase in resistance to conventional antibiotics, have in recent years become a promising alternative to antibiotics. The relative advantages and disadvantages of bacteriophage therapy have been discussed in detail in Chapter 1. In order to be a viable therapeutic for use in medical applications a bacteriophage must exhibit certain characteristics. Firstly, bacteriophage can be extremely specific, with one bacteriophage sometimes only able to infect one bacterial strain; in this case a bacteriophage with a wide host range (able to infect multiple strains of a species) must be chosen, or used in combination with other phages with different infectivity in a phage cocktail. Secondly, the bacteriophage must contain no toxic elements within its genome[1]; this can be remedied through whole genome sequencing. The bacteriophage must also have good temperature stability in order to survive use at room and body temperature, as well as during incorporation into hydrogel matrices. In this investigation Bacteriophage K was used as it is

known to have a broad host range against *S. aureus*, as well as having its entire genome sequenced.

In this system, the hydrogel layer will not only provide a highly hydrated environment which prevents bacteriophage desiccation, but it will also be a semi-solid framework that retains bacteriophage whilst still allowing bacteriophage diffusion and infection at a slowed rate. This can be achieved by altering the crosslinking density, chemical structure or composition.

A vast number of polymeric systems can be used to form hydrogels to immobilise bacteriophage, however two were focussed on during this study; the synthetic polymer poly(vinyl alcohol) and the natural biopolymer agarose. In both cases the hydrogel is formed through physical, as opposed to chemical means. This was to minimise possible damage to bacteriophage through reaction with chemical crosslinkers, solvents or curing techniques.

Poly (vinyl alcohol), PVA, was chosen as it is non-toxic and biocompatible. The polymer is available in a range of molecular weights meaning that hydrogel properties could be altered easily. Gelation is primarily carried out through freeze/thawing to form a solid, durable, highly flexible hydrogel that is clear to opaque depending on polymer concentration.

Agarose is a natural polysaccharide biopolymer derived from seaweed which is already widely used in biological applications (e.g. agarose gel electrophoresis). It is again non-toxic and biocompatible, and forms highly hydrated hydrogels with relatively low polymer concentrations. Hydrogels are formed though cooling of agarose solution, which again forms clear to opaque hydrogels depending on polymer concentration. Agarose hydrogels are solid and retain structure, however are not flexible at high concentrations which can lead to cracking and shearing.

4.2. Materials and Methods

4.2.1. Formation of PVA

PVA (M_w = 146,000 – 186,000) solutions were made up in SM buffer and heated to 95 °C until dissolved. The solutions were then allowed to cool to room temperature. To form bacteriophage or non-bacteriophage hydrogels, 900 µL PVA solutions were added to either 100 µL bacteriophage lysate or 100 µL SM buffer respectively. The final polymer concentrations in solution were 2%, 5% and 10% w/v PVA. Once mixed, 1 mL hydrogel mix per well was added to a 12-well plate and frozen at -20 °C for 18 hours. Hydrogels were then allowed to thaw at room temperature for 2 hours before use.

4.2.2. Formation of agarose

Agarose (low gelling temperature) solutions were made up in SM buffer and heated to above 95 °C in a microwave until dissolved. The liquid hydrogels were then cooled, and kept at 50 °C until needed. To form bacteriophage or non-bacteriophage hydrogels, 900 µL agarose solutions were added to 100 µL bacteriophage lysate or 100 µL SM buffer respectively. The final polymer concentrations in solution were 0.2%, 0.4%, 0.7%, 1.4% and 2% w/v agarose. Once mixed, 1 mL mix per well was added to a 12 well plate and allowed to cool for 1 hour at room temperature. Plates were then cooled further at 4 °C overnight before use.

4.2.3. Bacteriophage methods

The standard protocols for bacteriophage harvesting, isolation, purification and quantification can be found in Chapter 2.

4.2.4.1. Disc diffusion assay

Agarose and PVA hydrogel discs containing 10^8 pfu/mL Bacteriophage K were formed as described in Section 4.2.1. and 4.2.2.. Bacterial lawn plates were formed as previously described with *S. aureus* H560 as the host bacterium. 8 mm discs were then cut with a cork borer and placed on the bacterial lawn plates. The plates were incubated at 37 °C overnight. The zone of inhibition caused by bacteriophage diffusing from the hydrogel was measured as the whole zone diameter (including 8 mm hydrogel disc) in triplicate.

4.2.3.2. Temperature Stability of Bacteriophage K

In brief, 100 µL bacteriophage lysate solution (10^8 pfu/mL) was placed in a 1.5 mL Eppendorf tube and incubated in a heating block at 25, 37, 45 and 60 °C for 1 hour with mild shaking. After 1 hour vials were cooled in ice for 5 minutes and kept at 4 °C until needed. The concentration of viable bacteriophage after heating was then calculated using previously described methods.

4.2.4.3. UV stability of Bacteriophage K

400 µL Bacteriophage K lysate solution (10^8 pfu/mL) was placed in a 12-well plate and exposed to 30, 60, 120 and 300 seconds of UV irradiation (UV flood lamp, Dymax 5000 Flood curing system (400 W). The plate was then placed at 4 °C for 5 minutes to cool and bacteriophage concentration calculated using previously described methods.

4.3. Results and Discussion

4.3.1. Bacteriophage

4.3.1.1. Bacteriophage isolation and plaque morphology

Bacteriophage K was propagated and isolated using *S. aureus* H560 as a host bacterium. The bacteriophage was chosen as it has been well investigated, is lytic (as opposed to lysogenic), has a broad host range and has its entire genome sequenced, and so is contains no toxic elements[2]. On incubation with host bacteria, bacteriophage create clear 'plaques' where bacteria have been lysed (Figure 4.2). Plaques formed were small and circular in shape, with a size of approximately 1 – 1.5 mm in diameter. As bacteriophage lysate was diluted, single isolated plaques could be seen and so could be used for concentration calculation.

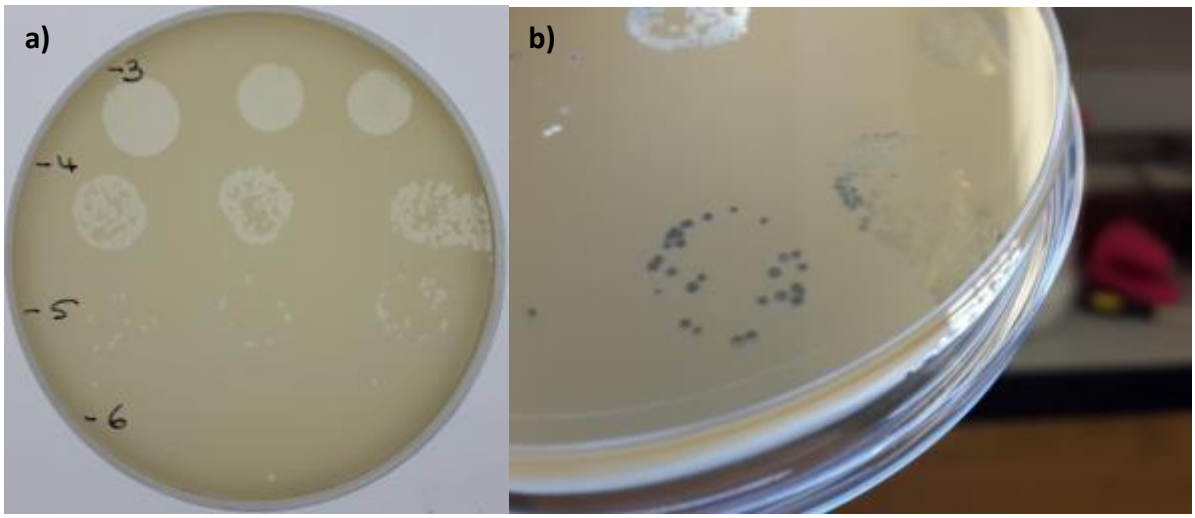

4.3.1.2. TEM imaging of bacteriophage

Although Bacteriophage K morphology has already been documented by O'Flaherty et al, TEM imaging was still carried out to verify bacteriophage size, type and structure[3]. The protocol for TEM imaging of bacteriophage particles is explained in Section 2.4.3.5. Bacteriophage were immobilised on hydrophilised TEM grids and then negatively stained using 1% uranyl acetate solution (pH 4). Images can be seen in Figure 4.3.

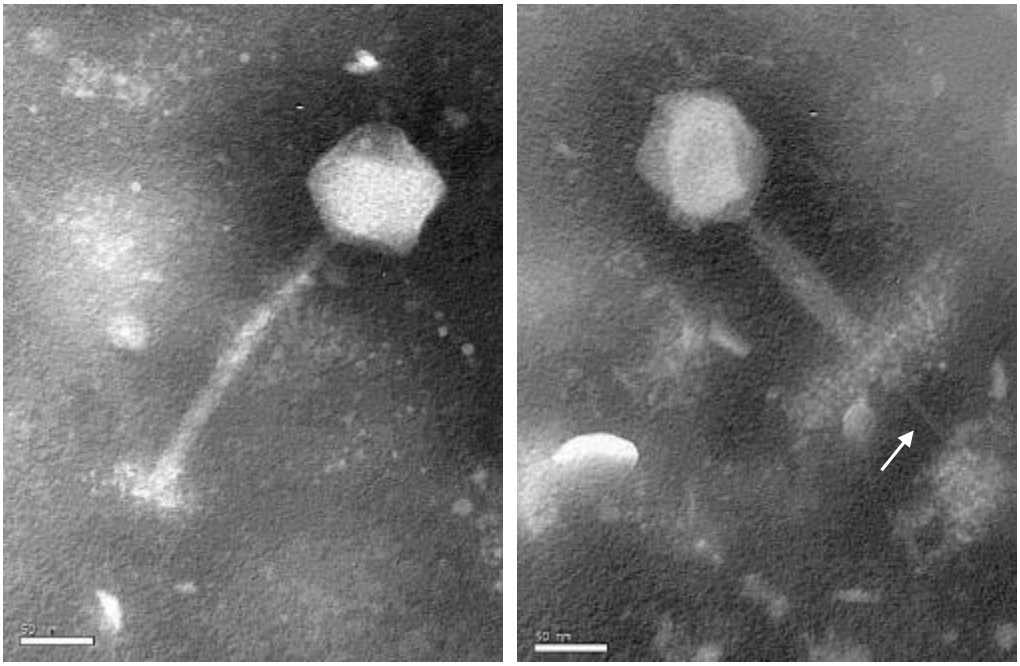

TEM images of Bacteriophage K show it to be part of the most common bacteriophage family, the *Myoviridae*. The bacteriophage comprises an icosahedral capsid head of approximately 100 nm in diameter and a long contractile tail of approximately 400 nm in length, as well as short tail fibres. In Figure 4.3, Bacteriophage with tails in both the relaxed (left) and contracted state (right) can be seen. The contracted tail also shows the central tail tube, which is used for the injection of genetic material through the cell membrane into the host bacterium (see arrow). To a certain extent, the protein subunits that make up the bacteriophage tail structure can also be seen as organised lines made up of small globular units. This is limited by the photographic resolution of the TEM, and could be improved by better sample clean-up before staining, different negative stains or the use of cryo-TEM.

4.3.1.3. Bacterial sensitivity to bacteriophage

The sensitivity of a number of bacterial species to Bacteriophage K was determined by the steak test. For a bacteriophage to be a useful therapeutic, it is important that the virus has activity against a broad range of strains within a species. In a clinical setting it is often time-consuming to initially identify the species, let alone the strain responsible for infection. A broad spectrum bacteriophage has a higher chance of eradicating infection than a bacteriophage that only has activity against a small number of strains within a species.

As Bacteriophage K is primarily an *S. aureus* infecting virus, the bacteriophage was tested against 86 *S. aureus* strains, as well as other clinically relevant pathogens including *S. epidermidis*, *E. coli* and *P. aeruginosa*. Streaks of bacterial overnight culture were allowed to dry on agar plates, and then 10 µL spots of Bacteriophage K lysate solution (10^8 pfu/mL) were added to the bacterial streak. The sensitivity of the strain to Bacteriophage K was then assigned depending on the amount of bacterial killing seen after overnight incubation at 37 °C.

Strains that exhibited total killing by Bacteriophage K were assigned as "Susceptible" to phage infection (Figure 4.4, left). Large, clear areas of killing were seen in the area where the lysate solution had been placed, with no resistant colonies being present. Strains with "Intermediate" killing by Bacteriophage K showed areas of slight but not total killing by the bacteriophage (Figure 4.4, centre). A characteristic spotted pattern is seen where some bacteria have been killed, but other resistant colonies are present. Where no killing at all is seen, these strains were assigned as "Resistant" to Bacteriophage K (Figure 4.4, right). The bacteriophage have no activity against the strain, allowing normal bacterial growth to occur.

In general, the majority of *S. aureus* strains tested with Bacteriophage K were found to either be completely sensitive, or intermediately sensitive. Of the 86 strains tested, only five strains were completely resistant (Table 4.1). 59% strains showed total killing, whilst 35% showed intermediate killing; these strains encompassed hospital and community acquired strains with varying susceptibility to methicillin. There appeared to be no correlation between country of origin, or susceptibility to methicillin, and sensitivity to Bacteriophage K.

Non *S. aureus* strains were also tested to determine sensitivity to bacteriophage in other species (Table 4.2). In the 7 *Staphylococcus* species tested, all showed intermediate killing by Bacteriophage K, meaning that the bacteriophage has a broader spectrum than most other phages. However, in *E. coli* DH5α and *P. aeruginosa* PAO1 no killing was seen, with strains being completely resistant to Bacteriophage K. This was expected, as the strains are Gram-negative, so

contain different bacteriophage receptor molecules, and are completely unrelated to *Staphylococci* in morphology, genome and outer membrane structure.

Susceptible		Intermediate	Resistant
8325-4	Germany131/98	15981	D551
963Small	H40	BK1563	MRSA 378
99ST10345	H402	Btn2299	ST239 µ1
Btn2164	H417	C125	ST239 µ2
C13	H42	C160	TW20
C154	H560	C253	
C3	HT2002-0635	CAN6820-0616	
C390	HT2004-0991	CDC201078-USA700	
C427	JE2	Cuba4030	
C49	lac (USA300)	D22	
C56	MSSA 476	D279	
CAN6428-011	MRSA 71	D316	
CDC12	MRSA 252	D470	
CDC16	MW2 (USA400)	D473	
CDC201114-USA300	Mu3	D98	
CDC980193-USA800	Newman	EMRSA 6	
col	NE334 (hys-)	H050960412	
Cuba4005	Not116	Fra97392	
D302	Not161	HT2001-634	
D318	Not266	HT2005-0306	
D49	Not290	KD12943	
EMRSA 16	RN6911	MRSA 4JJ	
H118	RN4282	MRSA 707	
H560	SwedenAO17934/9	Not271	
Fin62305	WBG8343	Not380	
Fin76167		Not98-53	
		RN6390B	
		ST239 µ20	
		SwedenON408/99	
		SwedN8890/99	

Table 4.1: Sensitivity of *S. aureus* species to Bacteriophage K. Tests were carried out jointly by Jessica Bean and Diana Alves

Intermediate	Resistant
S. epidermidis 12228	*E. coli* DH5α
S. epidermidis RP62A	*P. aeruginosa* PAO1
S. xylosus ATCC29971	
S. chromogenes CCM3387	
S. arlettae N910-254	
S. simulans N920-197	
S. sciuri subsp. Sciuri ATCC29062	

Table 4.2: Sensitivity of other bacterial species to Bacteriophage K. Tests were carried out by Diana Alves

The broad spectrum of Bacteriophage K makes it an ideal candidate for use in the proposed hydrogel system. In the bacterial screen, 94% *S. aureus* strains assessed showed complete or intermediate killing by Bacteriophage K. In cases where complete killing is seen, all infective

bacteria can be effectively removed by the phage. Even in cases where only intermediate killing is seen, the bacteriophage can still reduce bacterial numbers, which could aid the treatment of infection when used in combination with other phage (in phage cocktails) or antibiotics. Further research in the group by Diana Alves has developed a novel phage cocktail containing Bacteriophage K and another bacteriophage, DRA88 with increased *S. aureus* activity compared to pure Bacteriophage K[4].

4.3.1.4. Bacteriophage growth curves in liquid culture

S. aureus strains that had been assigned as "Susceptible", "Intermediate" or "Resistant" to Bacteriophage K by the streak assay were then incubated overnight in liquid culture. The optical density at 600 nm was measured and so the growth curves of the bacteria in solution could be followed.

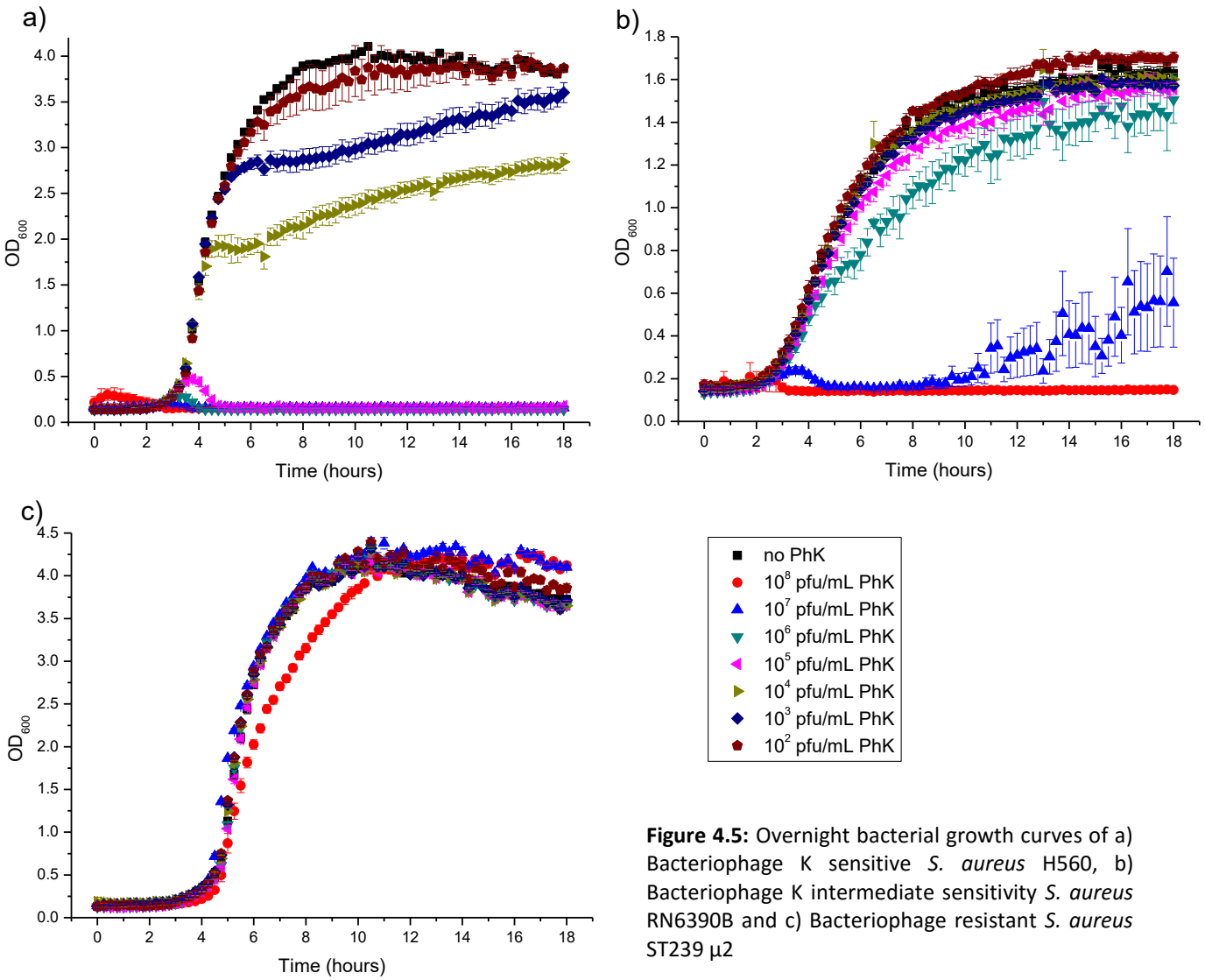

Figure 4.5: Overnight bacterial growth curves of a) Bacteriophage K sensitive *S. aureus* H560, b) Bacteriophage K intermediate sensitivity *S. aureus* RN6390B and c) Bacteriophage resistant *S. aureus* ST239 µ2

The *S. aureus* strains used were H560 (Susceptible), RN6390B (Intermediate) and ST239 µ2 (Resistant). The strains were also incubated with a range of Bacteriophage K concentrations (10^2 – 10^8 pfu/mL) to determine the minimum concentration needed for complete killing.

Overnight growth curves for *S. aureus* H560, RN6390B and ST239 µ2 incubated with varying concentrations of Bacteriophage K can be seen in Figure 4.5. In general, killing by Bacteriophage was seen in Susceptible and Intermediate strains, whereas in *S. aureus* ST239 µ2, which is resistant to Bacteriophage K, no killing was seen in live culture.

In *S. aureus* H560, a characteristic dilution dependent killing by Bacteriophage K is seen. Between dilutions of 10^5 and 10^8 pfu/mL bacteriophage, there is no growth after 18 hours implying that the bacteriophage have successfully infected and lysed all bacteria. Bacterial growth does occur until approximately 4 hours; this is due to the fact that bacteriophage are most able to infect actively growing bacteria in the exponential cycle, and lysis is slow before this point. In 10^4 and 10^3 pfu/mL, the bacteriophage concentration is sufficient to cause a slight reduction in bacterial growth; however bacteria are still present in high concentrations after 18 hours. By 10^2 pfu/mL, there are not sufficient bacteriophage to cause significant killing and growth follows the normal bacterial growth curve (black).

In the intermediately sensitive *S. aureus* RN6390B, a similar pattern is seen to that observed for *S. aureus* H560, however growth is only prevented by far higher bacteriophage concentrations. Where killing was seen down to 10^5 pfu/mL, here killing is only seen in 10^8 and 10^7 pfu/mL Bacteriophage K. In fact in 10^7 pfu/mL bacteriophage, after initial killing growth is able to restart after 8 hours. Here, either not all bacteria were killed in the first place or resistant cells had evolved which are not killed by Bacteriophage K. This mirrors what is seen in in the streak test, where resistant clusters of bacteria are present after incubation with bacteriophage. In all lower dilutions, normal bacterial growth was seen.

S. aureus ST239 µ2 exhibits complete resistance to Bacteriophage K, with normal bacterial growth seen in all cases after 18 hours incubation. In bacteria incubated with 10^8 pfu/mL lysate, a slight slowing of the rate of bacterial growth is seen in the exponential phase, however after 10 hours the same final concentration is still reached.

4.3.1.5. Temperature stability of Bacteriophage K

Although bacteriophage are extremely resilient and capable of existing in a range of environments, their protein structure makes them temperature sensitive. Normally bacteriophage lysate solutions are stored for years at 4 °C without a significant loss in titer. It is

also possible to freeze bacteriophage at –80 °C, or liquid nitrogen, or freeze/dry them[5, 6]. However, each bacteriophage has a different sensitivity to freezing.

High temperatures can cause more serious, irreversible damage to bacteriophage than lower temperatures[7]. Heat is able to denature bacteriophage proteins and (especially due to damage of the delicate tail fibres) causes a loss in bacteriophage infectivity. In 2012, Qiu et al were able to examine the heat-induced disassembly of Bacteriophage λ using DSC, SLS and Electron Microscopy. Above approximately 68 °C they found that proteins in the capsid head began to melt, releasing bacteriophage DNA into the surrounding environment[8]. It is important to note that some bacteriophage (e.g. isolated from hot springs) have exhibited higher stability in higher temperatures[9].

Bacteriophage K was incubated in a heating block at 25, 37, 45, 60 and 70°C for one hour to determine if a significant loss in titer would be seen. The solution was also frozen at -20 °C to assess bacteriophage damage by freezing. The bacteriophage titer after one hour incubation can be seen in Figure 4.6:

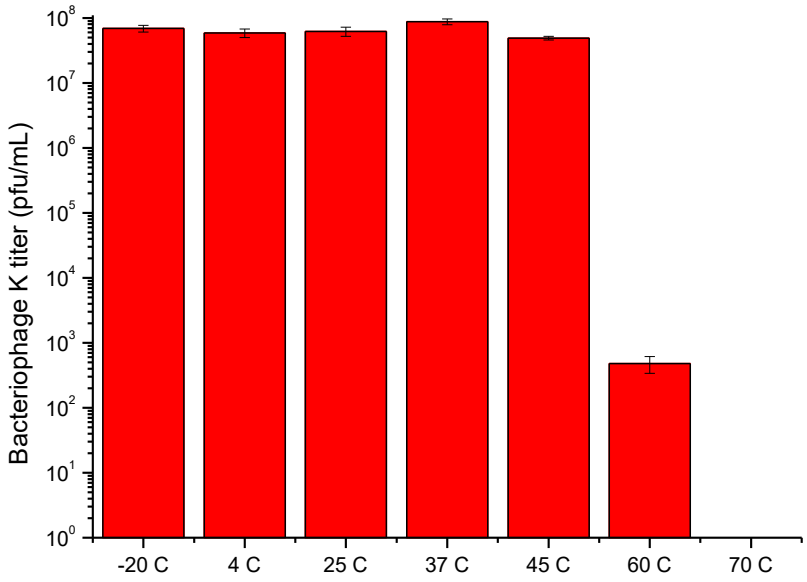

Figure 4.6: Titer of Bacteriophage K solutions incubated at -20, 4, 25, 37, 45, 60 and 70 °C for one hour

Bacteriophage K virions were found to be stable after one hour incubation at 4, 25, 37 and 45 °C; no significant change in titer was seen which implies that the bacteriophage were not damaged by heating at these temperatures. Also, after freezing at -20 °C the bacteriophage were similarly

unaffected, with a concentration of 10^8 pfu/mL being seen. At 60 °C however, a significant loss in bacteriophage concentration occurred, with titer dropping from 10^8 to 10^2 pfu/mL. No bacteriophage were detected after incubation at 70 °C, as bacteriophage particles had become damaged and unable to infect.

4.3.1.6. UV stability of Bacteriophage K

Bacteriophage are also inherently susceptible to damage by UV light. In fact, irradiation by UV is a common method for the bacteriophage sterilisation of microbiological flow hoods and instruments. The highly energetic radiation affects bacteriophage in many ways. DNA and proteins which make up bacteriophage virions are known to be physically altered or damaged by UV irradiation; this can be through mechanisms such as reaction with reactive oxygen species, genetic mutation, crosslinking with aromatic amino acid residues or formation of single strand breaks in DNA[10-12]. Damage can also be due to an increase in temperature caused by the radiation[13]. This reduces the ability of bacteriophage to infect and multiply.

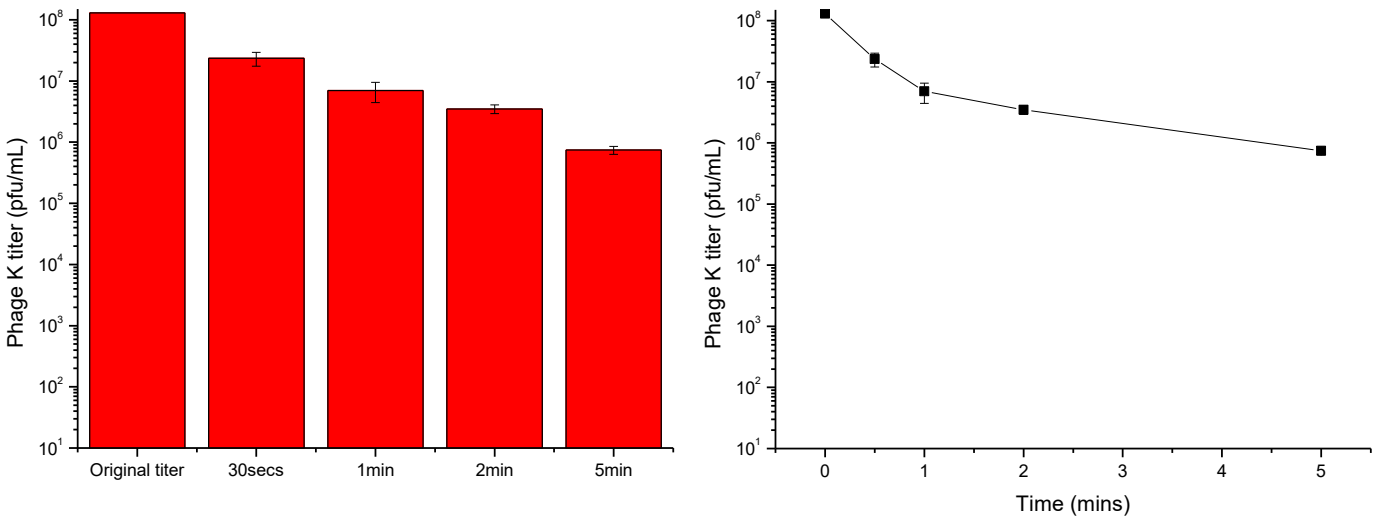

Figure 4.7: Titer of Bacteriophage K exposed to UV flood irradiation for 30 seconds, 1, 2 and 5 minutes

Bacteriophage K was irradiated in a UV flood curer for 30, 60, 120 and 300 seconds to ascertain if a significant loss in bacteriophage titer would be seen (Figure 4.7). This was important to determine, as (if Bacteriophage K were to be incorporated into a device) UV may be needed in other processes such as polymer crosslinking or bacterial sterilisation.

As expected, after 300 seconds of UV exposure a high loss of bacteriophage concentration was seen, with an initial concentration of 10^8 pfu/mL dropping to approximately 10^6 pfu/mL. A high rate of loss was seen until 60 seconds, where the rate of loss then slowed with increasing time. The quantity of UV irradiation that bacteriophage were exposed to was sufficient to affect concentration of viable virions.

In general, it is unlikely that UV experiments involving bacteriophage or polymers will exceed 60 seconds in length, as prolonged UV exposure results in increased temperature as well as physical damage and breakdown of materials. Therefore, a loss bacteriophage titer of approximately a factor of 10 after 60 seconds is not high enough to be regarded as considerable. From experiments carried out in Section 4.3.1.4., 10^7 pfu/mL Bacteriophage K is still sufficient to cause significant killing in “Susceptible” and “Intermediate” *S. aureus* strains.

In truth, in a commercial setting any irradiation of a bacteriophage with UV would be discouraged, as it would not be possible to ensure that the bacteriophage genome was not damaged or mutated into a possibly dangerous species.

4.3.1.7. Use of Bacteriophage K for further development

In general, Bacteriophage K is an ideal bacteriophage candidate for use in an antimicrobial wound dressing. The bacteriophage has a broad spectrum over *S. aureus* and other *Staphylococci*, meaning that there is a higher chance that on bacterial infection, the bacteriophage will be active. The whole genome of the bacteriophage has also been sequenced which allows examination of possible toxic genetic elements. For incorporation into a hydrogel matrix, the bacteriophage has high temperature and UV stability, allowing a range of hydrogel formulations to be tested. Despite this, high temperatures, desiccation, chelating ligands, solvents and extensive UV should be avoided to minimise bacteriophage damage.

4.3.2. Bacteriophage K in poly(vinyl alcohol) (PVA) hydrogels

PVA hydrogels were the first hydrogel candidates to be investigated. The structure of the polymer can be seen in Figure 4.8. PVA is a synthetic, biocompatible hydrogel that forms solid, flexible gels under mild conditions. It is available in a range of molecular weights; in this investigation 146,000 – 186,000 was used as it formed very solid hydrogels.

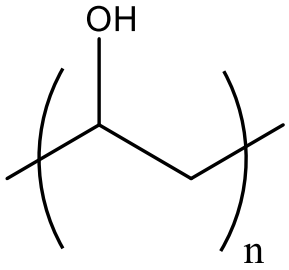

Figure 4.8: Structure of PVA repeating unit

4.3.2.1. PVA hydrogels

PVA hydrogels were formed by heating varying concentrations of polymer in SM buffer until dissolved. Once cooled, the dissolved polymer remained liquid when kept at room temperature. PVA can be crosslinked to form solid hydrogels chemically (with sodium tetraborate or dimethyl sulphoxide) or physically (with freeze/thawing)[14, 15]. Here, freeze/thawing was chosen as it does not introduce potentially harmful chemicals into the hydrogel which could damage the bacteriophage.

On freeze/thawing dissolved PVA undergoes physical crosslinking between chains. The formation of ice crystals during freezing is thought to push polymer chains together, allowing hydrogen bonds to form between hydroxyl groups[16]. There is high control over PVA gelation with freeze thawing, as the polymer solution remains liquid until it is frozen. The porosity and strength of cast hydrogels can also be altered by changing the number of freeze/thaw cycles, addition of salts or altering PVA molecular weight.

Cast 2%, 5% and 10% PVA hydrogels after one freeze/thaw cycle can be seen in Figure 4.9. The formed hydrogels are strong and flexible, with the hydrogel resistant to cracking or breaking. The hydrogels were also slightly opaque in appearance. Structural rigidity of hydrogels increases with polymer concentrations; 2% PVA hydrogels are highly hydrated, with structure collapse seen, whereas 10% hydrogels appear less hydrated and are extremely strong and robust.

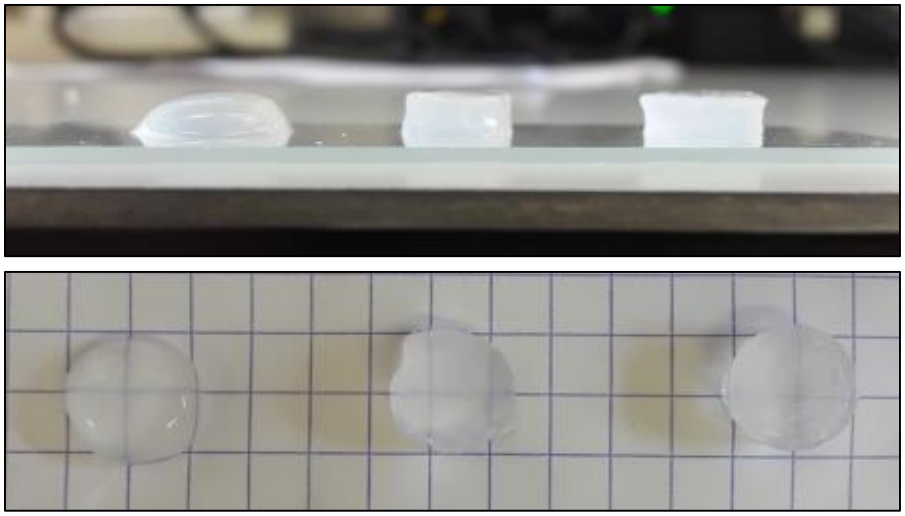

Figure 4.9: 10 mm discs of freeze/thawed hydrogels containing (left to right) 2%, 5% and 10% PVA

The swelling ratio of 2%, 5% and 10% PVA hydrogels was calculated using previously described methods. In general, the swelling ratio decreases sharply with increasing polymer concentration (Figure 4.10).

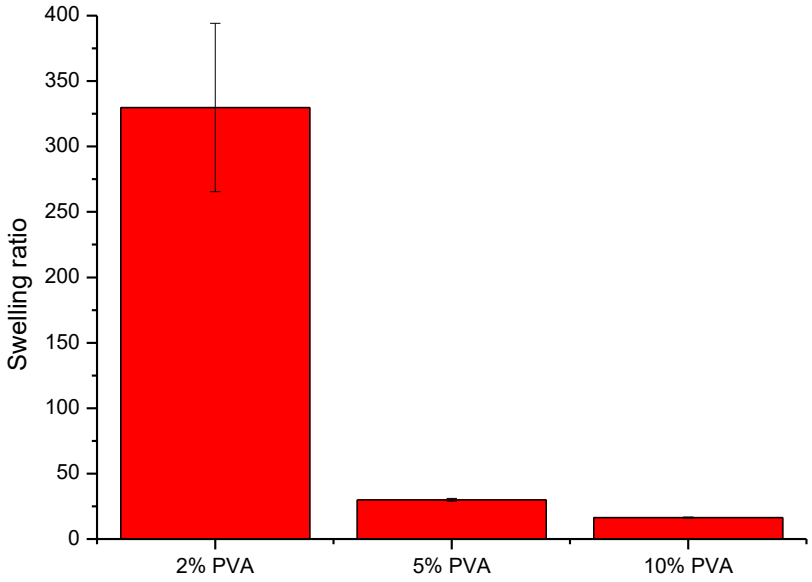

Figure 4.10: Swelling ratio measurements of 2%, 5% and 10% PVA hydrogels

The swelling ratio for 2% PVA mirrored the highly hydrated, weak hydrogel that was seen after freeze/thawing. The high concentration of absorbed water causes the structure to become soft

and unstructured. In 5% and 10% PVA hydrogels, the swelling ratio decreased significantly compared to 2% PVA, with swelling ratios of approximately 30 and 16.4 being seen respectively. These ratios imply a denser, less hydrated, more crosslinked network.

The weight loss of 5% PVA hydrogels was assessed by incubating hydrogels at varying temperature to determine the extent of water evaporation (Figure 4.11). This was important to understand if the hydrogel is to be used as a dressing; significant water loss during use could collapse the hydrogel structure and damage immobilised bacteriophage.

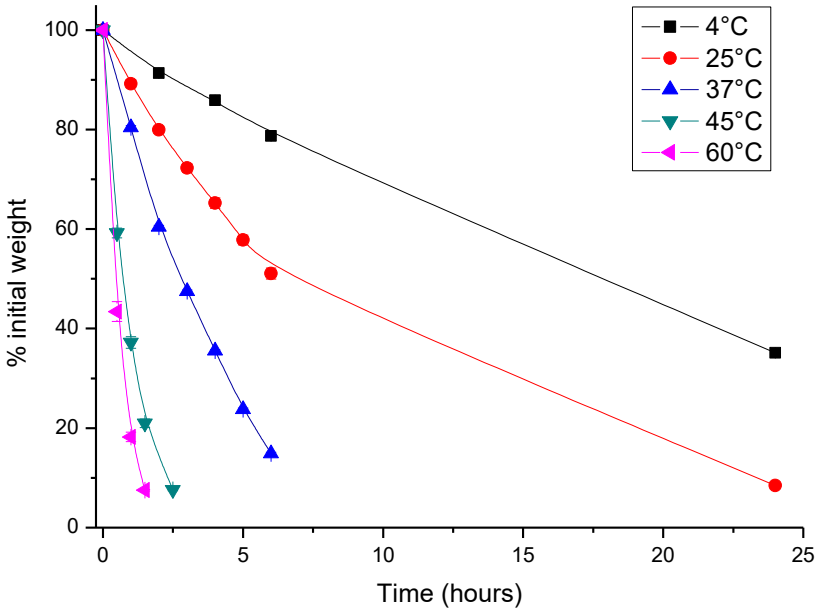

Figure 4.11: Water loss measurements of 5% PVA hydrogels at 4, 25, 37, 45 and 60 °C

In general, weight loss due to water evaporation occurred at a higher rate as temperature increased. At 4 °C the rate of water loss was comparatively slow, with a loss of approximately 3 %/hr. At room temperature (25 °C), water loss rate increased to 8 %/hr, whilst at body temperature (37 °C) water loss occurred at 15.4 %/hr. In hotter temperatures, the rate of water loss increased sharply, with water loss occurring at 37 %/hr at 45 °C and 62 %/hr at 60 °C. Although these results were significant, it is important to note that in a clinical setting, the hydrogels would not be stored or used at elevated temperatures, and would be covered in a protective plastic cover to prevent water loss.

4.3.2.2. SEM imaging of PVA hydrogels

SEM images of freeze/dried PVA hydrogels were taken to analyse the internal structure of the hydrated hydrogel (Figure 4.12). Although there is a certain amount of hydrogel collapse during

the freeze/drying process, this is the same in all cases and so differences due to PVA concentration can still be observed.

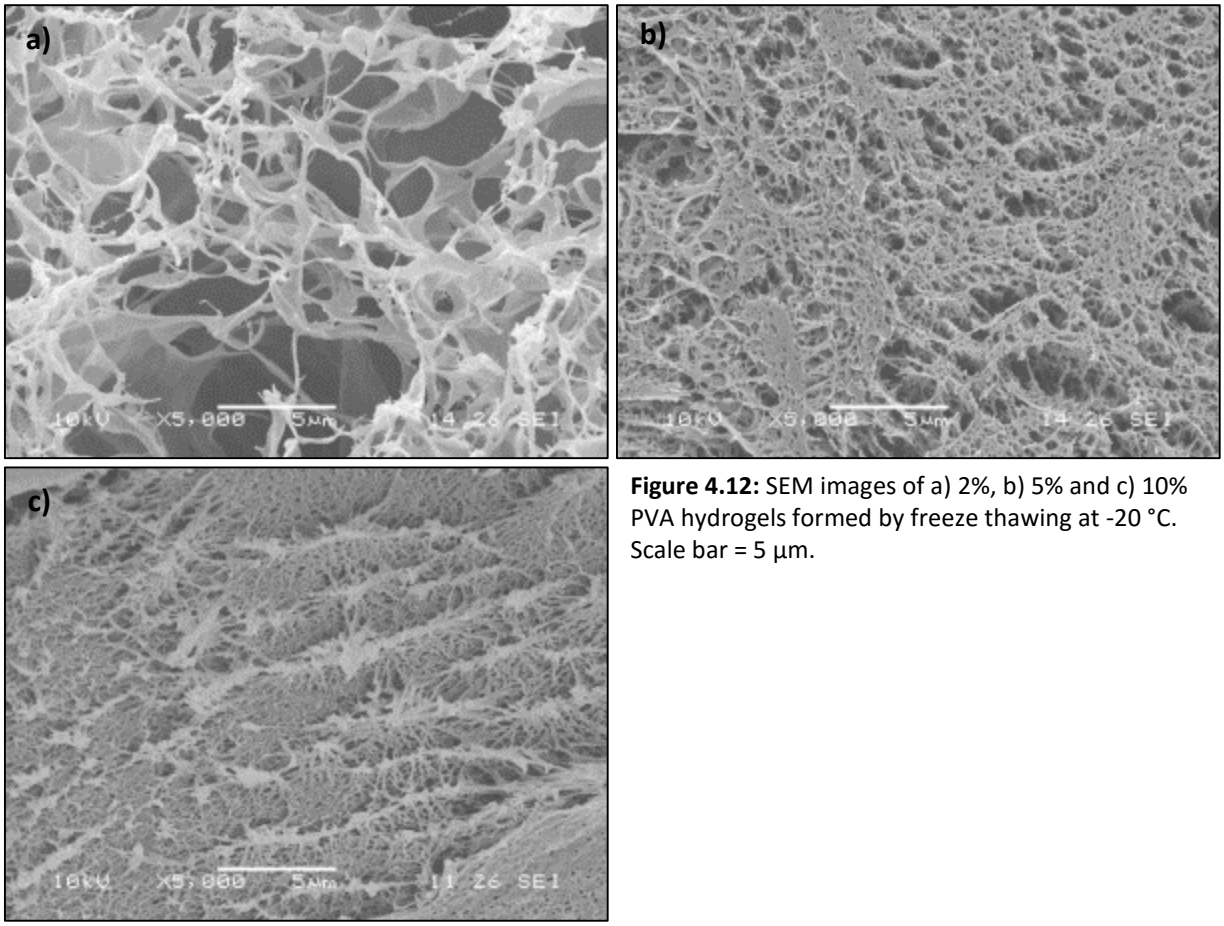

Figure 4.12: SEM images of a) 2%, b) 5% and c) 10% PVA hydrogels formed by freeze thawing at -20 °C. Scale bar = 5 µm.

In general, as PVA concentration increased the hydrogel pore size decreased; all hydrogels exhibited a highly porous internal structure. In 2% PVA hydrogels pores were very large (> 5 µm) with uneven size distribution, reflecting the high swelling ratio seen in Section 4.3.2.1. In 5% PVA hydrogels the hydrogel had a significantly smaller pore size (1 – 0.2 µm) with a more uniform porosity. By 10% PVA hydrogels appeared almost solid in nature, with a highly compact porosity of < 200 nm pores. In both 5% and 10% PVA the highly dense porous structure is reflected in the low swelling ratio observed in swelling measurements.

For the immobilisation of Bacteriophage K in these hydrogels, it was expected that the porosity would play a key factor in diffusion of the bacteriophage. In 2% PVA the large pore structure would allow near-free diffusion of the bacteriophage, whereas in 10% PVA very low or no diffusion was expected to be seen.

4.3.2.3. Release of bacteriophage from PVA hydrogels

The diffusion of bacteriophage from PVA hydrogels was investigated by measuring the concentration change over time (Figure 4.13). 1 mL PVA solutions (2%, 5% and 10% PVA) containing 10^8 pfu/mL Bacteriophage K were cast into a 12-well plate and freeze/thawed to form crosslinked hydrogels. 1 mL SM buffer per well was then added and the concentration of bacteriophage calculated at determined timepoints.

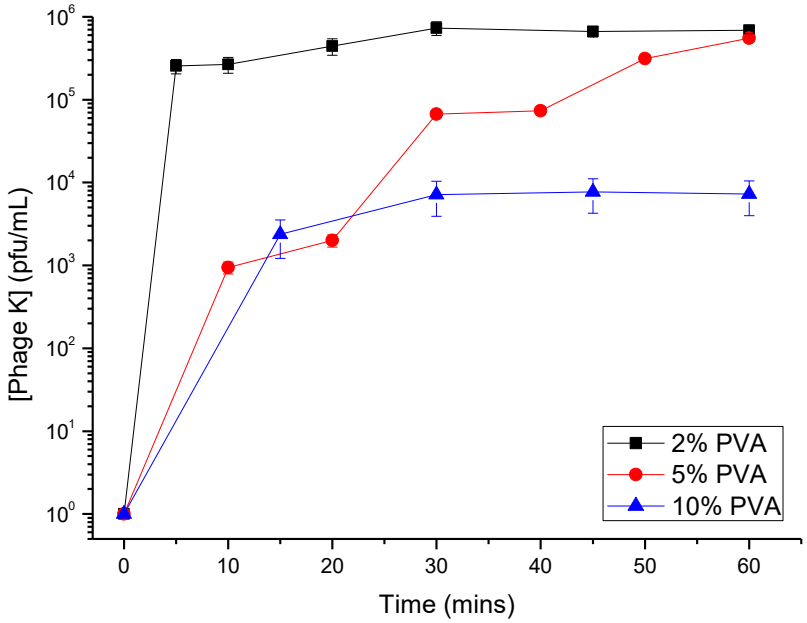

Figure 4.13: Bacteriophage release from 2%, 5% and 10% PVA hydrogels

In general, a faster diffusion of bacteriophage was seen in less concentrated hydrogels; 2% PVA exhibited a very fast 'burst' of bacteriophage release, whereas in 10% PVA hydrogels a slower release was seen. In 2% and 5% PVA hydrogels a final concentration of approximately 5 x 10^5 pfu/mL was seen, whereas in 10% a lower concentration of 10^4 pfu/mL was determined.

In all cases, a low percentage of bacteriophage appeared to be released compared to the initial loading concentration. Bacteriophage concentration reached a plateau at approximately 5 x 10^5 pfu/mL from a hydrogel concentration of 10^8 pfu/mL. This could be due to a number of factors. Firstly, the highly dense pore structure of 5% and 10% PVA hydrogels seen in SEM images (Figure 4.12) implies that the structure significantly restricts the free movement of bacteriophage; however if this was the case, in networks with a larger pore size such as 2% would show an increased concentration of released bacteriophage. Also, the freezing process in the presence of

polymer could damage bacteriophage and prevent them from infecting, and so the number seen in this experiment could be the number of virions that were able to survive the conditions. From Section 4.3.1.5, it was known that freezing at -20 °C did not cause a significant reduction in bacteriophage titer, however this was only after one hour freezing. A prolonged exposure could be sufficient to damage bacteriophage, especially if immobilised in a polymer network that prevents movement and expansion.

4.3.2.4. Kinetics of bacteriophage release

The kinetics of bacteriophage diffusion and the diffusion coefficient of bacteriophage in varying concentrations of PVA was then analysed using Fick's Law[17, 18]. The apparent diffusion coefficient, $D_{app,}$ is obtained from the slope of C_t/C_0 versus time plots, where C_t is the bacteriophage concentration at time t, C_0 is the initial bacteriophage concentration, S is the diffusion area, V is the solution volume and X is the membrane thickness:

$$\frac{C_t}{C_0} = \frac{SD_{app}}{VX}t \tag{4.1}$$

The concentration of bacteriophage released was measured as previously described before the system reached the steady state. This can be seen in Figure 4.14.

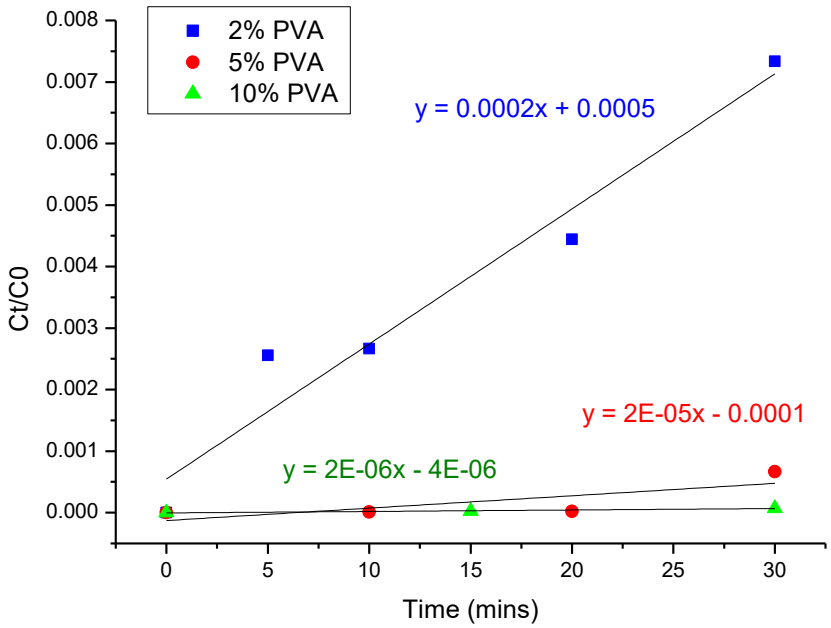

Figure 4.14: Graph of C_t/C_0 of 2%, 5% and 10% PVA hydrogels

The slopes calculated in Figure 4.14 were then used to calculate D_{app} for each concentration of PVA (Figure 4.15 and Table 4.3). Here, the solution volume, V, was 1 x 10^{-6} m^3 and membrane thickness, X, was 2.6 x 10^{-3} m for all measurements. The diffusion area, S, was calculated from the 12-well plate well diameter as 3.8 x 10^{-4} m^2.

% PVA (w/v)	C_t/C_0	V (10^{-6} m^3)	X (10^{-3} m)	S (10^{-4} m^2)	t (secs)	D_{app}(m^2sec^{-1})
2	0.0002	1	2.6	3.8	1800	7.6E-13
5	0.00002	1	2.6	3.8	1800	7.6E-14
10	0.000002	1	2.6	3.8	1800	7.6E-15

Table 4.3: D_{app} calculations for Bacteriophage K diffusion from 2%, 5% and 10% PVA hydrogels

In general, the D_{app} values calculated for Bacteriophage K in PVA were extremely low. The diffusion constant for bacteriophage decreases significantly as % PVA (and so hydrogel density) increases. The more concentrated polymer network physically slows diffusion of bacteriophage particles. 2% PVA, being the most fluid and least rigid hydrogel showed the highest D_{app} of 7.6 x 10^{-13} m^2sec^{-1}. With more concentrated PVA hydrogels D_{app} values decreased by a factor of 10 each time, with 7.6 x 10^{-14} m^2sec^{-1} for 5% PVA and 7.6 x 10^{-15} m^2sec^{-1} for 10% PVA.

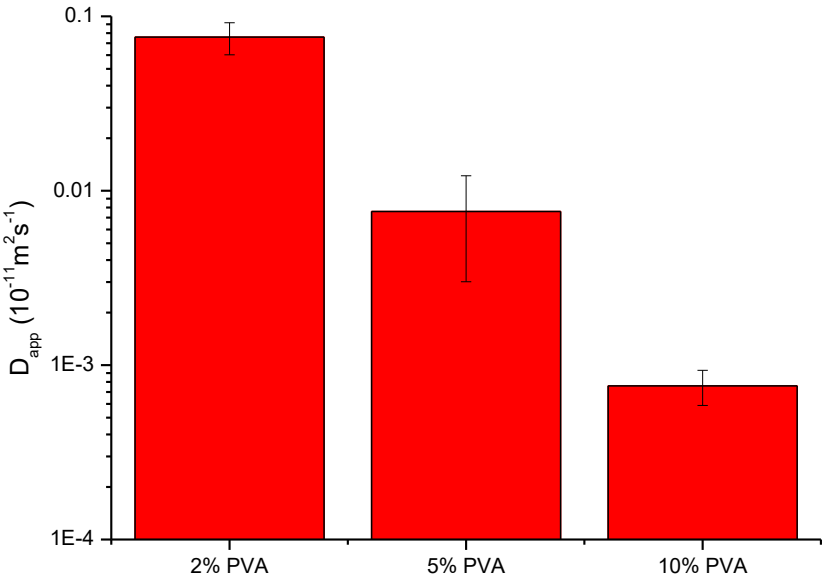

Figure 4.15: Diffusion coefficient values (10^{-11} m^2sec^{-1}) for 2%, 5% and 10% PVA

This is thought to be due to the shape of bacteriophage particles; Bacteriophage K is a long tailed phage of approximately 100 nm x 400 nm in size. The long tail is more likely to become entangled in the polymer matrix, or prevent movement through smaller pores. Also, as PVA crosslinks through physical interactions of the polymer chains, semi-crystalline domains in the hydrogel could entrap bacteriophage more strongly than in amorphous regions.

4.3.2.5. Zones of inhibition

PVA hydrogels containing 10^8 pfu/mL Bacteriophage K were incubated on bacterial lawns containing *S. aureus* H560 to assess bacteriophage diffusion out of the hydrogel. Bacteriophage are able to diffuse through the matrix into the bacterial lawn where they are able to infect in lyse bacteria present; this results in zones of inhibition where no growth is seen (Figure 4.16).

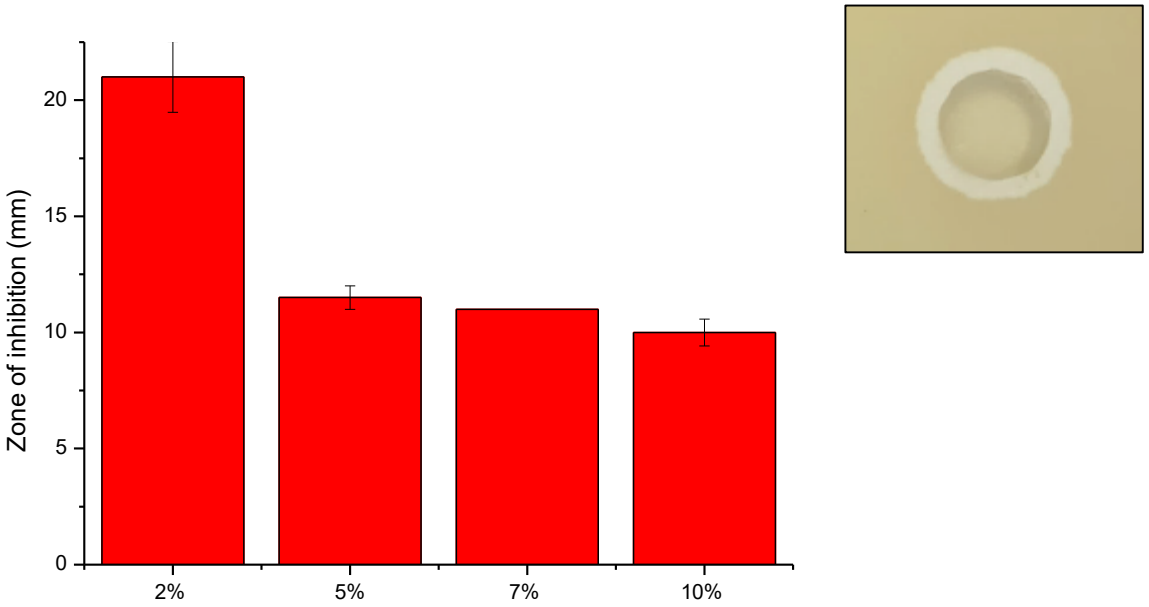

Figure 4.16: (left) Zone of inhibition measurements of 8 mm diameter PVA hydrogels containing 10^8 pfu/mL Bacteriophage K on *S. aureus* H560. (right) Image of zone of inhibition surrounding 7% PVA

The zone of inhibition seen around bacteriophage-containing PVA hydrogels decreased with increasing polymer concentration. In 2% a very high diffusion was seen of approximately 22 mm in diameter. This correlates well with the diffusion experiments in Section 4.3.2.3. where 2% PVA showed a significantly faster and higher bacteriophage release compared to more concentrated hydrogels. In 5%, 7% and 10% PVA, the zone of inhibition was smaller with 11.5, 11, 10 mm respectively.

4.3.2.6. Bacteriophage hydrogels in overnight culture

2%, 5% and 10% PVA hydrogels containing Bacteriophage K were formed into 24-well plates with 500 µL per well. The hydrogels were crosslinked by freezing overnight at -20 °C and subsequent thawing at room temperature for one hour. The hydrogels were then incubated with actively growing bacteria in liquid culture to determine if enough bacteriophage were able to diffuse to initiate bacterial killing (Figure 4.17). From the diffusion experiments carried out in Section 4.3.2.3., bacteriophage were able to diffuse, however in 5% and 10% PVA hydrogels, the concentration released could not be high enough to cause sustained killing.

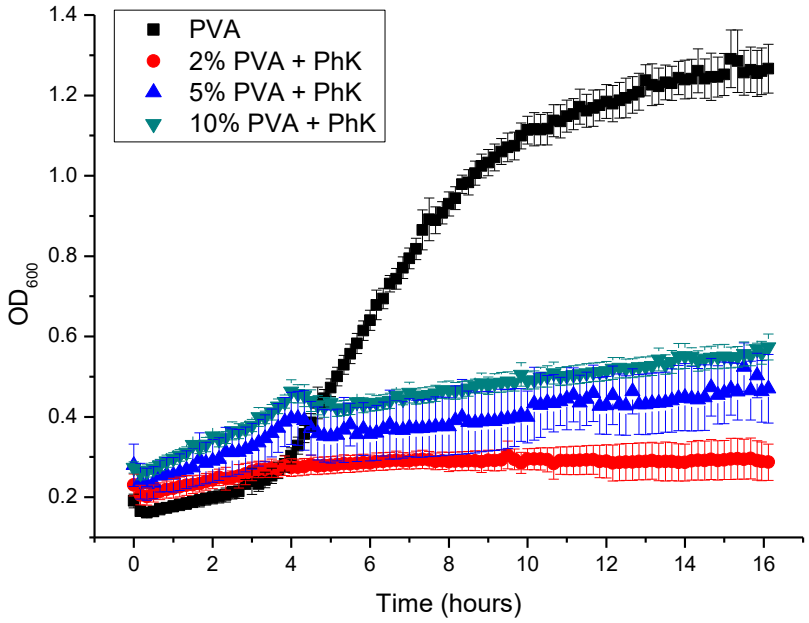

Figure 4.17: Growth curves *of S. aureus* H560 liquid cultures incubated with 2%, 5% and 10% PVA containing 10^8 pfu/mL Bacteriophage K.

A high background in bacteriophage hydrogels was seen during the experiment, as with increasing PVA concentration hydrogels became more opaque which interfered with absorbance measurements. As this was constant throughout the experiment, it was not significant when following bacterial growth. Similarly, a higher starting OD_{600} was seen in bacteriophage containing hydrogels compared to standard PVA as the lysate solution also contributes to a change in the opacity of the hydrogels.

Killing of *S. aureus* H560 was seen in all concentrations of PVA compared to PVA hydrogels containing no bacteriophage. A higher baseline OD_{600} was seen with increasing PVA concentration, however as previously discussed this was due to the hydrogel opacity and not a

loss in bacterial killing. In all hydrogels, active bacteriophage were able diffuse out of the hydrogel into bacterial solution in a high enough concentration (> 10^5 pfu/mL) to initiate killing. A characteristic "bump" in bacterial growth is seen at approximately 4 hours, where bacteria begin to grow and then are killed again. This is frequently seen in bacteriophage infection curves (see Section 4.3.1.4.). Killing by bacteriophage only begins to occur in the exponential phase, when bacteria are actively metabolising and reproducing. The bacteria start to grow, increasing the OD_{600}, and then bacteriophage begin to lyse bacteria once the exponential phase is reached, causing a decrease in OD_{600}.

4.3.2.7. UV irradiation

Bacteriophage can become damaged in UV light, as reactive radical species generated by UV can react with the delicate protein structure. In Section 4.3.1.6. it was shown that UV irradiation caused a loss of infective bacteriophage titer, with up to 10^3 pfu/mL loss after 5 minutes irradiation. The effect of UV irradiation on bacteriophage in PVA hydrogels was measured to determine if the hydrogel protected or damaged further immobilised bacteriophage. Here, only 5% PVA hydrogels containing 10^8 pfu/mL were investigated with UV irradiation for 10, 30 and 60 seconds. 2% and 10% PVA hydrogels were not taken on for further development; 2% hydrogels did not show a strong enough structure after crosslinking, and uncrosslinked 10% PVA was too viscous to mix, measure or add other components successfully.

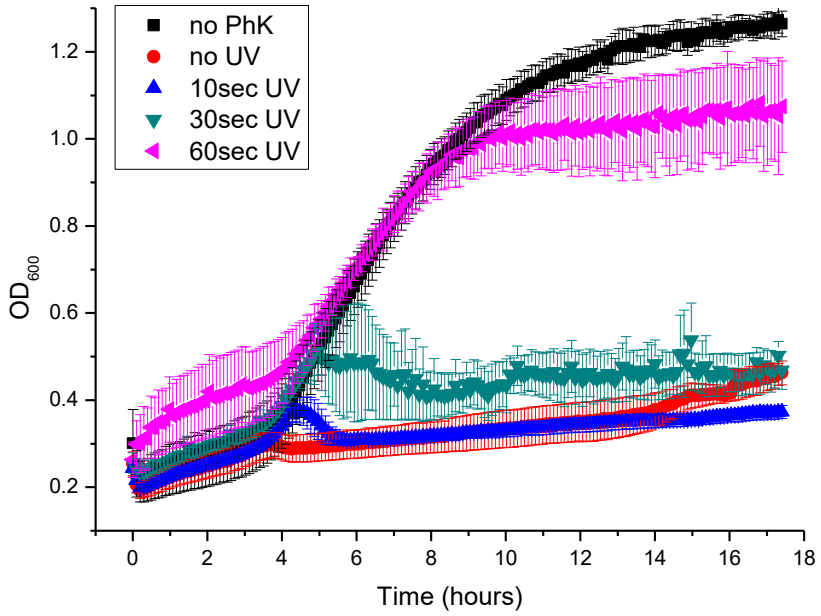

Figure 4.18: Incubation of *S. aureus* H560 with 5% PVA containing 10^8 pfu/mL Bacteriophage K which has been irradiated with flood UV for 10, 30 and 60 seconds

In general, as exposure of bacteriophage PVA hydrogels to UV increased, the lytic ability of immobilised bacteriophage significantly decreased (Figure 4.18). With no UV irradiation, normal killing of *S. aureus* H560 was seen compared to the normal growth curve. Even after 10 seconds of UV exposure, bacteriophage damage was seen with a shift in the initiation of bacterial lysis from four to five hours. Similarly, this was shifted further after 30 seconds irradiation to six hours. Despite this, overall bacterial killing was seen in both cases. After 60 seconds UV irradiation no bacterial killing was seen compared to normal bacterial growth, implying that bacteriophage had become damaged and unable to infect.

This could be due to a number of reasons. Firstly, after 60 seconds UV irradiation the local temperature of the hydrogel was significantly increased. High temperatures are known to damage bacteriophage proteins and nucleic acids, as well as altering the more complex virion structure. Secondly, in the case of PVA the polymer is known to form highly reactive free radical species on UV irradiation, as described by Niki et al[19]. These species can not only cause damage to bacteriophage particles through absorption of photons by DNA and proteins and subsequent oxidation, but on reaction with PVA, acidic species can be formed which lower the local pH [20].

4.3.2.8. Overview

In general, PVA hydrogels were a promising vehicle for the immobilisation of bacteriophage. The optimum PVA concentration was determined as 5% PVA, as this formed a strong, flexible hydrogel that retained structure whilst allowing high bacteriophage diffusion. The highly hydrated matrix provided an environment where bacteriophage could diffuse and successfully infect live bacterial culture on incubation. However, the loss of bacteriophage infectivity seen after UV irradiation would prevent the use of PVA where UV is required (e.g. for photopolymerisable hydrogels).

4.3.3. Bacteriophage K in agarose hydrogels

Agarose was the second candidate for use as a hydrogel to embed Bacteriophage K. The structure of agarose can be seen in Figure 4.19. The polymer was chosen as it is natural, non-immunogenic and biocompatible, whilst also forming solid hydrogels under mild conditions.

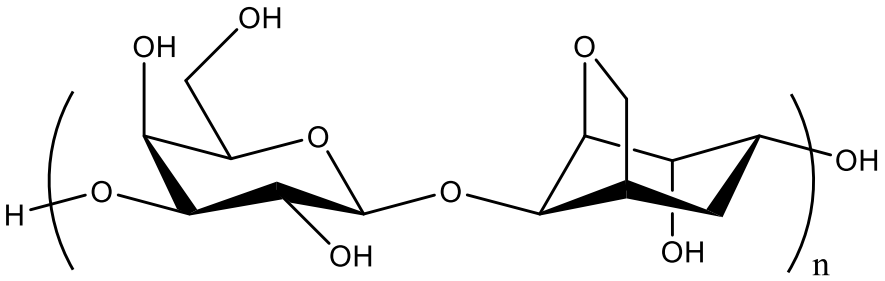

Figure 4.19: Structure of agarose repeating unit

4.3.3.1. Agarose hydrogels

Agarose hydrogels were formed by heating varying % low melting point agarose in SM buffer at 95 °C until dissolved. The liquid mixture sets into a solid hydrogel on cooling at different rates depending on agarose concentration; solidification usually occurs below 30 °C.

Agarose is ideally suited for bacteriophage immobilisation. It forms a highly hydrated, non-toxic hydrogel that is able to hold its shape at relatively low polymer concentrations. The hydrogels are clear to slightly opaque depending on polymer concentration (Figure 4.20), meaning they can be seen through, and the polymer itself is a natural polysaccharide requiring no additional molecules for hydrogel formation. The hydrogel is already commonly used in molecular biology for the analysis of proteins and nucleic acids in gel electrophoresis.

One drawback of agarose hydrogels is that they are mechanically quite fragile. They are not flexible and form into solid blocks that are irreversibly damaged on crushing or bending. There is also less control over gelation than with PVA hydrogels. The agarose must be kept above the setting temperature to mix in bacteriophage particles, but not so hot as to cause bacteriophage damage. In highly concentrated mixtures (e.g. > 1.5% w/v agarose) solidification can occur before bacteriophage have been mixed in and the agarose solution has been transferred to the desired mould. This can result in solidification in situ, either in the mixing vessel, the pipette tip or in a half filled mould. Because bacteriophage are temperature sensitive, it is not possible to reheat agarose to the pre-solidified state in these cases.

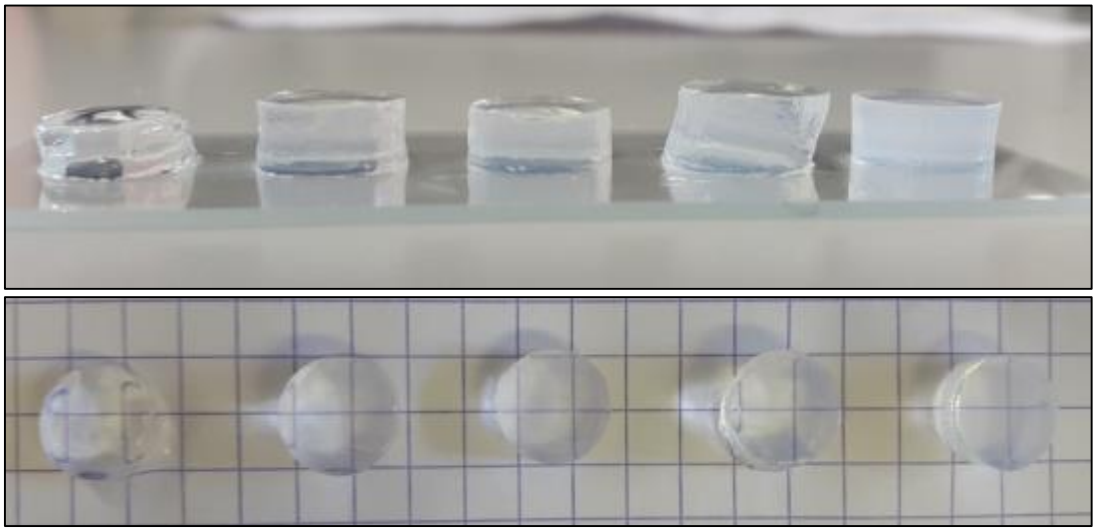

Figure 4.20: 10 mm discs of hydrogels containing (from left to right) 0.2%, 0.4%, 0.7%, 1.4% and 2% agarose

The swelling ratios of agarose hydrogels were again determined by swelling measurements (Figure 4.21). Compared to PVA hydrogels, in general agarose hydrogels were more hydrated and exhibited higher swelling ratios. Due to the poor structure of 0.2% agarose gels, the swelling ratio is significantly higher than more concentrated gels. Once the hydrogel has been swollen overnight the gel must be blotted to remove excess water; in 0.2% agarose gels the water content is so high that the structure is delicate and easily damaged when blotted. With 0.4%, 0.7%, 1.4% and 2% agarose hydrogels the structure is far more solid and the swelling ratio is more accurately measured. As agarose concentration increases, the swelling ratio decreases, with swelling ratios of 58.6±1.3 for 0.4%, 53.4±0.4 for 0.7%, 39.0±0.5 for 1.4% and 31.4±0.3 for 2% agarose.

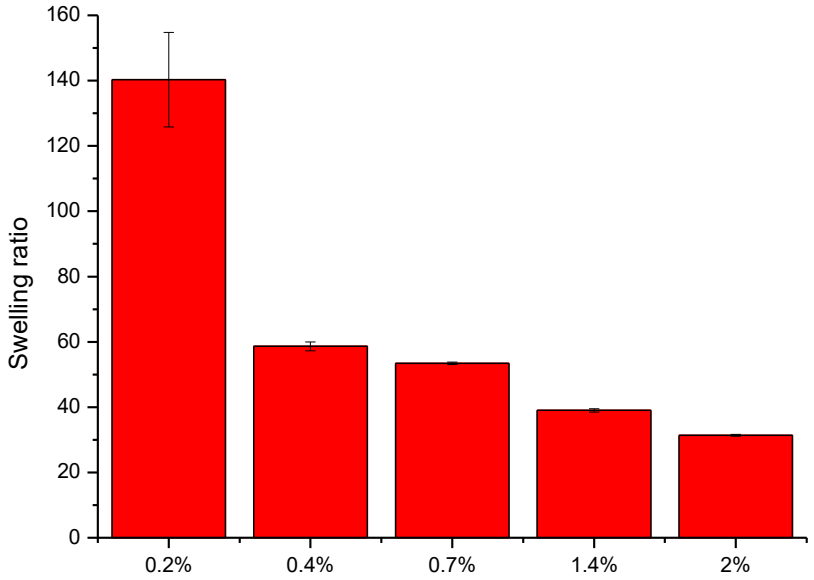

Figure 4.21: Swelling ratio measurements of 0.2%, 0.4%, 0.7%, 1.4% and 2% agarose hydrogels

0.7% agarose hydrogels were incubated at various temperatures to measure the % weight loss due to water evaporation of the hydrogel (Figure 4.22). As expected, weight loss occurred at a faster rate as temperature increased, in a linear fashion. At 4°C, weight loss decreased at a rate of approximately 7 %/hr, at room temperature (25 °C) weight loss occurred at 12 %/hr and at body temperature (37 °C) weight loss occurred at 30 %/hr. At higher temperatures, weight loss was far faster; at 79 %/hr for 45 °C and 95 %/hr for 60 °C. Again it is noted that in a clinical setting, any hydrogels used would be protected by a plastic cover to prevent water loss.

In comparison to PVA hydrogels, the rate of water loss seen in agarose is far higher. This is thought to be due to the higher porosity of agarose hydrogels, which allows water molecules to evaporate from a greater surface area of hydrogel compared to PVA.

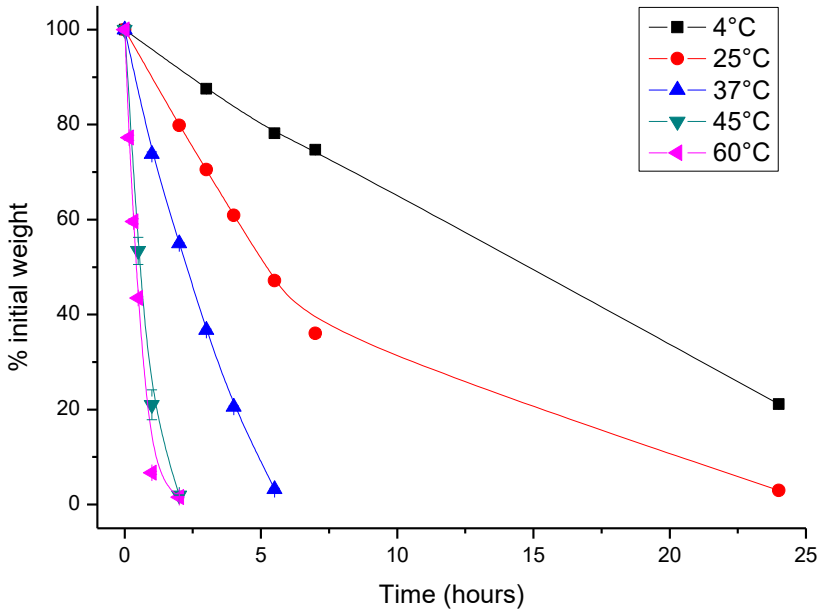

Figure 4.22: Water loss measurements of 0.7% agarose hydrogels at 4, 25, 37, 45 and 60 °C

4.3.3.2. SEM imaging of agarose hydrogels

SEM images of agarose hydrogels were taken to analyse the internal structure of agarose hydrogels (Figure 4.23). Here, 0.2%, 0.4%, 0.7%, 1.4% and 2% agarose hydrogels were cast and allowed to set. 2 x 2 mm samples were then cut and freeze dried to preserve the hydrated structure. In all cases, images taken were of the internal cut side of the hydrogel, not the air-facing top.

Agarose hydrogels formed showed a less obvious pore structure than that seen in PVA hydrogels. In general, hydrogels appeared more solid as agarose concentration increased, with 1.4% and 2% agarose hydrogels showing no pores, even at high magnification (x 10,000, images not shown). The gelation mechanism of agarose in solution is generally thought to be via a liquid-liquid phase separation that occurs in the sol-gel trasition on cooling[21]. Polymer chains are able to aggregate in the polymer-rich phase, surrounded by a polymer-poor phase. The agarose chains then form thick bundles crosslinked by hydrogen bonds[22].

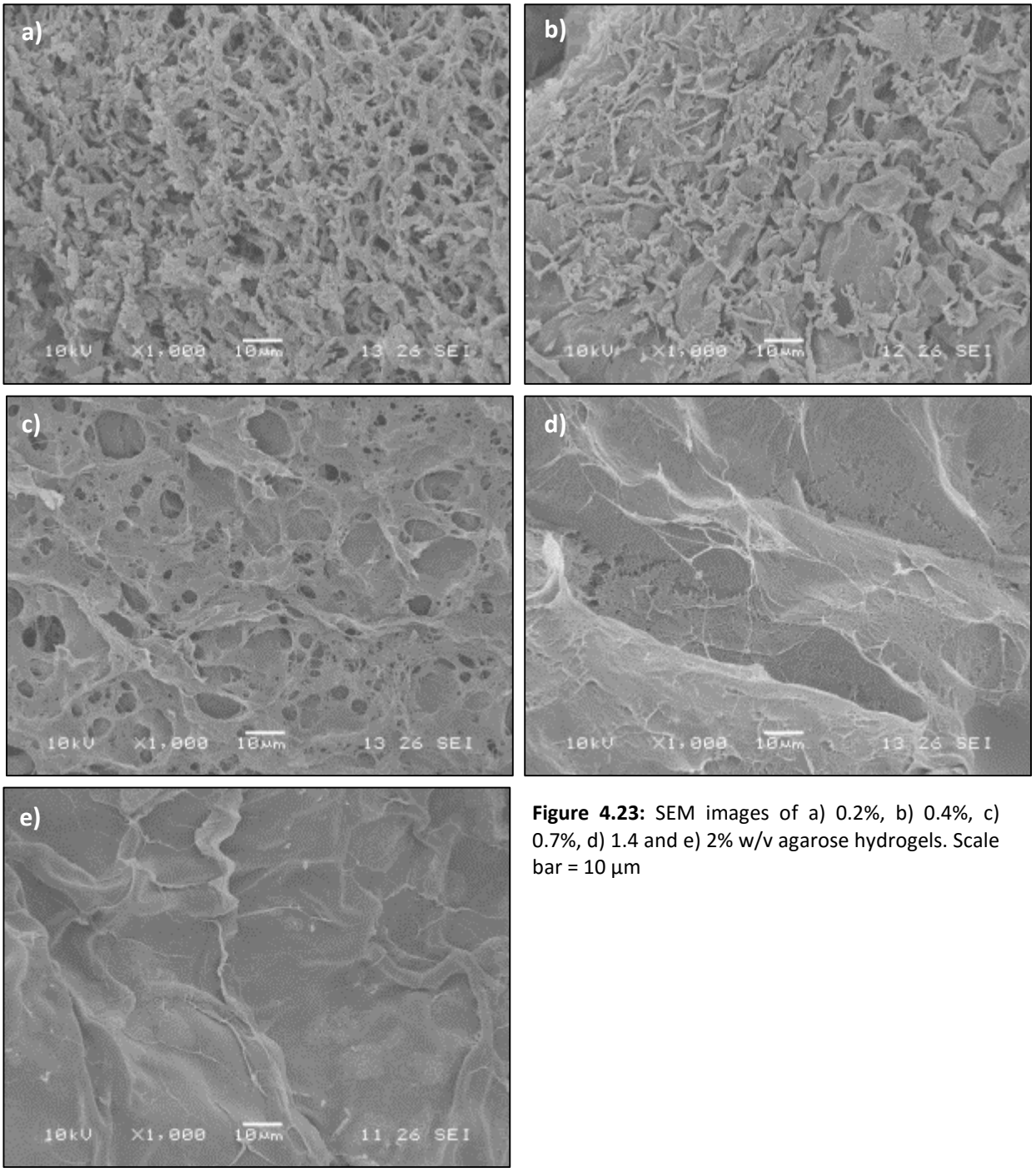

Figure 4.23: SEM images of a) 0.2%, b) 0.4%, c) 0.7%, d) 1.4 and e) 2% w/v agarose hydrogels. Scale bar = 10 µm

In 0.2% agarose, a flaked appearance was seen with pores of approximately 5 µm. 0.4% agarose also exhibited this, however the hydrogel seemed less porous with a more solid structure. In 0.7% agarose, the flaked appearance has given way to a solid structure which was interdisperced with a low number of larger pores of approximately 10 µm in diameter. 1.4% and 2% agarose hydrogels appeared as solid sheets with a rouge surface but no visible pores. This was most likely not that the hydrogel had an absence of pores, but that they were too small to be seen by SEM; with SEM very small pores could be hidden or filled during sputter coating.

4.3.3.3. Release of bacteriophage from agarose hydrogels

To analyse bacteriophage release from agarose hydrogels, 1 mL of agarose (0.2 – 2% w/v) containing 10^8 pfu/mL bacteriophage was cast in triplicate in a 12-well plate and allowed to set overnight at 4 °C. The concentration of released bacteriophage was then measured after the addition of 1 mL SM buffer per well.

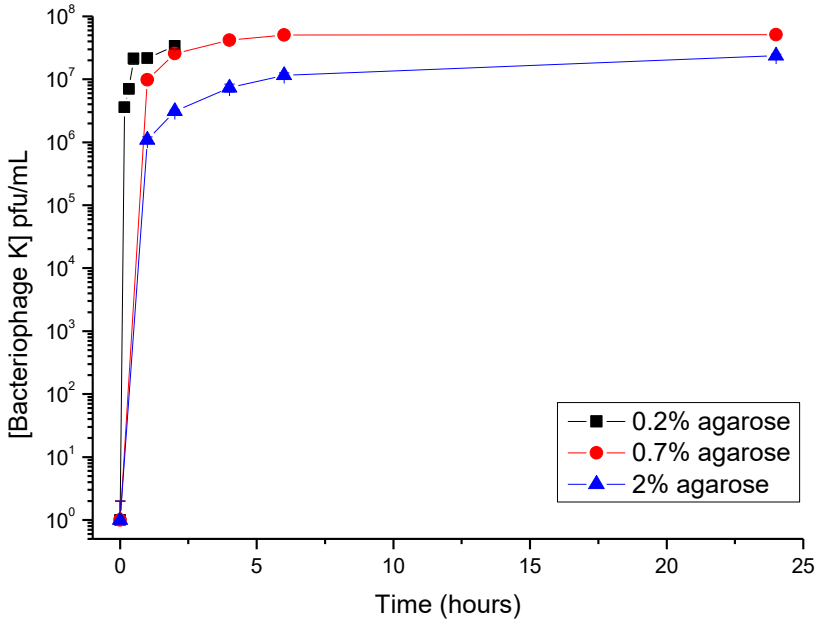

Figure 4.24: Bacteriophage release from 0.2%, 0.7% and 2% agarose hydrogels

In general, a higher concentration of released bacteriophage was seen in agarose hydrogels compared to PVA. A burst release of bacteriophage was seen, with the majority of bacteriophage being released in less than 10 minutes in most agarose concentrations (Figure 4.24). The lowest concentration (and so most porous) 0.2% agarose hydrogel exhibited very fast release, with bacteriophage concentration reaching a plateau after 7.5 minutes. In 0.7% hydrogels, release was slightly slower but the majority of bacteriophage had been released by 10

minutes. The more concentrated 2% agarose hydrogel showed a far shallower release curve, with eventually 10^7 pfu/mL bacteriophage released.

4.3.3.4. Kinetics of bacteriophage release from hydrogels

To analyse the fast diffusion of bacteriophage from agarose, the concentration of bacteriophage released was assessed over a shorter timeframe (Figure 4.25). Here, 0.2% agarose was chosen as a highly porous, highly hydrated hydrogel, 0.7% was chosen as a porous, solid hydrated hydrogel and 2% agarose was chosen as a dense, less hydrated hydrogel. 1 mL SM buffer was then added per well and the bacteriophage concentration again measured at various timepoints before the system had reached the steady state. The kinetics of bacteriophage diffusion in agarose were again calculated using Fick's Law (see Section 4.3.2.4.).

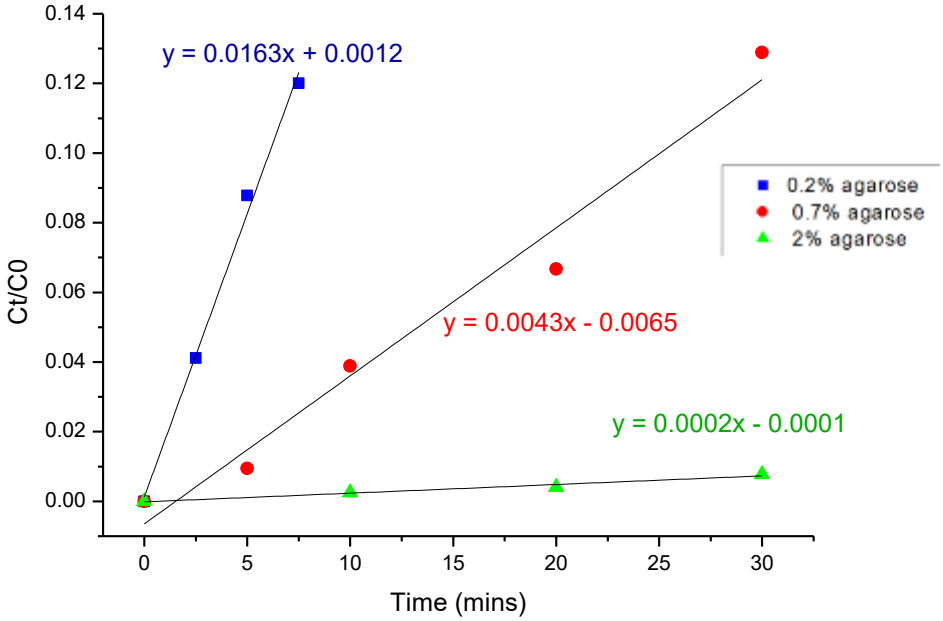

Figure 4.25: Graph of C_t/C_0 0.2%, 0.7% and 2% agarose hydrogels

The slopes calculated in Figure 4.25 were then used to calculate D_{app} for each concentration of agarose. Here, solution volume, V, was 1 x 10^{-6} m^3 and membrane thickness, X, was again 2.6 x 10^{-3} m for all measurements. The diffusion area, S, was calculated from the 12-well plate well diameter as 3.8 x 10^{-4} m^2.

% agarose w/v	C_t/C_0	V (10^{-6} m^3)	X (10^{-3} m)	S (10^{-4} m^2)	t (secs)	D_{app}(m^2sec^{-1})
0.2	0.0163	1	2.6	3.8	450	2.48E-10
0.7	0.0043	1	2.6	3.8	1800	1.63E-11
2	0.0002	1	2.6	3.8	1800	7.60E-13

Table 4.4: D_{app} calculations for Bacteriophage K diffusion from 0.2%, 0.7% and 2% agarose hydrogels

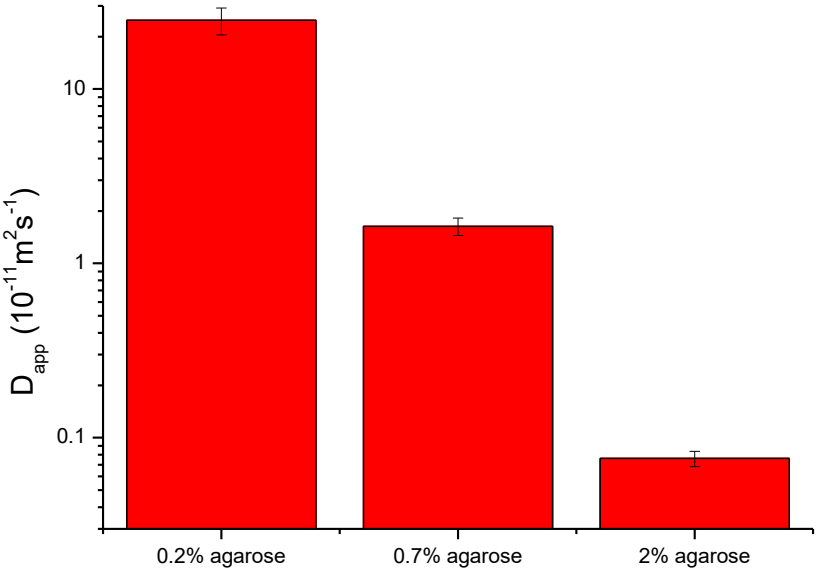

Figure 4.26: Diffusion coefficient values (10^{-11} m^2sec^{-1}) for 0.2%, 0.7% and 2% agarose

As expected, again the diffusion constant for bacteriophage decreases significantly as % agarose (and so hydrogel density) increases (Table 4.4 and Figure 4.26). The more concentrated polymer network physically slows diffusion of bacteriophage particles. The D_{app} values calculated correlate extremely well with those reported by Hu et al in 2010, where they analysed the diffusion of T4 phage in agarose[17, 23]. In this case, 0.2% agarose (the most porous gel that could form a solid gel) showed the highest D_{app} of 2.48 x 10^{-10} m^2sec^{-1}. As agarose concentration increased, D_{app} values decreased with 1.63 x 10^{-11} m^2sec^{-1} for 0.7% agarose and 7.60 x 10^{-13} m^2sec^{-1} for 2% agarose. In general all agarose hydrogels showed significantly higher release and D_{app} values than PVA hydrogels.

This could be due to the nature of each hydrogel gelation mechanism. In PVA the gel forms semi-crystalline areas which are highly packed and could entrap bacteriophage. With agarose the structure is more homogenous, meaning a less tight entrapment.

4.3.3.5. Zones of inhibition

Agarose hydrogels containing 10^8 pfu/mL Bacteriophage K were incubated on bacterial lawns containing *S. aureus* H560 to assess bacteriophage diffusion out of the hydrogel. Again the diameter of bacteriophage lysis around the hydrogel disc was measured.

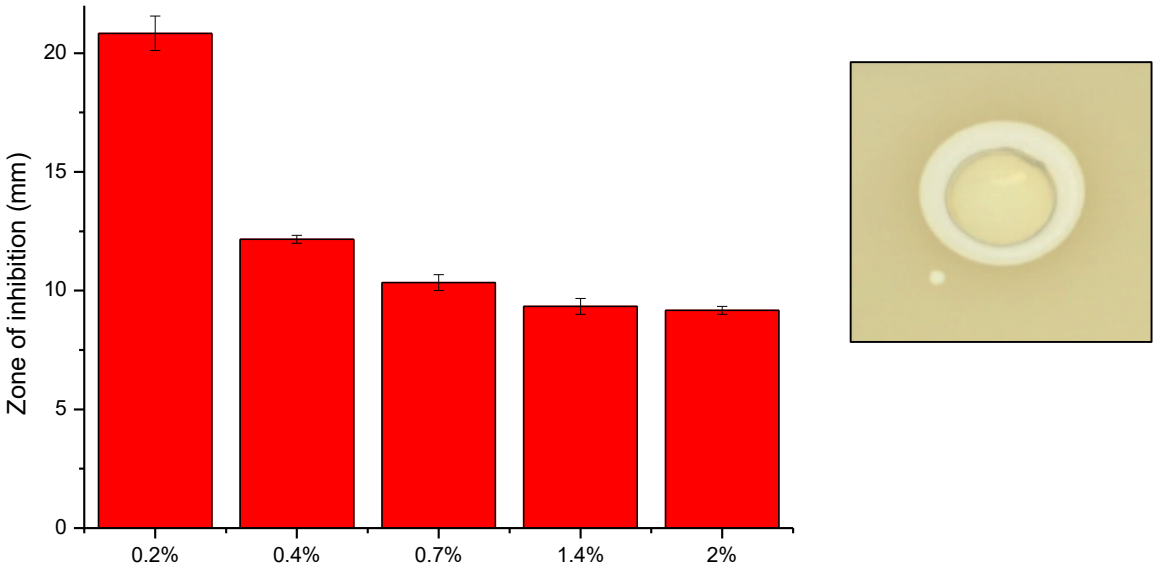

Figure 4.27: (left) Zone of inhibition measurements of 8 mm diameter agarose hydrogels containing 10^8 pfu/mL Bacteriophage K on *S. aureus* H560. (right) Image of zone of inhibition surrounding 0.4% agarose

The ability of bacteriophage to diffuse out of agarose hydrogels was reduced with increasing agarose concentration (Figure 4.27). However in all cases, bacteriophage were able to diffuse and infect bacteria present in the agar plate. In 0.2% a very high diffusion was seen of approximately 20 mm in diameter. This correlates well with the diffusion experiments in Section 4.3.3.3. where 0.2% agarose showed very high release of Bacteriophage K after one hour. In more concentrated hydrogels the zone of inhibition appears significantly smaller with 12.2, 10.3, 9.8 and 9 mm for 0.4%, 0.7%, 1.4% and 2% hydrogels respectively.

4.3.3.6. Bacteriophage hydrogels in overnight culture

0.4%, 0.7%, 1.4% and 2% agarose hydrogels containing 10^8 pfu/mL Bacteriophage K were formed into 24-well plates with 500 µL per well. 0.2% agarose was not investigated further as its lack of structure retention, high swelling ratio and fast bacteriophage diffusion meant that it would not be suitable for further development. The hydrogels were allowed to set overnight at 4 °C and then incubated with *S. aureus* H560 subculture. Now that the diffusion of bacteriophage from agarose hydrogels into buffer solution and bacterial lawns had been assessed, it was again important to measure the bacteriophage infectivity in actively growing liquid culture. The growth of the bacteria overnight was measured to determine if bacteriophage were still infective against actively metabolising and replicating bacterial culture once immobilised in the hydrogel matrix (Figure 4.28).

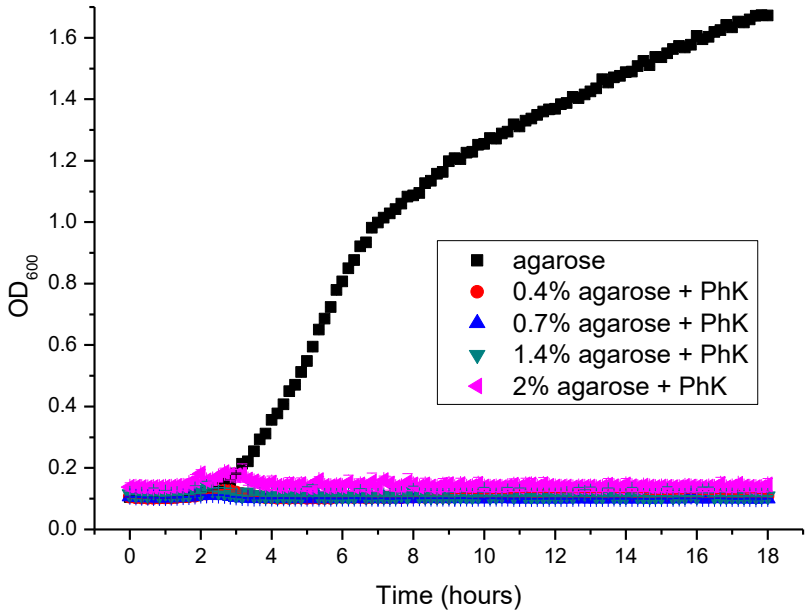

Figure 4.28: Growth curves of *S. aureus* H560 liquid cultures incubated with 0.4%, 0.7%, 1.4% and 2% agarose containing 10^8 pfu/mL Bacteriophage K.

Bacteriophage immobilised in 0.4%, 0.7%, 1.4% and 2% agarose all exhibited complete killing of *S. aureus* H560 in solution compared to agarose containing no bacteriophage (in this case 0.7% but the bacterial growth curve was the same in all agarose concentrations). It was already understood from Section 4.3.3.3. that after one hour, bacteriophage were able to diffuse enough into SM buffer from all agarose concentrations to exhibit a high enough concentration to kill bacteria (> 10^5 pfu/mL). This was seen in practice here, as killing was observed in all cases. The "bump" seen at approximately two hours is again characteristic of bacteriophage infection as described in Section 4.3.2.5.

4.3.3.7. UV irradiation

Once immobilised in agarose, it was again important to determine that on UV irradiation the polymer structure did not generate reactive radicals which would lower bacteriophage infectivity (as was seen in PVA). *S. aureus* H560 was incubated with agarose hydrogels that had been exposed to flood UV curing for 10, 30 and 60 seconds.

Bacteriophage K immobilised in agarose hydrogels were successfully able to prevent bacterial growth after UV irradiation (Figure 4.29). This implied that the more complex polysaccharide

structure of agarose is less susceptible to radical formation in the presence of UV, or that radicals quickly react together to terminate before reaction with bacteriophage.

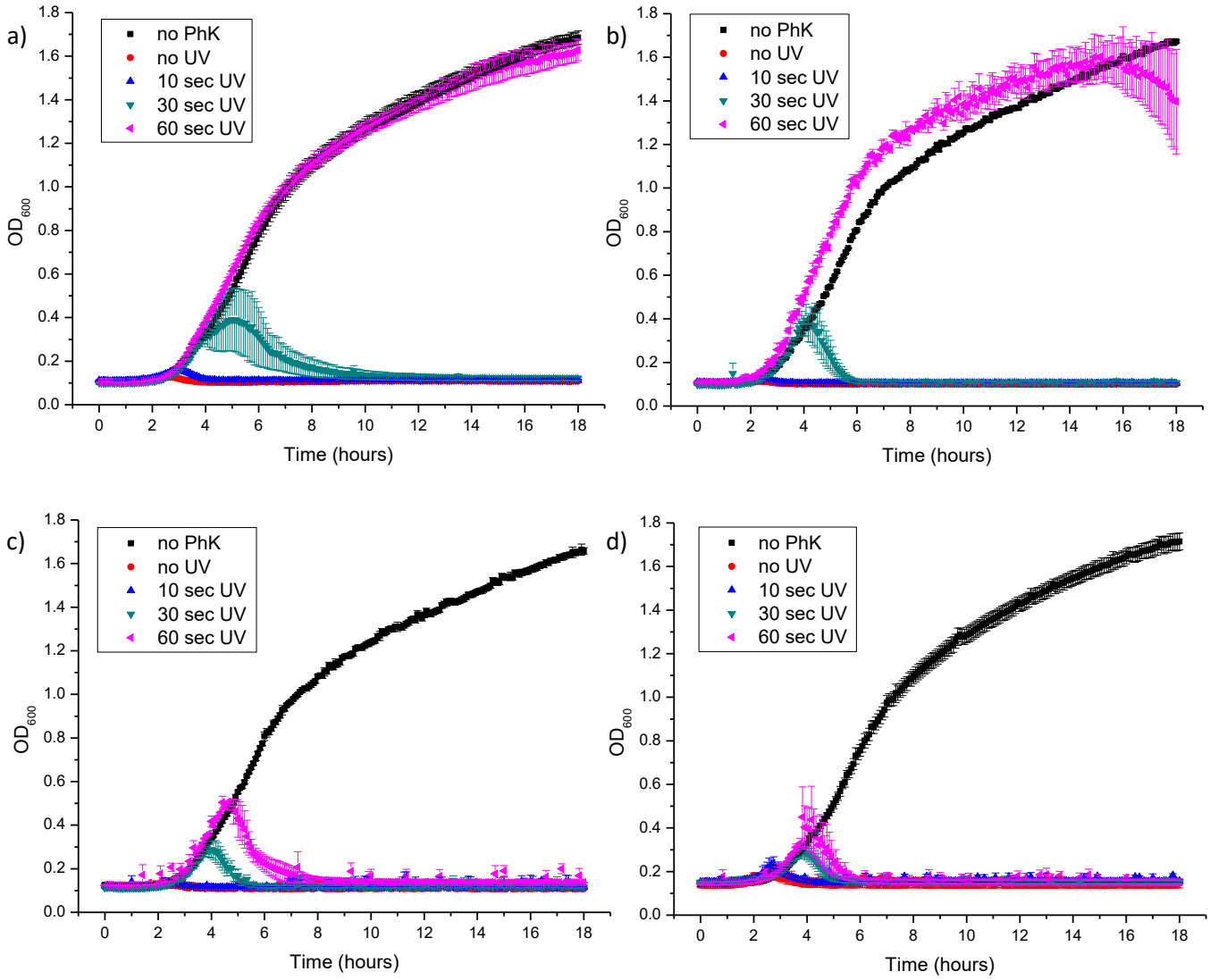

Figure 4.29: Incubation of *S. aureus* H560 with a) 0.4%, b) 0.7%, c)1.4% and d)2% agarose containing 10^8 pfu/mL Bacteriophage K which has been irradiated with flood UV for 10, 30 and 60 seconds

In general, the extent of *S. aureus* killing by Bacteriophage K was again reduced with more UV irradiation. In all cases killing was seen with Bacteriophage K hydrogels that had been UV cured for 0, 10 and 30 seconds; by 60 seconds bacterial killing was only seen in 1.4% and 2% agarose hydrogels. It was hypothesised that the concentration of the agarose hydrogel exhibits a protective effect over the bacteriophage, shielding the viral particles from damaging UV irradiation. The higher the concentration, the more protection; this can explain why in less

concentrated hydrogels (0.4% and 0.7%) after prolonged UV irradiation a loss of bacteriophage activity is seen compared to more concentrated hydrogels.

In 1.4% and 2% agarose hydrogels, killing was also initiated at later stages as irradiation time increased. For example after 10 seconds UV irradiation, killing started at the beginning of the exponential phase at 2 hours. After 30 seconds UV irradiation killing commenced later at 4 hours. By 60 seconds UV irradiation killing only commenced after 5 hours. This is thought to be due top UV damage of the bacteriophage slowing or reducing the infectivity of bacteriophage.

4.3.3.8. Overview

Overall, agarose hydrogels were found to be good vehicles for the immobilisation of bacteriophage. Agarose gels showed high swelling and allowed bacteriophage to diffuse at varying rates depending on polymer concentration. Bacteriophage were also able to successfully infect live bacteria on plates and in liquid culture. Additionally, the hydrogel actually showed protective properties over bacteriophage when UV irradiated.

4.4. Conclusions

In this chapter, the therapeutic use of Bacteriophage K as an active bacteriophage against *Staphylococcus aureus* infections was investigated. Here, agarose and PVA hydrogel systems were also used in order to immobilise the bacteriophage in a protective, highly aqueous environment. Although some research has been carried out into bacteriophage in agarose hydrogel matrices, immobilisation in poly (vinyl alcohol) has not been reported. In both cases the hydrogels were assessed for activity against live bacterial cultures. This chapter set out to answer a number of questions:

- Is Bacteriophage K a suitable bacteriophage for use in *S. aureus* infections?
- Can bacteriophage be immobilised in hydrogel matrices?
- Are bacteriophage able diffuse through the matrices, and if so, how?
- Once diffused out, are bacteriophage able to remain active against *S. aureus*?

Bacteriophage K proved to be a highly active bacteriophage with a broad host range against *S. aureus*. Diffusion of the bacteriophage in both hydrogels was investigated with diffusion significantly higher in agarose hydrogels. Furthermore, it could be successfully immobilised in both agarose and PVA hydrogels whilst retaining infectivity.

4.5. References

1. P. L. Wagner and M. K. Waldor, *Infection and Immunity*, 2002, **70**, 3985-3993.
2. S. O'Flaherty, A. Coffey, R. Edwards, W. Meaney, G. F. Fitzgerald and R. P. Ross, *Journal of Bacteriology*, 2004, **186**, 2862-2871.
3. S. O'Flaherty, R. P. Ross, W. Meaney, G. F. Fitzgerald, M. F. Elbreki and A. Coffey, *Appl Environ Microbiol*, 2005, **71**, 1836-1842.
4. D. R. Alves, A. Gaudion, J. E. Bean, P. Perez Esteban, T. C. Arnot, D. R. Harper, W. Kot, L. H. Hansen, M. C. Enright and A. T. A. Jenkins, *Applied and environmental microbiology*, 2014, **80**, 6694-6703.
5. P. Golec, K. Dąbrowski, M. S. Hejnowicz, A. Gozdek, J. M. Łoś, G. Węgrzyn, M. B. Łobocka and M. Łoś, *Journal of Microbiological Methods*, 2011, **84**, 486-489.
6. M. Merabishvili, C. Vervaet, J.-P. Pirnay, D. De Vos, G. Verbeken, J. Mast, N. Chanishvili and M. Vaneechoutte, *PLoS ONE*, 2013, **8**, e68797.
7. E. Jonczyk, M. Klak, R. Miedzybrodzki and A. Gorski, *Folia Microbiol (Praha)*, 2011, **56**, 191-200.
8. X. Qiu, *PLoS ONE*, 2012, **7**, e39793.
9. M. Breitbart, L. Wegley, S. Leeds, T. Schoenfeld and F. Rohwer, *Appl Environ Microbiol*, 2004, **70**, 1633-1640.
10. O. Blokhina, E. Virolainen and K. V. Fagerstedt, *Annals of Botany*, 2003, **91**, 179-194.
11. A. L. Santos, C. Moreirinha, D. Lopes, A. C. Esteves, I. Henriques, A. Almeida, M. R. Domingues, I. Delgadillo, A. Correia and A. Cunha, *Environ Sci Technol*, 2013, **47**, 6306-6315.
12. M. T. Neves-Petersen, S. Petersen and G. P. Gajula, in *Molecular Photochemistry - Various Aspects*, ed. S. Saha, InTech, 2012.
13. S. Bryant, R. Rahmanian, H. Tam and S. Zabetian, *Journal of Experimental Microbiology and Immunology*, 2007, **11**, 66 - 72.
14. M. Bercea, S. Morariu and D. Rusu, *Soft Matter*, 2013, **9**, 1244-1253.
15. U. Manna and S. Patil, *J Phys Chem B*, 2009, **113**, 9137-9142.
16. E. Otsuka and A. Suzuki, *Journal of Applied Polymer Science*, 2009, **114**, 10-16.
17. J. Hu, K. Miyanaga and Y. Tanji, *Biotechnol Prog*, 2010, **26**, 1213-1221.
18. A. Pluen, P. A. Netti, R. K. Jain and D. A. Berk, *Biophys J*, 1999, **77**, 542-552.
19. E. Niki, Y. Yamamoto and Y. Kamiya, 1978, **169**, 78-95.
20. D. I. Pattison and M. J. Davies, *Exs*, 2006, 131-157.
21. J. Y. Xiong, J. Narayanan, X. Y. Liu, T. K. Chong, S. B. Chen and T. S. Chung, *J Phys Chem B*, 2005, **109**, 5638-5643.
22. D. Nordqvist and T. Vilgis, *Food Biophysics*, 2011, **6**, 450-460.
23. J. Hu, K. Miyanaga and Y. Tanji, *Biotechnol Prog*, 2012, **28**, 319-326.

Chapter 5 : Development of Crosslinkable Hyaluronic Acid and Subsequent Sensitivity to *Staphylococcal* Hyaluronidase

5.1. Introduction

This section will focus on the development of an enzymatically degradable upper layer which will be added to the top of the bacteriophage hydrogel (described in Chapter 4) to create a 'smart' release wound dressing. On bacterial infection, the upper layer will be degraded by secreted *S. aureus* virulence factors, exposing the lower bacteriophage hydrogel. The bacteriophage can then diffuse out of the hydrogel and go on to infect (Figure 5.1).

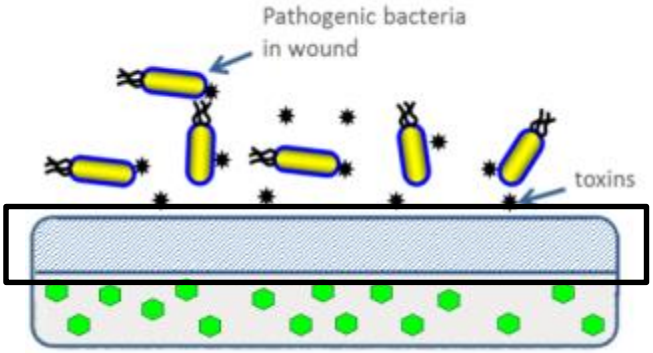

Figure 5.1: Schematic diagram of bilayered hydrogel system: upper hydrogel layer containing degradable crosslinked HA.

The upper hydrogel layer ideally needs to include a number of key properties; the hydrogel needs to be flexible, dense and enzymatically sensitive, whilst also promoting wound healing:

- **Flexibility:** A flexible hydrogel is required to prevent the wound dressing degrading or breaking during normal patient movement.
- **High crosslinking density:** In order to form a sturdy barrier to prevent release of bacteriophage from the lower layer, the hydrogel must be highly crosslinked without excess swelling.
- **Enzyme sensitivity and selectivity:** The trigger mechanism of this dressing is introduced by forming the upper layer from a polymer that is selectively degradable by *S. aureus* virulence factors. The polymer must be very sensitive to bacterial enzymes; a low amount of enzyme must be able to cause considerable degradation. Selectivity is also

important as the polymer must be broken down by an enzyme that is not produced by all bacterial species.

- **Wound healing:** Ideally the dressing must also promote wound healing. In the presence of *S. aureus*, the layer will degrade and bacteriophage will be released, but in the presence of no infection, the upper layer polymer must still aid healing as this is the layer in contact with the wound.

Hyaluronic acid was chosen as the enzyme-sensitive polymer which makes up the upper layer. The polymer is natural, non-immunogenic, non-toxic and is known to aid wound healing. Its structure also contains a number of chemically active groups which can be used to crosslink the polymer into hydrogel networks. The enzyme hyaluronidase (which breaks down HA) is known to be mainly secreted by *S. aureus*, meaning that the upper layer will only be degraded in the presence of that species.

HA must be crosslinked in order to form a solid hydrogel. A number of crosslinking methods were investigated to find an optimal HA formulation which encompassed the majority of desired characteristics. Alongside this, HAase expression and reactivity was investigated in *S. aureus* to ensure that HAase expressed was active, secreted in high enough concentrations and also that it was secreted by the majority of strains. The crosslinked hydrogels were tested with purified and *Staphylococcal* HAase and the structural breakdown during degradation followed through SEM and quantitatively with the Carbazole assay.

5.2. Materials and Methods

Hyaluronic acid sodium salt from *Streptococcus equi* (M_w = 1.8 x 10^6 g/mol), EDC, sodium periodate, ethylene glycol, *tert*-butyl carbazate, trichloroacetic acid, trinitrobenzene sulphonic acid solution (TNBS), adipic dihydrazide, glycidyl methacrylate, triethylamine (TEA), tetrabutyl ammonium bromide (TBAB), Irgacure 2959, PEG diacrylate (M_n = 575), PEG diglycidyl ether (M_n = 500), sodium azide, sodium chloride, hyaluronidase from bovine testes (Type I-S, 400-1000 U/mL), N-acetyl glucosamine, sodium tetraborate, p-dimethylaminobenzaldehyde (DMAB), acetic acid and hydrochloric acid were purchased from Sigma-Aldrich (Poole, Dorset, UK). Phosphate buffered saline (PBS) was purchased from Oxoid (Basingstoke, Hamps, UK)

5.2.1. Carbodiimide crosslinking

40 mL 2% w/v HA solution was dissolved overnight and then sonicated to remove air bubbles. The solution was then poured into a 120 x 120 mm square petri dish and the solution was allowed to settle to form an even distribution. The dish was incubated at 37 °C overnight to form a dry HA film. The film was then cut into 10 x 10 mm squares for further tests.

To crosslink, dried HA films were immersed in acetone:H_2O solution (80:20) containing EDC and HCl, as well as varying concentrations of PEG diglycidyl ether (0.5 – 20 equivalents) overnight at room temperature. Films were then washed in acetone:H_2O and allowed to air dry.

5.2.2. Aldehyde/adipic dihydrazide crosslinking

5.2.2.1. Synthesis of oxidised HA (oxi-HA)

Oxidisation of HA was carried out using a modified method based on the work described by Yeo et al[1, 2]. 1 g HA was dissolved in 100 mL distilled water (1% w/v) at room temperature until homogenous. 5 mL 0.5 M sodium periodate was then added and thoroughly mixed. The reaction was carried out for 2 hours at room temperature in the dark. The reaction was then terminated with the addition of 500 µL ethylene glycol to quench the reaction. Oxidised HA was purified by dialysis in deionised water for 3 days, with water changes every 12 hours. The product was then freeze dried and stored at -20 °C until needed. Oxi-HA structure was confirmed using FTIR and the TNBS assay.

5.2.2.2. TNBS assay

The TNBS assay was used to determine the degree of oxidisation of oxi-HA[3]. In brief, 25 µL 0.6% oxi-HA in water was added to 25 µL *tert*-butyl carbazate (t-BC) solution (30 mM *tert*-butyl carbazate in 1% w/v aqueous trichloroacetic acid) in a 1.5 mL Eppendorf tube and reacted at room temperature for 24 hours. 0.5 mL TNBS solution (6 mM TNBS, 0.1 M borate buffer, pH 8) was then added to each vial and allowed to react for a further hour at room temperature. 50 µL of the final mixture was then removed and placed in a 96-well plate, where it was diluted with 200 µL 0.5 M HCl per well. Absorbance was measured at 340 nm. A standard calibration curve of aqueous t-BC (5 – 30 mM) was used to calculate the concentration of unreacted t-BC in the test solution, and subsequently concentration of aldehyde groups per molecule. All experiments were done in triplicate.

5.2.2.3. Crosslinking of oxi-HA with adipic dihydrazide

Oxi-HA and adipic dihydrazide (ADH) were allowed to thaw for 1 hour at room temperature before use. Separate solutions were then made of oxi-HA (6% w/v) and ADH (8% w/v) in deionised water, and the solutions allowed to dissolve until homogenous. To form crosslinked hydrogels, 200 µL ADH solution was added to 800 µL oxi-HA solution and immediately vortexed. A solid hydrogel was seen to form after approximately 30 seconds. Hydrogel crosslinking was confirmed with FTIR.

5.2.3. Photopolymerisation crosslinking

5.2.3.1. Synthesis of hyaluronic acid methacrylate (HAMA)

Photo-crosslinkable HA methacrylate (HAMA) was prepared using the method described by Leach et al[4]. In brief, 1 g of HA (M_w = 1.8 x 10^6 g/mol) was dissolved in water overnight to form a 1 % w/v solution. 2.2 mL TEA, 4.4 mL glycidyl methacrylate and 2.2 g TBAB were then added sequentially, with each reagent fully dissolved before the addition of the next. The solution was stirred at room temperature for 24 hours, followed by 1 hour incubation at 60 °C. HAMA was then recovered by precipitation with acetone (20 x volumes) and re-dissolved in distilled water to remove excess reactants. The HAMA was lyophilised and stored at 4 °C until needed. ^{1}H NMR was used to determine the percentage of methacrylation. HAMA samples were dissolved in D_2O and spectra were recorded with a Bruker 450 MHz NMR.

5.2.3.2. Photopolymerisation of HAMA

Solutions of varying concentration of HAMA (0.5 – 5% w/v) and PEG diacrylate (0 – 10% v/v) were dissolved in deionised water overnight to form a homogenous mixture. The photoinitiator Irgacure 2959 was then added, the solution mixed, and then incubated at 50 °C for 5 minutes to aid solvation. The mixture was then kept in the dark at room temperature for up to 2 weeks until needed. To photocrosslink the HAMA mix, 400 µL mix was added per well to a 12-well plate with the plates then incubated under UV light (Dymax 5000 Flood curing system, 400 W) for 60 seconds.

5.2.4. Carbazole assay

The concentration of HA breakdown products after breakdown by HAase was quantified using a modified version of the Carbazole assay described by Makris et al[5]. Bacterial overnight cultures (approximately 10^9 cfu/mL) in TSB broth were centrifuged at 4,000 rpm for 15 minutes and the supernatant filter sterilised with 0.22 µm filters. 125 µL supernatant was then added to 250 µL

pre-warmed HA solution (0.6 % HA, 1 % NaN_3 and 200 mM NaCl). The vials were mixed and incubated at 37 °C for 2 hours with mild shaking (120 rpm). After this time, 125 µL was removed and added to vials containing 125 µL water and 25 µL 0.8 M sodium tetraborate. The vials were then boiled at 95 °C for 3 minutes to stop further enzyme activity. Samples were cooled and stored at 4 °C until needed. A standard curve was simultaneously carried out using 125 µL N-acetyl-glucosamine (0.5 - 0.05 mM) mixed with 125 µL water and 25 µL 0.8 M sodium tetraborate. Vials were boiled at 95 °C for 3 minutes and again allowed to cool.

A colour change was seen on the addition of 750 µL 0.1x DMAB reagent (10% w/v DMAB, 12.5 % v/v 10 M HCl, 87.5 % v/v glacial acetic acid) and subsequent incubation at 37 °C for 20 minutes. The absorbance at 544 nm was measured on a BMG SPECRAstar spectrometer.

5.2.5. Hyaluronidase production in biofilms

5.2.5.1. *S. aureus* biofilm formation

S. aureus biofilms were formed using previously reported methods[6]. In brief, 10 µL bacterial overnight culture was added to 10 mL TSB broth supplemented with 1% D-(+)-glucose. 1 mL solution was then added per well to a 12-well plate, as well as three wells containing TSB broth as a negative control; the plates were then incubated at 37 °C with no shaking to form biofilms.

Biofilm plates were removed at 6, 24 and 48 hours to determine HAase concentration and biofilm biomass. Biofilm supernatant was removed, centrifuged and filter sterilised with a 0.22 µm to remove any planktonic bacteria. HAase concentration of the sterilised supernatant was then measured using the Carbazole assay (Section 5.2.4).

5.2.5.2. Crystal violet assay

Biofilm biomass was quantified using the Crystal Violet assay. After the removal of supernatant for HAase analysis, each well was washed twice with PBS to remove planktonic bacteria. Plates were then dried for one hour at 50 °C. After drying, 500 µL 0.1% crystal violet staining solution was added and the plates left at room temperature for 20 minutes. The stain was then removed and the wells washed twice again with PBS. To dissolve the dye, 1 mL ethanol was added per well and, following a 10-fold dilution, the absorbance was measured at 590 nm.

5.3. Results and Discussion

5.3.1. Crosslinking of HA

5.3.1.1. Carbodiimide crosslinking

One of the most common methods of crosslinking HA with itself is through the use of water soluble diimides such as EDC. Here, dried HA films were immersed in acidified 80:20 acetone:water containing EDC, HCl and PEG diacrylate; the acetone:water mixture here allowed for solvation and reaction of EDC without further solvation of the HA film. PEG diglycidyl ether was also introduced as a crosslinker in order to form more crosslinks with the HA, and to also improve hydrogel properties by increasing hydrogel strength. An example reaction scheme for EDC crosslinking of HA can be seen in Figure 5.2.

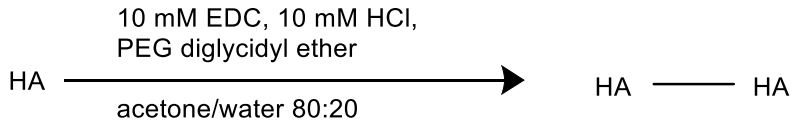

Figure 5.2: Reaction scheme for the crosslinking of HA with EDC and PEG diglycidyl ether

Carbodiimides are the most popular, best understood and most versatile methods for the chemical crosslinking or functionalisation of carboxylic acids, with the water soluble EDC the most commonly used. On reaction of HA with EDC, the EDC reacts with HA carboxylic acid groups to form an active O-acylisourea intermediate. This group can then go on to react in a number of different ways to form crosslinks (Figure 5.3). Both the carboxylic acid and secondary alcohol groups can attack the intermediate forming zero-length HA-HA crosslinks. With the addition of other molecules, such as diethers or diamines, longer crosslinks can be formed.

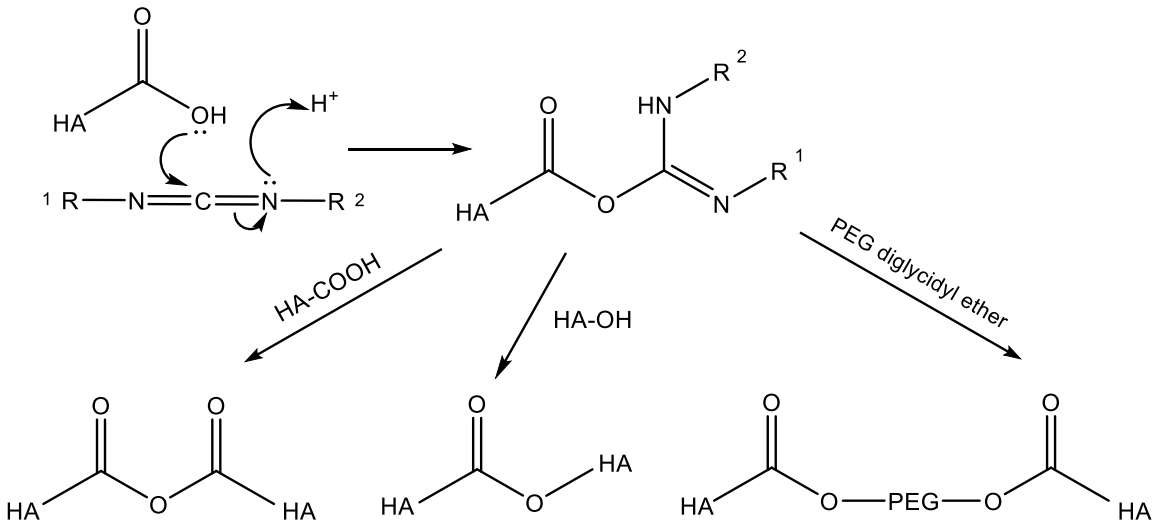

Figure 5.3: Reaction mechanism for the EDC mediated crosslinking of HA

The crosslinking of HA films in acetone:water containing EDC and crosslinker resulted in the formation of highly crosslinked hydrogel films. On crosslinking, the dry hydrogel films did not appear different from native HA films; they were slightly flexible and easily cut with scissors (Figure 5.4). After hydration, crosslinked HA films did not swell to high amounts, and although very flexible, could be easily ripped and were prone to curling into tubes.

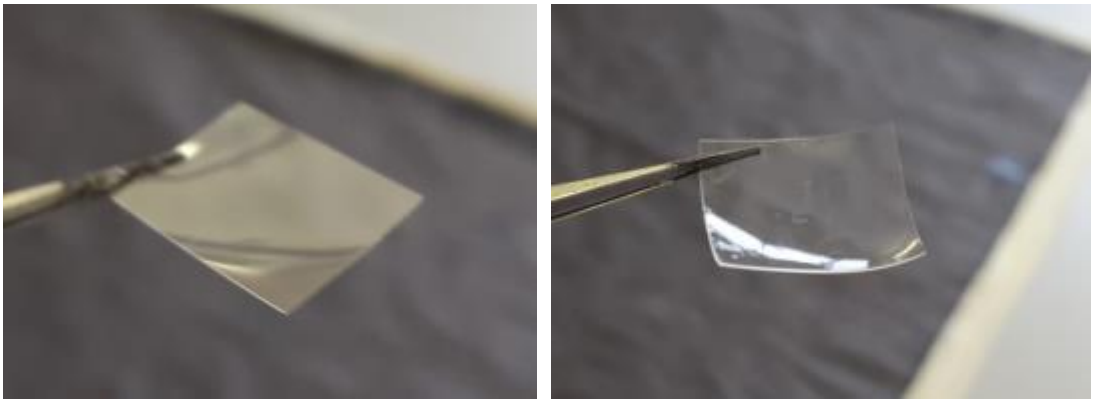

Figure 5.4: a) dry HA film before crosslinking, b) crosslinked HA film (10 mM EDC, 10 mM HCl, 250 mM PEG diglycidyl ether) after swelling in PBS buffer overnight

Firstly, a previously reported standard crosslinking mix was assessed to crosslink HA using 10 mM EDC, 10 mM HCl and 250 mM PEG diglycidyl ether crosslinker. The structure of crosslinked HA was confirmed by FTIR, with the appearance of a new C=O ester stretch at approximately 1730 cm^{-1} compared to non-crosslinked HA (Figure 5.5). It was not possible to tell from FTIR

spectra which major crosslinking route was followed, however it is most likely a mixture all three mechanisms.

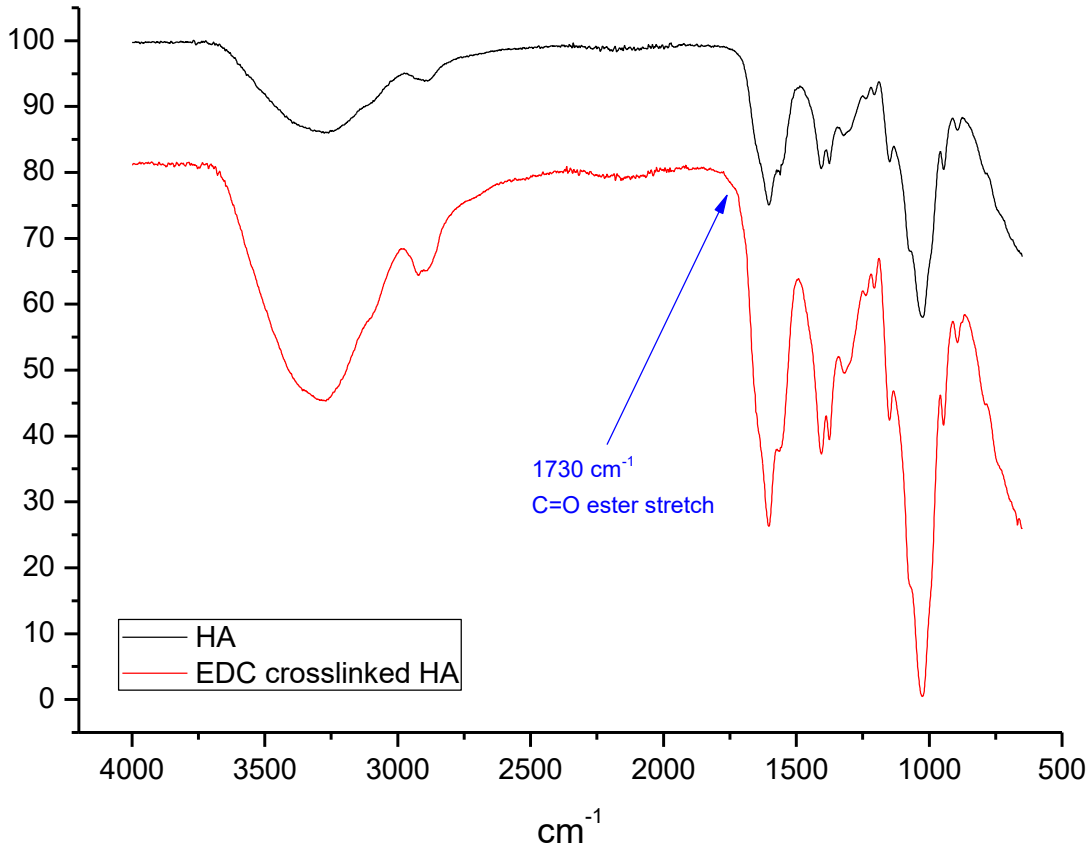

Figure 5.5: FTIR spectrum of HA and HA sheets crosslinked with 10 mM EDC, 10 mM HCl and 250 mM PEG diglycidyl ether.

A screen of reaction conditions was carried out to analyse how changing EDC, HCl and PEG diglycidyl ether concentration would affect the hydrogel swelling ratio (Table 5.1). Here, HA films were immersed overnight with varying concentrations of EDC (1 – 100 mM), HCl (10 – 50 mM) and PEG diglycidyl ether (25 – 500 mM). Mixtures containing no EDC and no PEG diglycidyl ether were also assessed. The swelling ratio was then calculated using previously described methods.

	EDC (mM)	HCl (mM)	PEGDE (mM)	Swelling ratio
1	0	10	250	no crosslinking
2	1	10	250	7.9 ± 1.3
3	2	10	250	4.8 ± 0.1
4	5	10	250	2.6 ± 0.1
5	10	10	250	1.8 ± 0.1
6	50	10	250	1.2 ± 0.2
7	100	10	250	0.7 ± 0.2
8	10	0	0	1.4 ± 0.1
9	10	10	0	no crosslinking
10	10	10	25	16.2 ± 1.2
11	10	10	50	4.5 ± 0.4
12	10	10	100	2.6 ± 0.2
13	10	10	250	1.5 ± 0.2
14	10	10	500	1.2 ± 0.03
15	0	10	0	no crosslinking
16	10	10	250	2.1 ± 0.1
17	10	20	250	2.9 ± 0.1
18	10	50	250	3.7 ± 0.3
19	0	0	0	no crosslinking

Table 5.1: Swelling ratio calculations for HA sheets crosslinked with EDC (1 – 100 mM), HCl (10 – 50 mM) and PEG diglycidyl ether (0 – 500 mM)

Firstly, swelling ratio generally decreased with increased concentration of EDC or PEG diglycidyl ether. With EDC, swelling ratio reduced from 7.9 ± 1.3 for 1 mM to 0.7 ± 0.2 for 100 mM. With PEG diglycidyl ether a similar trend was seen, with a reduction of 16.2 ± 1.2 for 25 mM to 1.2 ± 0.03 for 500 mM. This implied that in both cases the number of crosslinks was increasing as more crosslinking species were available. The concentration of HCl was also assessed, with a slight increase in swelling ratio as concentration increased (2.1 ± 0.1 for 10 mM, 2.9 ± 0.1 for 20 mM and 3.7 ± 0.3 for 50 mM). This could be due to hydrolysis of HA repeating units causing a breakdown of polymer structure at low pH.

In all samples where no EDC was present (samples 1, 15, and 19), no crosslinking of HA films was seen, showing that EDC was essential for successful crosslinking. In sample 15, only HCl was present to determine if crosslinking could occur through acid catalysed esterification, however this proved unsuccessful.

In general, although strong highly crosslinked HA hydrogels were formed through crosslinking with carbodiimides, the films were not chosen for further development due to the fact that the hydrogel could not be crosslinked in situ. For the proposed sandwich hydrogel, it would not be

possible to add second layers to the hydrogel once crosslinked. Also the presence of an acetone:water based crosslinking solution would damage any bacteriophage virions immobilised in the second layer.

5.3.1.2. Aldehyde/adipic dihydrazide crosslinking

Next, sodium periodate was chosen to oxidise certain groups on HA, as although it results in the degradation of HA primary structure (unlike Dess-Martin periodinane or TEMPO oxidation), the reaction is fast and the number of aldehydes formed per repeating unit is two as opposed to one (Figure 5.6). The viscosity of the HA reaction solution was visibly reduced after 24 hours, implying breakdown of the HA ring structure.

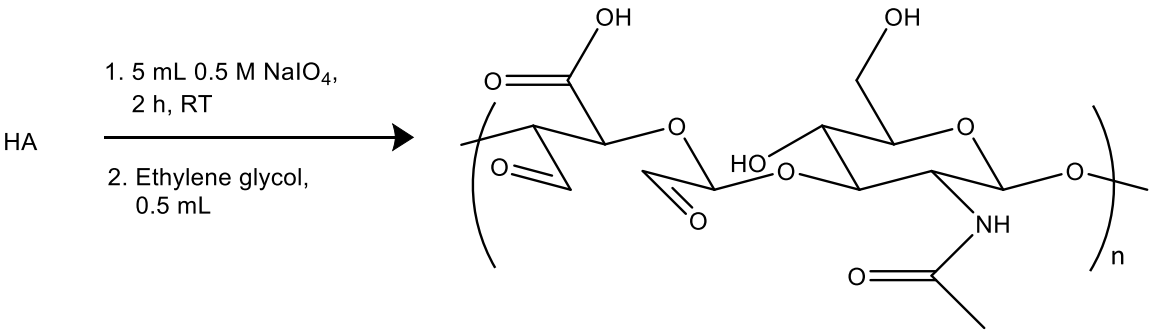

Figure 5.6: Reaction scheme for the oxidation of HA by sodium periodate

On reaction of oxi-HA with adipic dihydrazide, the nucleophilic ADH amine attacks the electrophilic oxi-HA aldehyde groups. This goes on to form a stable imine bond, through a carbinolamine intermediate, between one aldehyde group and one end of the ADH molecule. Because the ADH molecule is a diamine, it can act as a crosslinker which reacts with two sites on one HA molecule, or with two different molecules. The reaction mechanism for oxidised HA crosslinking with dihydrazide groups can be seen in Figure 5.7.

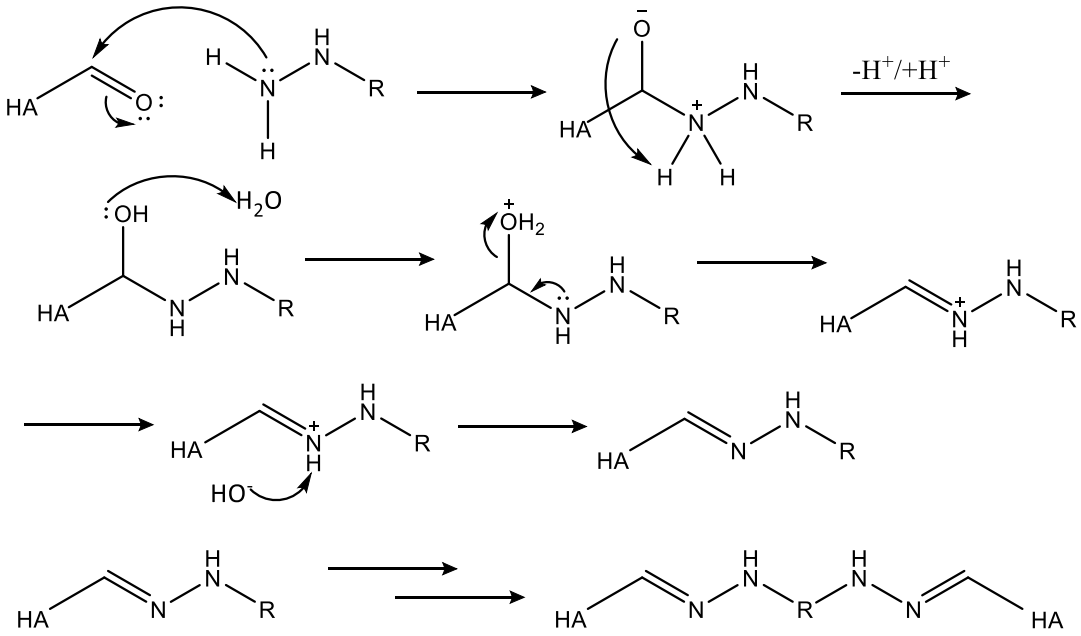

Figure 5.7: Reaction mechanism for the nucleophilic addition of adipic dihydrazide to oxi-HA

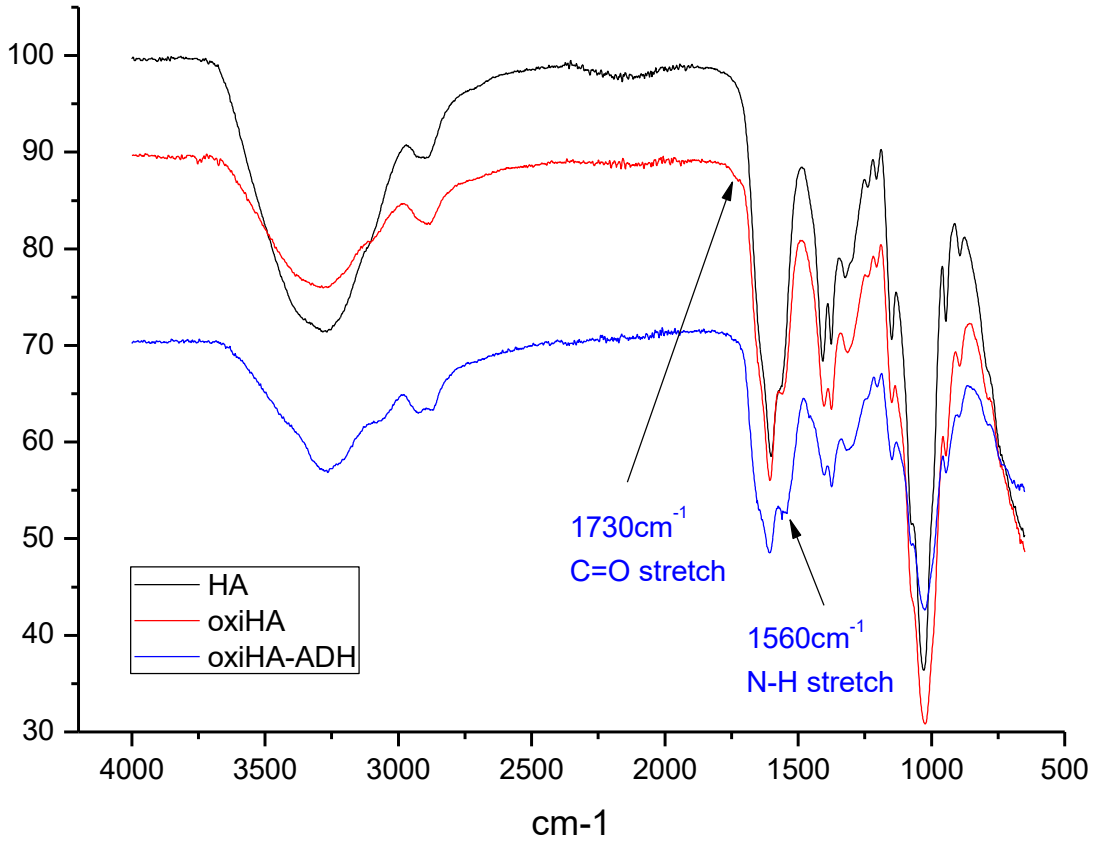

Figure 5.8: FTIR spectrum of HA, oxidised HA and oxidised HA crosslinked with adipic dihydrazide, aldehyde groups, and subsequent HA crosslinking

HA was oxidised by reaction with sodium periodate, which opens the glucuronic acid ring and forming two aldehyde groups per ring. FTIR was used to confirm the presence of aldehyde groups in oxi-HA (Figure 5.8). The appearance of a new peak at 1730 cm^{-1} showed the presence of a C=O aldehyde stretch. After crosslinking with adipic dihydrazide, the hydrogel was dried overnight at 50 °C. The crosslinked structure was again confirmed by FTIR with the simultaneous appearance of a peak at 1560 cm^{-1} (N-H stretch) and loss of the C=O peak at 1730 cm^{-1}.

The TNBS assay was used to calculate the degree of oxidation of oxi-HA, as the aldehyde groups were not stable with other quantitative methods such as NMR. A standard curve of *tert*-butyl carbazate was initially formed, and the concentration of t-BC remaining after reaction with oxi-HA subsequently quantified. The calculated number of aldehyde groups was then divided into the number of repeating units of HA, giving an approximate degree of oxidation of 70%.

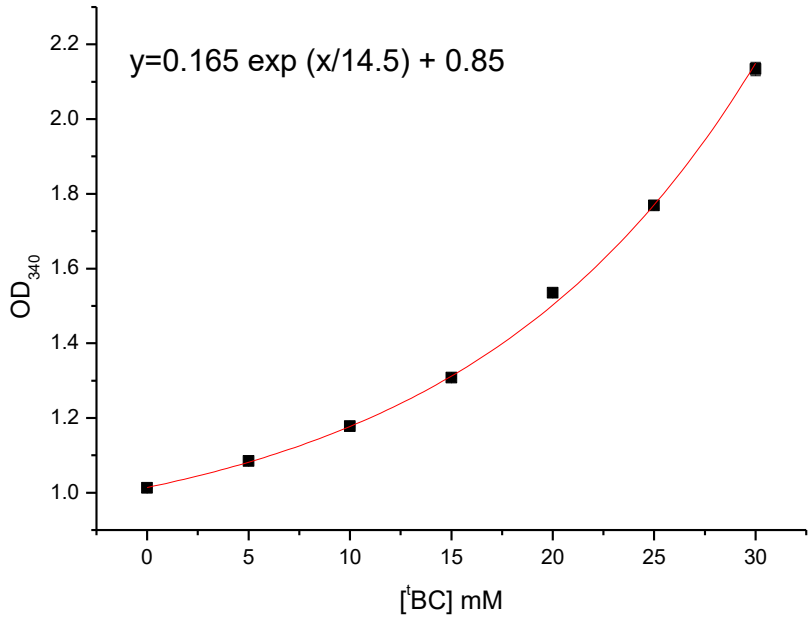

Figure 5.9: Standard curve of OD_{340} measurements of 0 – 30 mM tert-butyl carbazate used to calculate aldehyde concentration in oxidised HA

Oxi-HA/ADH hydrogels were formed by mixing 6% oxi-HA with 8% ADH in aqueous solution. Crosslinking occurred extremely quickly after mixing at room temperature, with a solid hydrogel being seen after approximately 30 seconds compared to the viscose liquids of the reactants (Figure 5.10). The hydrogel formed was clear and elastic, with polymerisation occurring so quickly that air bubbles became entrapped in the matrix. On removal of the gel from the reaction vessel hydrogel shape was kept slightly, however it did not retain a defined structure.

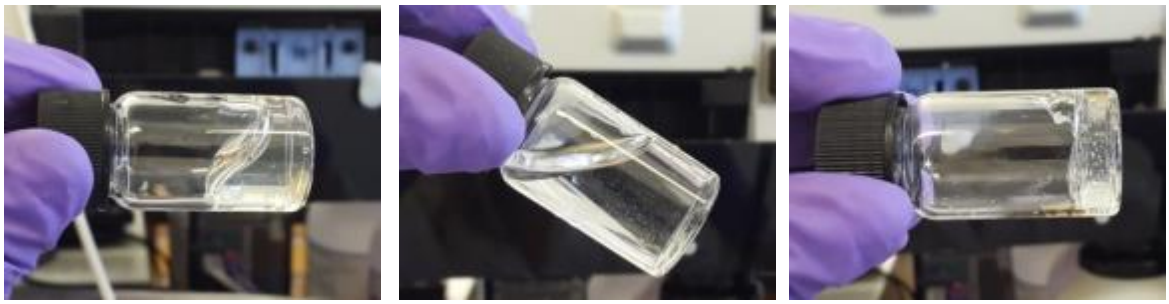

In general, although a fast and reliable way of crosslinking HA without the addition of toxic crosslinking agents, this approach was not investigated further. This was primarily due to the speed of crosslinking; although this could be altered by tailoring the % oxidation of oxi-HA or the concentration of ADH, the removal of entrapped air bubbles would still be an issue.

5.3.1.3. Photopolymerisation crosslinking

A photo-crosslinkable HA was next investigated as crosslinking with UV light offers a number of benefits over purely chemical crosslinking; the degree and time of polymerisation can be controlled, and hydrogels can be crosslinked in situ. The polymer can also be crosslinked in aqueous solution and can be co-polymerised with other photoactive or inert polymers. This also offers the opportunity of forming interpenetrating polymer networks (IPNs) where a polymer scaffold is soaked in a photocrosslinkable polymer mixture and then UV crosslinked forming an interlaced framework.

The methacrylation of HA to form a photoactive HA is predominantly carried out using methacrylic anhydride or glycidyl methacrylate, however the use of methacrylic anhydride gives low control of methacrylation and can yield methacrylic acid by-products[4, 7, 8]. HAMA was synthesised by reacting HA with 10 molar equivalents of glycidyl methacrylate in an excess of TEA and TBAB. In the presence of TEA, the basic conditions favour the ring-opening of glycidyl methacrylate epoxide by the secondary alcohol on the N-acetyl glucosamine unit of HA, as opposed to the glucuronic acid carboxylate (which is favoured at pH 3.5)[9]. The reaction scheme can be seen in Figure 5.11.

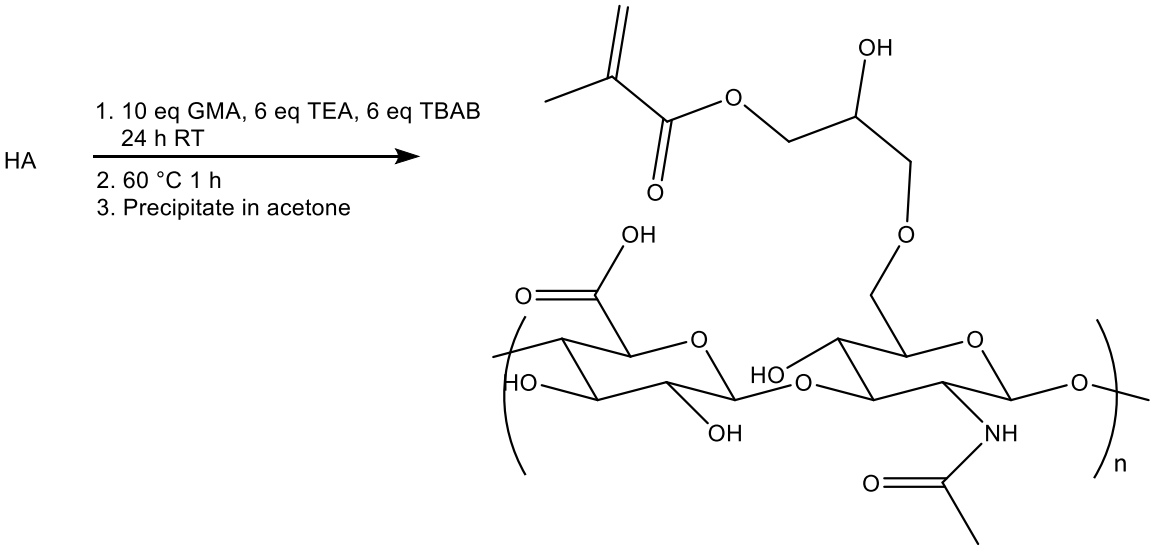

Figure 5.11: Reaction scheme for the methacrylation of HA using glycidyl methacrylate

Once purified, aqueous HAMA solution was UV crosslinked with the use of the photoinitiator Irgacure 2959; this was chosen predominantly because of its low cytotoxicity[10]. In UV light Irgacure 2959 homolytically cleaves to form two different radical species. The benzaldehyde radical species then goes on to attack the methacrylate double bond, initiating polymerisation (Figure 5.12). Diacrylates were also introduced as a crosslinker to strengthen gel and increase crosslink density; PEG diacrylate, ethylene glycol dimethacrylate and ethylene diacrylate were all initially tested.

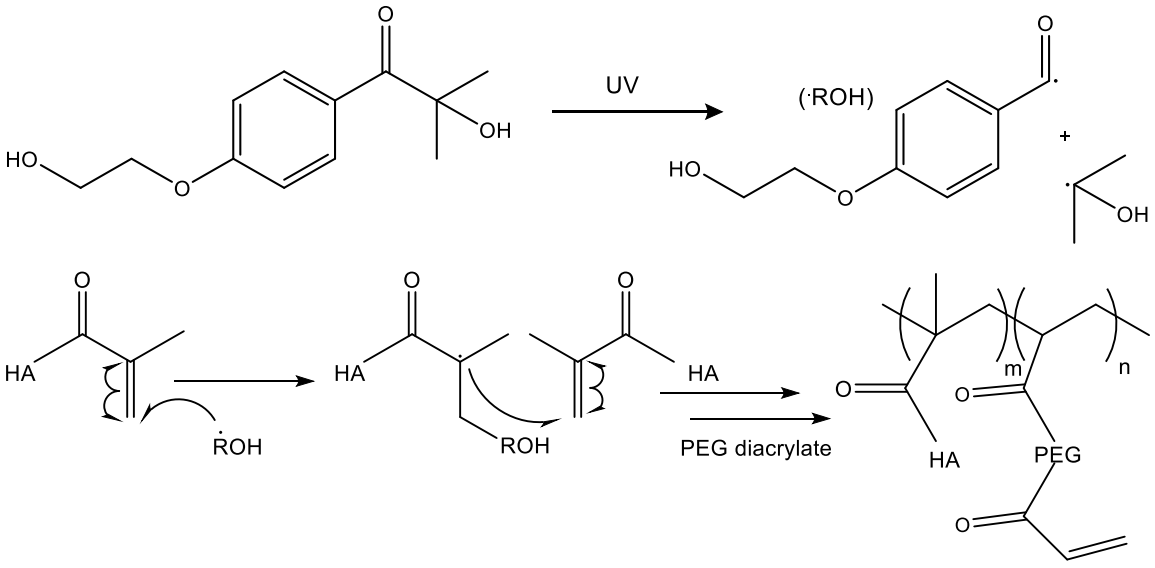

Figure 5.12: Reaction mechanism of radical formation of Irgacure 2959 by UV light and subsequent polymerisation initiation of HAMA.

HAMA hydrogels containing 1, 2 and 5% diacrylate were crosslinked for 1 minute in a UV reactor. As seen in Figure 5.13, hydrogels crosslinked with the longer chain PEG diacrylate were clear, whereas those crosslinked with ethylene glycol dimethacrylate and ethylene diacrylate were opaque. A clear hydrogel layer is advantageous in this system, as in a wound dressing it is beneficial to be able to see the progression of healing without disturbing the dressing. A clear gel means that wound healing instead can be assessed by looking through the hydrogel. Because of this, HAMA crosslinked with PEG diacrylate was taken on for further investigation.

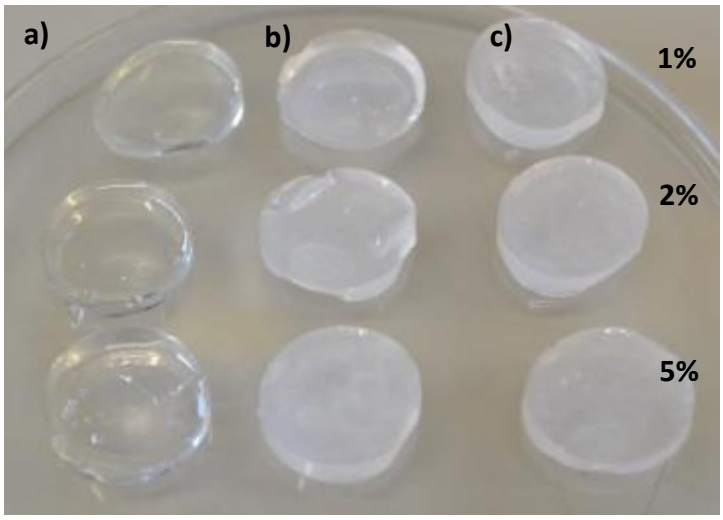

FTIR analysis of HAMA verified methacrylation with peaks at 1455 cm^{-1} corresponding to C=C stretching (Figure 5.14). The structure of HAMA was also confirmed by ^{1}H NMR. Resonances at 5.6 and 6.2 ppm verified the presence of methylene protons coupled to the grafted methacrylate (Figure 5.15). The integration ratio of methacrylate methylene protons and the N-acetyl glucosamine methyl proton peak allowed the approximate % methacrylation to be calculated as 7%.

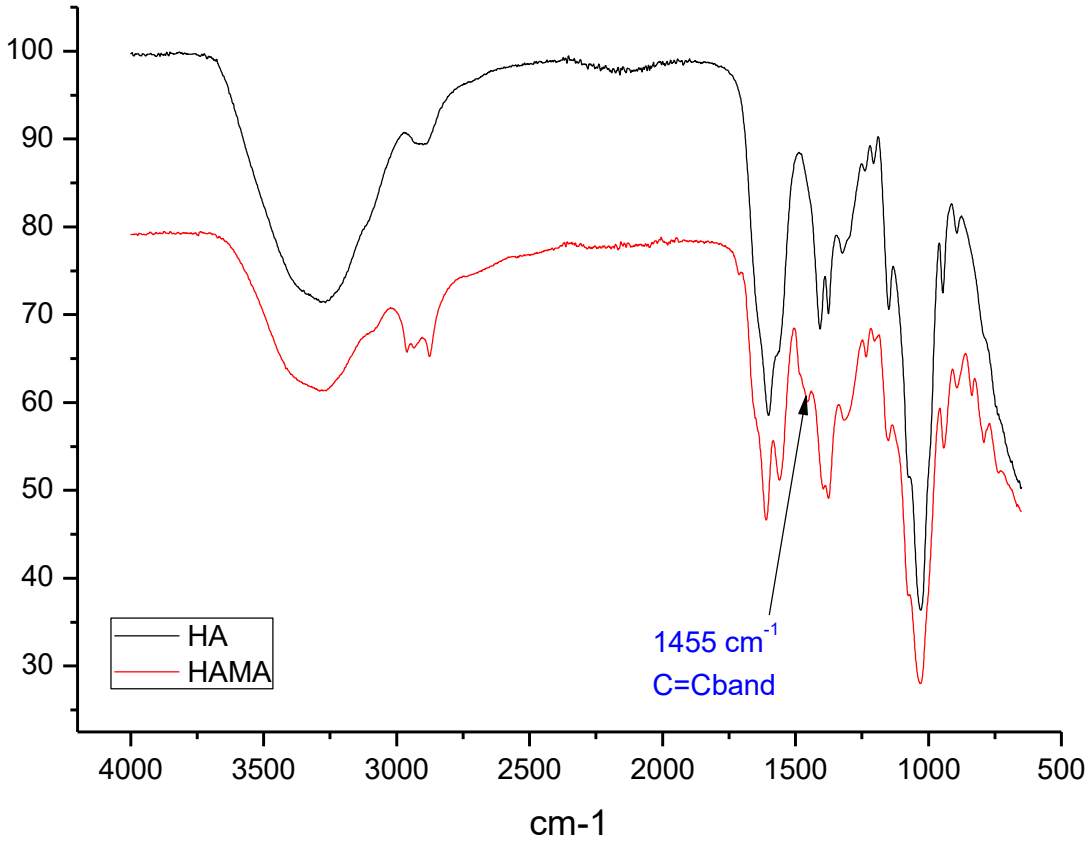

Figure 5.14: FTIR spectra of hyaluronic acid and hyaluronic acid methacrylate (HAMA)

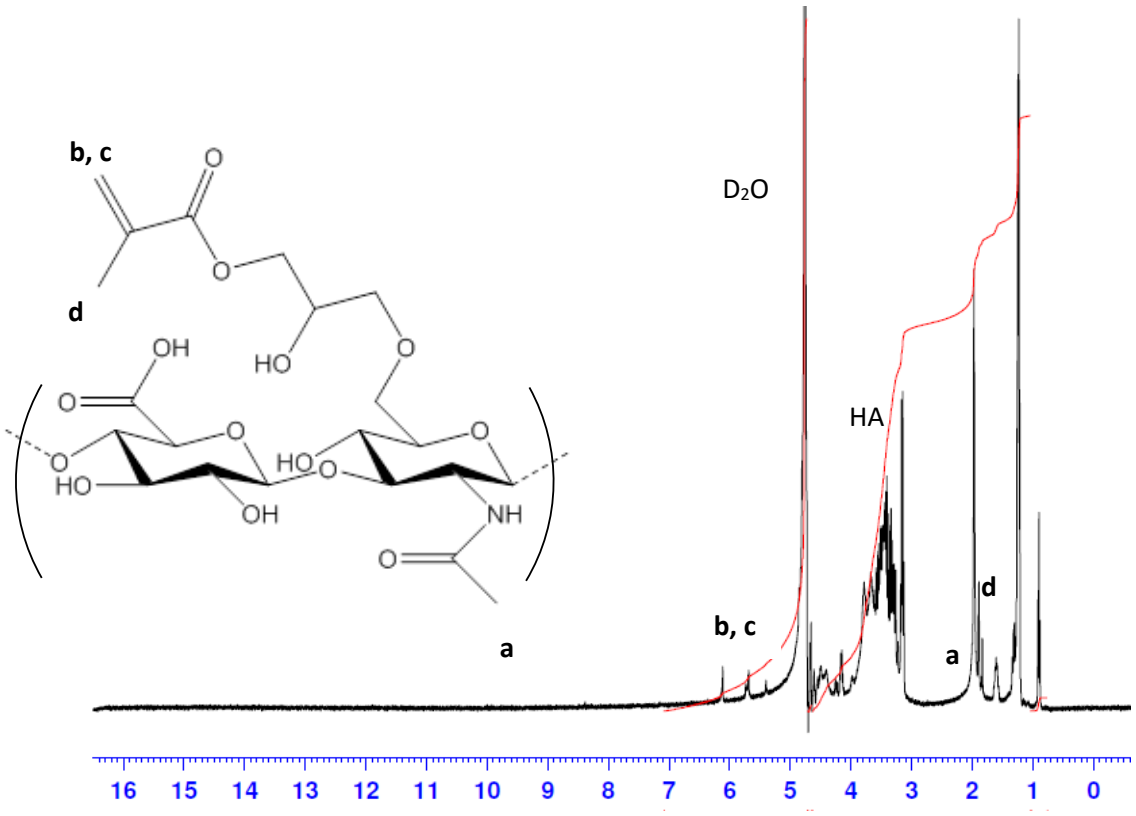

Figure 5.15: ^{1}H NMR spectrum of HAMA in D_2O. Resonances at 5.6 and 6.2 ppm verified the presence of methylene protons.

2% w/v HAMA was co-crosslinked with a range of concentrations of PEG diacrylate, along with 1% Irgacure 2959 photoinitiator through free radical polymerisation. The hydrogels could be crosslinked for up to 1 minute without visible signs of degradation (e.g. yellowing, structure breakdown or fluid exudate).

The swelling ratio of hydrogels changed inversely with the concentration of PEG diacrylate (Figure 5.16). For 0, 1, 5 and 10% w/v PEG diacrylate, the swelling ratio was determined as 67.4±3.9, 41.5±0.7, 14.6±0.1 and 7.7±0.3 respectively (n=3). This indicates an increased crosslinking density and a smaller hydrogel mesh size. This could also be due to the increasing % of PEG in the hydrogel compared to HA. As HA is more hydrophilic than PEG, and is thought to hold more water molecules per chain than PEG, this could contribute to a lower interaction of the hydrogel with water and subsequent swelling.

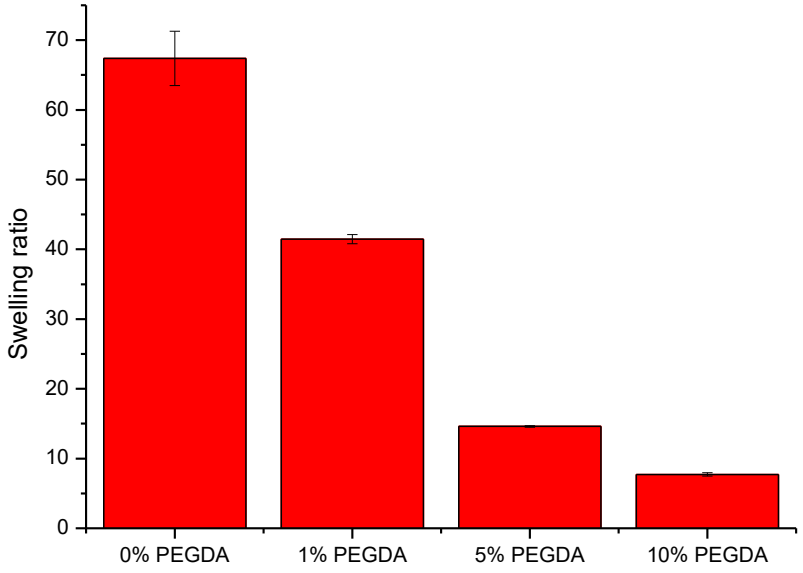

Figure 5.16: Swelling ratio measurements of 2% HAMA hydrogels containing varying % PEG diacrylate with 1% initiator and 1 minute UV exposure

A better understanding of hydrogel networks can be found using Florey-Rehner calculations, however in this case the heterogeneity of the system meant a too simplistic approximate was given. For 0% PEG diacrylate HA hydrogels (a one component system well explained by Florey-Rehner), the mesh size was found to be approximately 6.6 µm, with a crosslink density of 1.65 x 10^{-8} mol/cm^3. On the addition of PEG diacrylate however, Florey Rehner cannot now be reliably used. An indication of mesh size and crosslink density can be gained from swelling data by utilising the Florey parameter and specific dry polymer volume of HA throughout. By doing this,

a mesh size of 3.1, 0.6 and 0.2 µm respectively was seen for 1%, 5% and 10% PEG diacrylate hydrogels; however this was not completely illustrative of the real system.

SEM images of 2% HAMA hydrogels containing 0, 1, 5, and 10% PEG diacrylate were taken to assess internal structure and mesh size (Figure 5.17). In general, as PEG diacrylate concentration increased hydrogel structure became more ordered, implying that the long PEG chains are orienting together. A definite columnar structure is seen in hydrogels containing 5 and 10% PEG diacrylate.

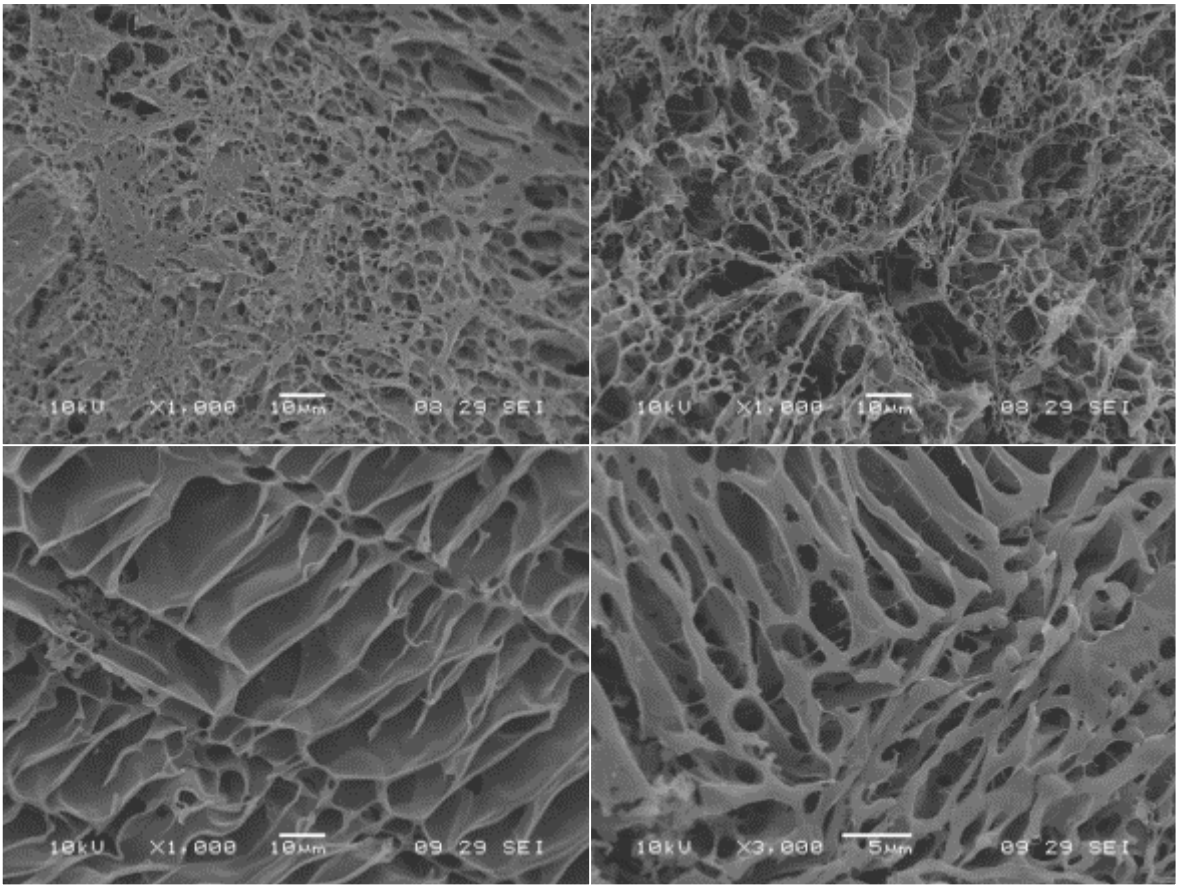

Figure 5.17: Side-on SEM images of 2% HAMA hydrogels containing 0, 1, 5 and 10% v/v PEG diacrylate with 1% initiator and 1 minute UV exposure.

After investigation of structure and swelling properties of HA crosslinked by various methods, it was decided that photocrosslinked 2% HAMA hydrogels co-crosslinked with 1% PEG diacrylate and 1% Irgacure 2959 was an optimal formulation to take on for further testing. The hydrogels formed were robust, and had a significantly small pore size and swelling ratio to ensure the retention of active molecules stored in the lower hydrogel layer. HAMA could be easily polymerised in situ, with good control of the hydrogel properties and without the fast gelation time seen with oxi-HA/ADH gels. The HAMA gels formed were then analysed for their reaction with HAase, both purified and from *S. aureus* cultures.

5.3.2. Hyaluronidase production by *S. aureus*

5.3.2.1. Screen of bacterial hyaluronidase activity

A screen of 116 clinical strains was carried out to assess HAase expression in a wide range of bacterial strains and species (Figure 5.19), which gave an 82.7% overall activity and 86% activity in *S. aureus*. These included hospital and community acquired MSSA and MRSAs, coagulase positive and negative *S. aureus*, as well as other medically important species such as *E.coli*, *P. aeruginosa*, and *S. epidermidis*. An additional screen of 33 *Proteus mirabilis* strains was also carried out, however no HAase activity was seen.

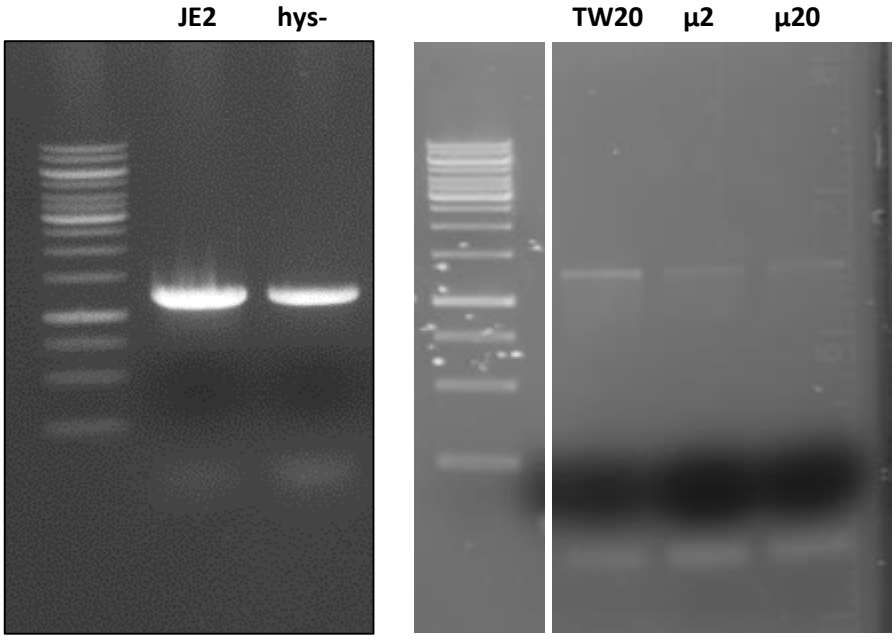

Figure 5.18: 2% agarose gels of hysA gene in JE2, NE334 (hys-), TW20, ST239 µ2 and ST239 µ0. Ladder =1 kB

HAase activity was calculated using the Carbazole assay, by incubating HA solution with bacterial supernatant. In brief, the assay involves the reaction of HA NAG at the reducing end with borate to form a monoanhydro sugar. On subsequent addition of acidified p-dimethylaminobenzaldehyde (DMAB), the DMAB is able to react with the sugar to form a red/purple complex with maximum absorbance at 544 nm.

The level of activity between strains ranged up to approximately 1.2 mM NAG in 2 hours. There was no apparent correlation between bacterial virulence and HAase activity. This also did not appear to be determined by methicillin resistance or origin of species.

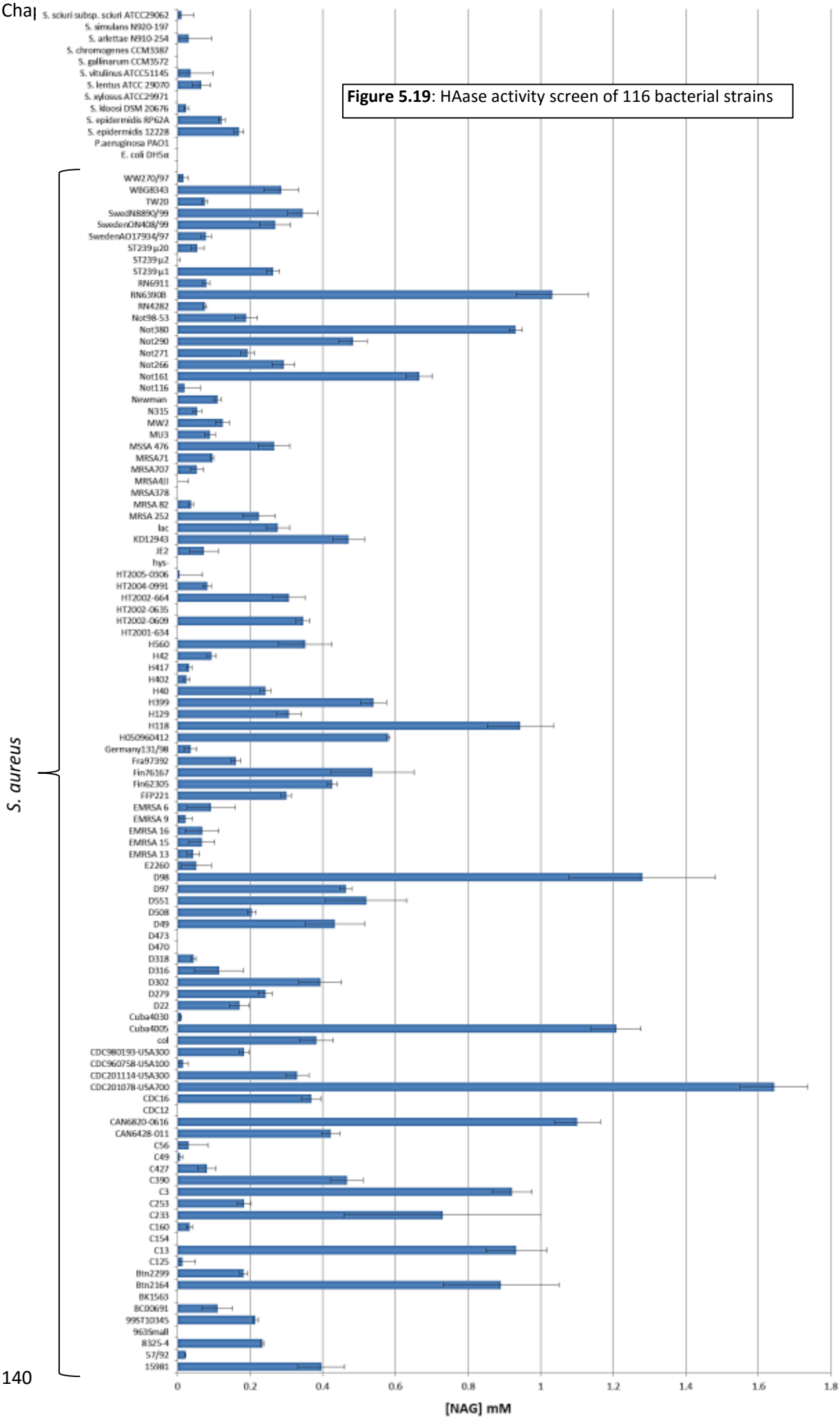

Figure 5.19: HAase activity screen of 116 bacterial strains

A number of *S. aureus* strains were found to show no HAase activity. *S. aureus* NE334 (hys-) is distinctive from other HAase negative *S. aureus* strains found in the screen, as it has been genetically engineered to exhibit no HAase activity by insertion of a transposon. Bacterial DNA was extracted and then analysed for the *hysA* gene, to asses if hysA is removed in non-engineered strains (Figure 5.18). Alongside hys-, JE2 was analysed as the parent strain of hys- (which does show activity). Also, ST239 µ2 and µ20 were analysed alongside their parent strain TW20. In all cases, the hysA gene was present.

S. aureus NE334 (hys-) does not exhibit HAase activity as the inserted transposon prevents the correct gene transcription. In other cases this also could be true; however it is more likely that the gene is downregulated by other mechanisms (e.g. the gene is silenced or repressed).

5.3.2.2. Hyaluronidase expression during *S. aureus* growth

The secretion of HAase was monitored over the growth cycle of both HAase positive (H560) and negative (ST239 µ2) *S. aureus* strains (Figure 5.20 and Figure 5.21). Bacterial subcultures were grown in 50 mL centrifuge tubes in a shaking incubator at 37 °C. Samples were then removed at certain timepoints; for each timepoint the bacterial OD_{600} and the HAase activity ([NAG] $ml^{-1}min^{-1}OD_{600}^{-1}$) was measured using the Carbazole assay.

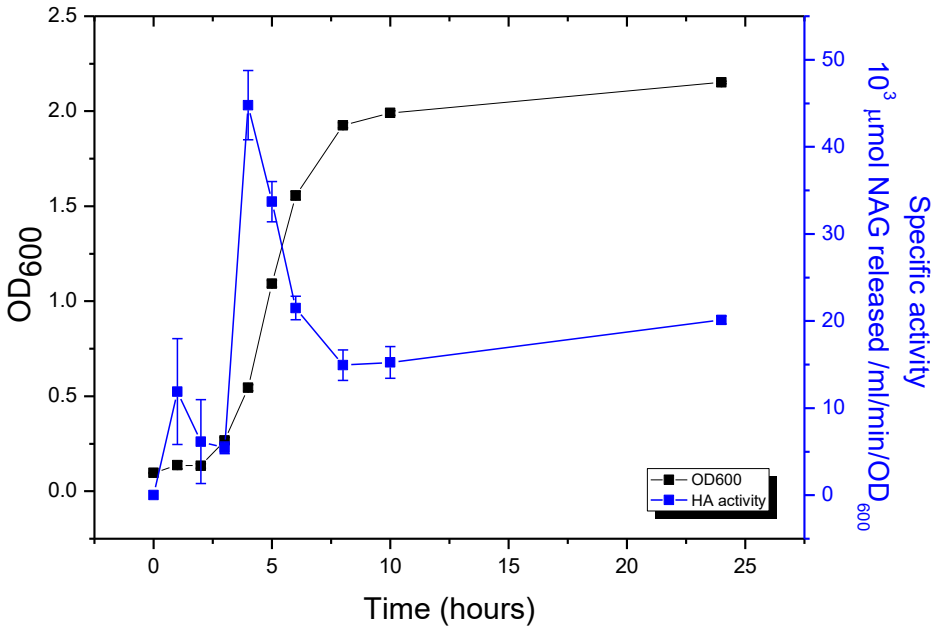

Figure 5.20: HAase production during the growth of *S. aureus* H560

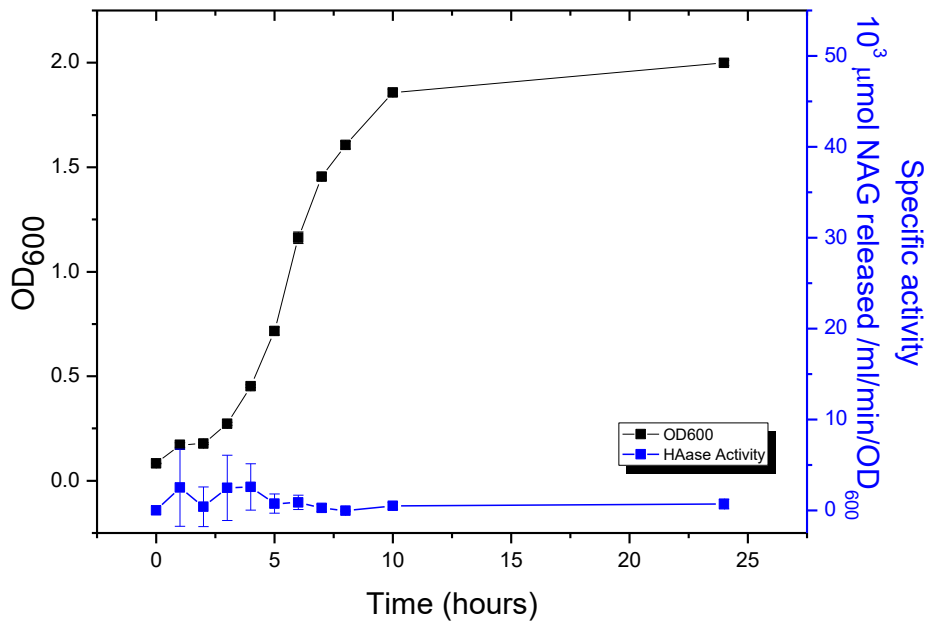

Figure 5.21: HAase production during the growth of *S. aureus* ST239 µ2

In *S. aureus* H560, HAase expression was predominantly seen in the early exponential phase of bacterial growth, with a peak after 4 hours growth, followed by a gradual decrease in expression once the stationary phase was reached. This was consistent with HAase being a spreading factor involved in early bacterial invasion of hosts, and also mirrored the results of Makris et al[5, 11]. In HAase negative *S. aureus* ST239 µ2, no expression of HAase was detected at any timepoint.

5.3.2.3. Expression of hyaluronidase by *S. aureus* biofilms

S. aureus biofilms were formed using a high HAase producing strain (C3), a low HAase producing strain (H560) and a non-producing strain NE334 (hys-). It was also recently reported by Hart et al that mutant bacteria deficient of HAase activity showed no significant change in biofilm production[12]. In that case however, HAase activity was only measured using zone of inhibition diameters.

HAase activity and biofilm biomass measurements can be seen in Figure 5.22. It is important to note that the three strains tested are example strains, and in order to get a better understanding of HAase expression in biofilms, more strains must be analysed. At different stages of biofilm formation, the biofilm biomass and concentration of HAase secreted was measured to determine three things. Firstly, if HAase was expressed differently in a biofilm compared to planktonic bacteria, and secondly, if HAase was expressed at different times over the biofilm growth cycle and finally, if there was a correlation between biofilm and HAase production.

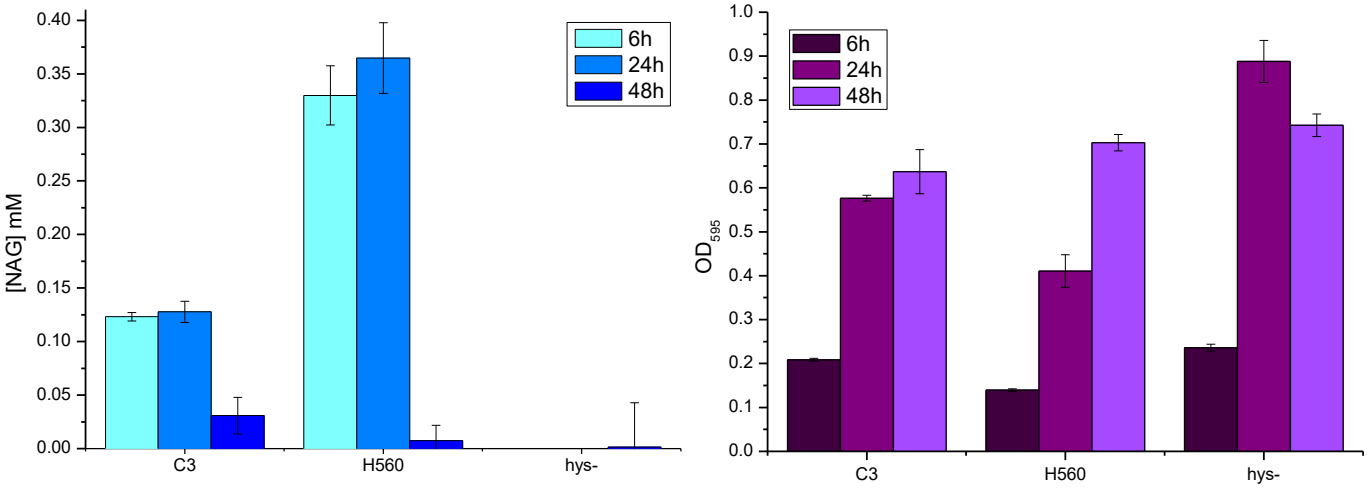

Figure 5.23: (left) HAase activity and (right) biofilm biomass in *S. aureus* C3, H560 and hys-

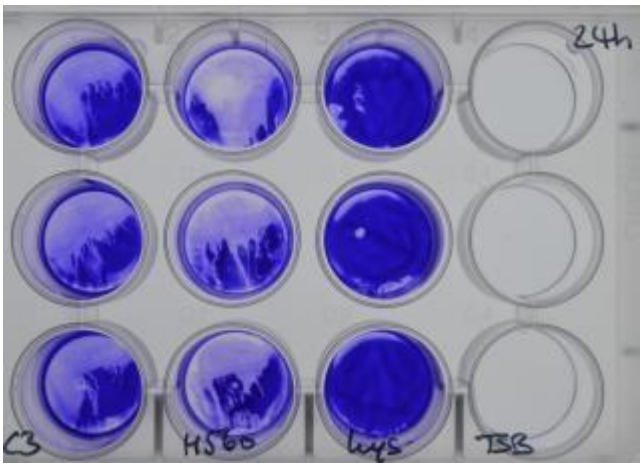

Figure 5.22: Example biofilm plate stained with 0.1% crystal violet solution after 24 hours growth

Firstly, comparing HAase activity at 24 hours in planktonic and biofilm systems, it was found that especially for strains that showed a high HAase activity as planktonic cells, a reduction was seen once in a biofilm. In *S. aureus* C3, HAase activity was reduced from approximately 0.9 mM NAG to 0.125 mM. Strains which exhibited a lower HAase activity in planktonic culture, such as H560, did not change significantly once in a biofilm. In both growth environments, *S. aureus* hys- showed no HAase activity. It is widely understood that bacteria in biofilms behave completely differently compared to planktonic bacteria. They have vastly different metabolism and susceptibility to antibiotics, as well as being phenotypically different exhibiting varied gene expression[13, 14]. *S. aureus* C3 could be exhibiting a genetic 'compromise' when forming a biofilm; overly high HAase expression could be downregulated to concentrate on biofilm formation.

Secondly, it was shown that in both HAase positive cases, HAase expression continued for approximately 24 hours until a sharp reduction was seen by 48 hours. HAase, as primarily an invasion enzyme, is likely to be downregulated after the initial invasion period (~ 24 hours) in order to concentrate bacterial resources in other areas.

Finally, normal biofilm production was seen in all three strains, implying that there is no correlation between biofilm and HAase production; production was seen in both HAase positive and negative strains. Biofilm biomass increased with time, as bacteria replicated and began to secrete EPS to form mature biofilms.

5.3.3. Sensitivity of HAMA-co-PEG films to hyaluronidase

HAMA-co-PEG hydrogels were incubated in a range of concentrations of HAase (Figure 5.23). Purified HAase was obtained from bovine testes; although this is not derived from microbial producers, it still degrades HA through hydrolysis of the sugar at the same position that would be seen after bacterial degradation. The enzyme is approximately 55 kDa and has a calculated size of 52 x 44 x 39 nm[15] - although large for an enzyme, this is still small enough to diffuse into the HAMA network based on theoretical mesh size calculations.

The concentration of the HA breakdown product NAG was quantified, however in the case of crosslinked HA, the NAG source was now from the hydrogel and not from added HA solution.

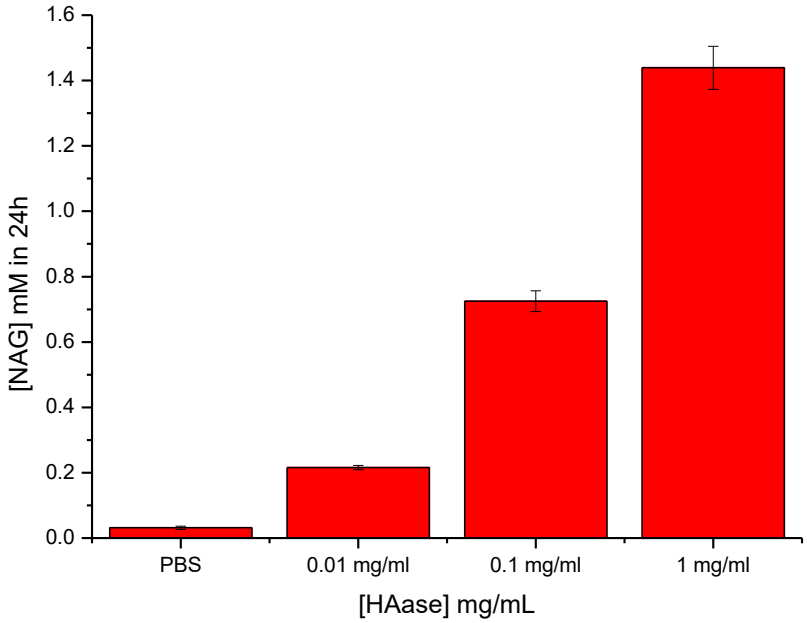

Figure 5.24: Concentration of NAG from 2% HAMA /1% PEGDA gels, after incubation with PBS, 0.01, 0.1 and 1 mg/mL HAase

On incubation with HAase, an increase in the concentration of NAG was seen compared to hydrogels incubated with PBS buffer solution, showing that although modified with methacrylate, HAMA was still susceptible to enzymatic degradation. Hydrogels were also seen to disappear by 6 hours in all HAase concentrations, with degradation continuing past this time as longer polymer chains were made smaller.

The degradation process was analysed through SEM after 2 hours incubation with HAase at 37 °C (Figure 5.25). On incubation with PBS no damage to hydrogel morphology was seen; gel homogeneity and a general absence of cavities implied the gel does not undergo significant hydrolysis with buffer. Hydrogels incubated with 0.01 mg/mL HAase showed small pores of approximately 5 µm in diameter, which were consistent throughout the gel. An increased concentration of 1 mg/mL gave considerably larger pores of 15-20 µm, with evidence of collapse between the layers also being apparent.

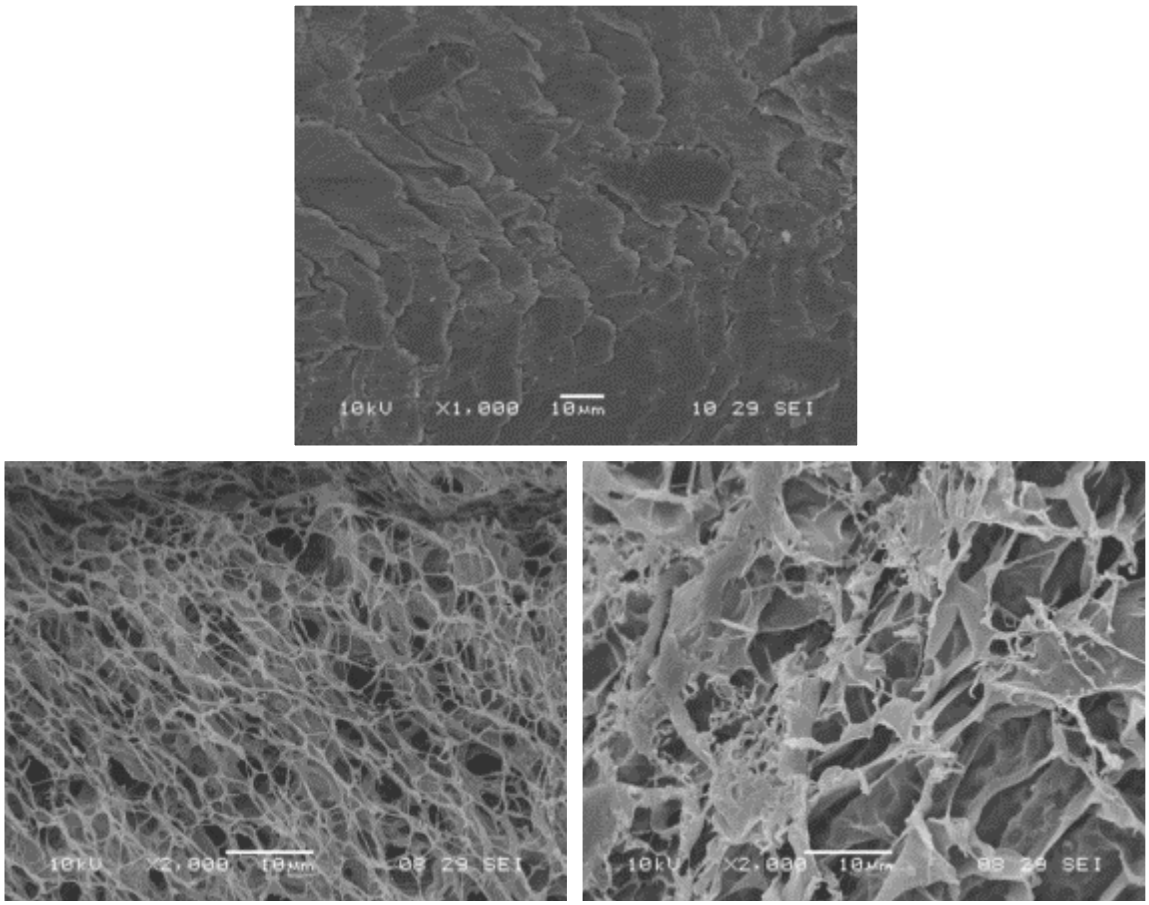

Figure 5.25: Top view SEM images after 2 hour incubation of 1% PEG diacrylate + 2% HAMA hydrogels with a) PBS, b) 0.01 mg/mL HAase and c) 1 mg/mL HAase

HAMA hydrogels containing a range of PEG diacrylate concentrations were then incubated with HAase, and the extent of breakdown of the cross-linked hydrogel measured after 24 hours

through the measurement of the formation of NAG breakdown product, using the Carbazole assay (Figure 5.26).

It can be seen that an increase in HAase concentration increases breakdown of cross-linked HAMA; an increase in the relative proportion of PEG-diacrylate however decreases the susceptibility of the cross-linked polymer to HAase. The breakdown of 10% PEG diacrylate co-gels was roughly a third of that seen for pure HAMA gel. It was hypothesised that in high co-polymer hydrogels, the viscosity of the polymer gel greatly increases slowing diffusion of HAase into the matrix.

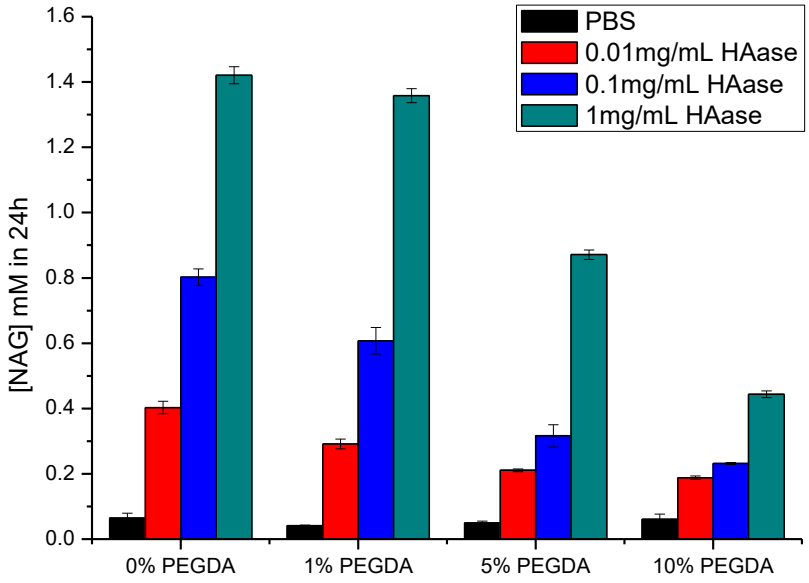

Figure 5.26: Degradation of HAMA hydrogels containing 0%, 1%, 5% and 10% PEGDA by HAase.

5.3.4. Sensitivity of HAMA-co-PEG films to *S. aureus* supernatant

HAMA-co-PEG hydrogels were also then incubated with overnight bacterial supernatant for 2 hours. Top view SEM images of the hydrogels after incubation showed significant differences in hydrogel morphology (Figure 5.27). HAMA hydrogels incubated with strains known to secrete HAase (images a), b), c)) all exhibited clear visual signs of enzymatic degradation. Large areas of hydrogel loss were seen that permeated through the entire matrix. This enzymatic hydrolysis leads to increased permiability and eventual dissolution of the gel.

Hydrogels were also incubated with *S. aureus* strains which showed no HAase activity in the initial strain screen. *S. aureus* hys- (image d) showed no changes compared to the negative

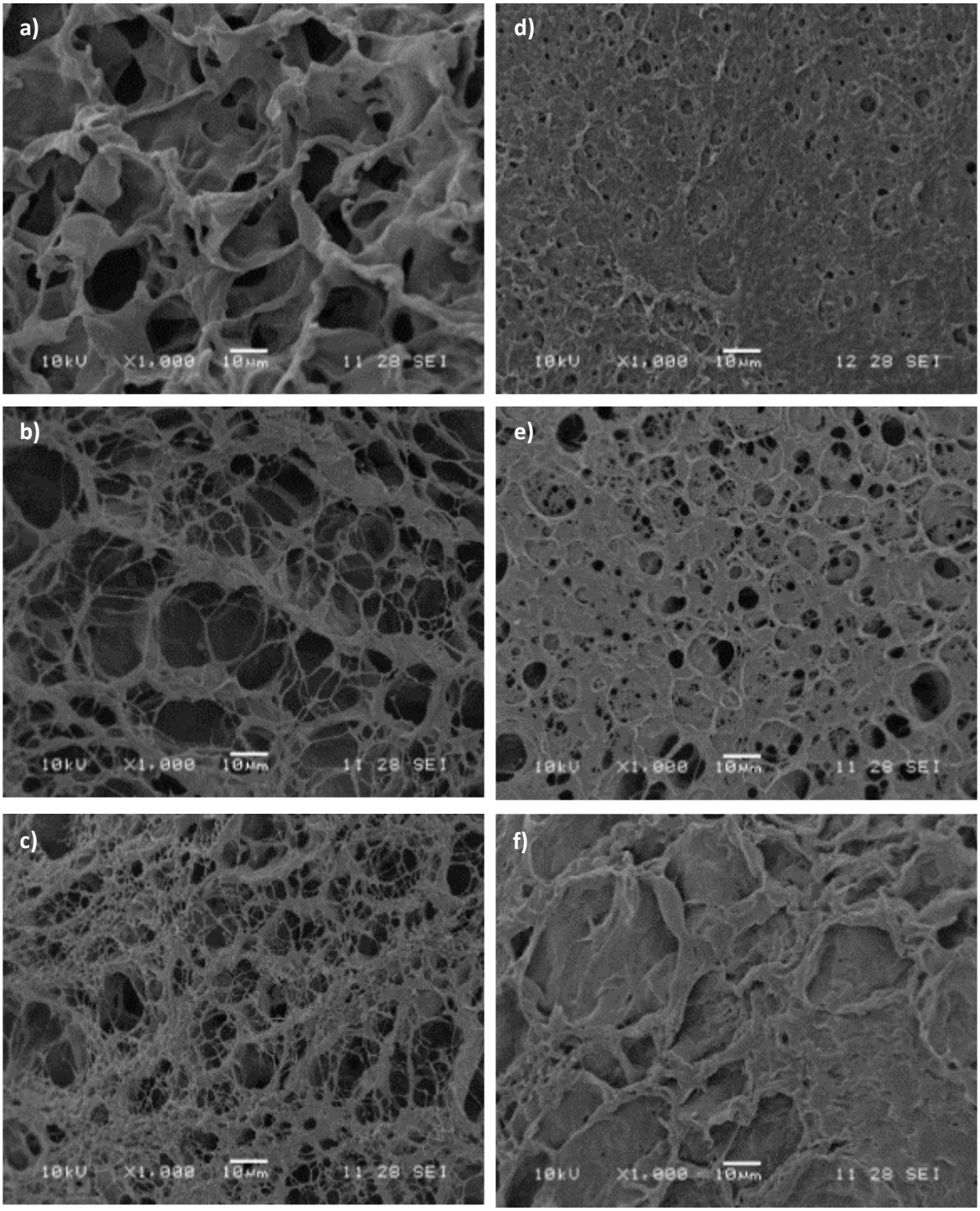

Figure 5.27: SEM images of HAMA hydrogels after 2h incubation with *S. aureus* supernatant. HAase positive strains: a) RN6390B, b) H560, c) lac. HAase negative strains: d) hys-, e) ST239 µ2, and f) TSB.

control (TSB growth medium, image f)). The hydrogel top layer remained confluent with no pores formed.) On incubation with ST239 µ2 (image e), a phenotypic mutant where despite *hysA* being present, no activity was seen in the strain screen, small circular pores were seen in some parts of the hydrogel. This could have been due to low levels of HAase being present which were undetectable by the Carbazole assay, or damage to the structure during freeze-drying.

Again the concentration of NAG breakdown products on incubation with supernatant were measured over the course of 24 hours (Figure 5.28). Firstly, no significant breakdown was seen in HAase negative strains (ST239 µ2 and hys-) compared to the negative control (TSB). With strains known to produce HAase however, the concentration of NAG breakdown products increases as the polymer was broken down. The rate at which this was done is different between strains. High HAase producers RN6390B, H560 and lac exhibited relatively fast breakdown with a plateau seen after 6 hours. Visually, hydrogels were completely dissolved after incubation with HAase positive *S. aureus* supernatant.

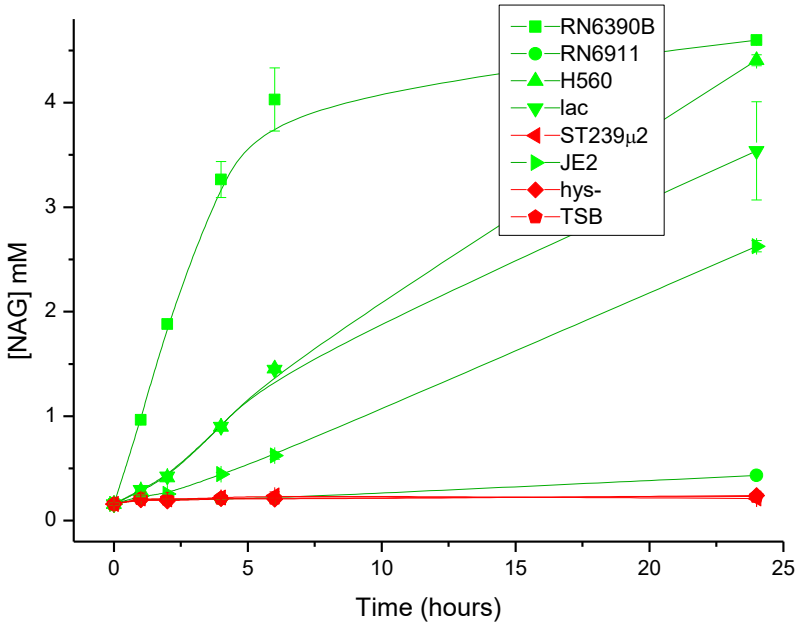

Figure 5.28: Degradation of HAMA hydrogels by HAase positive (green) and HAase negative (red) *S. aureus* supernatant.

5.4. Conclusions

This chapter focussed on the interactions of hyaluronic acid, HA and the enzyme hyaluronidase, HAase, a virulence factor of *S. aureus*. HA was chosen as an enzyme-sensitive release mechanism for immobilised bacteriophage as it already is widely used in medical therapeutics. It was crosslinked into hydrogel matrices of varying strength and flexibility. The secretion of HAase by 116 bacterial strains (predominantly *S. aureus*) was also assessed with the Carbazole assay to confirm that the enzyme was secreted by the majority of strains. Finally, crosslinked HAMA-co-PEG hydrogels were degraded by commercially available and bacterial HAase, as well as with *S. aureus* mutants with no activity. The degradation of these hydrogels was then analysed using

SEM imaging and quantitatively. In conclusion the final crosslinked HA formulation was found to be selectively degraded by *Staphylococcal* HAase, making it a viable hydrogel mechanism for triggered release.

5.5. References

1. Y. Yeo, C. B. Highley, E. Bellas, T. Ito, R. Marini, R. Langer and D. S. Kohane, *Biomaterials*, 2006, **27**, 4698-4705.
2. N. Shoham, A. L. Sasson, F.-H. Lin, D. Benayahu, R. Haj-Ali and A. Gefen, *Journal of the Mechanical Behavior of Biomedical Materials*, 2013, **28**, 320-331.
3. W. Y. Su, Y. C. Chen and F. H. Lin, *Acta Biomater*, 2010, **6**, 3044-3055.
4. J. B. Leach and C. E. Schmidt, *Biomaterials*, 2005, **26**, 125-135.
5. G. Makris, J. D. Wright, E. Ingham and K. T. Holland, *Microbiology*, 2004, **150**, 2005-2013.
6. N. Cerca, R. Oliveira and J. Azeredo, *Lett Appl Microbiol*, 2007, **45**, 313-317.
7. M. H. M. Oudshoorn, R. Rissmann, J. A. Bouwstra and W. E. Hennink, *Polymer*, 2007, **48**, 1915-1920.
8. J. Patterson, R. Siew, S. W. Herring, A. S. Lin, R. Guldberg and P. S. Stayton, *Biomaterials*, 2010, **31**, 6772-6781.
9. A. V. Reis, A. R. Fajardo, I. T. A. Schuquel, M. R. Guilherme, G. J. Vidotti, A. F. Rubira and E. C. Muniz, *The Journal of Organic Chemistry*, 2009, **74**, 3750-3757.
10. C. G. Williams, A. N. Malik, T. K. Kim, P. N. Manson and J. H. Elisseeff, *Biomaterials*, 2005, **26**, 1211-1218.
11. C. R. Starr and N. C. Engleberg, *Infect Immun*, 2006, **74**, 40-48.
12. M. E. Hart, L. H. Tsang, J. Deck, S. T. Daily, R. C. Jones, H. Liu, H. Hu, M. J. Hart and M. S. Smeltzer, *Microbiology*, 2013, **159**, 782-791.
13. K. E. Beenken, P. M. Dunman, F. McAleese, D. Macapagal, E. Murphy, S. J. Projan, J. S. Blevins and M. S. Smeltzer, *Journal of Bacteriology*, 2004, **186**, 4665-4684.
14. L. D. Handke, K. M. Conlon, S. R. Slater, S. Elbaruni, F. Fitzpatrick, H. Humphreys, W. P. Giles, M. E. Rupp, P. D. Fey and J. P. O'Gara, *Journal of Medical Microbiology*, 2004, **53**, 367-374.
15. Z. Marković-Housley, G. Miglierini, L. Soldatova, P. J. Rizkallah, U. Müller and T. Schirmer, *Structure*, 2000, **8**, 1025-1035.

Chapter 6 : A Bilayered Hydrogel System for Triggered Release of Bacteriophage K by *Staphylococcal* Hyaluronidase

6.1. Introduction

This chapter will focus on the combination of work described in Chapters 4 and 5 to create a bilayered hydrogel system which gives triggered release of Bacteriophage K on incubation with hyaluronidase. This bilayered hydrogel comprises two hydrogel matrices: firstly an agarose or PVA hydrogel containing immobilised Bacteriophage K, and secondly a crosslinked hyaluronic acid layer which will become degraded in the presence of *Staphylococcal* hyaluronidase.

On infection with hyaluronidase secreting bacteria (*S. aureus*), the HA-based upper layer will be degraded, allowing bacteriophage to be released into the surrounding environment and subsequently go on to infect and lyse live bacteria. In this way, bacteriophage are released *only* in the presence of pathogenic bacteria and by doing so the development of bacterial resistance to bacteriophage will be reduced. A diagram of triggered bacteriophage release from bilayered hydrogels can be seen in Figure 6.1.

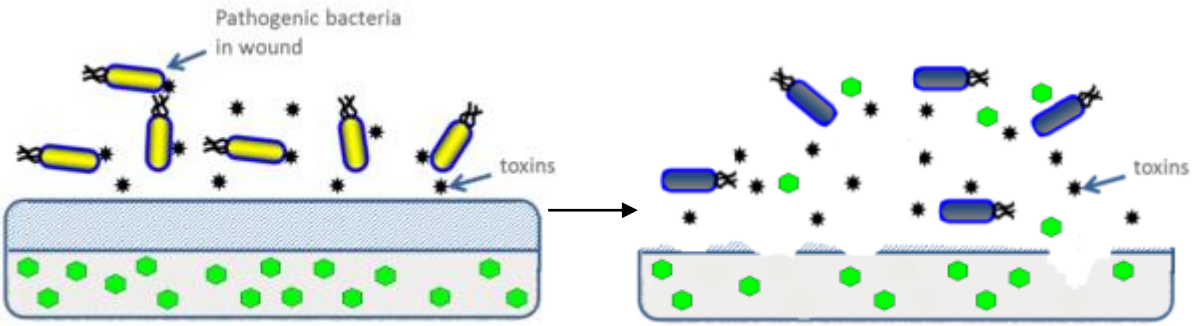

Figure 6.1: Schematic diagram of bilayered hydrogel system: degradation of the upper HAMA layer causes release of immobilised bacteriophage, causing bacterial death

With non-pathogenic or non *S. aureus* species, no hyaluronidase is expressed and so the upper HAMA layer does not break down, causing no bacteriophage to be released. As the bacteriophage used (Bacteriophage K) only has efficacy against *S. aureus*, this is not an issue as even if the bacteriophage were released they would not cause lysis. Bacteriophage are only released by bacteria that are susceptible to them.

Bilayered hydrogels have been used in a number of biomedical applications. Firstly, they are commonly used in tissue engineering in order to build up stratified hydrogels which mimic the structure and mechanical properties of tissue[1-4]. These are predominantly tissues which already exhibit a highly ordered structure in the body, such as dermal or osteochondral tissue[5, 6].

Secondly, double or triple network hydrogels can be used to increase the mechanical strength of a hydrogel[7-10]. These are referred to as interpenetrating polymer networks, IPNs, and can demonstrate dramatically different properties from their constituent polymers[11]. The IUPAC definition of an IPN is "a polymer comprising two or more networks which are at least partially interlaced on a molecular scale but not covalently bonded to each other and cannot be separated unless chemical bonds are broken"[12]. In general to form IPNs, firstly one polymer is crosslinked into a matrix and then another is crosslinked around it *in situ*.

6.2. Materials and Methods

6.2.1. Formation of bilayer hydrogel

Bilayered hydrogels were formed in 12-well (for hyaluronidase and supernatant tests) and 24-well (for live bacteria tests) cell culture plates. Different hydrogel volumes were used for each plate, retaining the same hydrogel volume ratio:

- 12-well plate = 1 mL lower layer + 400 µL HAMA
- 24-well plate = 500 µL lower layer + 200 µL HAMA

Lower layer hydrogel formation has been previously described in Chapter 4, whilst upper layer development has been described in Chapter 5. In all experiments, HAMA mix (2% HAMA, 1% Irgacure 2959, 1% PEG diacrylate) was crosslinked in a UV flood crosslinker.

A schematic representation of bilayer hydrogel formation can be seen in Figure 6.2. Lower layer hydrogels containing SM buffer or 10^8 pfu/mL Bacteriophage K were cast and allowed to set; for agarose, plates were cooled overnight at 4 °C, for PVA, plates were frozen overnight at – 20 °C and then thawed at room temperature for 1 hour. HAMA mix was then added and allowed to completely cover and seal the lower hydrogel. Plates were then exposed to UV irradiation to crosslink the upper layer and used immediately.

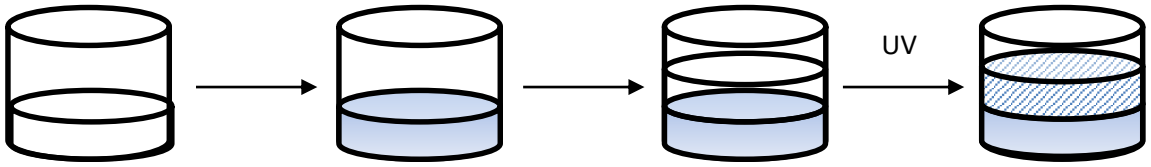

6.2.2. Measurement of bacteriophage release by hyaluronidase

Triggered bacteriophage release from bilayered hydrogels by hyaluronidase was measured by casting bacteriophage containing hydrogels into a 12-well plate, as shown in Figure 6.3. Column 1 contained control bacteriophage hydrogel with no HAMA layer, and columns 2 and 3 contained bacteriophage hydrogel with a HAMA layer. 1 mL per well SM buffer was then added to columns 1 and 2, and 1 mL 1 mg/mL was added to column 3.

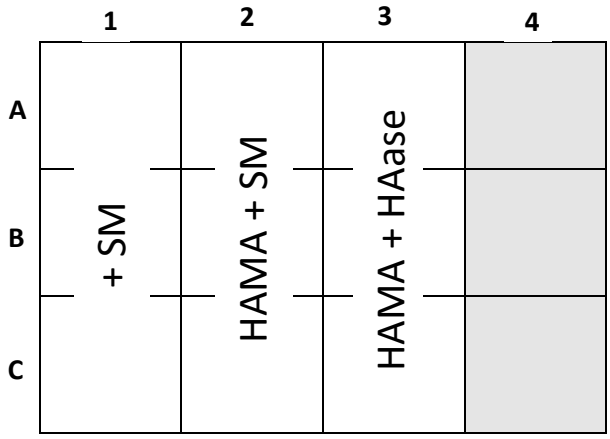

Figure 6.3: 12-well plate layout for 1 mg/mL hyaluronidase breakdown measurements of bilayer hydrogel experiments

Plates were incubated at 37 °C with 120 rpm shaking. Time point measurements at 2, 4 and 6 hours were taken after addition of hyaluronidase, and (100 µL) samples were stored at 4 °C until required. After removal, liquid was replaced by SM buffer or HAase solution to keep test volume constant. Bacteriophage concentration was measured using standard protocols described in Chapter 2.

6.2.3. Measurement of bacteriophage release by bacterial supernatant

Triggered bacteriophage release from bilayered hydrogels by bacterial supernatant was measured by casting bacteriophage containing hydrogels into a 12-well plate, as shown in Figure 6.4. Column 1 again contained control bacteriophage hydrogel with no HAMA layer, whilst

columns 2, 3 and 4 bacteriophage hydrogel with a HAMA layer. 1 mL per well TSB was then added to columns 1 and 2, whilst 1 mL *S. aureus* C3 supernatant was added to column 3 and 1 mL *S. aureus* hys- supernatant was added to column 4.

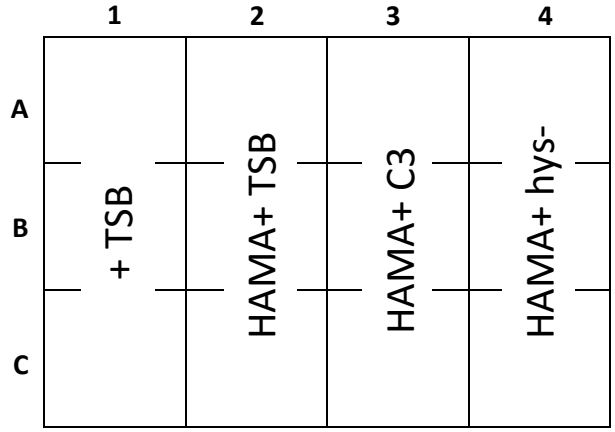

Figure 6.4: 12-well plate layout for bacterial supernatant breakdown measurements of bilayer hydrogel experiments

Plates were again incubated at 37 °C with 120 rpm shaking. Time point measurements at 1, 2 and 4 hours were taken after addition of hyaluronidase, and (100 µL) samples were stored at 4 °C until required. After removal, liquid was replaced by TSB or bacterial supernatant to keep test volume constant. Bacteriophage concentration was measured using standard protocols described in Chapter 2.

When incubating the bilayered hydrogel systems with bacterial supernatant instead of HAase, a faster timeframe was analysed as the concentration of HAase in bacterial supernatant was much higher than 1 mg/mL. As the enzyme was able to work faster, triggered release was seen at an earlier time. Also, as seen in Section 5.3.2.2., peak HAase production in *S.aureus* is seen in the early exponential phase, at approximately 4 hours.

6.2.4. Live culture with bilayer hydrogels

Bilayer hydrogels (with and without Bacteriophage K) were cast in a 24-well plate as previously described. Lower layers with no HAMA layer were also included to determine non-triggered response. *S. aureus* H560 and hys- subculture was formed by mixing 10 µL overnight culture with 10 mL TSB. Broth for growth of *S. aureus* hys- strains was additionally supplemented with 5 µg/mL erythromycin. 500 µL per well was then added to each well and OD_{600} measurements were taken during the overnight incubation at 37 °C with shaking.

6.3. Results and Discussion

6.3.1. Bilayer hydrogels

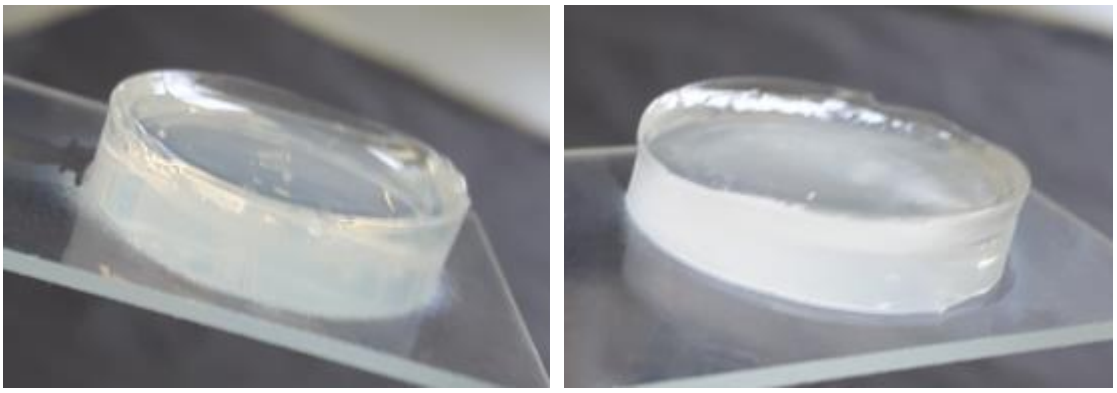

Figure 6.5: (left) Bilayered 2% agarose hydrogel with HAMA layer, (right) bilayered 5% PVA hydrogel with HAMA layer

Bilayered hydrogel systems could be formed easily with both agarose and PVA solutions (Figure 6.5). With agarose, an inflexible hydrogel was seen that formed a solid system with defined layers; an opaque agarose layer and a clear HAMA layer. With PVA, a more elastic hydrogel was formed with could be bent without breaking. The bilayered system again formed two defined layers however the hydrogels were clearer, with a higher binding between the two layers.

6.3.2. Optimisation of HAMA crosslinking

As the main cause of bacteriophage killing during the hydrogel making process is UV exposure, the shortest time needed to effectively crosslink HAMA without the loss of the structure seen in Chapter 5 was determined. Here, the swelling ratios and rate of degradation by HAase were measured to assess if the hydrogel properties were altered. In general, all HAMA hydrogels became solid ("fully-crosslinked") after a minimum of 10 seconds. Because of this, hydrogels were irradiated for 10, 20, 30 and 60 seconds to determine if there was a significant change from lowering the crosslinking time from 60 to 10 seconds.

Firstly, the swelling of hydrogels crosslinked for varying times was measured; this gives an indication of the extent of crosslinking. If crosslinking has not gone to completion, the hydrogels would exhibit a higher swelling (and higher pore size). If crosslinking is completed by 10 seconds, the same swelling should be seen in all cases. Swelling ratio values for 10, 20, 30 and 60 seconds UV exposure can be seen in Figure 6.6. In general, the swelling ratio values measured for HAMA did not change with irradiation time, implying total crosslinking had occurred before 10 seconds.

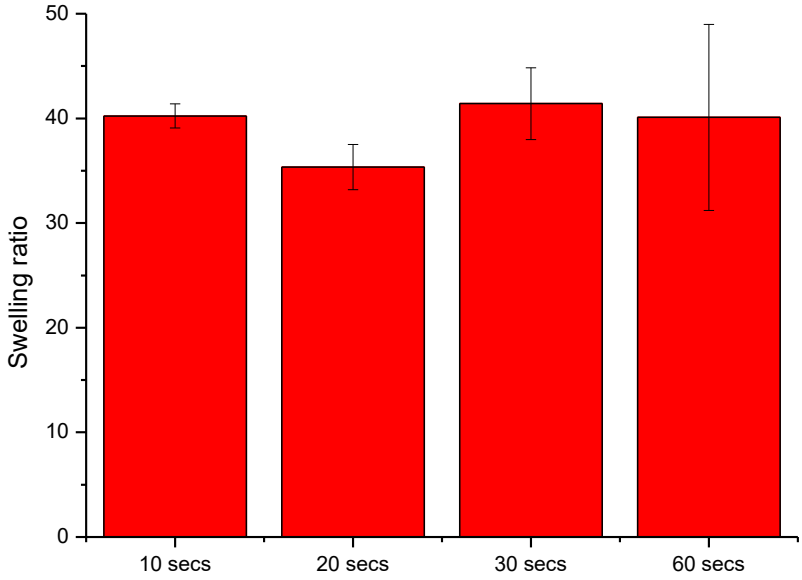

Figure 6.6: Swelling ratio measurements of HAMA hydrogels after 10, 20, 30 and 60 sec UV irradiation

The HAMA hydrogels were then incubated with 1 mg/mL HAase solution to determine if changing the crosslinking time affected the rate of enzymatic degradation Figure 6.7. In general, hydrogels exhibited a slightly slower initial degradation when irradiated for 10 seconds compared to longer exposure times. However, by 45 minutes incubation, the concentration of breakdown products (NAG) present had become equal. By 1 hour there was no significant difference in NAG concentration, implying that the rate of degradation was not dependent on irradiation time. This again implies that crosslinking had gone to completion at or before 10 seconds.

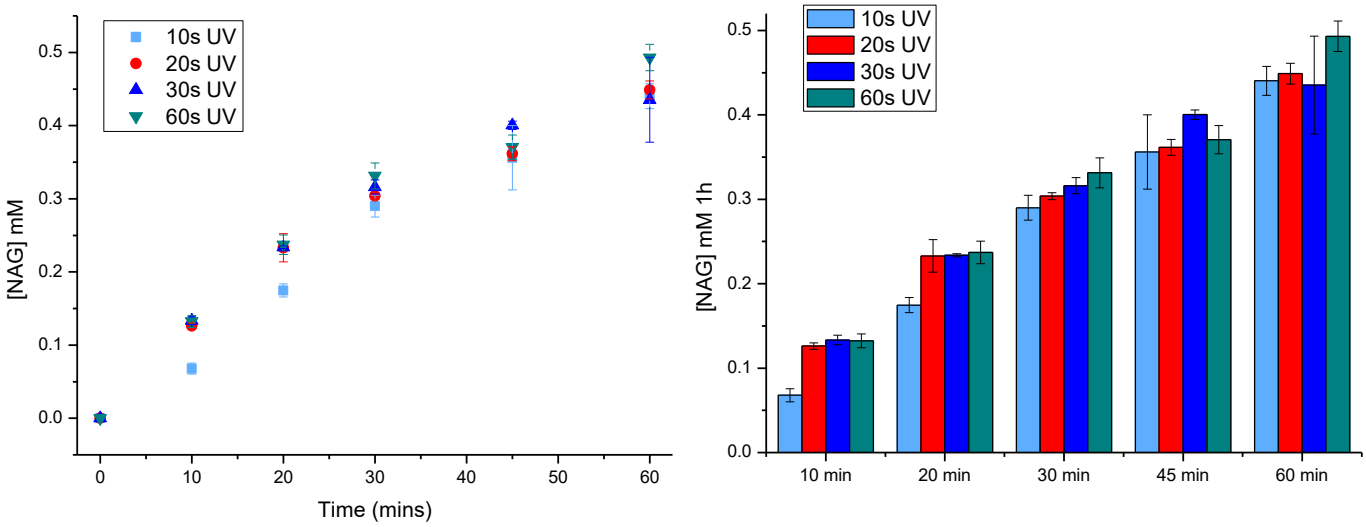

Figure 6.7: Degradation of HAMA hydrogels crosslinked for 10, 20, 30 and 60 seconds with 1 mg/mL HAase

It was decided that 10 seconds UV exposure would be sufficient to completely crosslink HAMA hydrogels judging by swelling and enzymatic degradation results. It was then important to determine if this UV irradiation time was damaging to bacteriophage in the lower layer.

6.3.3. Optimisation of agarose hydrogels

From Chapter 4, it was known that after UV irradiation of bacteriophage immobilised in 5% PVA of up to 30 seconds, sufficient bacteriophage remained to cause lysis and killing of bacterial live culture. However, even 10 seconds of UV irradiation was found to affect the onset of lysis compared to non-irradiated samples. This, combined with the general knowledge that UV is highly damaging to bacteriophage and their genetic material when combined with PVA, meant that PVA was not used as the lower layer hydrogel.

Instead, agarose was used for lower layer development. Agarose is not thought to form (as many of) the highly damaging radicals seen in PVA during UV exposure. When agarose systems were incubated with live culture, a less extreme effect was seen compared to PVA, with full lysis occurring in all cases, except those with a very long exposure time and a very low polymer concentration (60 seconds, 0.4% and 0.7% agarose). In fact with agarose the polymer appeared to shield the bacteriophage from UV.

In this respect, it was firstly important to determine the concentration of bacteriophage remaining in agarose hydrogels after 10 seconds UV exposure. Hydrogels containing 10^8 pfu/mL Bacteriophage K were formed using standard protocols and then exposed to UV for 10 seconds. SM buffer was then added to each well and the plates were incubated with slight shaking for 4 hours (the time *S. aureus* normally takes to reach the early exponential phase; the phase where bacteriophage are most infective). The bacteriophage concentration present after 4 hours was then measured (Figure 6.8).

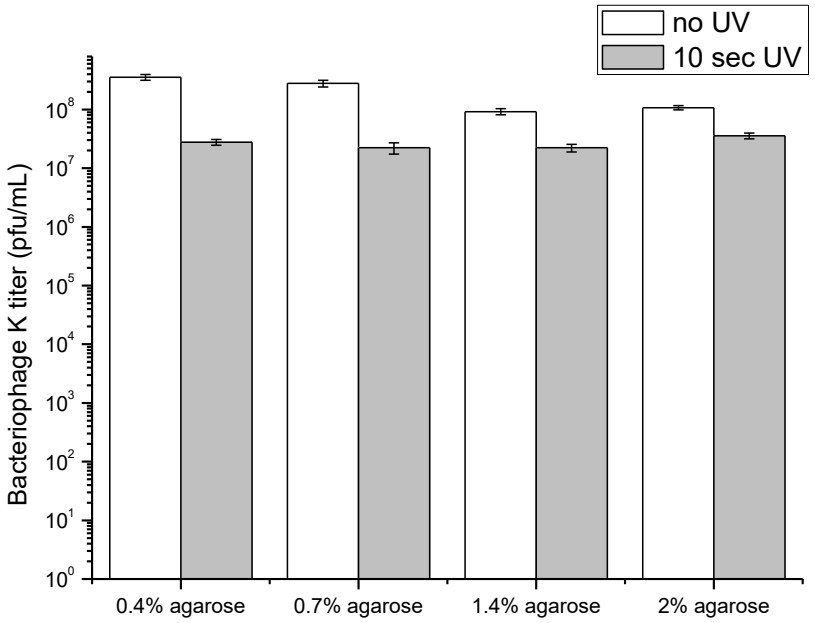

Figure 6.6: Bacteriophage K concentration released from agarose hydrogels exposed to no and 10 sec UV after 4 hours

After 10 seconds UV exposure, the concentration of infective bacteriophage released into the SM buffer from agarose hydrogels decreased by approximately a factor of 10 compared to non-exposed hydrogels. In hydrogels exposed to no UV, a concentration of approximately 10^8 pfu/mL was seen, with a slight decrease as agarose concentration increased. This mirrors the results seen in Chapter 4, where the higher polymer concentration slows the diffusion of bacteriophage particles out of the hydrogel. When exposed to 10 seconds of UV, the bacteriophage concentration present was lower (10^7 pfu/mL), implying a certain amount of bacteriophage damage. However, this was still a high enough concentration to cause complete killing of infecting bacteria in live culture.

6.3.4. 0.4% agarose bilayer hydrogel

0.4% agarose based hydrogels were first investigated. From previous experiments, it was known that the hydrogel exhibited extremely high bacteriophage diffusion whilst retaining hydrogel structural stability. The more bacteriophage able to diffuse, the more that can go on to infect pathogenic bacteria.

6.3.4.1. Triggered release of Bacteriophage K by hyaluronidase

Bilayered 0.4% agarose/HAMA hydrogels were incubated with 1 mg/mL hyaluronidase solution and bacteriophage concentration measurements taken at 2, 4 and 6 hours (Figure 6.9).

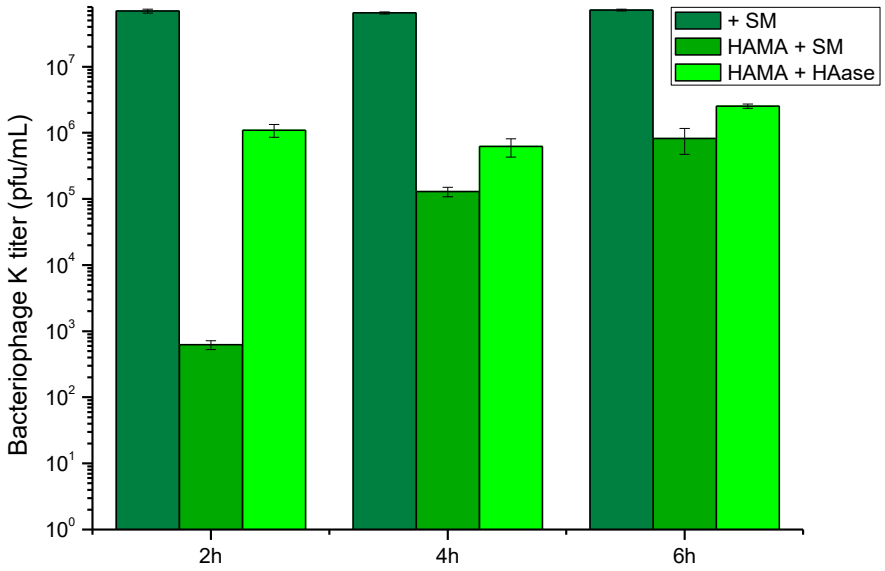

Figure 6.7: Bacteriophage titer after hyaluronidase degradation of bilayer 0.4% agarose / HAMA hydrogel

Firstly, in wells where only bacteriophage-containing agarose was present (no HAMA layer) a very high concentration of bacteriophage (almost 10^8 pfu/mL) was seen after two hours, which was constant throughout the experiment. From this, it could be confirmed that a high concentration of bacteriophage were able to diffuse out of 0.4% agarose (as also seen in Chapter 4).

Once the HAMA layer was added, bacteriophage release became significantly reduced compared to pure agarose. The HAMA was able to form a barrier to prevent or slow bacteriophage movement. When SM buffer (no HAase) was added, a low number of bacteriophage were released, whereas in comparison HAase addition caused a significantly higher release (10^6 pfu/mL). A significant difference between SM buffer and HAase, especially after two hours incubation, implied that the HAMA had an active role in triggered release. The HAase was able to successfully degrade the HAMA layer quickly, even after two hours.

On the other hand, after two hours, a high concentration of bacteriophage were found in samples incubated with SM buffer. The HAMA layer did not give selective release of bacteriophage, most probably due to the passive diffusion of bacteriophage from the agarose matrix. The high diffusion in 0.4% agarose meant that too many bacteriophage were able to diffuse out before the HAase could elicit an effect.

6.3.4.2. Triggered release of Bacteriophage K by bacterial supernatant

Bilayered 0.4% agarose/HAMA hydrogels were then incubated with HAase positive *S. aureus* supernatant (C3) and HAase negative *S. aureus* supernatant (NE334 (hys-)), as well as TSB growth medium. Bacteriophage concentration measurements were then taken at 1, 2 and 4 hours (Figure 6.10).

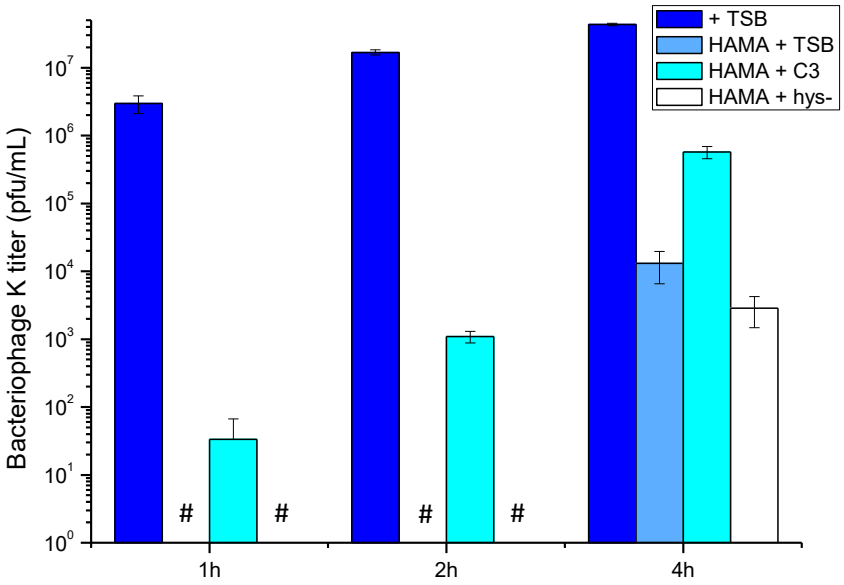

Figure 6.8: Bacteriophage titer after *S. aureus* C3 and hys- supernatant degradation of bilayer 0.4% agarose / HAMA hydrogel. # = no bacteriophage detected

Again, control wells containing bacteriophage agarose but no HAMA layer showed a high release of bacteriophage, with 10^6 pfu/mL after 1 hour and 10^7 pfu/mL after 2 hours. In hydrogels containing the HAMA layer, no bacteriophage were detected when incubated with TSB or *S. aureus* hys- supernatant (both contain no HAase). However, when incubated with *S. aureus* C3 supernatant (HAase positive) bacteriophage were found, albeit in low concentrations.

After 4 hours incubation, the unspecific release of bacteriophage seen with HAase was again seen with bacterial supernatant. Approximately 10^4 pfu/mL bacteriophage were detected in HAase negative wells, implying that passive diffusion was seen. Despite this, a significant difference in bacteriophage concentration was seen between *S. aureus* C3 and hys- supernatant, implying that the HAMA layer was forming a HAase sensitive barrier to release.

6.3.5. 0.7% agarose bilayer hydrogel

0.7% agarose based hydrogels were then investigated as the more concentrated hydrogel shows slower bacteriophage diffusion. In this way, passive release of bacteriophage would be prevented, allowing the degradation of HAMA to be the only way of causing bacteriophage release.

6.3.5.1. Triggered release of Bacteriophage K by hyaluronidase

Bilayered 0.7% agarose/HAMA hydrogels were incubated with 1 mg/mL hyaluronidase solution and bacteriophage concentration measurements taken at 2, 4 and 6 hours.

In wells where only bacteriophage-containing agarose was present a high concentration of bacteriophage (10^7 pfu/mL) was still seen after two hours, which was constant throughout the experiment. Bacteriophage were able to diffuse out of 0.7% agarose (as again seen in Chapter 4) quickly and in high concentrations (Figure 6.11).

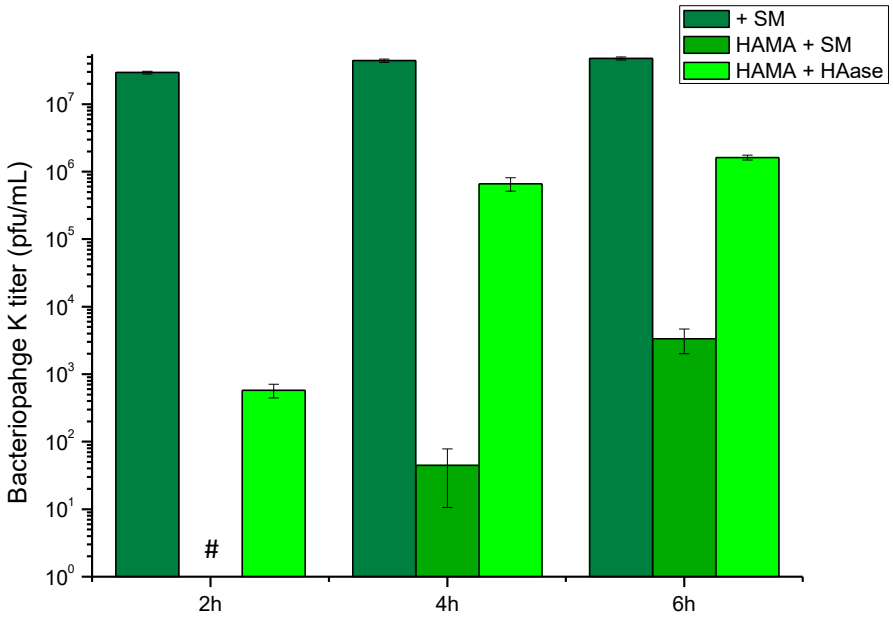

Figure 6.9: Bacteriophage titer after hyaluronidase degradation of bilayer 0.7% agarose / HAMA hydrogel. # = no bacteriophage detected

In hydrogels containing the HAMA layer, after two hours incubation triggered release was seen, with bacteriophage only detected in systems containing HAase. After 4 hours this was still generally the case; however a low concentration of bacteriophage was detected after SM incubation. After 6 hours, 10^3 pfu/mL bacteriophage was detected after SM incubation. In both cases, 10^6 pfu/mL bacteriophage were released after incubation with HAase, meaning a

significant difference was seen between SM and HAase. In this respect triggered release was still apparent; however passive bacteriophage diffusion was still seen.

6.3.5.2. Triggered release of Bacteriophage K by bacterial supernatant

Bilayered 0.7% agarose/HAMA hydrogels were again incubated with HAase positive *S. aureus* supernatant (C3) and HAase negative *S. aureus* supernatant (NE334 (hys-)), as well as TSB growth medium. Bacteriophage concentration measurements were then taken at 1, 2 and 4 hours (Figure 6.12).

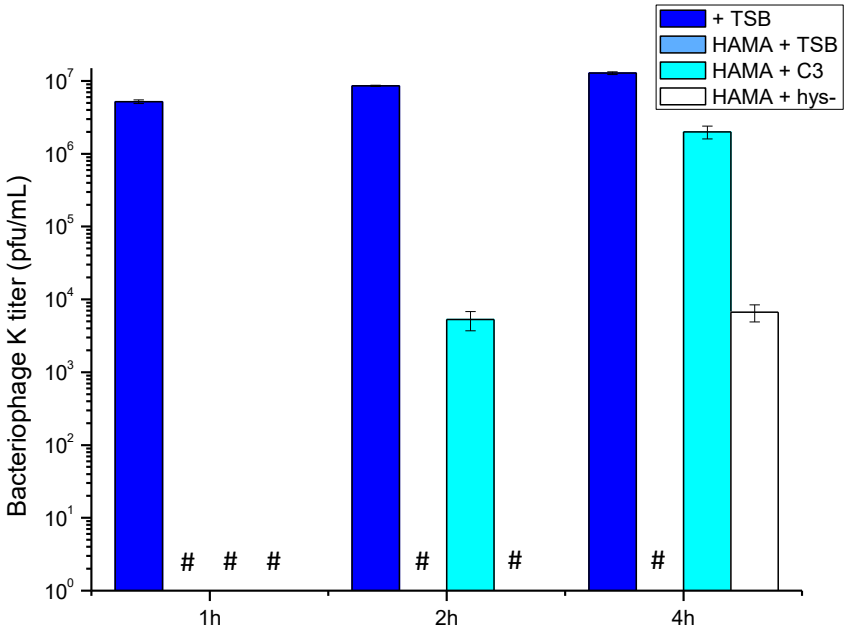

Figure 6.10: Bacteriophage titer after *S. aureus* C3 and hys- supernatant degradation of bilayer 0.7% agarose / HAMA hydrogel. # = bacteriophage not detected

In this system, control hydrogel wells with no HAMA layer showed a high bacteriophage release, however understandably slightly less than in 0.4% agarose. The rate of bacteriophage diffusion however appeared to be significantly slower, as after 1 hour no bacteriophage were detected in HAMA layer hydrogels, even in HAase positive strain supernatant. After 2 hours, triggered release was seen, with 10^4 pfu/mL bacteriophage released by *S. aureus* C3 (HAase positive) and none found in control or *S. aureus* hys- (HAase negative) wells.

Although initially promising, after 4 hours unspecific release was seen with bacteriophage present after incubation with HAase negative *S. aureus* hys- supernatant. In this case however, no bacteriophage were found after addition of TSB. The difference in concentration between C3

and hys- was significant, and far higher than in 0.4% agarose systems. The use of 0.7% agarose enabled a reduction in passive diffusion of bacteriophage whilst retaining HAase sensitivity.

6.3.5.3. Triggered release of Bacteriophage K by multiple bacterial supernatants

Due to the promise of the 0.7% agarose system, it was assessed with more *S. aureus* strain supernatants (8 HAase positive strains and 8 HAase negative strains). Strains were chosen from the strain screen carried out in Chapter 5 which exhibited very high or no HAase activity. HAase positive strains were *S. aureus* RN6390B, Not380, H050960412, D98, Cuba4005, CDC201078-USA300, C3 and CAN6820-0616. HAase negative strains were *S. aureus* 963Small, D470, D473, HT2001-634, hys-, HT2002-0635, MRSA378 and C154.

After 4 hours incubation with bacterial supernatant, bacteriophage concentration was measured for each strain (Figure 6.13). Here, all HAase positive strains were coloured in green, and all HAase negative strains were coloured in red.

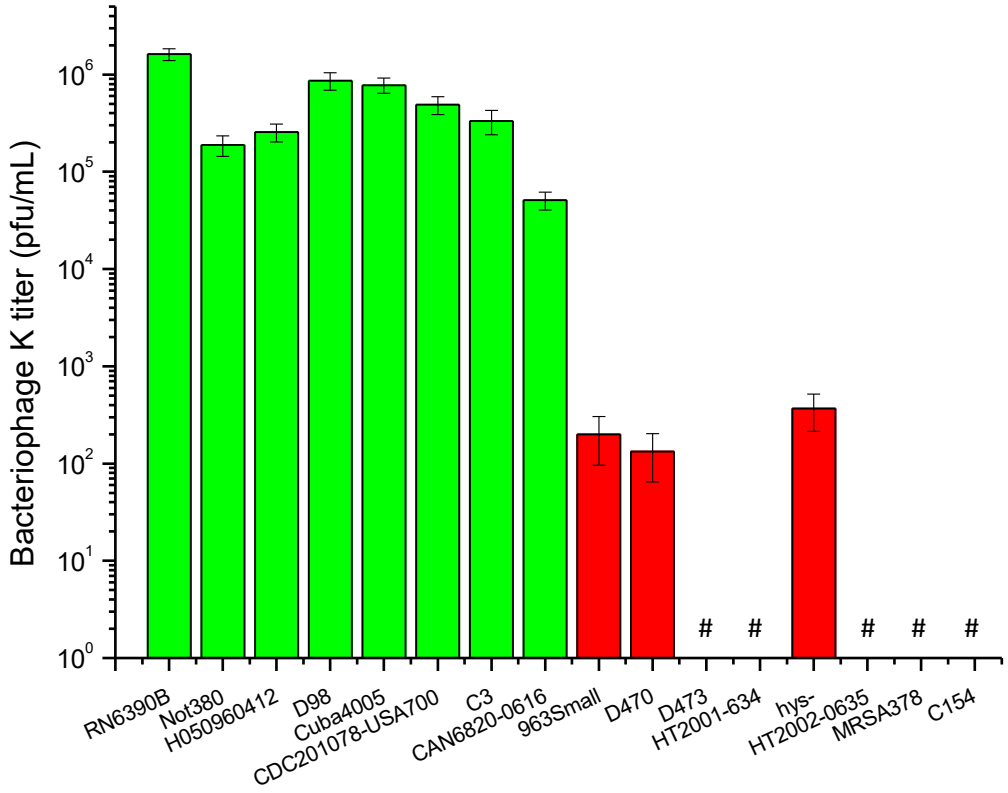

Figure 6.11: Bacteriophage titer after 4 hour incubation of bilayered 0.7% agarose / HAMA hydrogels with 8 HAase positive and 8 HAase negative strains. # = no bacteriophage detected

When incubated with HAase positive *S. aureus* strains, in all cases a high concentration of approximately 10^5 to 10^6 pfu/mL bacteriophage were released from bilayered 0.7% agarose

based hydrogels. In HAase negative strains, out of 8 strains tested, 5 strains showed no bacteriophage release after 4 hours and 3 strains released 10^2 pfu/mL. Although some strains did exhibit some phage release, in all cases HAase positive strains caused a significant release of bacteriophage compared to HAase negative strains. In this respect, triggered release was seen.

6.3.6. 2% agarose bilayer hydrogel

2% agarose based were finally assessed as the hydrogel exhibits very low bacteriophage diffusion. Even though this may result in fewer bacteriophage available to infect and lyse pathogenic bacteria, killing should still be possible for two main reasons. Firstly, killing of *S. aureus* is seen by Bacteriophage K in concentrations as low as 10^5 pfu/mL. Secondly, bacteriophage multiply in number as they infect, so a low initial concentration results in exponential-type growth, resulting in millions of further bacteriophage progeny.

6.3.6.1. Triggered release of Bacteriophage K by hyaluronidase

Bilayered 2% agarose/HAMA hydrogels were incubated with 1 mg/mL hyaluronidase solution and bacteriophage concentration measurements taken at 2, 4 and 6 hours (Figure 6.14).

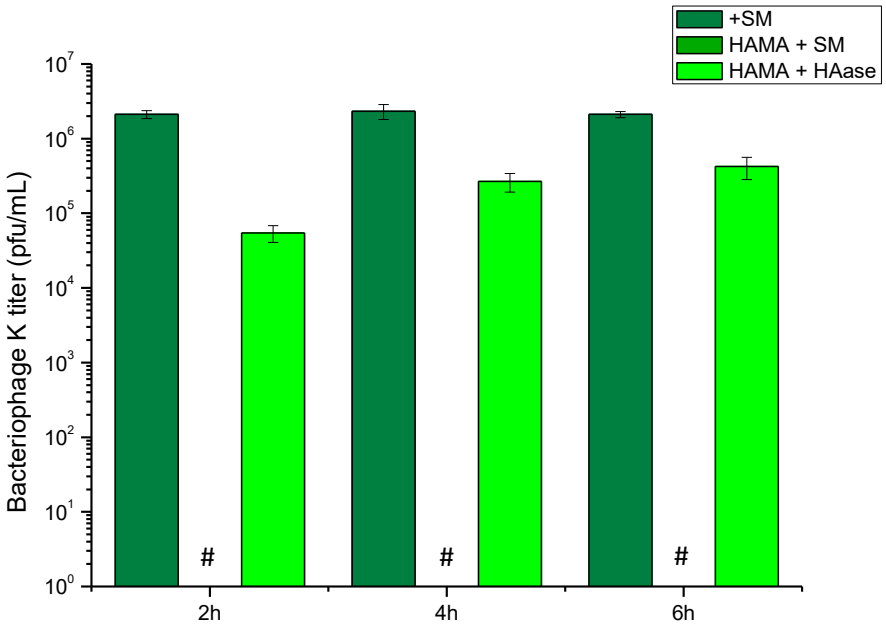

Figure 6.12: Bacteriophage titer after hyaluronidase degradation of bilayer 2% agarose / HAMA hydrogel. # = no bacteriophage detected

Firstly, in this experiment 2% agarose hydrogels which contained no HAMA layer exhibited a high concentration of bacteriophage release; however this was slightly less than less concentrated

hydrogels (10^6 pfu/mL) due to the dense nature of such concentrated agarose. The bacteriophage concentration would still be sufficient to cause high levels of *S.aureus* killing.

Triggered release of Bacteriophage K by HAase was seen in all timepoints. In Bilayer hydrogels incubated with SM buffer, no bacteriophage were released as the lower agarose layer was now dense enough to retain bacteriophage and prevent passive leakage. When incubated with pure HAase, a high concentration of bacteriophage were detected with concentrations of 5 x 10^5 pfu/mL after 6 hours. This significant difference in release was initially purely because of HAMA layer degradation by the HAase enzyme.

6.3.6.2. Triggered release of Bacteriophage K by bacterial supernatant

Bilayered 2% agarose/HAMA hydrogels were incubated with HAase positive *S. aureus* supernatant (C3) and HAase negative *S. aureus* supernatant (NE334 (hys-)), as well as TSB growth medium. Bacteriophage concentration measurements were then taken at 1, 2 and 4 hours (Figure 6.15).

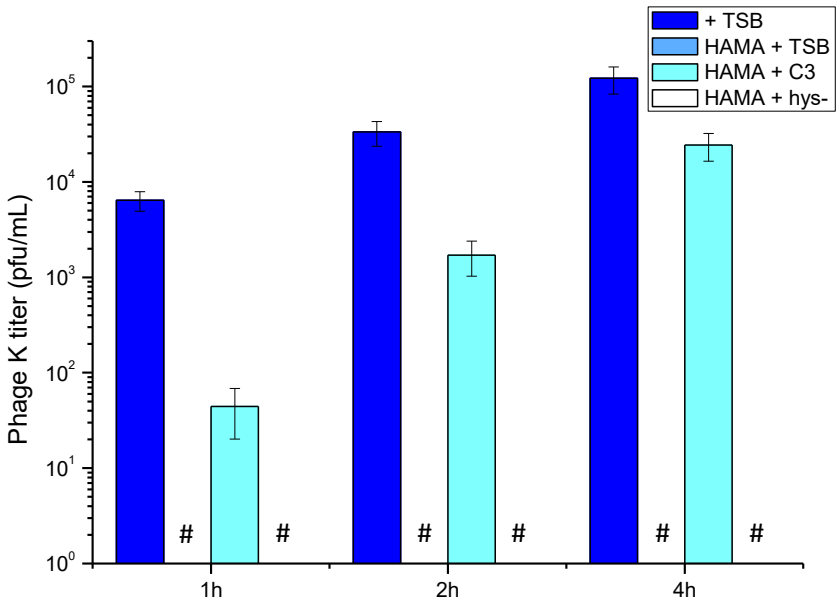

Figure 6.13: Bacteriophage titer after *S. aureus* C3 and hys- supernatant degradation of bilayer 2% agarose / HAMA hydrogel. # = no bacteriophage detected

Generally, bacteriophage release was significantly lower in this experiment compared to tests with pure HAase and tests with less concentrated agarose. In 2% agarose hydrogels containing no HAMA layer, only 10^5 pfu/mL bacteriophage were detected after 4 hours. This may be due to

a combination of the high agarose concentration and the bacterial growth medium (TSB) composition slowing bacteriophage diffusion.

Despite this, triggered release of Bacteriophage K by HAase positive *S. aureus* supernatant was seen at all time points. On incubation of bilayered hydrogels with TSB growth medium or *S. aureus* hys- supernatant, no bacteriophage release was seen. However when incubated with C3 supernatant, a high bacteriophage concentration was eventually seen. Bacteriophage release was initially slow, but increased with time as HAase enzymes degraded the HAMA layer.

6.3.6.3. Triggered release of Bacteriophage K by multiple bacterial supernatants

The *S. aureus* strains assessed in Section 6.3.5.3. were then incubated again with the 2% agarose based bilayer hydrogel. The 8 HAase positive and 8 HAase negative strain supernatants were added to the bilayered hydrogels and incubated for 4 hours, and the concentration of bacteriophage released calculated (Figure 6.16).

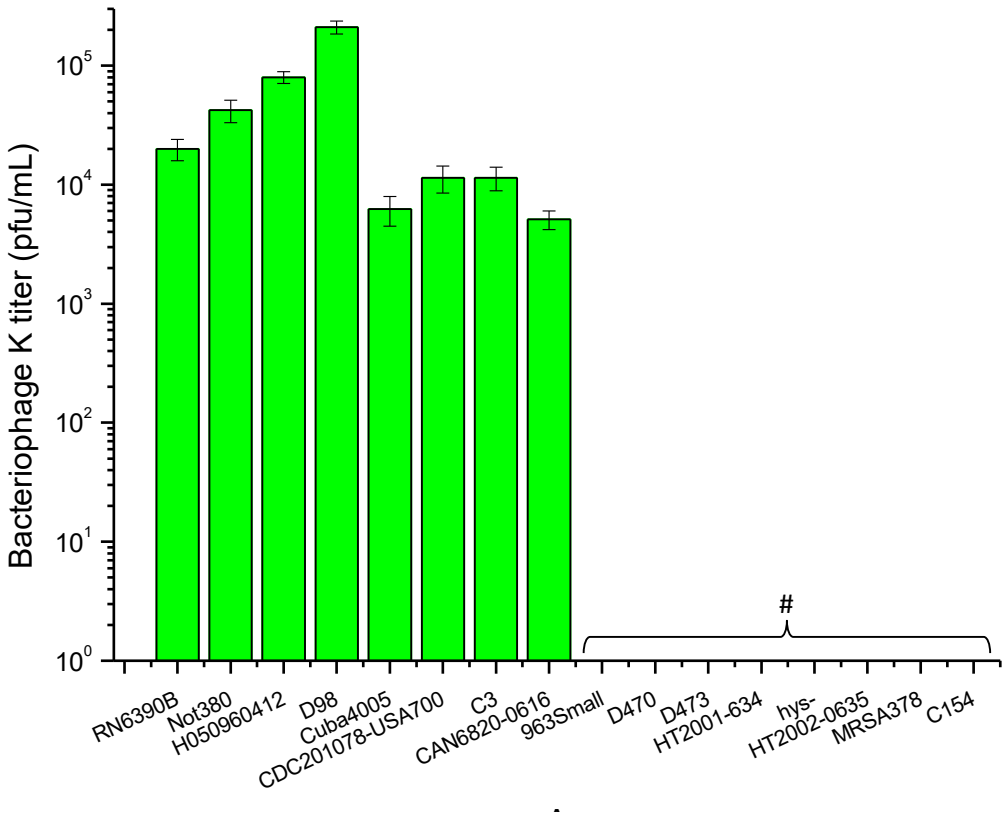

Figure 6.14: Bacteriophage titer after 4 hour incubation of bilayered 2% agarose / HAMA hydrogels with 8 HAase positive and 8 HAase negative strains. # = no bacteriophage detected

On incubation with HAase positive strains, a release of bacteriophage was seen in all cases. This concentration, although low (10^4 – 10^5 pfu/mL) compared to 0.7% based systems, would still be enough to elicit a therapeutic effect. With added time this would also increase. In HAase negative strains, no bacteriophage were detected after incubation in all cases. From this, it can be said that triggered release was seen only by *S. aureus* strains which were known to secrete HAase.

6.3.6.4. Incubation with live *S. aureus* culture

After the success of triggered release seen in incubation of 2% agarose bilayer hydrogels with hyaluronidase and bacterial supernatant, the hydrogels were then assessed using live bacterial liquid culture. Bilayer hydrogels were formed in 24-well plates with and without Bacteriophage K. They were then inoculated with *S. aureus* H560 (HAase positive) and hys- (HAase negative) live subculture and incubated at 37 °C for 18 hours. The OD_{600} was measured to assess bacterial growth and the graphs plotted can be seen in Figure 6.16.

Here, as bacteria grow, levels of HAase will increase as HAase is secreted into the surrounding environment (as examined in Chapter 5). The HAase will then degrade the HAMA layer causing release of Bacteriophage K and killing of *S. aureus* H560. In the case of hys-, no HAase is expressed so normal growth should be seen.

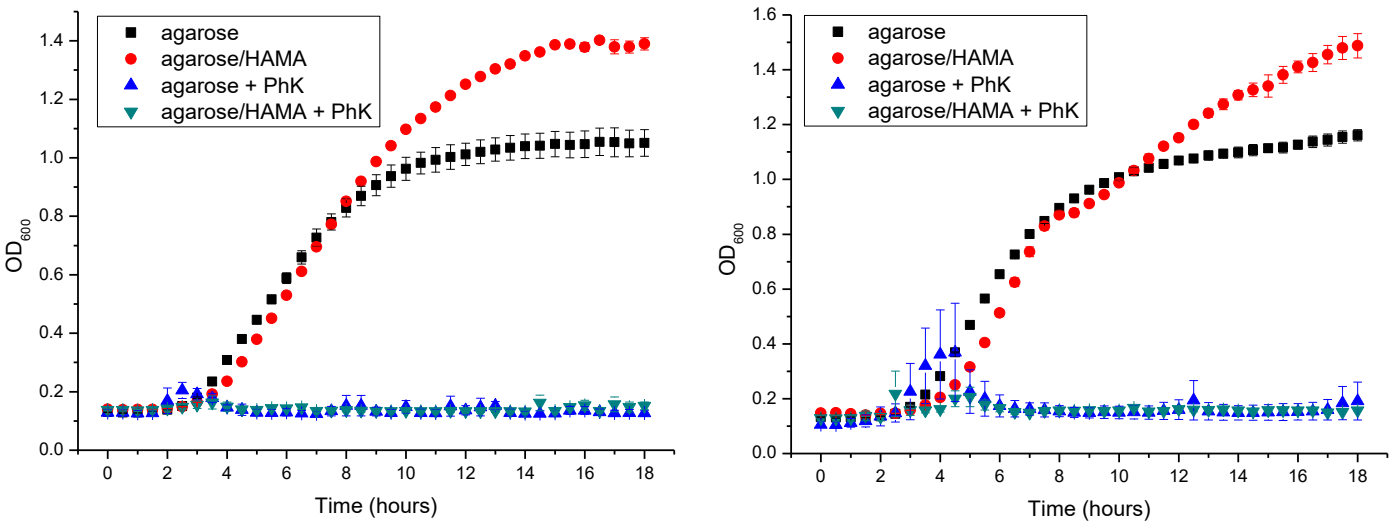

Figure 6.15: 2% agarose/ HAMA bilayer hydrogels containing Bacteriophage K incubated with (left) *S. aureus* H560 and (right) *S. aureus* hys- live culture

In *S. aureus* H560, systems were found to respond as expected. In hydrogels with no bacteriophage present (with and without HAMA) normal bacterial growth was seen. A slightly higher growth was seen with bilayer systems, as the additional HAMA provides a superb energy source for the growing bacteria. In both hydrogels that contained bacteriophage, killing was seen. The bacteriophage were able to diffuse out of the 2% agarose in a high enough concentration to cause killing. In the bilayered system, the HAMA layer was degraded by HAase produced by H560, and so bacteriophage were released.

In *S. aureus* hys- however, the same result was seen. Normal growth was seen in hydrogels containing no bacteriophage, and in both hydrogels (with and without HAMA) which contained bacteriophage bacteria were killed. This indicated that the HAMA layer was not able to cause triggered release of bacteriophage, as if this was the case normal bacterial growth would be seen in bilayered hydrogels.

It is most probable that passive diffusion of bacteriophage was apparent in the system; this could be due to a number of reasons. The seal between the well and the hydrogel, or the HAMA and agarose layer could not be intact or sealed enough to prevent bacteriophage diffusion over 18 hours. In Section 6.3.6.1., no bacteriophage were detected after 6 hours of incubation in SM buffer (no HAase), however after this time bacteriophage in low numbers could eventually diffuse out. Also, the shaking of the plate reader used for live experiments was far more aggressive than the shaking used for HAase and supernatant experiments; this could dislodge the HAMA layer causing un-triggered bacteriophage release.

6.4. Conclusions

In conclusion, this chapter combined work carried out in Chapters 4 and 5 to create a bilayered hydrogel comprising of a lower bacteriophage-containing layer and an upper layer formed of crosslinked HAMA. PVA was not investigated, as when exposed to UV the polymer is known to form highly damaging free radicals which can harm bacteriophage. Instead, agarose was used as a biocompatible, non-toxic hydrogel. HAMA was crosslinked in situ on top of the set agarose layer for a shorter time than in previous experiments in order to minimise bacteriophage damage.

The aim of this chapter was to form a hydrogel system which selectively gave triggered release of bacteriophage only in the presence of HAase. In this way, bacteriophage are only released in the presence of bacterial infection, therefore reducing the unnecessary release of bacteriophage and the possibility of resistance evolving.

The bilayered hydrogel system was assessed with varying concentrations of agarose in order to tune the triggered release. The system was then assessed with pure HAase, bacterial supernatant and live cultures. The 2% agarose system was found to be most sensitive, with bacteriophage only released when HAase was present (either from pure commercially available HAase or bacterial supernatant).

The system was then taken on for further assessment with HAase positive and negative *S. aureus* live culture to see if HAase secreted during the normal growth cycle was capable of initiating triggered release of bacteriophage (and so triggered killing of the HAase positive strain).When incubated with live culture, bacterial killing was seen in all cases where bacteriophage were present compared to normal growth curves. In this case it was most probable that bacteriophage were able to diffuse out of the hydrogel due to a poor seal with the culture well.

6.5. References

1. S. Lu, J. Lam, J. E. Trachtenberg, E. J. Lee, H. Seyednejad, J. J. van den Beucken, Y. Tabata, M. E. Wong, J. A. Jansen, A. G. Mikos and F. K. Kasper, *Biomaterials*, 2014, **35**, 8829-8839.
2. X. Zhao, Q. Lang, L. Yildirimer, Z. Y. Lin, W. Cui, N. Annabi, K. W. Ng, M. R. Dokmeci, A. M. Ghaemmaghami and A. Khademhosseini, *Adv Healthc Mater*, 2015.
3. J. Jiang, A. Tang, G. A. Ateshian, X. E. Guo, C. T. Hung and H. H. Lu, *Ann Biomed Eng*, 2010, **38**, 2183-2196.
4. H. Geckil, F. Xu, X. Zhang, S. Moon and U. Demirci, *Nanomedicine (Lond)*, 2010, **5**, 469-484.
5. P. Nooeaid, V. Salih, J. P. Beier and A. R. Boccaccini, *Journal of Cellular and Molecular Medicine*, 2012, **16**, 2247-2270.
6. S. P. Zhong, Y. Z. Zhang and C. T. Lim, *Wiley Interdiscip Rev Nanomed Nanobiotechnol*, 2010, **2**, 510-525.
7. A. Nakayama, A. Kakugo, J. P. Gong, Y. Osada, M. Takai, T. Erata and S. Kawano, *Advanced Functional Materials*, 2004, **14**, 1124-1128.
8. L. Weng, A. Gouldstone, Y. Wu and W. Chen, *Biomaterials*, 2008, **29**, 2153-2163.
9. H. Shin, B. D. Olsen and A. Khademhosseini, *Biomaterials*, 2012, **33**, 3143-3152.
10. S. Yan, Q. Zhang, J. Wang, Y. Liu, S. Lu, M. Li and D. L. Kaplan, *Acta Biomaterialia*, 2013, **9**, 6771-6782.
11. P. Matricardi, C. Di Meo, T. Coviello, W. E. Hennink and F. Alhaique, *Adv Drug Deliv Rev*, 2013, **65**, 1172-1187.
12. A. D. Jenkins, P. Kratochvil, R. F. T. Stepto and U. W. Suter, *Pure & Appl. Chem.*, 1996, **68**, 2287-2311.

Chapter 7 : Nano-imprint lithography of photocrosslinkable hyaluronic acid/gelatin hydrogels for cell proliferation

7.1. Introduction

In a similar fashion to prokaryotes, eukaryotic cells are inherently driven to bind to surfaces during growth. Because of this, it is important to assess the growth and interactions of eukaryotic cells on a device if it is to be used as a therapeutic. Hydrogels have been widely used in cell culture for a number of years, either as scaffolds to immobilise cells, or as platforms to grow cell sheets on top of. The hydrogel chemical structure greatly determines the extent of cell binding and can be incorporated with polymers, proteins (e.g. growth factors) or other additives which promote cell growth. Also, the polymer structure can be altered to make the hydrogel more or less hydrophilic, and so changing how cells adhere to the surface.

In this chapter, firstly the growth of NIH-3T3 mouse fibroblast cells on hydrogels derived from HA and gelatin was investigated. Fibroblasts are cells which secrete the extracellular matrix and collagen found in the skin and connective tissues; because of this they are critical for wound healing. A number of studies have reported the beneficial effect HA has on fibroblast growth[1, 2]. The cells are also known to have a number of cell-binding receptors for HA (CD44, RHAMM) which have been discussed previously in Chapter 1. Because of its close structural similarity to collagen, gelatin interacts with cells through the same receptors; the most prevalent of which are integrins and the RGD (Arg-Gly-Asp) amino acid sequence[3, 4].

In this investigation, nano-imprint lithography was also used to form printed hydrogels for use in cell culture. It was proposed that lithography of hydrogels could impart a surface roughness that could aid cell adherence, or direct cell growth (depending on print size and shape). The effect of surface roughness has been investigated at the nano and micro scale in hydrogels, as well as on implant surfaces, with positive results[5-7]. Cells have been successfully grown in a directed way with a high control over cell growth using lithography of a range of biocompatible hydrogels[8-11]. Here, hydrogels were printed with a pre-patterned stamp, with cells either incorporated into the hydrogel structure or subsequently being grown on top.

A schematic representation of this process can be seen in Figure 7.1. Polypropylene moulds can be formed with surface patterns in a variety of shapes and sizes. These then can be placed on top of a pre-polymer solution that when exposed to UV light, can be crosslinked to form a solid

hydrogel (a) which contains a print. On removal of the mould, an inverted print is seen in the hydrogel surface (b).

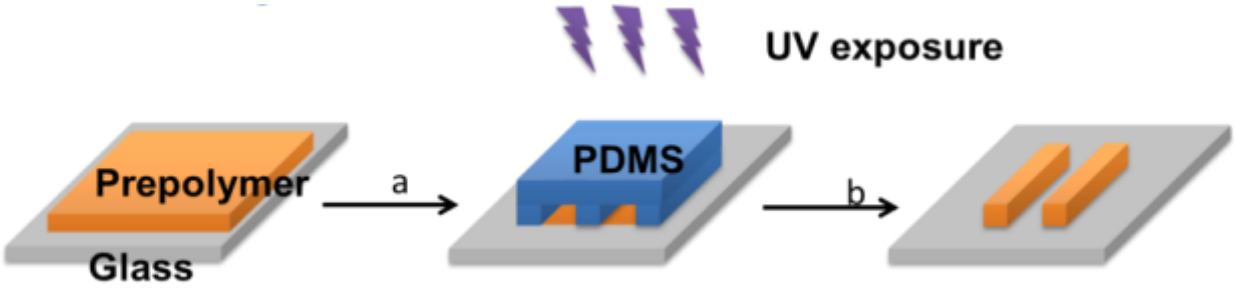

Figure 7.1: Diagram of nano-imprint lithography using PDMS moulds to emboss photo-crosslinkable polymers. Diagram by Ping Li

Due to the previous work carried out on UV crosslinkable HA, it was decided that this mix would be the foundation for lithographic printing and fibroblast cell tests.

7.2. Materials and Methods

7.2.1. Cast moulding of lithographic prints through Hot Embossing

A UV-reactive photoresist AZ125 was firstly spin-coated onto a clean silicon wafer. The coated wafers were then baked on a hot plate at 65 °C for 3 minutes followed by a second bake at 95 °C to remove organic solvents. A mask was placed on top of the wafer with the required design and the photoresist exposed to UV light. Post-exposure baking was performed for 1 minute at 65 °C, followed by a second bake for 3 minutes at 95 °C. Un-crosslinked photoresist was then washed away using developer and dried under nitrogen.

PDMS (Polydimethylsiloxane) moulds used for hot embossing were formed using the PDMS mix Sylgard® 184 in the ratio 1:9 curing agent:PDMS. PDMS mix was degassed under vacuum for 30 minutes and 1 mL poured over the spin-coated silicon pre-mould. Moulds were then incubated at 60 °C for 2 hours to cure. Hot Embossing was used to form durable prints for hydrogel nano-imprinting. Polystyrene sheets were cleaned to remove contaminating dust and placed over the PDMS mould. They were then heated in an Obducat Eitre 3 Hot Embosser to 140 °C at 5 bar for 120 seconds, and then allowed to air cool for 100 seconds.

7.2.2. Crosslinking of hydrogels

Casting of hydrogels was carried out in a similar way to that described in Chapter 5. 1 mL hydrogel mixture containing photoinitiator was added per well in a 12 well cell culture plate. In

non-printed hydrogels, gels were left and allowed to form a flat surface; in printed hydrogels, the cooled polystyrene print was placed on top of the hydrogel (with the printed side exposed to the hydrogel). Plates were then crosslinked using a UVP CL-1000 UV Crosslinker.

7.2.3. Characterisation of polystyrene prints and imprinted hydrogels

Light microscopy of polystyrene prints, printed hydrogels and all cell imaging was carried out on a Zeiss AxioCam ERc5s light microscope. Printed polystyrene patterns were gold sputter coated and Scanning Electron Microscopy (SEM) images were taken using a Carl Zeiss AG Zeiss Ultra 55 FESEM.

7.2.4. Cell culture on HAMA hydrogels

In brief, passaged NIH-3T3 fibroblasts were adjusted to 10^4 cells/mL with culture medium, and 1.5 mL added to precast hydrogels in a 12-well plate. Plates were then incubated for up to 48 hours at 37 °C at 5% CO_2.

7.2.5. Preparation of GelMA

Gelatin methacrylate (GelMA) was synthesised as described by Chen et al[12]. In brief, 2 g type A porcine gelatin was dissolved in 20 mL PBS at 60 °C to make a 10% w/v solution. Once gelatin was fully dissolved, 1.6 mL methacrylic anhydride was added at a rate of 0.1 mL/min with stirring. The mixture was then allowed to react at 50 °C for 3 hours and the reaction stopped by the addition of 60 mL PBS. The GelMA mixture was dialysed against deionised water to remove unreacted methacrylate and by-products using 50 kDa MWCO dialysis membrane for 7 days at 40 °C. The purified GelMA was then frozen at -80 °C, lyophilised and stored at 4 °C until needed. Methacrylation was confirmed by ^{1}H NMR using a Bruker 400 MHz NMR.

7.2.6. Cytotoxicity of Irgacure 2959

Cytotoxicity of Irgacure 2959 to NIH-3T3 fibroblasts was investigated using the method described by Williams et al[13]. Passaged NIH-3T3 fibroblasts were adjusted to 64,000 cells/mL with growth medium and seeded at 500 µL/well in a 24 well plate. Photoinitiator stock solutions were formed by dissolving 0, 0.03, 0.05 and 0.1 g Irgacure 2959 in 1 mL 70% ethanol. The solutions were then removed from light and kept at room temperature until needed. Immediately after seeding, 5 µL Irgacure 2959 solution was added to each well which exposed cells to a final initiator concentration of 0, 0.03, 0.05 and 0.1 % w/v. Plates were then incubated for 24 hours at 37 °C and 5 % CO_2. Control wells contained cells incubated with 5 µL 70% ethanol solution only.

7.2.7. MTT assay

In vitro cytotoxicity was assessed through the MTT (3-[4,5-dimethylthiazol-2-yl]-2,5 diphenyl tetrazolium bromide) assay. This involves the conversion of the water soluble MTT to insoluble formazan (Figure 7.2). After incubation with test chemical for the appointed time, medium was removed and replaced with 600 µL fresh DMEM medium. Standard curve wells were also included containing 500 – 128,000 cells/mL. 60 µL MTT solution (5 mg/mL in PBS) was then added per well and the plate incubated for 4 hours at 37 °C.

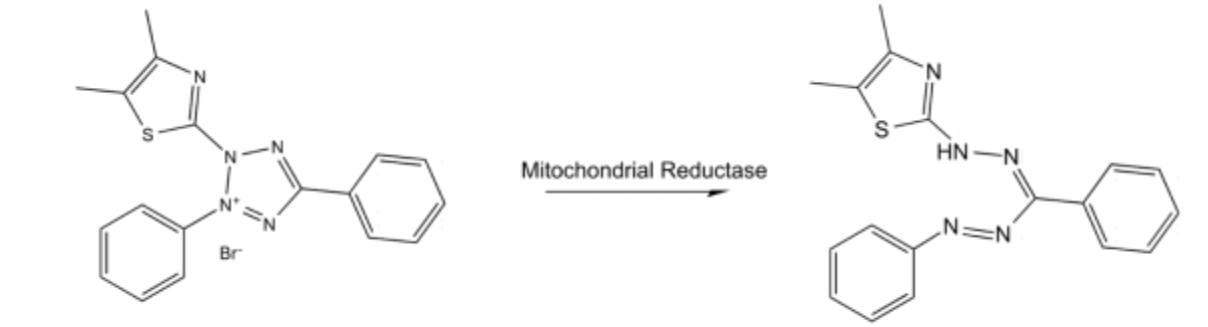

3-(4,5-dimethylthiazol-2-yl)-2,5-diphenyltetrazolium bromide
(MTT)

(*E*,*Z*)-5-(4,5-dimethylthiazol-2-yl)-1,3-diphenylformazan
(Formazan)

After 4 hours, 600 µL SDS solution (100 mg/mL in 0.01 HCl) was then added per well, the solutions mixed, and the plate incubated overnight at 37 °C. Solutions were mixed again thoroughly and the absorbance measured at 570 nm.

7.2.8. Hyaluronidase degradation of HA and Gelatin based co-gels

Hydrogels containing varying concentrations of HA, HAMA and GelMA were photocrosslinked as described previously. Hydrogels were then swollen overnight at room temperature in PBS to achieve complete swelling. Samples were weighed (100% hydrogel weight) and incubated with 1 mL 0.1 mg/mL hyaluronidase in PBS at 37 °C with mild shaking. After 2, 4, 6, 8 and 24 hours, all hyaluronidase solution was removed, remaining gels were blotted and the samples weighed. All hydrogel measurements were carried out in triplicate. The change in weight of hydrogels over time was then plotted as a % of the original weight.

7.3. Results and Discussion

7.3.1. Imprinting of hydrogels

7.3.1.1. Cast moulding of lithographic prints through Hot Embossing

Hot embossing was found to be a robust technique which gave good quality, reproducible prints with varying sizes and shapes. Silicon wafers (Figure 7.3 a) and b)) could be spin-coated with a variety of patterns and used repeated times to form PDMS pre-moulds. These PDMS moulds (Figure 7.3 c) could either be used directly to print hydrogels, or further used to print polystyrene prints, depending on the print properties required. Polystyrene was chosen for all printing as these formed hard prints that retained their pattern and which could be washed after each use through sonication.

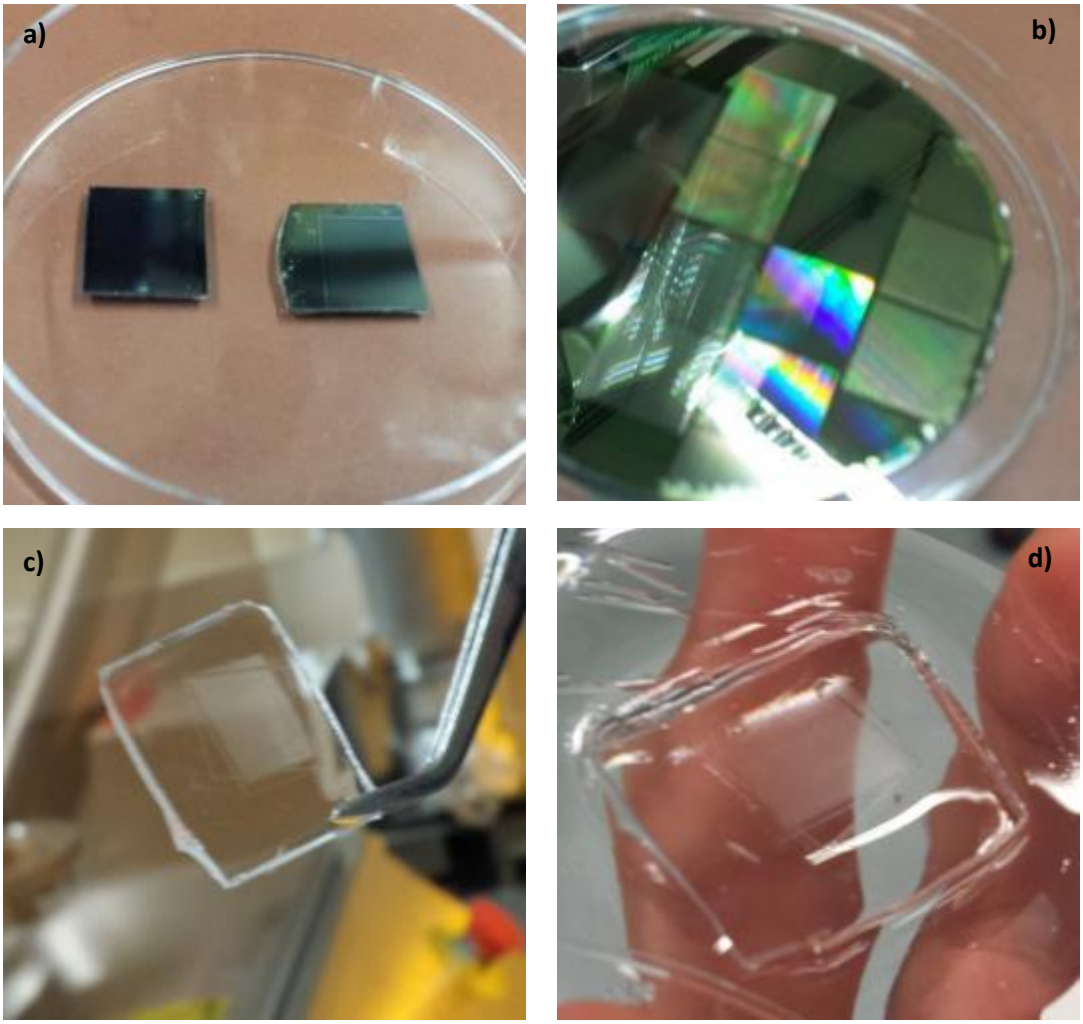

Figure 7.3: a) Silicon wafer line patterned with photoresist b) Large silicon wafer with multiple photoresist patterns c) PDMS mould of patterned silicon wafer leads to a negative patterning d) Polystyrene master formed through hot embossing with PDMS mould

SEM images (Figure 7.4) of polystyrene line prints with varying line width were taken to assess surface morphology. These sizes were thin line prints (10 and 15 µm line width) and large line prints (80 µm line width). In all sizes, a consistent straight line was seen with equal line spacing and no defects.

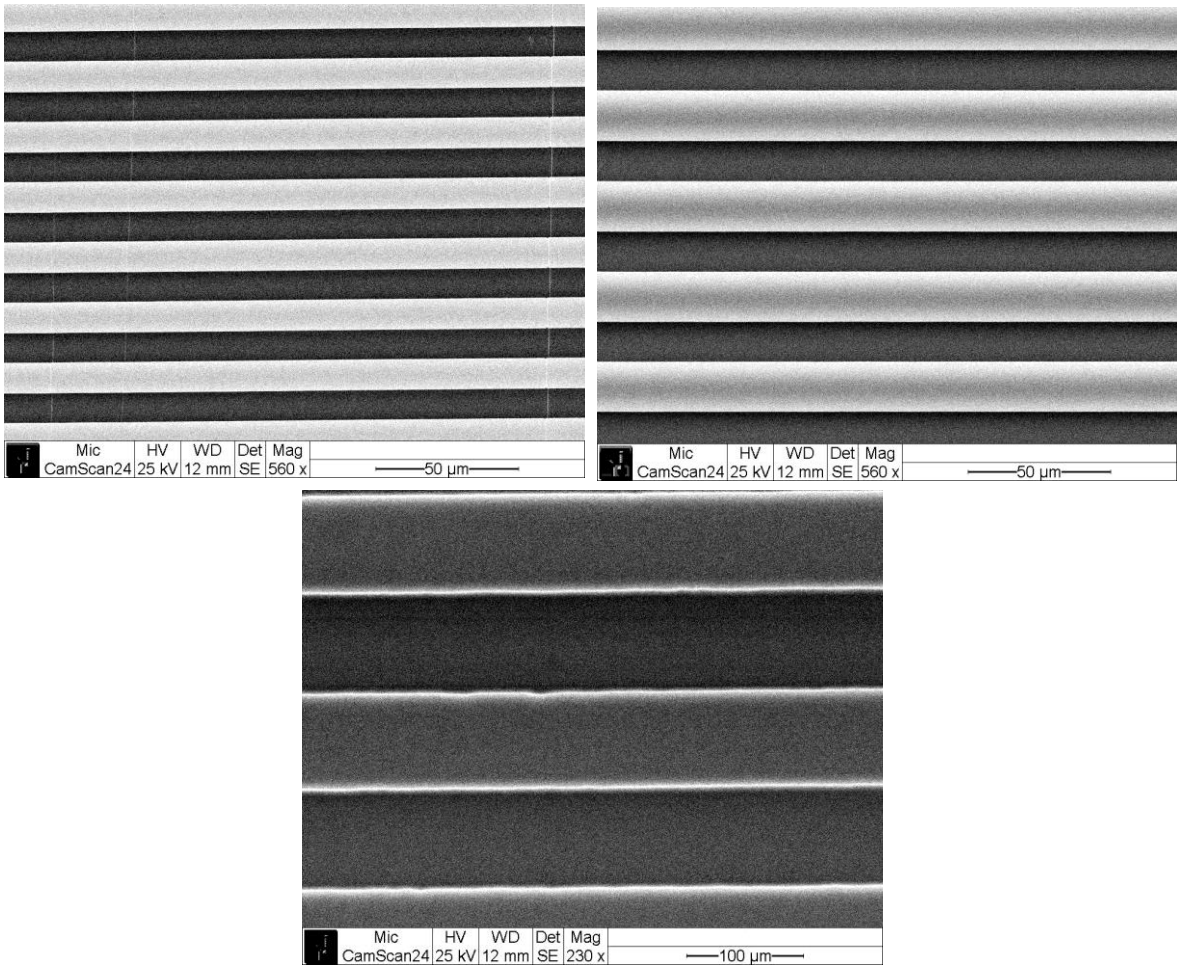

7.3.1.2. Printing of HAMA hydrogels

2% HAMA hydrogels containing a range of PEGDA concentrations were UV-irradiated with 10, 15, 50 and 80 µm line prints (20 µm deep). It was previously understood that with an increasing concentration of PEGDA, an increase in non-specific free radical polymerisation to the polystyrene mould occurs, making the mould hard to remove from the crosslinked hydrogel. Hydrogels containing 0% PEGDA were found to be too elastic to retain print on irradiation. Both 5% and 10% PEGDA hydrogels were too brittle to be removed from the polystyrene mould. It was also found that prints with smaller line spacing (10 and 15 µm) were harder to remove from

irradiated hydrogel than larger prints. It was decided that 1% PEGDA gave the optimum hydrogel properties for further nano-imprinting.

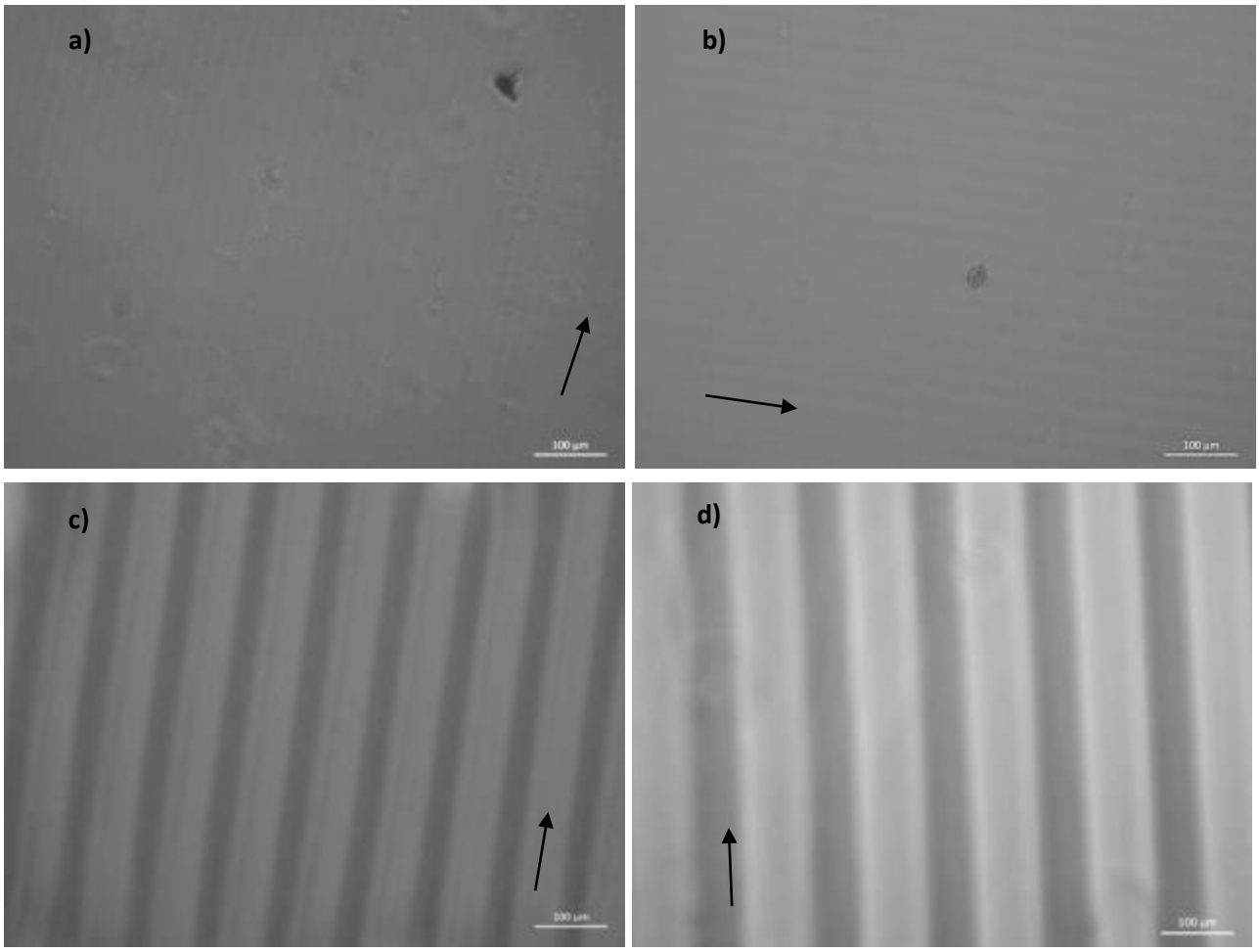

Figure 7.5: Light microscopy images of a) 10 µm, b) 15 µm, c) 50 µm and d) 80 µm line width prints formed on 2% HAMA/1%PEGDA/1%I2959 hydrogels. Scale bar = 100 µm

2% HAMA hydrogels containing 1% PEGDA co-crosslinker were printed with line prints of varying width: 10, 15, 50 and 80 µm (Figure 7.5). In all cases defined, regular prints were seen by light microscopy which retained structure over time. On swelling however, printed patterns became distorted (Figure 7.6). In 10 and 15 µm prints, no pattern was seen after 24 hours swelling in PBS buffer. In 50 and 80 µm prints, a patterned structure was still seen, although in a far less defined way with lines appearing broader in width.

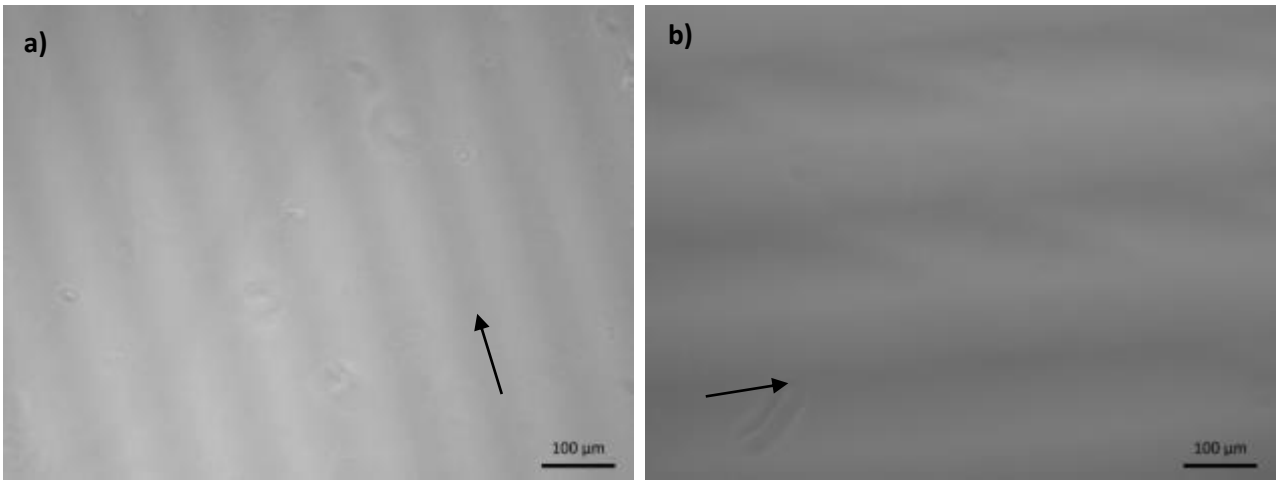

Figure 7.6: Light microscopy images of a) 50 µm and b) 80 µm line width prints formed on 2% HAMA/ 1%PEGDA/ 1%I2959 hydrogels after 24 hours swelling in PBS buffer. Scale bar = 100 µm

7.3.2. NIH-3T3 culture on HAMA hydrogels

7.3.2.1. Culture of NIH-3T3 fibroblasts

NIH-3T3 fibroblasts, originally isolated from mouse embryo tissue, are the standard cell line used in fibroblast cell culture experiments. Initial binding to flask bottoms is seen after approximately two hours; with cells appearing flattened and elongated (Figure 7.7). The doubling time for NIH-3T3 fibroblasts is approximately 20 hours, and as seen in Figure 7.7 b, once attached to the surface cells extend filopodia to their surroundings and to other cells. Nuclei also become bigger and more visible, with contracted genetic material visible as dark spots under the light microscope. After 48 hours a near confluent sheet of extended cells is seen.

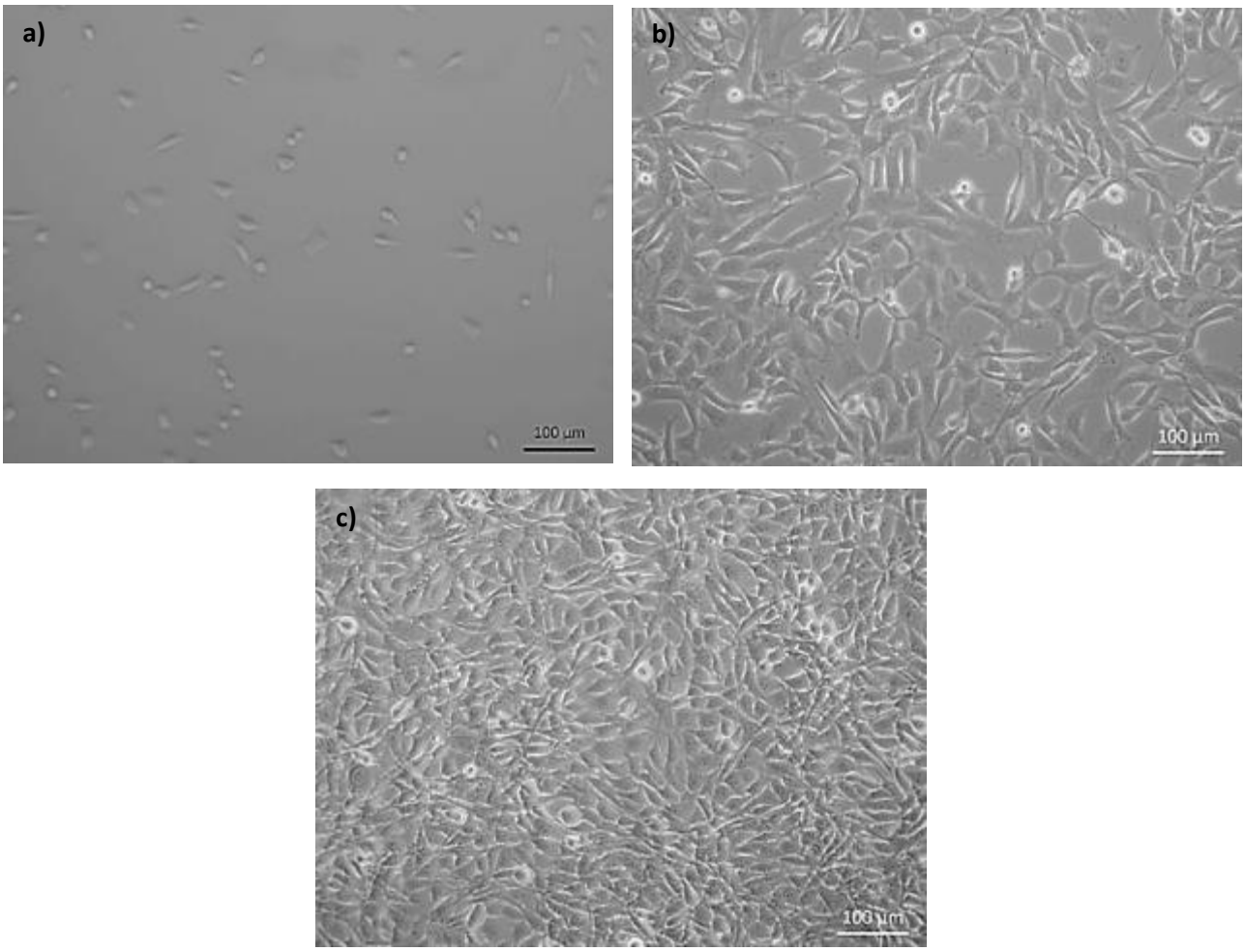

7.3.2.2. Cell culture on flat HAMA hydrogels

In recent years, a wide range of polymers, including HA and PEG, have been reportedly used in hydrogel systems for cell culture and tissue engineering. The long polymer chains provide an advantageous environment to promote cell attachment. In this respect, NIH-3T3 fibroblasts were firstly incubated on HAMA hydrogels co-crosslinked with PEGDA (the same HAMA mix investigated in detail in Chapter 5). It was hypothesised that by increasing the PEGDA concentration in HAMA gels, cell binding would increase. As described previously, ease of hydrogel printing changed depending on concentration of PEGDA; flat HAMA hydrogels containing varying concentrations of PEGDA were firstly incubated with NIH-3T3 fibroblasts.

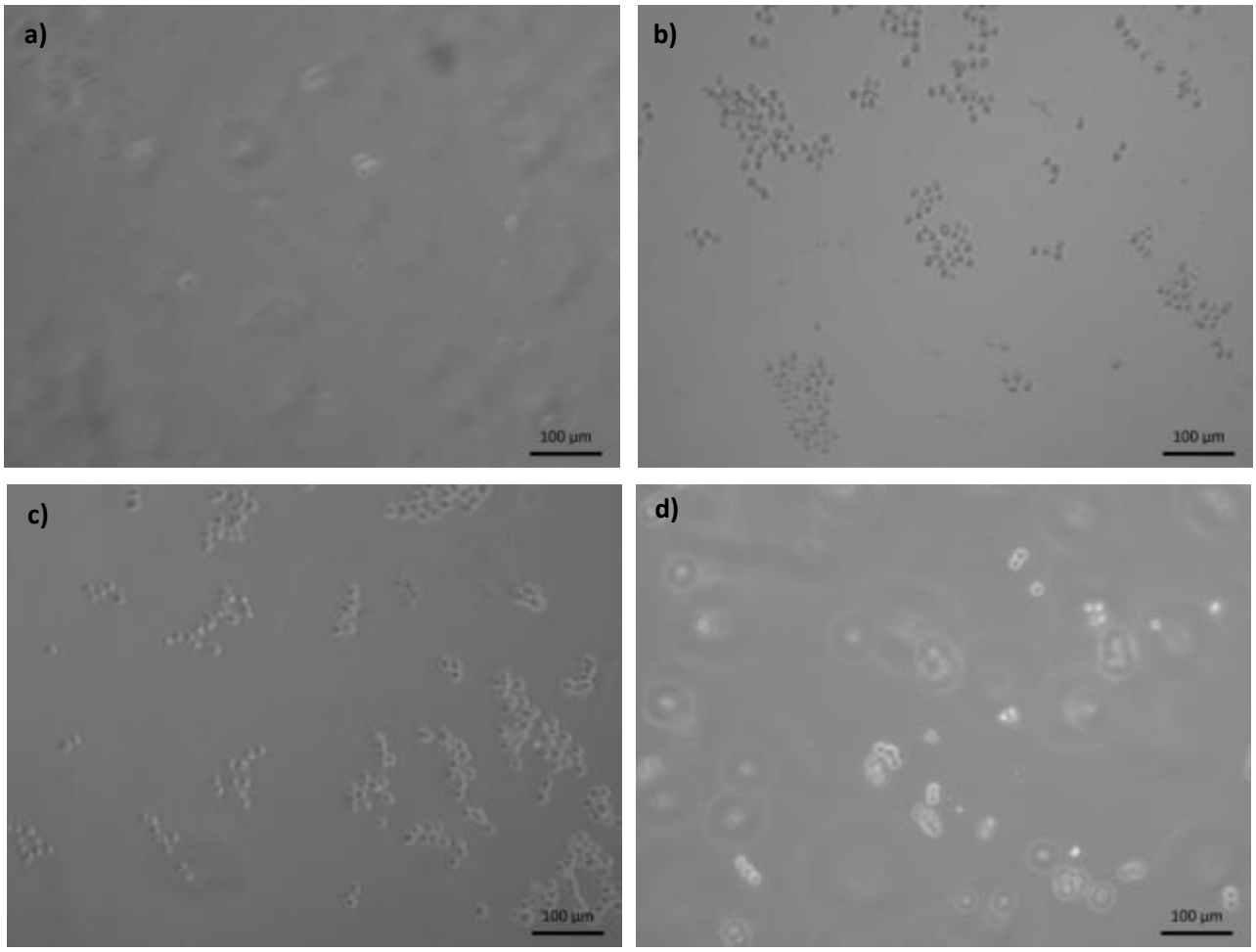

2% HAMA hydrogels containing 0, 1, 5 and 10% PEGDA with no print were incubated with NIH-3T3 fibroblasts for 48 hours (Figure 7.8). In all cases, no cell attachment was seen to hydrogels, with cells instead forming spherical aggregates that permeated through the gel. More aggregates were seen on incubation with 1% and 5% PEGDA, although in all cases no cell binding was seen to gels. This was most probably due to the chemical properties of HA. HA is inherently non-cell binding due their negative charge[14]. Also, because of the high water content of the gel it is possibly hard for cells to gain a strong binding between polysaccharide fibres as they are so far apart.

7.3.2.3. Cell culture on printed HAMA hydrogels

To increase cell binding, hydrogels were printed to impart a surface 'roughness'. Cells were investigated with 10, 15, 50 and 80 µm prints (Figure 7.9). NIH-3T3 fibroblasts were still found not to attach to hydrogel membranes after 48 hours, regardless of surface roughness. On attachment, NIH-3T3 fibroblasts normally exhibit a flattened shape as the cells bind to the

surface. As cells grow on an adherent surface, cells become increasingly branched and proliferate to a confluent sheet.

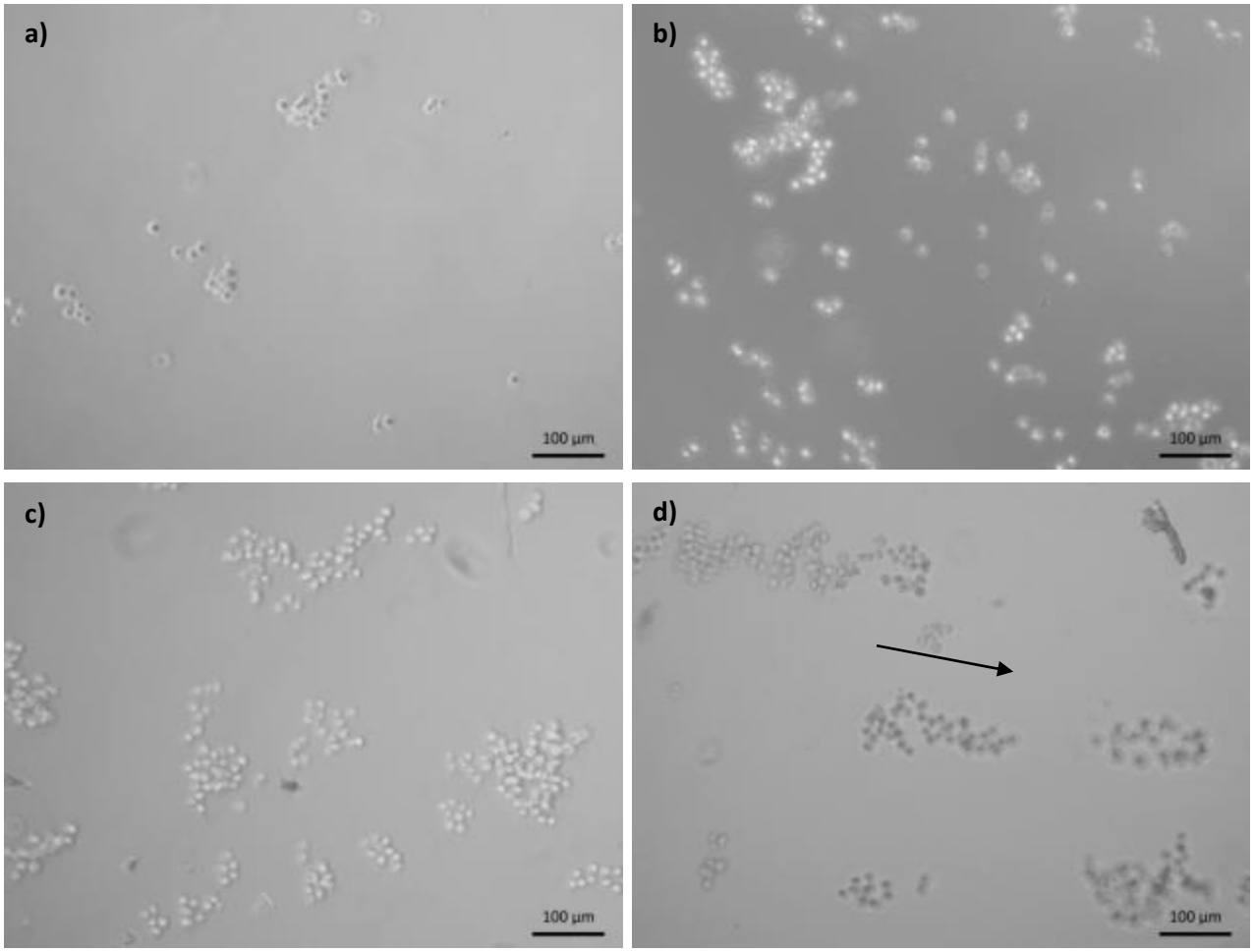

In this case, no branching was seen, with cells clustering into multicellular aggregates both on the surface and inside the hydrogel. This is characteristic of the surface being non-adherent and not conducive to cell binding. Hydrogels printed with 10, 15 and 50 µm lines did not induce directed growth. With 80 µm prints, although aggregated, cells did show directed growth with cells predominantly in the wells of the pattern. In Figure 7.9, direction of line print is shown by an arrow. In all cases, on washing with PBS buffer, no cells remained confirming non-adhesion.

7.3.2.4. Printing of HA hydrogels with varying concentration of HA

HA hydrogels were cast containing varying concentrations of HAMA to increase the crosslinking density and to decrease the length between polysaccharide fibres. By doing this it was proposed

that not only would a more sturdy print be formed (by making hydrogels with a decreased swelling ratio), but also that cells would have more polysaccharide fibres to bind to.

Hydrogels were investigated with concentrations of 1, 2, 3, 4, and 6% w/v HAMA and a line print of 80 µm; with any higher concentrations of HAMA the pre-crosslinked solution was found to be too viscous to reliably quantify. As expected, by increasing the concentration of HAMA in hydrogels, the swelling ratio decreased from 46.6 ± 2.7 for 1% HAMA gels to 20.0 ± 0.2 for 6% HAMA gels (Figure 7.10).

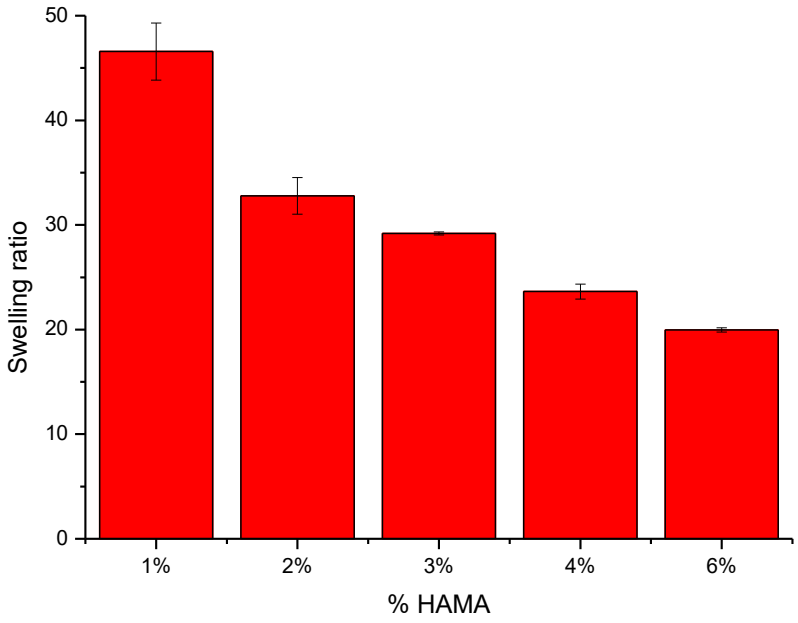

Figure 7.10: Swelling ratio values for varying 1% PEGDA/1% I2959 HAMA hydrogels containing 1 – 6% HAMA

Hydrogels were then printed, and NIH-3T3 fibroblasts incubated on these hydrogels to assess cell attachment (Figure 7.11). Firstly, as HAMA concentration increased, a more defined print was seen that was retained after swelling in cell solution for 48 hours. In hydrogels of lower concentration, prints were ill-defined after swelling and did not induce directed cell growth. However, 3, 4 and 6% HAMA printed hydrogels all showed defined prints and on incubation with cells, cells were predominantly found in the wells of the pattern. Even so, cells were still clustered and spherical in shape with no binding to hydrogel surfaces.

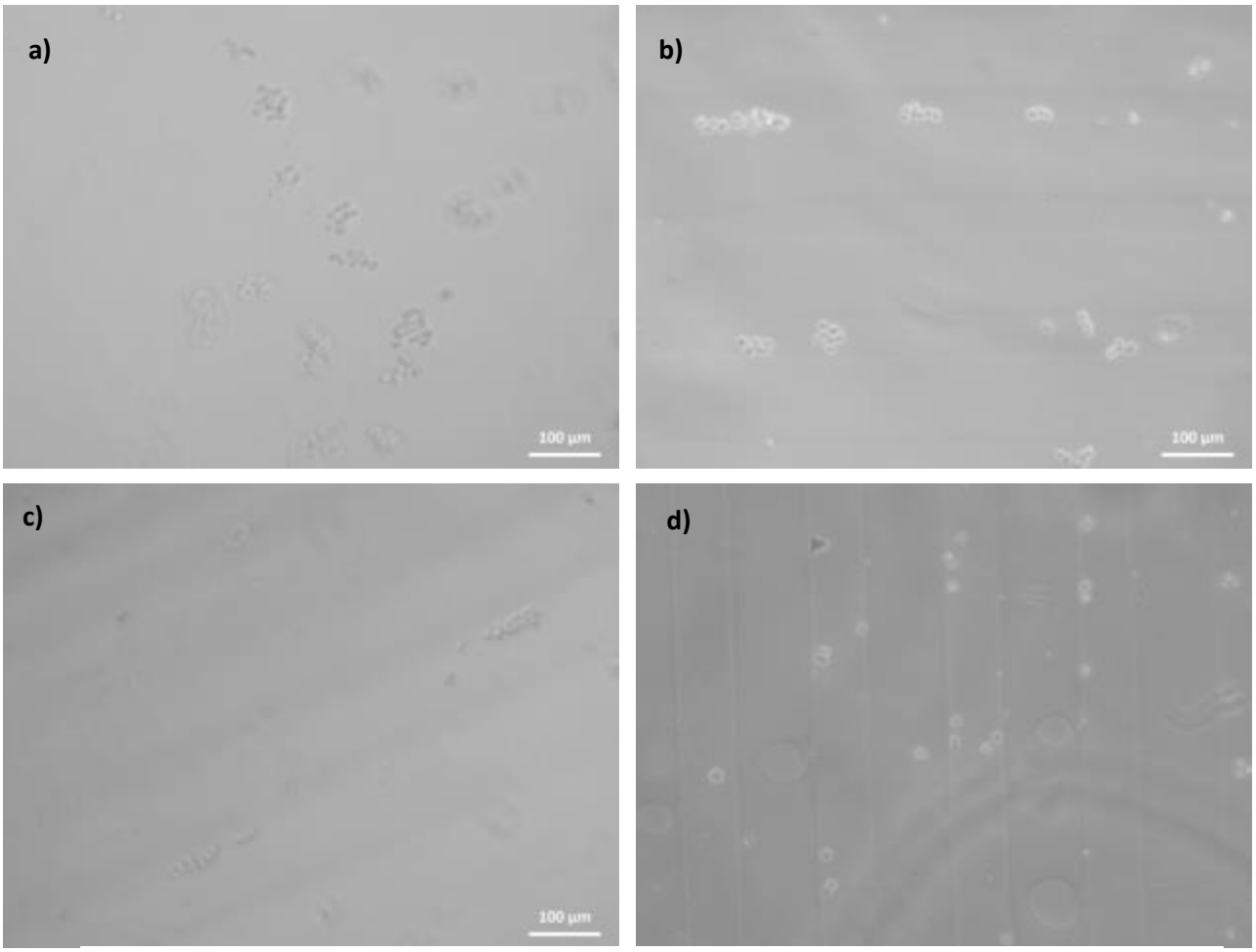

Figure 7.11: NIH-3T3 fibroblast growth on 80 µm hydrogel prints formed from varying HAMA concentrations – a) 2%, b) 3%, c) 4% d) 6% w/v HAMA/1% PEGDA/1% I2959. Scale bar = 100 µm

7.3.2.5. Cytotoxicity of Irgacure 2959

The cytotoxicity of Irgacure 2959 to NIH-3T3 fibroblast was measured to assess if cell damage was seen at high photoinitiator concentrations. On UV exposure, the free radicals created from photoinitiators are able to react with and damage eukaryotic cells. Radical species can react with a range of cellular components (e.g. cell membranes, DNA and proteins) causing damage. As previously described in Chapter 5, the photoinitiator Irgacure 2959 was chosen over other photoinitiators because of its low cytotoxicity. It has also been used successfully in a range of crosslinked polysaccharide hydrogels[15, 16].

The cytotoxicity of various photoinitiators (but not Irgacure 2959) to NIH-3T3 fibroblasts was assessed in 2000 by Bryant et al, showing that at high concentrations cell death can occur[17]. In 2005, Williams et al similarly reported on the cytotoxicity of Irgacure 2959 to six separate cell lines; however NIH-3T3 fibroblasts were not investigated[13]. Although in this investigation cells were not encapsulated in the hydrogel matrix, and so were not directly exposed to UV or free radicals created from Irgacure 2959, it was important to determine if cytotoxicity was seen at concentrations required to crosslink hydrogels.

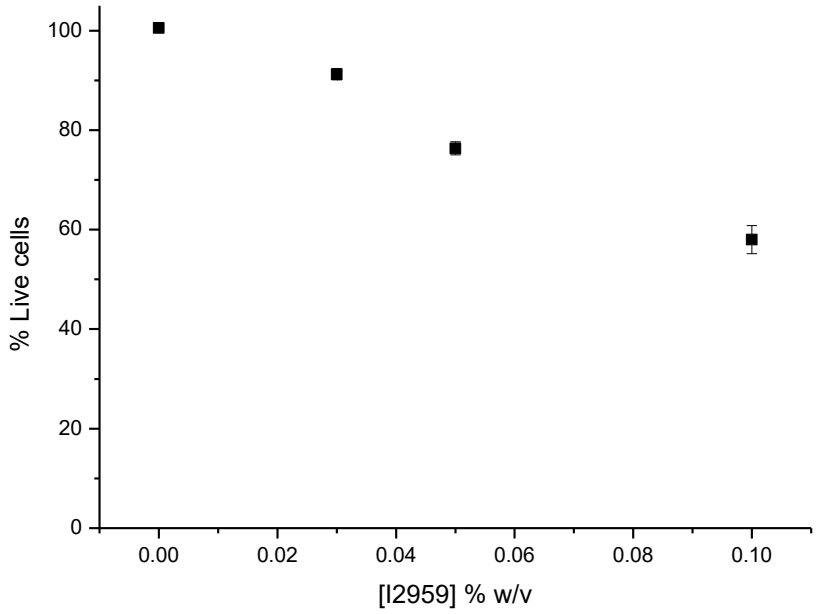

Figure 7.12: % live NIH-3T3 fibroblast cells after 24 hours incubation with 0, 0.03, 0.05 and 0.1% Irgacure 2959

NIH-3T3 fibroblasts were incubated for 24 hours in DMEM growth media containing 0, 0.03, 0.05 and 0.1% Irgacure 2959. In this case, higher concentrations of photoinitiator were not investigated because of solubility issues. The cellular metabolic activity was then measured using the MTT assay, alongside a calibration curve that allowed the number of live cells to be calculated (Figure 7.12).

In general, the % live NIH-3T3 fibroblast cells found to be actively metabolising after 24 hours incubation with Irgacure 2959 was found to decrease significantly with increasing photoinitiator concentration. Incubation with no photoinitiator was set at 100% live cells, which equated to approximately 75,000 cells/mL after 24 hours. Even low concentrations were able to lower live

cell number, with approximately 90% after incubation with 0.03%, 75% after incubation with 0.05% and 60% after incubation with 0.1% Irgacure 2959 respectively.

In the 12 well plates used for cell culture, 1 mL hydrogel solution is present per well containing 1% w/v Irgacure 2959. This is far higher than the concentrations investigated in the MTT assay, however after the UV irradiation of the hydrogel the photoinitiator is degraded and so would be present in far lower amounts when cell solution is added.

7.3.3. NIH-3T3 culture on HAMA/gelatin hydrogels

In order to improve the cell adhesive properties of the hydrogel, gelatin was then added as it contains the cell attachment motif RGD. Firstly, NIH-3T3 fibroblasts were incubated on hydrogels containing gelatin, gelatin + 1% I2959 and gelatin + 3% HAMA + 1% I2959 and imaged after 48 hours. Cell adhesion to hydrogels was investigated on both flat and 80 μm printed gels.

Firstly, as expected, on incubation at 37 °C gelatin hydrogels were not stable, with the hydrogel able to melt and mix into the cell culture medium (even after UV irradiation). This caused a positive effect on cell growth; more cells attached to the well bottom and cells were seen to link and extend more towards each other. However, eventually cells became overgrown compared to control wells. Example light microscopy images can be seen of cells incubated with and without 5% gelatin for 48 hours in Figure 7.13.

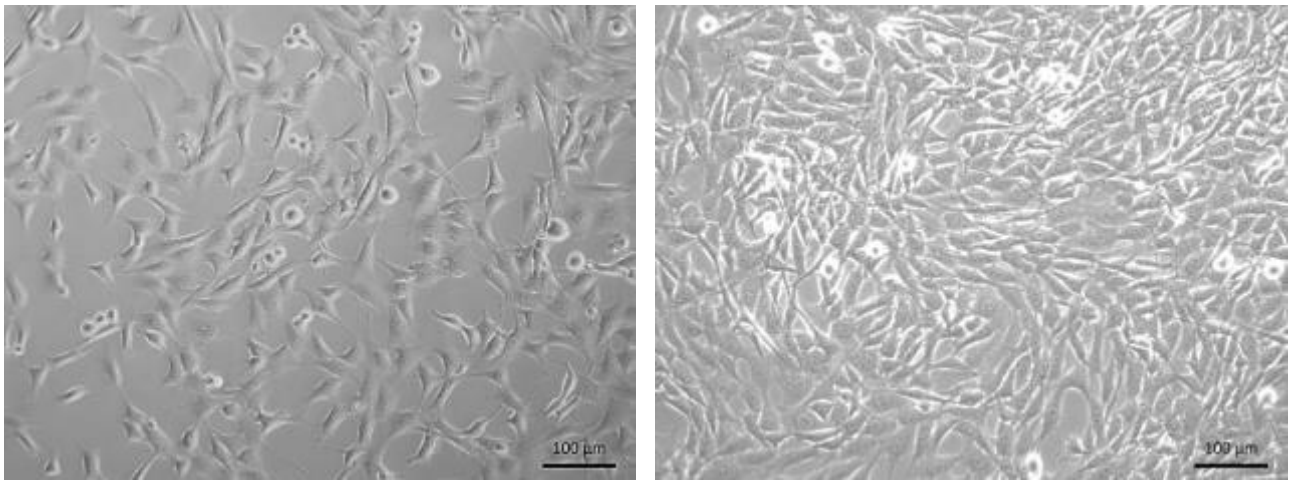

Cells were also incubated with hydrogels containing gelatin and the photoinitiator Irgacure 2959 (Figure 7.14). The incorporation of photoinitiator greatly affected the morphology and cell binding of NIH-3T3 cells.

Again, hydrogels did not retain shape and instead melted into the cell culture medium. In this case however, cells were now spherical and clumped together. Greater cell clumping was again seen with increasing gelatin concentration, however cells did not adhere to the surface and no filopodia were seen.

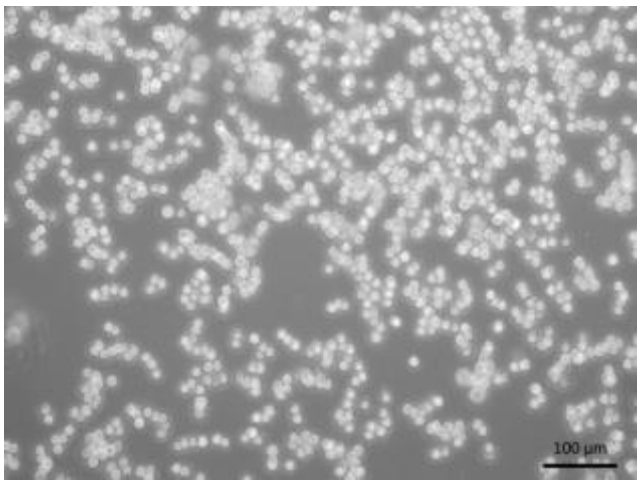

Figure 7.14: NIH-3T3 cell growth in 5% gelatin + 1% Irgacure 2959 after 48 hours. Scale bar = 100 µm

When 3% HAMA was added to gelatin solutions hydrogels retained shape on UV irradiation and did not dissolve into the surrounding environment. Because of this, the 80 µm print was also retained. In general, greater numbers of cells were seen on hydrogels containing more gelatin. Cells remained in an aggregated, spherical shape with no filopodia extending. In printed gels cells aligned in the bottom wells of the striped print, with the most defined lines of cells being seen in 10% gelatin 3% HAMA gels (Figure 7.15). Here cells aligned in the wells of the print.

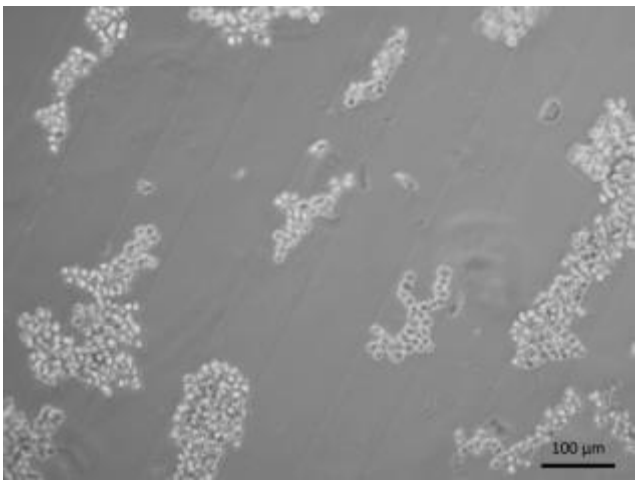

Figure 7.15: NIH-3T3 cell growth in 80 µm printed 3% HAMA/ 10% gelatin hydrogels after 48 hours. Scale bar = 100 µm

Overall, the incorporation of gelatin into the HAMA matrix did encourage cell growth; however cells did not bind and instead were spherical and aggregated. It was thought that the high

concentration of photoinitiator that could remain in the gels after crosslinking could contribute to the lack of cell binding.

7.3.3.1. Cell culture on HAMA-gelatin co-gels with 0.1% Irgacure 2959

The concentration of Irgacure 2959 was reduced from 1% to 0.1% w/v in order to promote cell adhesion onto the hydrogels. 3% HAMA was mixed with varying concentrations of gelatin and crosslinked with UV irradiation. Although gelatin was known to melt above room temperature, by co-crosslinking with HAMA, the HAMA crosslinks would entrap gelatin fibres within the matrix. 80 µm prints were also investigated to assess if directed growth was seen.

In general, as gelatin concentration increased a higher number of cells were seen on the hydrogel surface, with cells again aligning within the wells of the print (Figure 7.16). Hydrogels containing no gelatin showed very few cells on the surface; due to no gelatin being present, the hydrogel structure was soft and print was not retained well, meaning that cells diffused into the matrix.

In all hydrogels which contained gelatin, the improved structure meant the print was retained, allowing cells to align in the wells. In 10% gelatin gels the alignment is most defined as cells were able to replicate more. Although directed growth was seen, in all cases cells remained spherical and non-adhered.

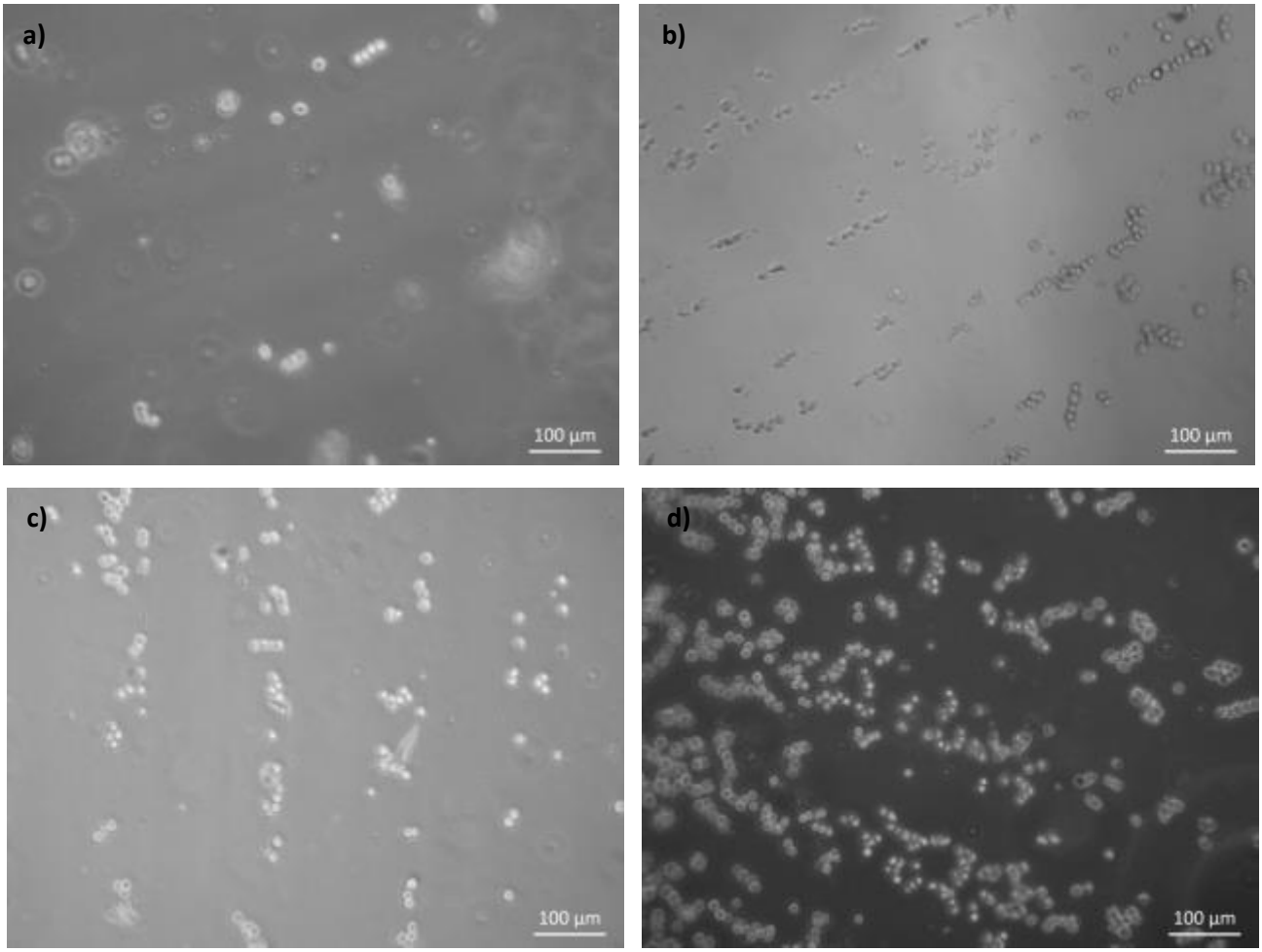

7.3.3.2. Cell culture on HAMA-gelatin co-gels with prewashing

In order to remove any Irgacure 2959 from the hydrogels after crosslinking but before the addition of cells, hydrogels were incubated in cell culture medium for 2 x 1 hour. The majority of unreacted photoinitiator would pass into the medium through diffusion and be removed from the hydrogel before cell addition. By lowering the photoinitiator concentration in cell culture medium, cells would be encouraged to bind to the hydrogel matrix and proliferate.

In this case, a positive effect on cell growth was seen with the removal of excess Irgacure 2959 (Figure 7.17). Instead of cells appearing to be spherical and aggregated in nature, cells had proliferated into multicellular growing clusters; this effect was similar to that seen by Park et al in 2003 where they incubated fibroblast cells on HAMA combined with RGD peptide[18]. With increasing gelatin concentration, cells were able to bind to the matrix and exhibit directed growth on printed hydrogels without clustering.

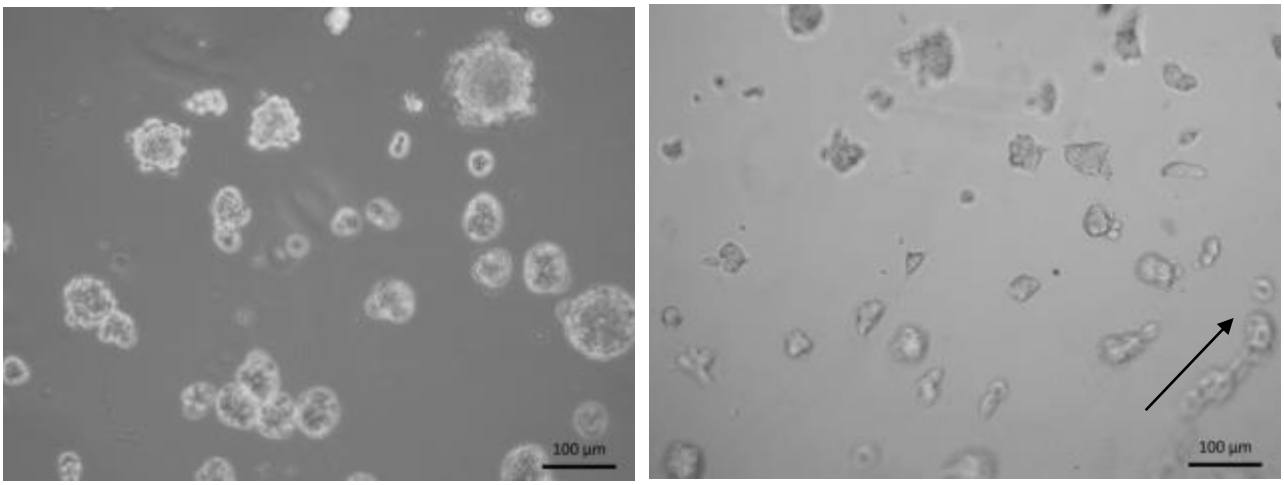

7.3.4. NIH-3T3 culture on gelatin methacrylate (GelMA) hydrogels

The use of gelatin as a photocrosslinkable hydrogel was then assessed for growth with NIH-3T3 fibroblasts. As described earlier, gelatin is useful as the protein structure contains cell-binding RGD sequences which could promote cell adhesion. Because non-modified gelatin hydrogels are able to melt at 37 °C, the gelatin was modified in a similar way to HA, with methacrylation and subsequent photo-crosslinking. From earlier experiments methacrylated HA gave a high degree of control over crosslinking as this only occurred in the presence of UV. Therefore gelatin was methacrylated to form gelatin methacrylate (GelMA) and crosslinked into temperature stable hydrogels with Irgacure 2959 and UV irradiation.

7.3.4.1. Preparation of GelMA

The reaction scheme for gelatin methacrylation and ^{1}H NMR spectrum can be seen in Figure 7.18 and Figure 7.19. Free amine groups in the protein structure (notably lysine and arginine) were reacted with methacrylic anhydride to form methacrylated gelatin and methacrylic acid by-

products. The lowering of pH by the production of the acid by-products was buffered by the use of PBS as a reaction buffer.

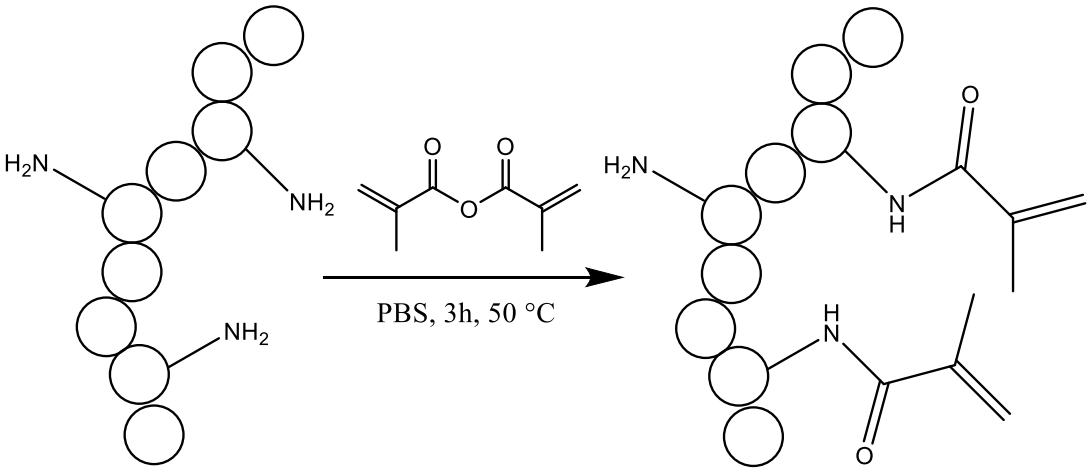

Figure 7.18: Reaction scheme for gelatin methacrylation with methacrylic anhydride

The degree of gelatin methacrylation was determined by ^{1}H NMR (Figure 7.19). NMR analysis on GelMA was carried out using the method described by Brinkman et al[19]. Peaks corresponding to methylene protons were seen at 5.2 and 5.4 ppm; the degree of functionalisation was calculated using the ratio of these peaks to aromatic protons found at 7.2 ppm as approximately 73%.

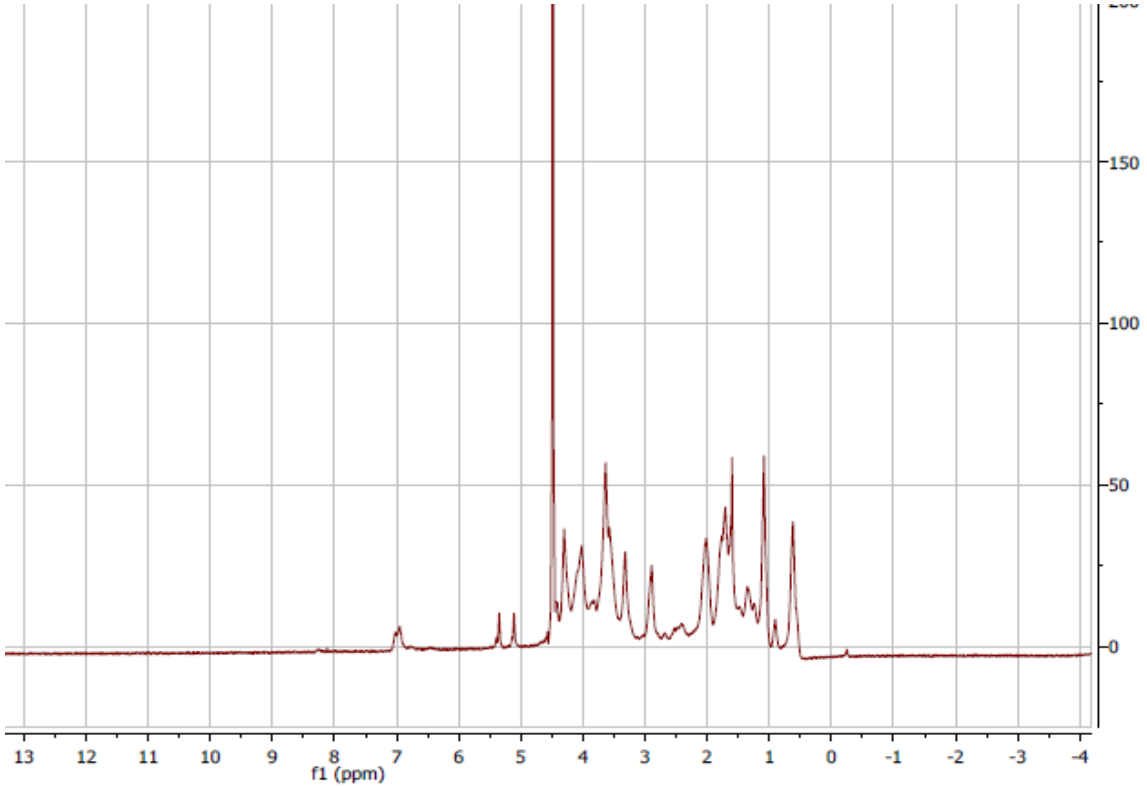

7.3.4.2. Swelling of GelMA hydrogels

Hydrogels containing varying concentrations of GelMA were formed (containing additional HA and HAMA) by exposure to UV light. Gels containing purely gelatin or HA were not investigated, as they could not be photo-crosslinked. In the case of gelatin the gels also melted at increased temperatures. Swelling ratios were calculated using previously described methods (Figure 7.20).

In general, in HA/GelMA gels a swelling ratio of approximately 20 was seen, with swelling decreasing with an increase in HA concentration. This trend however became less distinct with increasing GelMA concentration. Indeed by 10% w/v GelMA the trend switched, with a higher swelling seen in 3% HA. It was hypothesised that this was because at such high polymer concentrations complete dissolution and mixing of polymers became difficult; the polymers formed domains that made swelling measurements inaccurate.

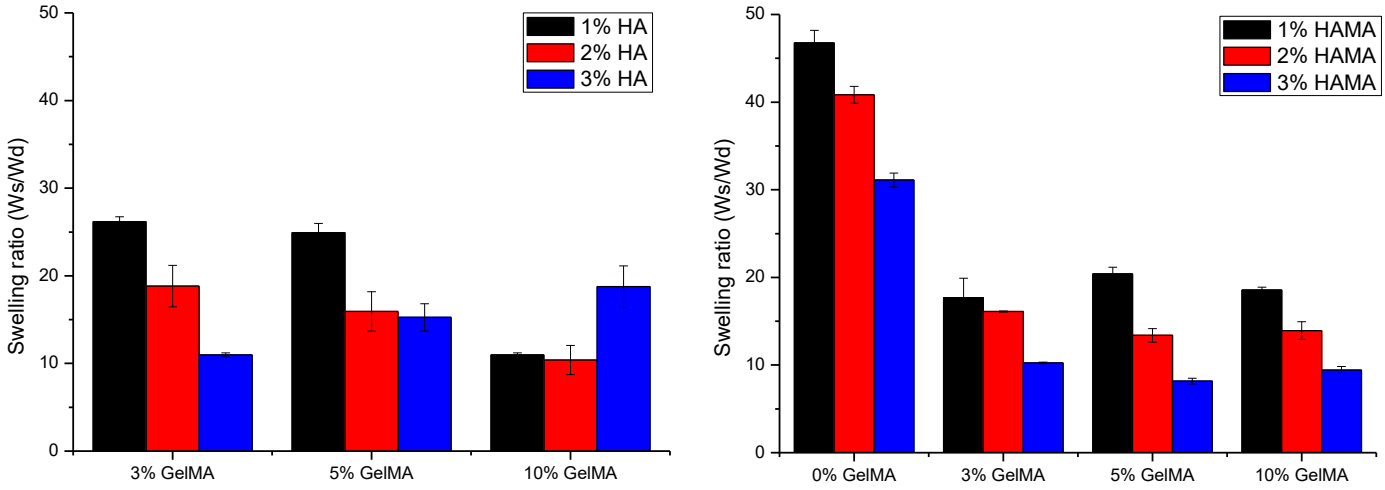

Figure 7.20: Swelling ratio values for hydrogels containing 1 – 3% HA (a) or HAMA (b) and 0 – 10% GelMA.

Compared to HA hydrogels, a lower viscosity was seen with HAMA/GelMA mixes; the addition of methacrylate groups to the HA reduced intermolecular attractive interactions, lowering viscosity. In general, swelling ratios decreased with the addition of more HAMA, as more crosslinks were able to be formed. Addition of GelMA did lower swelling ratios further, however significant differences were not seen with increasing GelMA concentrations.

7.3.4.3. Cell culture on GelMA

NIH-3T3 fibroblasts were incubated on 5% GelMA hydrogels crosslinked with 0.1% and 1% photoinitiator (Figure 7.21). In the presence of low concentrations of Irgacure 2959, a good degree of cell attachment and growth is seen. The cells adopted a highly branched shape with many filopodia and connections between cells; in fact the cells appear 'over-stretched' compared to cells incubated with no hydrogel. In 1% Irgacure GelMA hydrogels, the cells appear to have attached to the hydrogel surface, however growth and extension of cells is significantly reduced. Some cells were in the process of stretching and extending, suggesting that the growth rate is slowed by the higher photoinitiator concentration.

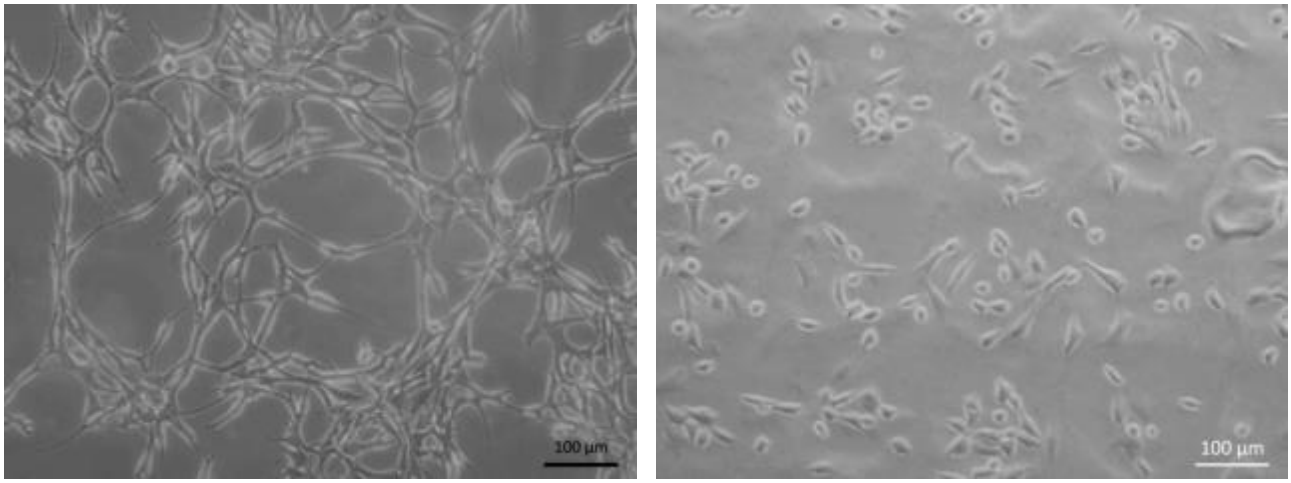

Figure 7.21: NIH-3T3 fibroblast growth on 5% GelMA hydrogels containing 0.1% (left) and 1% (right) I2959. Scale bar = 100 µm. Images courtesy of Ping Li

7.3.4.4. Cell culture on HAMA-GelMA co-gels

GelMA was added to 3% HAMA hydrogel mixes to form strong hydrogels with a higher crosslinking density and so lower swelling ratio. A higher crosslinking density was again hypothesised to give more points available for cell binding.

Firstly, the addition of GelMA did show higher crosslinking, with hydrogels binding very strongly to the prints used for patterning. Indeed, in most cases prints could not be removed successfully from hydrogels without considerable damage to the hydrogel print. Due to this, two parameters were altered to reduce the 'over-crosslinking' seen. Firstly, the overall concentration of photoinitiator was decreased from 1% w/v to 0.1% w/v. Not only would this reduce the number of crosslinks made, but also lower the cytotoxicity of the hydrogel. Secondly, the hydrogel was UV irradiated for a shorter time from 5 minutes to 3 minutes. After 3 minutes, the complete

hydrogel was still formed. Hydrogels were also investigated with and without prewashing in cell culture medium as previously described.

In general, the decrease in Irgacure 2959 concentration did not cause a significant change in cell appearance, with cells remaining spherical and non-adhered. The more defined hydrogel formed did allow more cells to assemble in the wells of the line prints used instead of in the matrix; here 3% HAMA/10% GelMA showed high directionality compared to gels containing no gelatin (Figure 7.22).

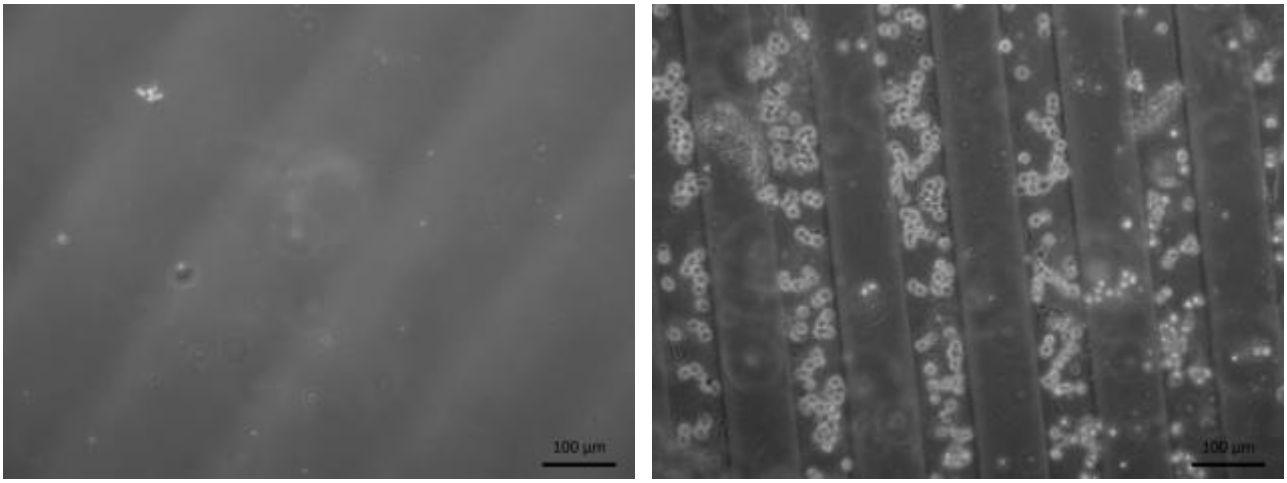

Prewashing of hydrogels before incubation with NIH-3T3 cells did show a slight improvement in cell morphology. Cells were still spherical in shape; however cells were now clumped together whilst still retaining directed growth (Figure 7.23).

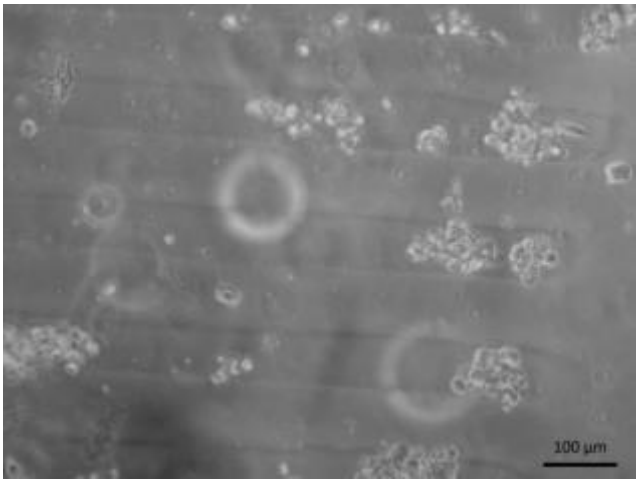

Figure 7.23: NIH-3T3 cell growth on 3% HAMA 80 µm printed hydrogels after 48 hours with (left) 0% GelMA and (right) 10% GelMA with prewashing. Scale bar = 100 µm

7.3.4.5. Cell culture on 5% GelMA hydrogels with and without HA and PEGDA

GelMA hydrogels were formed with and without HA and PEG diacrylate in order to assess if these additives influenced cell growth. 80 µm prints were also included to determine if cells were able to align with the print. In Figure 7.24, no HA was included in the hydrogels, and in Figure 7.25, hydrogels contained 1% HA.

Firstly, in Figure 7.24, it can be seen that hydrogels containing no HA and no PEG diacrylate show significantly different cell morphology than in hydrogels containing 1% PEG diacrylate. In images a) and c), cells are attached to the hydrogel and exhibiting a flattened shape with clearly visible filopodia. There is also a high extension to neighbouring cells. When incubated on a printed hydrogel, directed cell growth was not apparent. In the case of hydrogels containing 1% PEG diacrylate, clustering of cells is seen with no attachment to the surface. Cells are also spherical in shape implying cell distress.

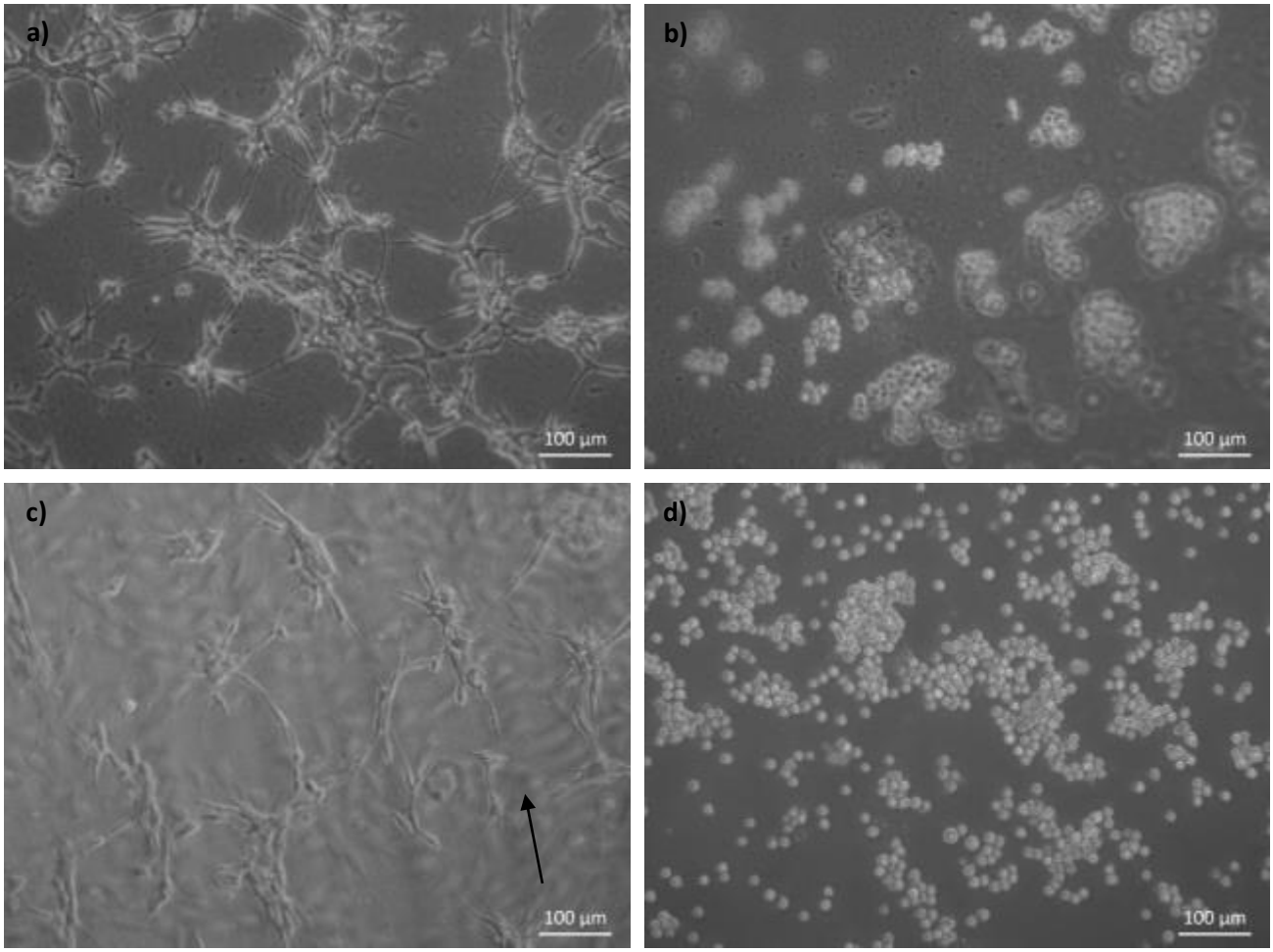

Figure 7.24: NIH-3T3 cell growth on crosslinked GelMA hydrogels containing no HA. No print with a) no PEGDA and b) 1% PEGDA. 80 µm line print with c) no PEGDA and d) 1% PEGDA. Scale bar = 100 µm

Cells were then incubated on hydrogels containing 1% HA as well as PEG diacrylate. Again, 80 µm line prints were also included (Figure 7.25). Here, the opposite trend to that described previously was seen; good cell growth was observed in hydrogels containing 1% PEG diacrylate, but cell growth was hindered with no PEG diacrylate. With no PEG diacrylate the cells adopted a spherical, clustered appearance with cells aggregating in the wells of the 80 µm print. In 1% PEG diacrylate hydrogels cells were able to adhere to the surface and extend filopodia to neighbouring cells.

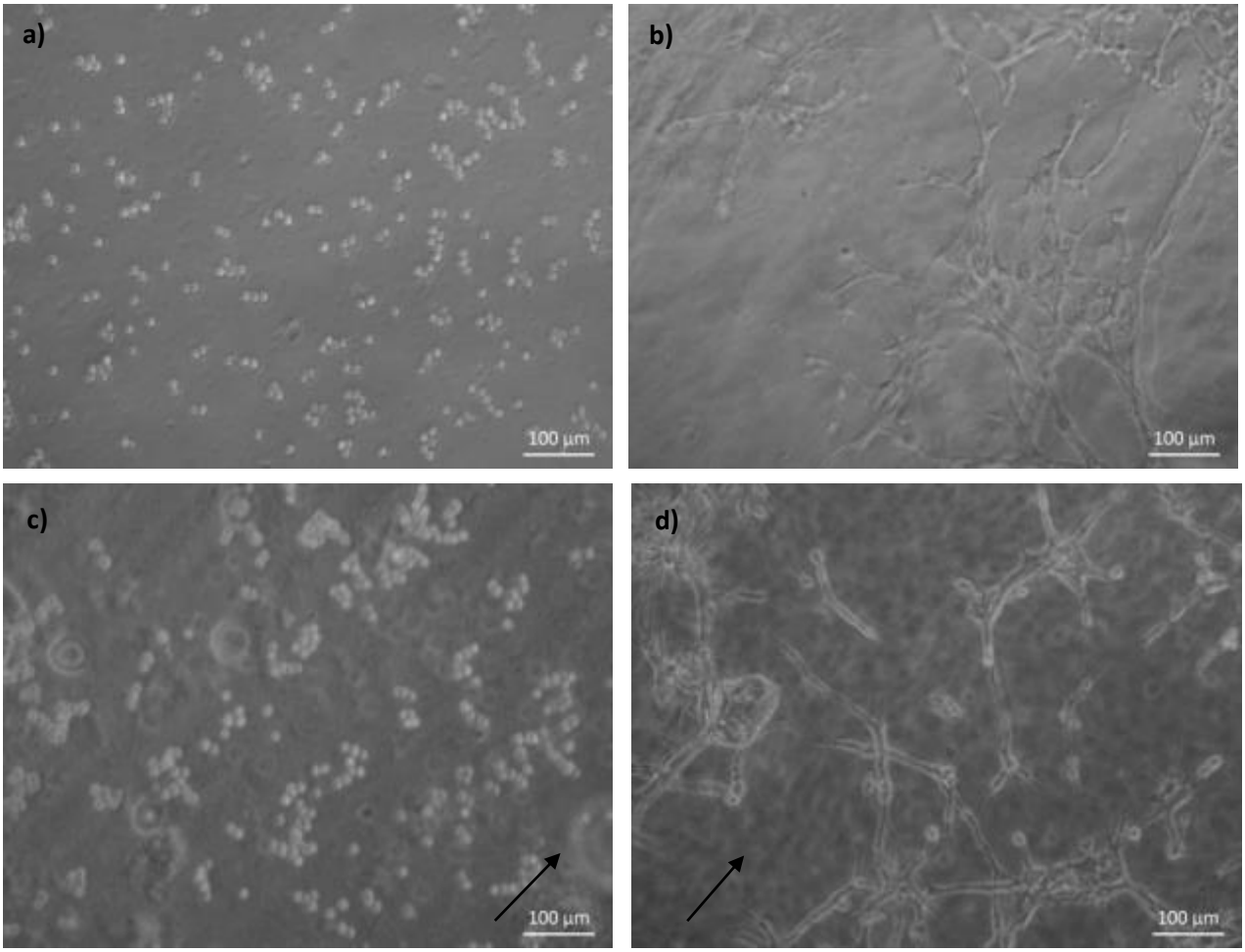

In general, cell attachment and growth was only seen here in two cases: either in hydrogels containing only GelMA or GelMA with HA and PEG diacrylate. In the first case, this is plausible as the cell-binding RGD sequence found in gelatin would promote cell attachment, as well as the hydrophilic polymer properties. In the second case, the reason why we see cell attachment and growth is more unclear. This could be due to the shear concentration of GelMA, HA and PEG

diacrylate polymer fibres in the hydrogel; the high density could be enough for cells to be able to attach across the polymer network.

7.3.4.6. Hyaluronidase degradation of GelMA gels containing HA

Hydrogels containing 5% and 10% GelMA were formed containing 1%, 2% and 3% unmodified HA, and were subsequently degraded with 1 mg/mL hyaluronidase solution, as described by Camci-Unal et al[20]. The degradation of the hydrogel was followed using the loss of weight of the hydrogel due to degraded polymer units going into solution (Figure 7.26).

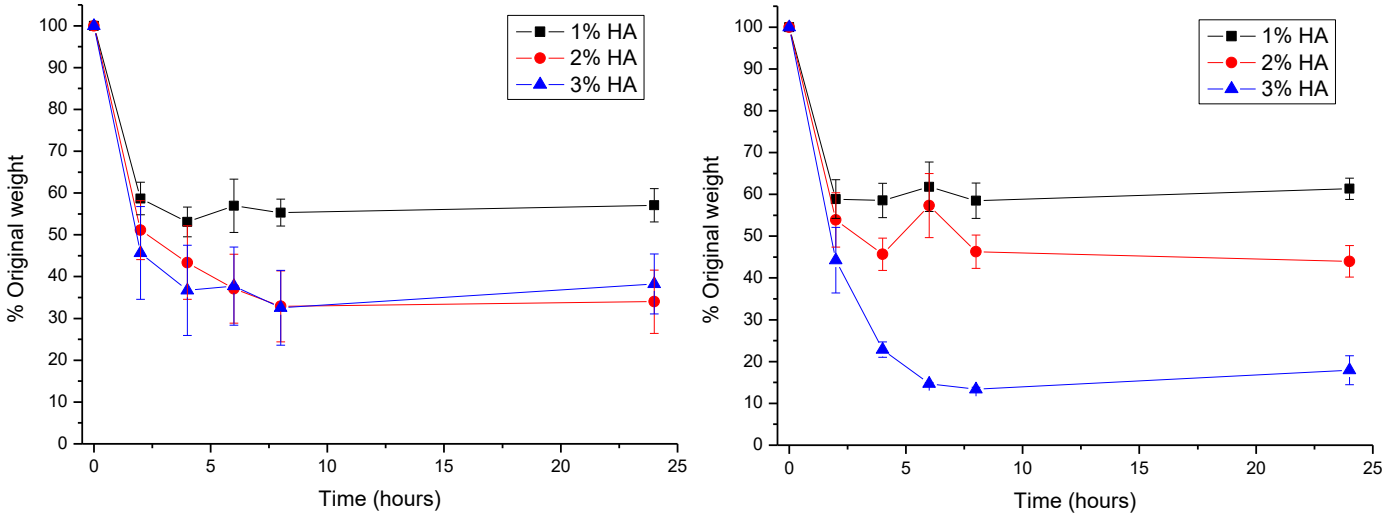

Figure 7.26: Weight loss of GelMA/HA hydrogels through degradation with 1 mg/mL hyaluronidase. (left) 5% GelMA and (right) 10% GelMA

In general, the extent and rate of weight loss seen during incubation with hyaluronidase increased with increasing HA concentration. In 5% GelMA hydrogels containing 1% HA, approximately 60% of the original hydrogel weight remained after 24 hours, whereas in 2% and 3% HA only 30% remained. In 1% HA degradation plateaued after 2 hours, and 2% and 3% HA a plateau was seen after 8 hours.

Similarly, in 10% GelMA hydrogels the extent and rate of degradation by hyaluronidase increased with increasing HA concentration. In 1% HA a similar response to hydrogel containing 5% GelMA was observed; approximately 60% initial weight remained after 24 hours. In 2% HA degradation was slightly more with approximately 45% remaining. Compared to 3% HA

hydrogels containing 5% GelMA, in 10% GelMA a significantly higher amount of degradation was seen; by 6 hours degradation only 15% of the initial weight remained.

7.3.4.7. Hyaluronidase degradation of GelMA gels containing HAMA

Hydrogels containing 1%, 2% and 3% HAMA were then also formed with 5% and 10% GelMA, and again degraded with 1 mg/mL HAase solution. The degradation of the hydrogel was determined using the loss of weight of the hydrogel due to degraded polymer units going into solution (Figure 7.27). This time, hydrogels were visibly more viscous in solution compared to HA/GelMA solutions.

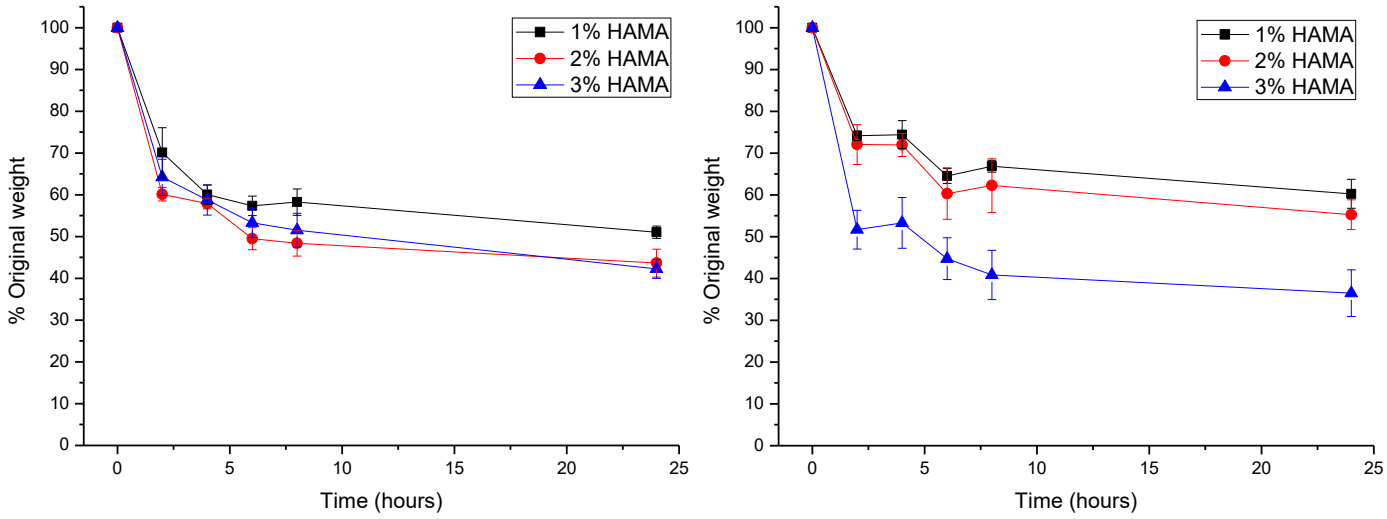

Figure 7.27: Weight loss of GelMA/HAMA hydrogels through degradation with 1 mg/mL hyaluronidase. a) 1% HAMA, b) 2% HAMA and c) 3% HAMA

Generally as the concentration of HAMA increased, the extent and rate of weight loss seen during incubation with HAase increased. With 5% GelMA hydrogels, the effect was less pronounced with approximately 50% initial weight remaining in 1% HAMA hydrogels and 40% in 2% and 3% HAMA hydrogels. In 10% GelMA hydrogels, the hydrogels were slightly more resistant to HAase degradations, with 65%, 60% and 40% initial weight remaining after 24 hours for 1%, 2% and 3% HAMA hydrogels respectively.

7.4. Conclusions

This chapter focussed on the use of hot embossed polystyrene lithographic prints to form hydrogels with a printed surface, in order to aid cell adherence or impart directed growth to

fibroblast cells. Hot embossing was found to be a useful technique which gave durable, high quality prints for hydrogel printing. HAMA was successfully printed with 50 and 80 µm line prints using UV irradiation. On seeding printed HAMA hydrogels with NIH-3T3 fibroblasts, directionality was seen as the cells aggregated in the line wells of the print, however they were unable to bind to the surface properly or proliferate. Gelatin methacrylate hydrogels were then investigated with and without HAMA, resulting in a more successful attachment to the surface.

7.5. References

1. R. M. Greco, J. A. Iocono and H. P. Ehrlich, *J Cell Physiol*, 1998, **177**, 465-473.
2. J. K. Kutty, E. Cho, J. Soo Lee, N. R. Vyavahare and K. Webb, *Biomaterials*, 2007, **28**, 4928-4938.
3. M. H. Zaman, *Biophysical Journal*, 2007, **92**, L17-L19.
4. E. Ruoslahti and M. D. Pierschbacher, *Science*, 1987, **238**, 491-497.
5. T. W. Chung, D. Z. Liu, S. Y. Wang and S. S. Wang, *Biomaterials*, 2003, **24**, 4655-4661.
6. R. A. Gittens, T. McLachlan, R. Olivares-Navarrete, Y. Cai, S. Berner, R. Tannenbaum, Z. Schwartz, K. H. Sandhage and B. D. Boyan, *Biomaterials*, 2011, **32**, 3395-3403.
7. *H.-I. Chang* and Y. W*ang* in *Regenerative Medicine and Tissue Engineering - Cells and Biomaterials*, ed. D. Eberli, InTech, 2011, ch. 27.
8. V. Chan, M. B. Collens, J. H. Jeong, K. Park, H. Kong and R. Bashir, *Virtual and Physical Prototyping*, 2012, **7**, 219-228.
9. M. M. Stevens, M. Mayer, D. G. Anderson, D. B. Weibel, G. M. Whitesides and R. Langer, *Biomaterials*, 2005, **26**, 7636-7641.
10. H. Schift and A. Kristensen, in *Springer Handbook of Nanotechnology*, ed. B. Bhushan, Springer Berlin Heidelberg, 2010, ch. 9, pp. 271-312.
11. J. Yeh, Y. Ling, J. M. Karp, J. Gantz, A. Chandawarkar, G. Eng, J. Blumling, 3rd, R. Langer and A. Khademhosseini, *Biomaterials*, 2006, **27**, 5391-5398.
12. Y. C. Chen, R. Z. Lin, H. Qi, Y. Yang, H. Bae, J. M. Melero-Martin and A. Khademhosseini, *Adv Funct Mater*, 2012, **22**, 2027-2039.
13. C. G. Williams, A. N. Malik, T. K. Kim, P. N. Manson and J. H. Elisseeff, *Biomaterials*, 2005, **26**, 1211-1218.
14. C. Fotia, G. M. Messina, G. Marletta, N. Baldini and G. Ciapetti, *Eur Cell Mater*, 2013, **26**, 133-149; discussion 149.
15. C. Zhong, J. Wu, C. A. Reinhart-King and C. C. Chu, *Acta Biomater*, 2010, **6**, 3908-3918.
16. A. D. Rouillard, C. M. Berglund, J. Y. Lee, W. J. Polacheck, Y. Tsui, L. J. Bonassar and B. J. Kirby, *Tissue Eng Part C Methods*, 2011, **17**, 173-179.
17. S. J. Bryant, C. R. Nuttelman and K. S. Anseth, *J Biomater Sci Polym Ed*, 2000, **11**, 439-457.
18. Y. D. Park, N. Tirelli and J. A. Hubbell, *Biomaterials*, 2003, **24**, 893-900.
19. W. T. Brinkman, K. Nagapudi, B. S. Thomas and E. L. Chaikof, *Biomacromolecules*, 2003, **4**, 890-895.
20. G. Camci-Unal, D. Cuttica, N. Annabi, D. Demarchi and A. Khademhosseini, *Biomacromolecules*, 2013, **14**, 1085-1092.

Chapter 8 : Conclusions and Future Project Development

8.1. General Conclusions

The development of resistance of bacteria to common antibiotics is, and will continue to be, widespread globally in the subsequent decades. It will remain an issue of critical political, medical and social importance. Although certain measures have been introduced to slow this, the seemingly universal and unregulated use of antibiotics (especially within agriculture and the developing world) means that the problem must be confronted on many lines of attack to be solved.

Research in the West into the use of bacteriophage as alternatives to antibiotics has increased significantly in response to antibiotic resistance. Combined with fast, modern sequencing techniques and a better understanding of bacteriophage genetics, bacteriophage therapy is a promising new way of treating common bacterial infections in humans, food and agriculture. Although most likely not a complete alternative to antibiotics, bacteriophage still can be active as another weapon in the antibacterial arsenal. In this work, Bacteriophage K was investigated as an active bacteriophage against *S. aureus*. The bacteriophage exhibited a broad efficacy and was effective against bacterial liquid culture and biofilms, as well as in both lysate solution and when combined into hydrogels.

In recent years, triggered release systems have been widely explored in order to reduce the overuse of antibiotics, and so curb the development of bacterial resistance. By preventing the exposure of bacteria to sub-lethal levels of antibiotic, the selection pressure on bacteria to mutate is reduced. In this way, the original aim of this project was to create a hydrogel system which gave triggered release of bacteriophage instead of antibiotics by pathogenic bacterial virulence factors. This was successfully accomplished through the formation of a bilayered hydrogel matrix comprising a lower hydrogel layer containing Bacteriophage K and an upper crosslinked hyaluronic acid layer. Hyaluronidase secreted by *S. aureus* was able to specifically degrade the upper layer and release bacteriophage compared to non-active strains.

The use of hydrogels in wound care has been proven to be beneficial in promoting wound healing. Hydrogels are able to protect the wound from the external environment, as well as provide a highly hydrated environment which allows for cell proliferation and migration. They combine the viscoelastic properties of a solid with the diffusive properties of a liquid. Additionally, they are generally biocompatible, non-toxic, non-immunogenic and in some cases

biodegradable. The chemical structure of the hydrogel can also be tailored for specific roles, by addition of other polymers, proteins or drug molecules.

HA was focussed on in this investigation, as in the body the biopolymer makes up a large part of skin and soft tissue and has many reported roles in wound healing. Additionally, the polymer can be selectively degraded by the *S. aureus* virulence factor, hyaluronidase. In this way, the polymer was used as a trigger mechanism for release of bacteriophage from other hydrogels. In general, the use of hydrogels (including hyaluronic acid) in wound dressings will only benefit wound treatment compared to conventional dressings, as they are able to play a more active role in the wound healing process.

In Chapter 7, the lithographic printing of hydrogels for use in cell culture was investigated. The technique is an effective way of imparting directional prints to a hydrogel, and subsequent directed growth of cells. However, the use of HA based hydrogels was found to give poor attachment compared to later gelatin-based hydrogels. This could be beneficial in a wound dressing, as this would prevent cell attachment to the dressing surface, allowing for easier removal.

8.1.1. Limitations of the presented work

Although the presented work showed novel findings, there are certain limitations which must be addressed in order to take the research further.

Firstly, the main limitation of the bilayer system described in Chapter 6 is that the HAMA upper layer does not give complete prevention of bacteriophage diffusion. Passive leakage is seen in some cases, and indeed when incubated with live culture (a more authentic model of how bacteria will affect the system) no triggered killing of *S. aureus* was seen.

Secondly, further investigation needs to be carried out into the type of hydrogel used for the lower layer. In this research, PVA was found to be damaging to bacteriophage on exposure to UV, and agarose has very poor mechanical properties which would be unsuitable in a normal environment (the hydrogel cracks and breaks when exposed to any external stress). Thankfully the vast selection of natural and synthetic polymers available means that there is a high chance that a suitable alternative could be found which does not damage bacteriophage, has mild gelation conditions and a high flexibility and strength.

The reliance of the system on hyaluronidase as a trigger mechanism is also an issue. Firstly, bacteria do not continually secrete the same quantity and type of virulence factors; it is

dependent on many external factors including the concentration of available oxygen and energy sources, temperature and if bacteria are planktonic or in a biofilm. In Chapter 5, the secretion of HAase in both planktonic and biofilm systems was investigated, however even these were in optimised laboratory conditions. Similarly, HAase is also prevalent in the human body, where it is secreted by cells during normal HA metabolism. For the system to be effective the concentration of HAase secreted by *S. aureus* on infection must be far higher than baseline HAase, as well as the concentrations found during inflammation. The secretion of HAase by NIH-3T3 fibroblasts was investigated which showed no HAase activity, however this is only one, non-human cell line. The breakdown products of the bilayered hydrogel system (low molecular weight HA) are also known to promote an inflammatory response during wound healing.

The UV irradiation of bacteriophage must also be discouraged, as it not only greatly decreases the concentration of bacteriophage available for bacterial infection, but also exposes the virions to possible genetic mutations or scission of toxic elements. These toxic elements could later be taken up by any bacteria present, causing the formation of dangerous bacterial mutants.

8.2. Future Project Development

The research presented in this thesis offers a number of avenues for future investigation and development.

8.2.1. Bacteriophage cocktails

The use of bacteriophage therapy in general will only escalate in the future, as more antibiotics become inactive against pathogenic bacteria. Single bacteriophage may be effective in certain cases, but in order to become a viable alternative (or addition) to antibiotics, bacteriophage cocktails are more useful. These are mixtures of two or more bacteriophage which when combined give a broader range of infectivity than single bacteriophage. Cocktails are more successful in hospital environments, where it is frequently not possible to quickly identify the exact strain (even species) of an infection. The addition of a bacteriophage cocktail into this system instead of only Bacteriophage K would be beneficial and more likely to be active with unknown bacteria.

Also, novel bacteriophage can be isolated from the surrounding environment (e.g. sewage, river water) which are able to infect different bacterial strains. In a clinical setting, a bacteriophage which has activity against any of the ESKAPE pathogens provides a valuable alternative treatment to antibiotics.

8.2.2. Theranostic wound dressings

A 1st generation antimicrobial hydrogel can be thought of as systems described in Chapter 4, where a passive release is seen. On addition of the virulence factor-sensitive HAMA layer (2nd generation) an active response is now seen, where incorporation of HAMA layer gives triggered release of bacteriophage. This bilayered hydrogel system then has the possibility of being incorporated into a theranostic wound dressing; a theranostic is a device which combines diagnostics and therapeutics into a single system. Here, the diagnostic component will be dye-containing phospholipid vesicles currently investigated by the group, which in the presence of pathogenic bacteria release the dye and cause a fluorescent warning that infection is present. The therapeutic component will be the bilayered hydrogel system described in this thesis, where on infection bacteriophage will be selectively released causing a therapeutic response through killing of bacteria.

8.2.3. Triggered release hydrogels

The formation of hydrogels which give a triggered release of bacteriophage by bacterial virulence factors still has leverage, and can be investigated in different ways.

Firstly, as mentioned earlier the structure and properties of the existing bilayered hydrogel system could be altered to prevent the passive diffusion of bacteriophage. This could be overcome in a number of ways. The bacteriophage particles could be physically immobilised in the lower hydrogel layer, either by chemical coupling to the main hydrogel polymer or to a separate polymer which can later be broken down. For example, the bacteriophage could be coupled to hyaluronic acid through reaction of the HA carboxylic acid and amine residues on the bacteriophage head, and then incorporated into the agarose lower layer before gelation. The bacteriophage are then prevented from passively diffusing by polymer entanglement, but in the presence of HAase the HA could be broken down into smaller units which could allow bacteriophage diffusion. Also, the bacteriophage could be immobilised into micro- or nanoparticles which are subsequently embedded in the lower layer. The upper layer could also be altered to take advantage of other bacterial virulence factors which can breakdown hydrogel forming polymers, e.g. ester based hydrogels which respond to lipase, or protein/amine linked hydrogels which respond to protease.

In the future, the bilayered hydrogel system for triggered release of bacteriophage originally described in this thesis can be adapted for different external triggers or bacterial systems. For example, these can include PNIPAAm based hydrogels which are temperature responsive, or pH

sensitive hydrogels. Recently within the group (Scarlet Milo) a bilayered hydrogel has been developed which gives triggered release of bacteriophage for the treatment of *Proteus mirabilis*, a common bacterium found in the majority of urinary tract infections. Here, the HAMA layer is replaced by the pH-sensitive polymer Eudragit®. When *P. mirabilis* grows, it secretes the enzyme urease which breaks down urea into ammonia and carbamate molecules. The excess ammonia causes a general increase in the urine pH from pH 5.5 - 6.5 to pH 8. The Eudragit coating exploits the change in pH, as it is selectively degraded at high pH, giving triggered release of *P. mirabilis* bacteriophage.

8.2.4. Testing with established biofilms

In the majority of cases, bacteria in a wound infection exist in a biofilm of either one or more species or strains, instead of isolated floating planktonic bacteria. An established biofilm is a complex community able to sense and respond to its external environment. As mentioned earlier, bacteria do not continually secrete the same quantity and type of virulence factors, and so any dressing which will be used on a wound must be tested with established biofilms (both *in vitro* and *in vivo*). Further work would include further assessment of HAase secretion from biofilms, and to see if triggered killing can be seen on incubation of the bilayered hydrogel system on biofilms.

8.2.5. In vivo testing

Any therapeutic that aims to be used in a clinical setting must be rigorously tested before being used on patients. Firstly, pre-clinical phase studies must be carried out in vivo, which evaluate the biocompatibility of the therapeutic, as well as its response in the presence of inflammation. This is initially carried out on small animals (mice and rats) before going on to higher species. In wound dressings used for the skin and soft tissues, testing is frequently done on pigs as they have a very similar dermal structure to humans.

If initial in vivo results prove promising, clinical trials on humans (Phase I – III) are then undertaken. Randomised double-blind clinical trials are seen as the best and most accurate, as the possibility of bias is prevented.

8.2.6. Hydrogels for eukaryotic cell culture

Although not particularly successful with HA based polymers, the use of gelatin hydrogels for cell culture still provides scope for future work. In general, hydrogels provide a good environment to promote cell proliferation and migration - both highly important in wound healing. By altering

the structure, porosity and chemical composition of hydrogels, growth of cells can be promoted, or suppressed (e.g. to prevent biofouling).

8.2.7. Lithographic printing of hydrogels

By printing a hydrogel, this gives a better opportunity for cell attachment or directed growth, depending on the size and shape of the print. The ordered and directed growth of cells has many applications in biomedicine and tissue engineering, such as in neurology. Lithographic printing allows the easy investigation of how the size and shape of a print affects cell growth.

In the Schönherr group, hydrogel printing technology has been adapted to form hydrogel cubes (instead of lines). These can then be used as hydrogel “building blocks” which can be stacked and arranged in different ways. Also, patterned hydrogels can be formed which contain either cell-adhesive or cell-repulsive regions. Again this enables the directed or patterned growth of cells on a surface. They have also investigated the printing of hydrogels with square wells which hold single cells; here to see how different factors affect single cells can be investigated.